THE UNIVERSITY OF SHEFFIELD

Department of Civil and Structural Engineering

INCORPORATING ACTIVE CONTROL OF HUMAN-INDUCED VIBRATIONS IN FLOORS INTO BUILDINGS

by

Emma Jane Hudson

A thesis submitted for the Degree of Doctor of Philosophy in Engineering

March 2013

Abstract

This thesis investigates the implications of incorporating active vibration control (AVC) into floor structures from the initial design stage, with the goal of enabling the construction of more slender long-span floors.

The original contributions to knowledge in this work are the investigations into: the development of a novel walking force that simulates the in-service loading of an office environment; the comparison between the effectiveness of AVC and tuned mass dampers (TMDs) when used on floor structures; the investigation into the effect of AVC over the entire floor area rather than considering single locations only, leading to conclusions about typical numbers of actuators that would be required; the investigation into the trade-off between power demand and the performance of an AVC system; and the initial life cycle analysis (LCA) of a floor that incorporates AVC at the design stage.

The force model utilises simultaneous pedestrians walking throughout the structure and was calibrated and verified using experimentally acquired data. AVC was found to be a significant improvement upon TMDs in that the response of the structure was reduced to a greater extent using a much smaller inertial masses. The effectiveness of AVC was generally limited to within a single bay. However, large reductions in response were observed within each controlled bay. Therefore, it is suggested that a rule of thumb of one actuator per significant panel is required to control a given floor area, and that the size of these bays should be maximised to increase the effectiveness of AVC.

High feedback gains resulted in only slight improvements in structural response, therefore improvements in the non-overhead power demand for AVC can be achieved through a simple decrease in the feedback gain. This has the additional benefit that smaller actuators could be utilised. The initial LCA highlighted the high financial cost of AVC but also demonstrated that potentially significant material savings could be realised through incorporation of AVC at the design stage.

Acknowledgements

When I look back at my time here I will do so with much fondness. All that I have achieved would not have been possible without the support, friendship and love of those close to me and I would like to take a moment to thank everyone who has helped me so much.

Firstly, I would like to thank my supervisor, Paul Reynolds. Throughout my PhD he has guided, challenged and inspired me to get the most out of my work. He has given me so many opportunities and experience by getting me involved in other projects and I am incredibly fortunate that he has as provided lots of 'toys' to play with; a sure fire way to keep a PhD student happy! Thank you for believing in me Paul and for helping me so much.

All my colleagues at VES throughout the years have been incredibly kind and supportive and I only wish I could personalise my thanks to you all! I would like to thank Chris for showing me that there's always time for a coffee! You've given me some great advice, both technical and personal, for which I am extremely grateful. Sharon, you've helped me so much and when times have been tough you have always been there for me. Your baked treats are always something to look forward to! And Donald, thank you for your guidance throughout my PhD. You have always been there to help out in the lab, or just to bounce ideas around with.

I would also like to thank those very close to me. Olivia, you have been so understanding and shared so much love. I truly cherished coming home to you at the end of a tough day and really appreciate how amazing you are. I would like to thank my fabulous sisters Beccy and Helen and tell them how grateful I am for always looking out for me. Finally, I would like to thank my parents. You bore the brunt of me worrying about my work, and despite my rants you would always ask again next time! You always believed in me when I doubted myself and for all these things and countless more I would like to dedicate this work to you.

Memorandum

The accompanying thesis entitled ”Incorporating Active Control of Human-Induced Vibrations in Floors into Buildings” is submitted for the degree of Doctor of Philosophy in the Faculty of Engineering at the University of Sheffield. The thesis is based entirely on the independent work carried out by the author in the University of Sheffield between August 2009 and March 2013 under the supervision of Professor Paul Reynolds. All the work and ideas recorded are original except where acknowledged in the text or by reference. The work contained in the thesis has not previously been submitted for a degree or diploma at this, or any other, University or Examining Body.

Emma Jane Hudson

March 2013

Contents

List of Figures

List of Tables

List of Symbols

$\mathbf{A}$	state matrix in state space
$\mathbf{B}$	input matrix in state space
C	damping matrix
$\mathbf{C}$	output matrix in state space
C_m	modal damping matrix
C^*	mass normalised modal damping matrix
$(CF)_i$	net cash flow in year i
$\mathbf{D}$	direct transmission matrix in state space
D_{CF}	annual cash flow to debt
E_{CF}	annual cash flow to equity
F	applied disturbance force
F_m	modal force vector
F_{wz}	transfer function between exogenous signals and error signals
G	static self weight of person
G_{ij}	structural dynamics for ij-th DOF
G_{aij}	actuator dynamics for ij-th DOF
H	modal amplitude vector
I	identity matrix
I_{eff}	effective impulse
J	performance index
K	stiffness matrix
K_{ij}	controller dynamics for ij-th DOF
K_G	constant gain
K_m	modal stiffness matrix
K^*	mass normalised modal stiffness matrix
M	mass matrix
M_m	modal mass matrix

N	number of years
$\mathbf{Q}$	state weighting matrix
R	Response factor
$\mathbf{R}$	input weighting matrix
T	time period used for RMS
T_a	duration of a particular activity
T_t	total time period
T_r	applicable tax rate
U	control force
W_c	controllability Gramian
W_o	observability Gramian
W_x	x-th frequency weighting curve
Y	structural displacement vector
$\dot{Y}$	structural velocity vector
$\ddot{Y}$	structural acceleration vector
$\mathcal{Y}$	displacement of structure in laplace domain
$\mathcal{Y}_\mathcal{T}$	displacement of TMD in laplace domain
a	acceleration
c_i	i-th DOF of modal damping matrix
c_{ij}	ij-th DOF of damping matrix
c_T	TMD damping
f_i	i-th DOF of force vector
f_{opt}	optimal TMD tuning frequency
f_p	walking pace
f_{pri}	natural frequency of mode of vibration to which TMD is tuned
f_{n1}	fundamental natural frequency
h	harmonic number
i	mode number
i_D	annual cost of debt

i_E	annual cost of equity
j	year number
k_i	i-th DOF of modal stiffness matrix
k_{ij}	ij-th DOF of stiffness matrix
k_T	TMD stiffness
m	number of modes
m_i	i-th DOF of modal mass matrix
m_{ij}	ij-th DOF of mass matrix
m_c	number of controlled modes
m_r	number of residual modes
m_T	TMD mass
n	number of nodes
n_a	number of times a particular activity will occur
r	discount rate
s	laplace operator
t	time
t_f	time period considered for LQR optimisation
$\mathbf{u}$	system inputs
v	physical location
w	exogenous signals to generalised plant
$\mathbf{x}$	internal states
y_i	i-th DOF of structural displacement
$\dot{y}_i$	i-th DOF of structural velocity
$\ddot{y}_i$	i-th DOF of structural acceleration
$\mathbf{y}$	output vector
z	error signals from generalised plant
ΔC	additional damping matrix
ΔK	additional stiffness matrix
Φ	mode shape matrix

α_h	Fourier coefficient for h-th harmonic of walking
γ	scalar weighting for importance of minimising effect of residual modes
δ	deflection of beam due to permanent loading
ε	lag term for actuator driven in voltage mode
ζ_a	damping ratio of actuator
ζ_i	damping ratio of i-th mode of vibration
ζ_{opt}	optimal TMD damping ratio
η_i	i-th modal amplitude
$\lambda_{1,2}$	complex conjugate poles
λ_{C_i}	i-th eigenvalue of controllability Gramian
μ	mass ratio of TMD relative to primary structure
ρ	scalar weighting factor between states and inputs
$\bar{\sigma}(\bullet)$	singular value of $(\bullet)$
ϕ_h	phase angle for h-th harmonic of walking
ϕ_{ij}	i-th mode shape value for the j-th mode
ψ	force voltage characteristic for actuator
ω	circular frequency
ω_a	circular natural frequency of actuator
ω_{n_i}	circular natural frequency of i-th mode of vibration
$(\bullet)_{RMS}$	RMS of $(\bullet)$
$(\bullet)_w$	frequency weighted value of $(\bullet)$
$\mathrm{tr}(\bullet)$	trace of matrix $(\bullet)$
$(\bullet)^T$	transpose of matrix $(\bullet)$
$\|(\bullet)\|_x$	x-norm of $(\bullet)$
$\dot{(\bullet)}$	derivative of $(\bullet)$ with respect to time
$(\bullet)^*$	complex conjugate transpose of $(\bullet)$

List of Abbreviations

ACB	Asymmetric Cellular Beam
AISC	American Institute of Steel Construction
AMD	Active Mass Damper
AVC	Active Vibration Control
BCR	Benefit-Cost Ratio
CAF	Compensated Acceleration Feedback
c/c	Centres
CDF	Cumulative Distribution Function
CLD	Constrained Layer Damping
DAF	Direct Acceleration Feedback
DECC	Department for Energy and Climate Change
DOF	Degrees of Freedom
DOFB	Direct Output Feedback (controller)
DVF	Direct Velocity Feedback
EC	Embodied Carbon
EE	Embodied Energy
EIA	Environmental Impact Assessment
EMA	Experimental Modal Analysis
FE	Finite Element
FRF	Frequency Response Function
FTT	Feed-Through Term (as in DVF with FTT)
HMD	Hybrid Mass Damper
ICC	Input Constrained Control
IMSC	Independent Modal Space Control
LCA	Life Cycle Analysis
LCI	Life Cycle Inventory
LQG	Linear Quadratic Gaussian

LQR	Linear Quadratic Regulator
LTI	Linear Time Invariant
MB	Model-Based (controller)
MDOF	Multiple Degrees Of Freedom
MIMO	Multiple Input-Multiple Output
MTVV	Maximum Transient Vibration Value
NHS	National Health Service
NPV	Net Present Value
OCC	Output Constrained Control
OC	Operating Carbon
OE	Operating Energy
PD	Probability Distribution
PG	Plate Girder
PM	Permanent Magnet
PVC	Passive Vibration Control
PI	Performance Index
RDVF	Response Dependent Velocity Feedback
RMS	Root Mean Square
SAVC	Semi-Active Vibration Control
SCI	Steel Construction Institute
SDOF	Single Degree of Freedom
TMD	Tuned Mass Damper
TP	Test Point
UB	Universal Beam
UC	Universal Column
ULS	Ultimate Limit State
VDV	Vibration Dose Value
WACC	Weighted Average Cost of Capital

Chapter 1

Introduction

1.1 Background

Problematic floor vibrations are increasingly being reported in newly constructed buildings, including offices, shops, classrooms and multi-purpose blocks (Hanagan, 1994; Setareh and Hanson, 1992b; Varela and Battista, 2011). Substantial improvements in design and construction techniques have enabled engineers to design much more slender floor structures and whilst these perform acceptably with regards to strength requirements, this type of structure is more prone to excessive vibrations which can result in complaints from occupants. In addition to this, for offices there is a trend that open plan layouts are being chosen in preference to the traditional compartmentalised layouts whose partitions add significant amounts of damping to the structure (Nyawako and Reynolds, 2007b; Díaz and Reynolds, 2010a; Hudson and Reynolds, 2010).

There are a number of approaches available to reduce these vibrations, including structural modification, passive vibration control and active vibration control (AVC). Often, only structural modification is considered when a vibration problem occurs and the solution typically involves the addition of extra concrete mass to the floor or the use of additional props. However, this approach negates the benefits of having the more slender structural form in the first place, so alternative technologies are being sought. Moreover, the construction work required to make these modifications can be very inconvenient and expensive.

AVC improves the vibration response of a structure by applying a force in response to its movement. However, in contrast with passive vibration control, the generation of this force requires an external energy source (Symans and Constantinou, 1999; Nyawako, 2009). AVC can be thought of as the use of force delivery devices, integrated with real-time processing controllers and sensors at pre-selected locations within the structure being controlled (Soong and Spencer, 2002).

Recent research has shown that AVC has the potential to achieve very signifi-

cant reductions in the structural response and has a number of advantages over structural modification and passive technologies. This research has focussed on incorporating AVC technology into existing structures that have exhibited vibration serviceability issues after construction (Hanagan, 2005a). However, because such large response improvements can be achieved with AVC, there is the potential to take the application of this technology further and to consider incorporating AVC from the initial design stage of a building.

The rationale behind this is that as spans increase and damping reduces, the governing criterion for slenderness shifts from one of strength or deflection requirements to that of vibration serviceability, so structures require more construction materials than would otherwise be the case. Hence, by using AVC to improve the vibration performance of a structure, more slender structural forms would be possible which also could potentially realise significant savings in construction materials.

Improvements in material efficiency alone are not sufficient to keep up with the demand for new constructions/products; indeed the efficiency of production for many materials is already high, so reductions in the amount needed to make each item are required (Gutowski et al., 2013; Allwood, 2013). These are some of the conclusions presented in the recent issue of the *Philosophical Transactions of the Royal Society A* which is dedicated to material efficiency and demonstrates the need for further research in this area.

However, there are a number of issues that must be addressed before this option becomes a reality. Firstly, the design of a robust control system with good performance is a complicated task and requires specialist knowledge that is not in the domain of structural engineers. Further research is required to develop a simplified design procedure that is more readily accessible. Also, the inclusion of AVC into a structural system may well have significant changes in the optimal structural layout compared with the structure without control. The combined control

and structure design is not well researched for floors, so further research is needed to give insights into what approaches may be better. Furthermore, no research currently exists examining the potential economic or environmental implications of incorporating AVC into a structural design. Both the initial savings from material costs and the initial and on-going costs of AVC would have to be quantified before recommendations could be made regarding the efficacy of this technology on these grounds.

1.2 The Research Problem

The research presented in this thesis was undertaken with the aim of enabling the construction of longer span, more slender, floor structures through the use of AVC. In order to achieve this, there are five key areas of research that must be addressed.

1. Firstly, in order to simulate the effect that AVC has within an office environment, a novel walking loading model must be developed. This should simulate the in-service loading that occurs in a typical office, taking into account the stochastic and spatially varying nature of the forces.

2. Following from this, a comparison of AVC with the alternative passive technology of tuned mass dampers (TMDs) should be performed. This investigation will indicate the effectiveness of AVC relative to the current alternative technology.

3. Thirdly, research must be focussed towards investigating how many actuators would be required for a particular floor area. In doing so, this must address the question of how effective AVC is at reducing the response of the entire floor structure, rather than just at one or two locations, as has been the focus of previous research. This work should consider the effect that different structural designs have on the effectiveness of AVC, with the aim of arriving at recommendations for optimal structural layouts when the

structural system is designed in parallel with that of the control system.

4. In addition to these, the trade-off between performance and power demand of the AVC system should be researched. This will provide insights into how future AVC implementations could be made to be more efficient and hence reduce some of the ongoing costs of AVC.

5. Finally, the inclusion of AVC at the design stage to enable more slender structures will result in a reduction in construction materials compared with a design without AVC. Therefore, an initial life cycle analysis should be performed to quantify these reductions with respect to some of the expected increase in running costs throughout the building life. This should consider both the financial and environmental implications, with the issues raised by this giving direction for future work in this area.

1.3 Organisation of Thesis

This thesis is comprised of seven chapters. A brief introduction to the research problem is provided in Chapter 1 and key aims and objectives of the thesis are detailed. A comprehensive review of the available literature relevant to this research problem is provided in Chapter 2. This includes a review of AVC, both in general terms and specifically with regards to the active control of floor vibrations. Additionally, the current design guidance for the construction of floors that are acceptable in terms of their vibration performance are investigated, along with a review of some of the issues surrounding environmental and economic analyses of buildings. Chapter 3 introduces the majority of the mathematical models used in simulations throughout this and following chapters. The development of the walking load is first introduced in this chapter and this is then used to provide a comparison between AVC and TMDs for the control of floor vibrations, hence addressing the first two research objectives. Chapter 4 introduces finite element models of two typical floor structures and details the calibration and verification

of the walking model that was first described in Chapter 3. Simulations are performed which investigate the number of actuators required to achieve satisfactory levels of structural response throughout the entire floor area and the effect that the different structural designs have on the performance of AVC are investigated. This chapter therefore directly addresses the third research objective. Following from this, the trade-off between performance and power demand for a variety of control laws is investigated in Chapter 5. Specifically, the fourth research objective is addressed by investigating a typical controller with a reduced feedback gain, and comparing this with a model-based controller that targets only particular modes of vibration and a controller which utilises a switching-off rule. Chapter 6 addresses the fifth and final research objective which is the initial life cycle analysis of a floor design that incorporates AVC. Here, the economic and environmental implications of the possible material savings that could be achieved and the ongoing electricity costs that could be expected from typical in-service office loading are investigated. Finally, conclusions from the thesis work are provided in Chapter 7 and recommendations for further work are made.

Chapter 2

Literature Review

The contents of this chapter are an adapted form of a published paper in the journal Engineering Structures. Details of this paper are as follows:

> M J. Hudson and P. Reynolds. Implementation considerations for active vibration control in the design of floor structures. *Engineering Structures*, 44:334–358, November 2012. ISSN 01410296. doi: 10.1016/j.engstruct.2012.05.034.

2.1 Introduction

2.1.1 Problem Definition

In recent years, the problem of excessive human-induced floor vibrations causing annoyance and disturbance has been noted in a wide range of newly built structures, including offices, retail areas, gymnasia and dance studios and laboratories (Ebrahimpour and Seek, 2005; Brownjohn and Middleton, 2008; Pavic et al., 2008; Sandun De Silva and Thambiratnam, 2009; Middleton and Brownjohn, 2010; Reynolds and Pavić, 2011). Improvements in design methods and construction technology and the use of steel-deck composite floor slabs have enabled the construction of longer span floors with less inherent damping (Setareh et al., 2007; Feldmann et al., 2009; Saidi et al., 2011; Živanović and Pavić, 2009; Varela and Battista, 2011) which are more prone to excessive vibrations. In addition, a shift in the division of office space from compartmentalised to open plan has reduced the level of damping present (Hudson and Reynolds, 2010; Miskovic et al., 2009; Setareh et al., 2006; Setareh, 2010). It is important to note that these vibrations rarely affect the safety of the structure and hence are a serviceability problem (Bachmann, 1992).

Various strategies exist that aim to reduce the response of the structure to dynamic loads, typically falling into one of the categories of structural modification, passive control, active control, semi-active control or hybrid control (a combination of active and passive control). Frequently, only structural modification is considered when a floor has been noted to have a serviceability problem after construction. However, research in the fields of passive and active control has shown that these strategies should also be considered for vibration mitigation in floors as they hold a number of advantages over structural modification.

To date, this research has focussed on applying these strategies to fix a problematic floor after construction (Hanagan, 2005a). However, incorporating these strategies

into the design of new buildings has the potential to allow slenderness to be pushed further without adverse effects on the vibration serviceability of the structure.

Active vibration control (AVC) is a very promising technique and could potentially yield significant performance enhancements when incorporated into a structure from the design stage (Nyawako, 2009). However, there are still a number of research challenges that must be addressed before the implementation of AVC becomes a more standard practice, namely:

- the general complexity of designing a robust control system with good performance when applied to civil engineering structures;
- a lack of suitable hardware for industrial implementation, particularly actuators;
- a lack of design guidelines for how an engineer could incorporate such a system, and
- a lack of an assessment of the potential environmental and economic implications the inclusion might have.

These items must be considered in future research if the potential benefits of using vibration mitigation systems are to be realised.

The predominant goal of this review is to work towards answering the question "is it practical and environmentally / financially beneficial to include AVC in the design of a new building?". To this end, this review begins with an overview of current vibration mitigation systems to provide the context of AVC. Following from this, in Section 2.2 the current guidance documents used to design floors are examined in an attempt to see how vibration controllers could be incorporated. The practical issues relating to the implementation of active control are examined in Section 2.3 so that the key aspects can be identified. In Section 2.4, current research for the environmental assessment of buildings and the potential application

of economic assessment tools are reviewed. This highlights some of the issues associated with performing such an evaluation, with particular interest towards an assessment including an AVC system. Finally, in Section 2.5 some concluding remarks are given.

2.1.2 Vibration Mitigation Systems for Floors

A review of the range of techniques that could be used to mitigate the effect of human-induced vibrations is provided below. This introduces the key topics of structural modification, passive, active, semi-active and hybrid control and briefly discusses their advantages and disadvantages.

Structural Modification

The traditional methods for improving the dynamic performance of a floor often involve major additions to the original structure. For example, the addition of non-structural full-height partitions has been shown to add support and increase the damping of a floor by up to 14% (Miskovic et al., 2009; Hanagan, 1994). Testing of two nominally identical floors, differing only by nonstructural elements, has also shown that both floor frequencies and the global or local nature of the mode shapes are greatly affected by these nonstructural elements (Miskovic et al., 2009). However, there is the possibility that annoying vibrations can be transmitted to other locations within the building after installation, which in this case might extend the problem to other locations within the building (Hanagan, 1994).

Alternatively, the framing members can be stiffened. This is most effectively achieved by installing extra columns to interrupt the most flexible members (Smith et al., 2007). The extra stiffness reduces the amplitude of vibration and also increases the frequencies of vibration of the floor. If the excitation frequency is known then it is possible to shift the floor frequencies such that resonance with the excitation source is avoided or reduced (Setareh and Hanson, 1992a).

Another commonly considered option is the addition of a concrete layer to the existing floor. This additional material acts to increase the damping and reduce both the frequency and amplitude of vibration (Hanagan, 1994). This can actually cause an increase in the perceived response if the natural frequencies are lowered to within a range excitable by human-induced forces (Smith et al., 2007) and the existing structure must be able to (or be made able to) support this additional weight. This modification is extremely disruptive if the building is occupied.

Passive Control

Types of passive vibration control (PVC) that have been used to reduce the response of floor structures to human-induced vibrations include tuned mass dampers (TMDs), viscous dampers, and viscoelastic layers. A thorough, state-of-the-art review of these is provided by Nyawako and Reynolds (2007a). PVC improves the vibration response of a structure by increasing its damping (i.e. energy dissipation) and/or stiffness (i.e. energy storage) through the application of forces generated in response to the movement of the structure, as shown in Figure 2.1 and Equation 2.1 (Soong and Spencer, 2002; Housner et al., 1996; 1997).

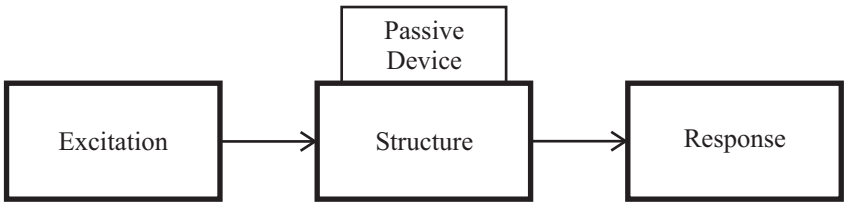

Figure 2.1: Passive Control, after Spencer and Soong (1999)

$$[M]\{\ddot{Y}(t)\} + ([C] + [\Delta C])\{\dot{Y}(t)\} + ([K] + [\Delta K])\{Y(t)\} = \{F(t)\} \quad (2.1)$$

where M, C and K are the primary structure's mass, damping and stiffness matrices respectively, $Y(t)$, $\dot{Y}(t)$ and $\ddot{Y}(t)$ are the structural displacement, velocity and accelerations respectively, $F(t)$ is the applied disturbance force and ΔC and ΔK are the respective additional damping and stiffness contributions from the PVC.

No external power source is used, which means that no energy can be added to the structural system for the purposes of control (Housner et al., 1996). The dynamic characteristics of the PVC remain relatively unchanged over time so suffer an inability to adapt to changes in the external loading conditions. Also, because they are generally tuned to deal with a specific frequency, as is the case for TMDs, if the structural parameters or excitation frequency vary over time then "de-tuning" can occur, which reduces their effectiveness (Jalili, 2002). Further to this, the reduction in response at one frequency may actually cause a greater response at other frequencies so care must be taken in the case of human-induced vibrations because excitation can occur over a range of frequencies. The performance of some TMDs has been observed to diminish once the amplitude of vibration reduces below a certain threshold (Eyre and Cullington, 1985). For example, the reductions in response amplitude observed by Casado et al. (2010) for running (high excitation levels) to walking (low excitation levels) on a lively footbridge reduce from 86% to 36%. Unfortunately even very low amplitude vibrations can still be found to be annoying. This means that this type of PVC may be of limited use when mitigating the effects of human-induced vibrations. Despite this, several implementations of passive tuned devices have been recorded. For example, the pendulum tuned mass damper (PTMD) used by Setareh et al. (2006) achieved reductions of 50% and 70% in the two permanent office floor installations considered.

Viscoelastic layers can be used to increase the level of damping in a structure without significant increase in mass or depth: one example of such being the Resotec system (Willford et al., 2006) for composite floors. However, it should be noted that the Resotec system requires the exclusion of shear studs along a portion of the steel beam's length - thereby reducing its stiffness (Willford et al., 2006).

Active Control

Active control is a natural development from passive control methods which have been used extensively due to their simplicity and reliability (Nyawako and Reynolds, 2007a). The concept of AVC was first introduced in the 1950s but a lack of the necessary technology delayed development (Housner et al., 1996). Similar to PVC, AVC improves the vibration response of a structure by applying a force in response to its motion. However in contrast with PVC, the force is generated with assistance from an external energy source (Symans and Constantinou, 1999; Nyawako and Reynolds, 2007a).

AVC can be thought of as force delivery devices, integrated with real-time processing controllers and sensors at pre-selected locations within the structure being controlled (Soong and Spencer, 2002). The sensors detect the motion of the structure and/or the external excitation. The signals from these sensors are then processed by controllers that use a particular algorithm to generate a desirable output command signal which is then used to drive the force delivery device (Spencer and Soong, 1999; Housner et al., 1997), as shown in Figure 2.2 and Equation 2.2.

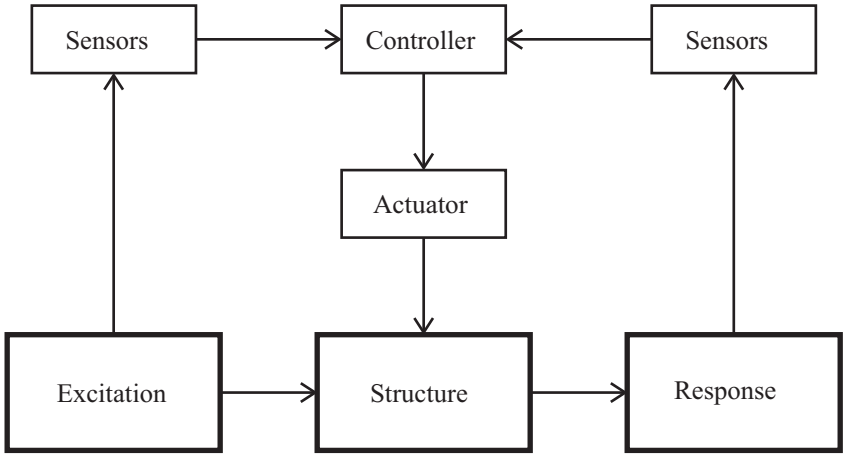

Figure 2.2: Active Control, after Spencer and Soong (1999)

$$[M]\{\ddot{Y}(t)\} + [C]\{\dot{Y}(t)\} + [K]\{Y(t)\} = \{F(t)\} + \{U(t)\} \tag{2.2}$$

where $U(t) = f(Y(t), \dot{Y}(t), \ddot{Y}(t), F(t))$ is the control force applied by AVC. For example, one common control law that features a velocity feedback scheme can be represented by Equation 2.3:

$$U(t) = f(\dot{Y}(t)) = -K_G \dot{Y}(t) \tag{2.3}$$

where K_G is a constant gain. This real-time response gives AVC enhanced effectiveness in response control and applicability to multi-hazard vibration mitigation systems (Soong and Spencer, 2002; Spencer and Soong, 1999). However, because additional energy is being brought into the system, it is possible to introduce instability in a previously inherently stable system (Jalili, 2002).

An advancement to this approach features the so-called hybrid mass dampers (HMDs) which combine both active and passive control systems. Since a portion of the control objective is met by the PVC, the energy demand from the AVC is reduced (Spencer and Soong, 1999). Active mass dampers (AMDs) are the most suitable devices for attenuating vibrations in floor structures because they generate the control force through an inertial mass. This means that the control force can be produced without a fixed reaction surface, which is unavailable around floor structures. However, other types of AVC do exist - often for applications such as full structure control due to seismic or wind loading. These include active tendon-control and active constrained layer damping (Nyawako and Reynolds, 2007a). More recently, an active momentum exchange impact damper has been suggested as a means to reduce shock vibration of floors (Son et al., 2008; 2010). However, it is not clear how effective such a method would be at dealing with the spatial variability associated with human-walking impacts. A more thorough analysis of the benefits and problems of using AVC is provided in Sections 2.3.1 and 2.3.2.

Semi-Active Control

Also known as adaptive-passive or controllable passive (Housner et al., 1997; Jalili, 2002), semi-active vibration control (SAVC) devices are similar to PVCs, both in the mechanism by which the corrective force is introduced and in that no mechanical energy is added to the system. However, some dynamic characteristics of the device can be altered in real-time, as shown in Equation 2.4 (Jalili, 2002). A schematic for how SAVC devices work is shown in Figure 2.3.

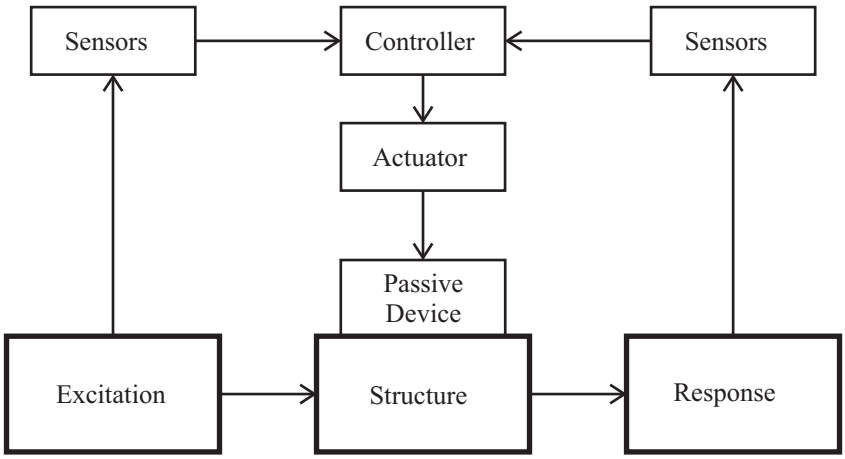

Figure 2.3: Semi-Active Control, after Spencer and Soong (1999)

$$[M]\{\ddot{Y}(t)\} + ([C] + [\Delta C(t)])\{\dot{Y}(t)\} + ([K] + [\Delta K(t)])\{Y(t)\} = \{F(t)\} \tag{2.4}$$

where $\Delta C(t)$ and $\Delta K(t)$ are the respective time varying additional damping and stiffness due to the semi-active controller.

This feature enhances the vibration mitigation performance of these devices over their passive counterparts, whilst still having some functionality during power-failure. The energy requirements are typically orders of magnitude less than that required for AVC (Housner et al., 1997) and because no mechanical energy is added to the system the devices are guaranteed to have a bounded output. Types of SAVC currently investigated include electrorheological and magnetorheological dampers, adjustable tuned liquid dampers, semi-active TMDs and semi-active

constrained layer damping (Nyawako and Reynolds, 2007a). This technology has great potential for the mitigation of vibration in floors, but more research is required before the technology is at a stage for implementation in floor structures.

2.2 Design Methodologies

Often, the response of a structure is not actually predicted - rather, the lowest natural frequency of its primary and secondary beams are checked to be greater than 4Hz (Smith et al., 2007). This is often performed by combining the equation for free elastic vibration of a uniform beam and the equation for the deflection due to a uniformly distributed load. In both the simply supported and fixed ended cases this yields the same formulation, shown in Equation 2.5.

$$f_{n1} \approx \frac{18}{\sqrt{\delta}} \tag{2.5}$$

where δ is the deflection of the beam due to permanent loading (in mm). The fundamental natural frequency of the floor as a combined system of the primary and secondary beams and the slab is then found through the use of Dunkerley's Method (Smith et al., 2007).

If this condition is met then the structure was deemed to be satisfactory. However, this approach merely reduces the likelihood of the first harmonic of walking causing resonant excitation (Smith et al., 2007). Indeed, there is now evidence that this method is unreliable and can result in uneconomical designs (Pavić and Willford, 2005). This has led to an increased need to predict what the actual structural response will be in order to determine if adverse comments will arise due to human-induced floor vibrations and/or verify that the floor is not being over-designed.

2.2.1 Walking Excitation

An appreciation of the nature of the force induced by walking is essential in order to predict the structural response from pedestrians. A typical walking force time history is shown in Figure 2.4a and the frequency spectrum of the ground reaction forces for this walking history are shown in Figure 2.4b (Racic, 2009).

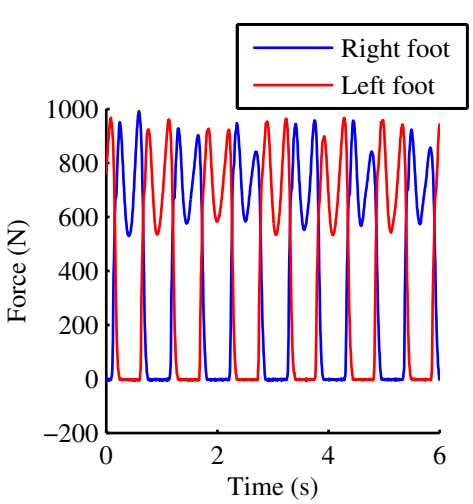

(a) Force Time History

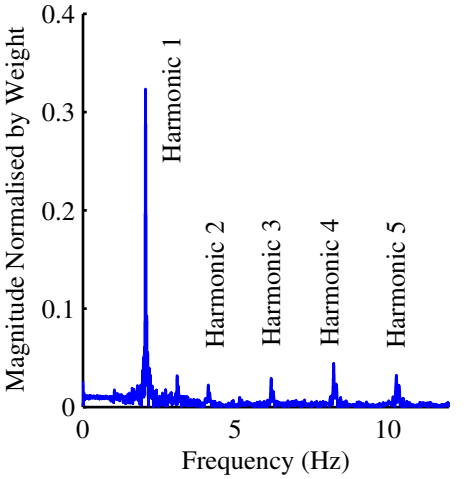

(b) Spectral Analysis (ignoring 0Hz magnitude for clarity)

Figure 2.4: Measured Walking Properties (Walking at 1.5 m/s)

Walking pacing rates have been measured to vary between 1.4Hz and 2.5Hz with velocities varying between 0.9m/s and 1.8m/s (Pachi and Ji, 2005), although typical pacing rates tend to lie in a narrower band. For example, the SCI guidance (Smith et al., 2007) recommends considering pacing frequencies between 1.8Hz and 2.2Hz. Frequencies for other activities can vary greatly, for example for climbing/descending stairs frequencies can range from 1.2Hz to 4.5Hz (Smith et al., 2007; Davis and Murray, 2009). The walking pace in Figure 2.4 is about 2.05Hz and the multiple harmonics of the walking force at integer multiplies of 2.05Hz are clearly observed. It is important to note that some of these harmonics have both a significant magnitude and a frequency that potentially could excite structural modes of vibration greater than 4Hz, which indicates that structural response prediction may be preferable over frequency limitation as a design method.

It is possible to use real walking force time histories in the design process. However, these are usually not available or are too complicated for design engineers to work with so simplified models have been developed as an alternative. One popular method is the decomposition to a Fourier series (Smith et al., 2007; Willford and Young, 2006; Pavić and Willford, 2005) as shown in Equation 2.6 (Živanović

et al., 2005) . Typical Fourier coefficients, α_h, and phase angles, ϕ_h, are given in Table 2.1.

$$F(t) = G + \sum_{h=1}^{n} G \cdot \alpha_h \cdot sin(2\pi h f_p t - \phi_h) \tag{2.6}$$

where $F(t)$ is the modelled periodic force, G is the static self weight of the person (commonly taken as 700N), f_p is the walking pace, h is the harmonic number and t is the time.

Harmonic Number	Frequency Range for f_p	Fourier Coefficient	Phase Angle
1	1.8-2.2	0.436(f_p-0.95)	0
2	3.6-4.4	0.006(f_p+12.3)	-π/2
3	5.4-6.6	0.007(f_p+5.2)	π
4	7.2-8.8	0.007(f_p+2.0)	π/2

Table 2.1: Fourier Coefficients for Design Walking Paces from Smith et al. (2007)

The coefficients shown in Table 2.1, from the SCI guidelines (Smith et al., 2007), appear to be based on the work by Young (2001) which are chosen from a probabilistic view due to the intra- and inter- variability of human walking such that the chance of exceedence is 25% (Willford and Young, 2006). Contrary to the phase angles provided here, Živanović et al. (2007) found no interdependence between the harmonic frequency and the phase angle: here it was found that the phases were uniformly distributed in the interval $[-\pi, +\pi]$.

Various models exist to model each individual footfall, such as: the 'kf' method (Ungar and White, 1979), Arup's effective impulse (Young, 2001) and the impulse used in the SCI guidelines (Smith et al., 2007) which is based on Arup's effective impulse. Arup's effective impulse (design value), I_{eff}, is given by:

$$I_{eff} = 54 \frac{f_p^{1.43}}{f_{n1}^{1.36}} \tag{2.7}$$

where f_p is the walking pace rate and f_{n1} is the lowest natural frequency of the

floor. This impulse was designed to contain sufficient energy to excite the higher frequency structural modes that provide the transient response to each footfall (Živanović and Pavić, 2009). This is in contrast with the previously described walking models that contain energy only at lower frequencies and are designed to simulate excitation achieving resonance with low frequency structural modes.

2.2.2 The Floor as a Dynamic System

An early floor vibration design guide by Wyatt (1989) considered the loss of energy for the higher harmonics of walking and concluded that the resonant behaviour of floors was not "an appropriate model where the natural frequency exceeds that of the third Fourier harmonic of the walking pace". Here, it was found that the response from each footfall dissipates before the next occurs, so the floor acts impulsively to each footfall (Middleton and Brownjohn, 2010). This difference leads to the division of floors into 'low frequency floors' and 'high frequency floors', a notion popular with some modern design guides (Pavić and Willford, 2005; Smith et al., 2007; Willford and Young, 2006; Murray et al., 1997). However, recently there have emerged examples of floors with significant responses in both the low and high frequency regions (Živanović and Pavić, 2009). This raises doubts about the suitability of a cut-off frequency to indicate how a floor will respond to walking excitation.

Another key parameter that determines the structural response is the level of damping present, however it is much more difficult to predict the levels of damping a priori than to predict the stiffness or mass of the structure. One of the reasons for this is that the mechanisms by which damping could be provided by a civil structure are not evident (Middleton and Brownjohn, 2010). Wyatt (1977) suggested that the damping is primarily frictional in nature, but that the summation of the contributions from the many different mechanisms that provide this results in damping that appears as viscous. Damping in structures has also been observed as increasing with amplitude (Jeary, 1986). For mathematical simplicity, damping is

generally modelled using a viscous damping formulation. Typical assumed damping values are shown in Table 2.2. The damping values provided by the Canadian guidance appear to be unrealistically high when compared with other guidance, which could lead to under-estimates of the response of a floor. Pavic et al. (2001) note that inadequate experimental damping estimation techniques have been used in the past - the techniques previously employed have typically utilised the half-power method or the amplitude decay method which, when applied to structures having closely spaced modes around the fundamental mode, can lead to overestimates of the damping value of the fundamental mode. This could account for the large differences observed in the 'typical' damping values.

Design Guide	**Bare floors**	**Floor with non-structural elements**	**Floor with many full-height partitions**
SCI P354 (Smith et al., 2007)	1.1	3.0	4.5
AISC (Murray et al., 1997)	2.0	3.0	5.0
Canadian (CSA, 1989)	3.0	6.0	12.0
Concrete Centre (Willford and Young, 2006)	0.8 - 2.0	2.0 - 3.5	3.0 - 4.5

Table 2.2: Typical Damping Values (% of critical damping)

These damping values highlight that, for typical structures, it is generally accepted that full-height partitions add to the level of damping in the structure. There is less consensus regarding the effects of non-structural elements such as raised flooring and suspended ceilings: Williams and Falati (1999) found that raised flooring on a post-tensioned model floor slab yielded no increase in damping or stiffness when rigidly attached, but increased the critical damping ratio for the fundamental mode from 1.1% to 1.8% when the panels edges were not rigidly connected to the floor slab. To the contrary, Reynolds and Pavić (2003) found that for one of the

structures tested the false flooring could contribute additional damping whether loosely laid or mechanically fixed, whilst for another structure tested with similar false flooring, the flooring that was mechanically fixed provided more significant increases in damping. It is important to note the conclusions of the authors (Reynolds and Pavić, 2003), that there existed "no discernible pattern regarding which modes would be affected and which would not".

One method for acquiring estimates of damping is through curve fitting of experimentally acquired data (Middleton and Brownjohn, 2010), though this is clearly only possible on existing structures and, in addition, the levels of excitation used during the measurement may not represent the actual day-to-day excitation levels.

The most comprehensive approach for the calculation of the structural response is through the use of a finite element (FE) model, then performing a modal analysis or direct integration methods. However, the creation of the FE model here follows a different procedure to that used for ultimate limit state (ULS) design, namely (Pavić and Willford, 2005; Smith et al., 2007; Willford and Young, 2006):

- generally only the floor in question and the columns above and below should be modelled
- the dynamic Young's modulus for concrete should be used
- connections should be modelled as continuous even if they are designed to be simply supported at ULS due to the relatively low levels of movement expected
- the imposed load should be taken to be 10% of the ULS imposed load to represent quasi-permanent loading
- non-structural partitions may be included in the model as these may cause modes to become more localised.

Several authors have examined FE models of floor structures and investigated how

closely the derived modal properties match with experimentally determined values. It is often the case that an FE model will require updating in some form, to match better with experimental results. For example, a relatively early investigation by Pavic et al. (2001) investigating post-tensioned concrete floors initially underestimated the natural frequency of the first six modes by between 19% and 23%. However upon updating, which included explicitly modelling the columns instead of using pin-supports as is now recommended to begin with (Pavić and Willford, 2005; Smith et al., 2007; Willford and Young, 2006), achieved frequencies correct to two significant figures for four of the six modes considered, whilst the other two differed by 2% and 4%. In addition to this, the mode shapes for the first three modes correlated very well. Similarly, an investigation into long-span flat concrete floors by El-Dardiry et al. (2002) matched frequencies to within 3% of experimental. However, no mode shapes were recorded because the experimental frequencies were determined by post-processing the recorded structural acceleration resulting from a heel-drop in the centre of each bay. The results from the FE analysis with various boundary conditions indicate that although the natural frequencies change, for this family of structures the mode shapes remained quite constant.

The Young's modulus of concrete that should be used in the FE model is a relatively uncertain parameter. Cracking in the concrete can require a reduction in this value. For example, Reynolds et al. (2002) achieved a strong correlation of both mode shapes and natural frequencies for the first seven modes of a steel/concrete composite floor following model updating which included reducing the Young's modulus of concrete from 38GPa to 32.6GPa. The reason cited for this was that the precast planks used were possibly suffering a loss of stiffness through shrinkage cracking. Similarly, Pavic et al. (2007) found that their initial FE model of an open-plan composite steel-concrete floor estimated natural frequencies with an error of 10-15% relative to measured frequencies. Cracking of the lightweight concrete was noted as being one possible cause of the discrepancy. However, it

has also been reported where a higher Young's modulus must be used: for example Reynolds and Pavić (2003) found that a value of 40GPa or slightly more was appropriate for the post-tensioned concrete floor examined.

The effect of cracking in a multi-panel steel/concrete composite floor was examined by Zheng et al. (2010). It was found that the continuity between panels was significantly reduced by the minor cracks present and this required modelling through the use of rotation spring connections. Importantly, the stiffness at the tested location was found to be significantly overestimated by assuming continuity in the FE model, even though the natural frequencies approximately matched the measured frequencies.

Miskovic et al. (2009) explored the contribution that non-structural partitions have on finite element modal analysis results. The steel/concrete composite structure considered had frequencies that differed by -11% to -25% before model updating. However after updating, which included explicit modelling of the full-height glass and full-height double boarded plasterboard partitions, much closer frequencies and mode shapes were obtained.

All these results demonstrate that finite element models created with the best information available to a design engineer will still generate modal results that have a degree of uncertainty attached to them. This is due in part to the uncertainties involved with the construction itself. It should also be noted that there are still only recommendations for approximate modal damping values, and certainly no methods that can predict what the damping ratio for each individual mode of vibration will be. The ability to generate accurate models of floor structures without the need for model updating is an area where more research is of great importance.

There have been several attempts to simplify the design procedure without the need for a full FE model because of this complexity (Smith et al., 2007; Willford and Young, 2006; CSA, 1989; Murray et al., 1997; Feldmann and Heinemeyer, 2007). The accuracy of these methods is naturally inferior to methods focussed

on a full FE model and as such are of limited use for the design of AVC systems. Whilst an approximate improvement could be derived when a simple feedback controller is used (see Section 2.3.4), the same would not be possible for a more complex controller (see Section 2.3.4) that has the potential for greater improvements to the dynamic response of the structure. Even the full FE method is just an approximation based on a model, so when it comes to designing the final characteristics of a vibration mitigation device it is usually best to use experimentally determined data, as will be discussed in Section 2.3.3.

2.2.3 Human Response to Vibrations

The human perception of vibrations depends on a number of factors that can be broadly divided between direct and indirect effects (ISO, 2007). The magnitude and frequency of vibration and the orientation of the body are examples of direct effects, whilst indirect effects include visual cues, audible noise and population type. Research has quantified the effects of frequency and orientation of the body, resulting in weighting functions that can be applied to the response. BS6841 (BSI, 1987), ISO2631 (ISO, 1989) and BS6472 (BSI, 2008) provide details for frequency and orientation weighting factors that can be applied which are all based on the basicentric coordinate system shown in Figure 2.6. These have been incorporated by the various floor-vibration design guidelines in the UK (Smith et al., 2007; Pavić and Willford, 2005; Willford and Young, 2006), although there exist differences between the standards as to which frequency weighting should be applied for particular situations. For example, the SCI guidance (Smith et al., 2007) recommends the use of W_g for vertical vibrations in "critical" working areas, W_b for vertical vibrations in "non-critical" working areas, and W_d for horizontal vibrations, as shown in Figure 2.5. This differs to the other guidance (Pavić and Willford, 2005; Willford and Young, 2006) which follows the recommendations in BS6472 (BSI, 2008) and uses W_b and W_d only.

Often acceleration is used to quantify vibration response because readily available

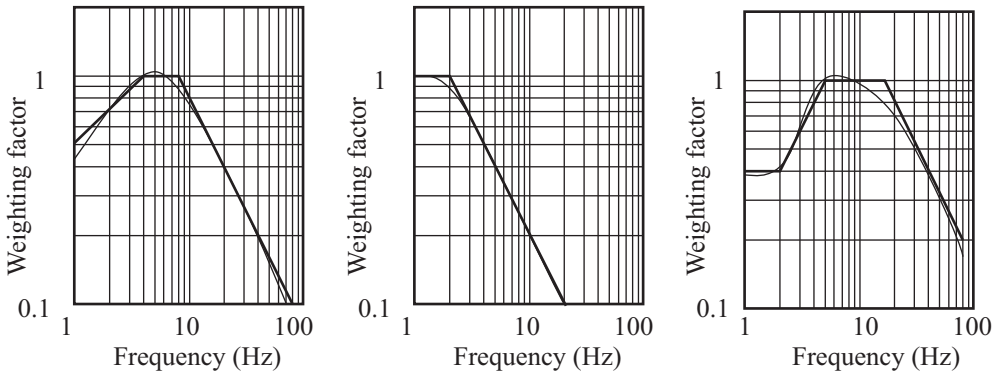

(a) W_g weighting for z-axis in critical working areas (b) W_d weighting for x- and y-axes (c) W_b weighting for z-axis in non-critical working areas

Figure 2.5: Frequency Weighting Curves, and their Simplifications, for Different Orientations, after Smith et al. (2007)

instrumentation for measuring vibrations typically measures acceleration. However, velocity is also used - in particular when sensitive equipment is under consideration (Gordon, 1991).

An acceleration time history is often characterised by a single number for ease of comparisons; often the peak value or the running root mean square (RMS) value are used. The running RMS value over a time period, T (usually 1s or 10s) is given in Equation 2.8.

$$a_{RMS} = \sqrt{\frac{1}{T}\int_0^T a(t)^2\,\mathrm{d}t} \qquad (m/s^2) \tag{2.8}$$

It should be noted that when assessing the vibration response from individual footfalls (as is commonly performed for high frequency floors) the relatively long periods used in the calculation of the running RMS neglect the effect of additional footfalls that would occur within that period. For this reason, it has been proposed (Živanović and Pavić, 2009) that a period of $1/f_p$ (where f_p is the pacing frequency) be used for this situation.

The most common form of limit placed upon acceleration values is the Response factor (or R factor). This is a multiple of the RMS level of continuous vibration

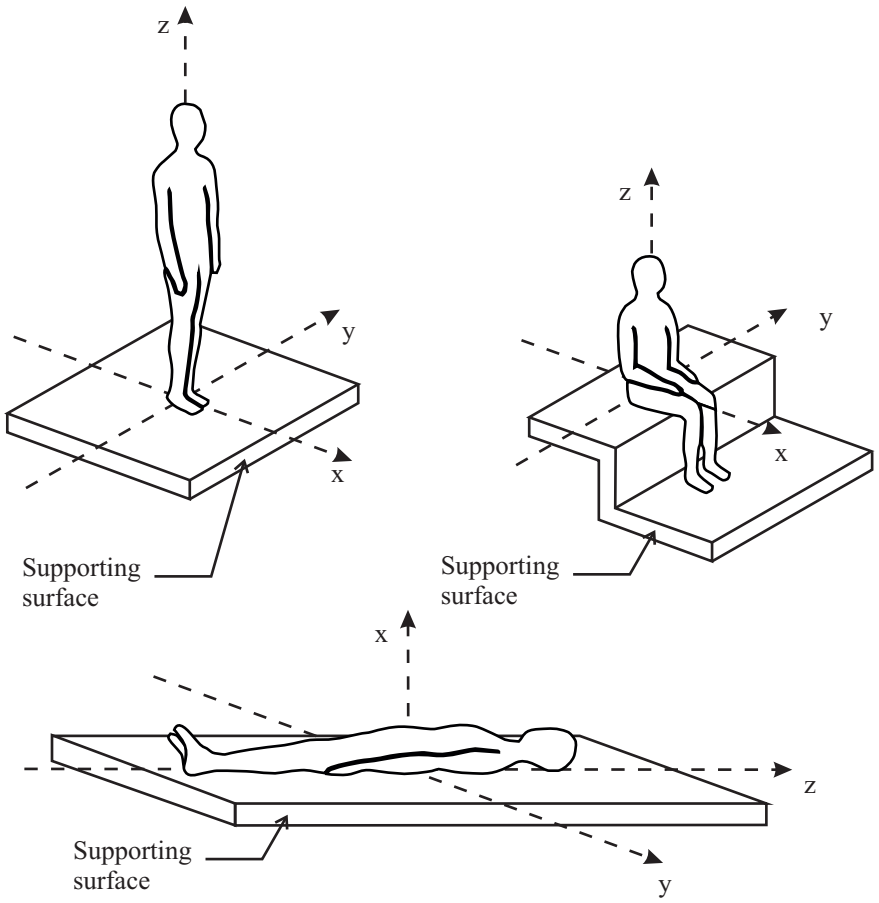

Figure 2.6: Directions for Vibration, after Smith et al. (2007)

that is at the average threshold of human perception (Willford and Young, 2006), as defined by Equation 2.9.

$$R = \max_{t} \left(\left(\int_{t-T/2}^{t+T/2} {a_w}^2(t)dt \right)^{0.5} \right) \times \frac{1}{0.005} \tag{2.9}$$

where:

T is the period used for the running RMS, s

$a_w(t)$ is the frequency weighted acceleration response of the structure in the time domain, m/s^2

The maximum value for a given time history gives the R factor for that vibration

response which can then be compared with recommended limits for the particular environment under consideration. Typical values for these are shown in Table 2.3.

Place	Time	Multiplying factor
Critical working areas	Day	1
	Night	1
Residential	Day	2 to 4
	Night	1.4
Quiet office, open plan	Day	2
	Night	2
General office	Day	4
	Night	4
Workshops	Day	8
	Night	8

Table 2.3: R limits for several locations, after ISO (2007)

The nature of walking excitation is intermittent in nature rather than continuous which potentially limits the usefulness of the R factor. However, the limits on the response implicitly consider this difference to some extent because they are based on feedback from users. Furthermore, BS6841 (BSI, 1987) restricts the use of the R factor to when the crest factor (the ratio of peak response to mean response) is less than 6. The vibration dose value (VDV) is another measured used to characterise the response and this explicitly considers the intermittent nature of the excitation, as seen in Equation 2.10 (BSI, 1992)

$$VDV = \left(\int_0^{T_t} a(t)^4 \, \mathrm{d}t \right)^{1/4} \qquad (m/s^{1.75}) \tag{2.10}$$

where T_t is the total time period.

The fourth power of the acceleration is used in this integration, placing greater emphasis on the magnitude of the response rather than the duration. The rather unusual units of m/s$^{1.75}$ for the VDV mean that this measure has no physical meaning, despite which Griffin (1998) asserts that since its inclusion in BSI 6841 (BSI,

1987) it has been used to evaluate a "very large number of widely differing exposures with reasonable conclusions". The VDV is referred to in several of the modern vibration guidelines (Smith et al., 2007; Willford and Young, 2006; Pavić and Willford, 2005). The limits placed on VDV values for offices are shown in Table 2.4, scaling factors can then be applied to these to account for different environments (e.g. residential, workshops). However, recent research on a problematic floor by Reynolds and Pavić (2011) has shown that these limits could result in floors that meet the VDV limits but are considered to have unacceptable vibration levels in reality.

Time	**Low Probability of Adverse Comments**	**Adverse Comments Possible**	**Adverse Comments Probable**
16h day	0.4-0.8	0.8-1.6	1.6-3.2
8h night	0.1-0.2	0.2-0.4	0.4-0.8

Table 2.4: VDV limits for offices, after BSI (2008)

The SCI guidelines (Smith et al., 2007) have used the work by Ellis (2001) in an attempt to make the VDV more accessible to engineers in practice, and so have recommended limits placed on the number of times an activity can occur, based on the frequency weighted RMS acceleration, $a_{w,rms}$, as seen in Equation 2.11.

$$n_a = \frac{1}{T_a}\left[\frac{VDV}{0.68 \times a_{w,rms}}\right] \tag{2.11}$$

where n_a is the number of times the activity will occur and T_a is the duration of the activity (e.g. time to walk along a corridor).

2.2.4 The Inclusion of Vibration Mitigation Measures

When considering incorporating vibration mitigation measures into a structure, a more detailed knowledge of the vibration characteristics of the structure is required compared with when only knowledge of the expected human response is

needed. Here, the specific dynamics that cause the high response must be identified - that is the modal mass, frequency, damping and shape of all relevant modes must be identified, particularly noting if the cause of the high response is a single mode or multiple modes (Johnson, 1995). For a preliminary design these parameters can be approximated through an FE model. However, for a final optimisation experimental data for the as-built structure may be required; previous investigations have shown that nominally identical structural floor systems can have very different dynamic properties once constructed (Živanović and Pavić, 2009; Miskovic et al., 2009).

Passive Devices

The relative simplicity of passive devices means that closed form solutions can often be formulated and/or tabulated to assist with the preliminary design. For example, for TMDs there are three key design parameters - in order of increasing importance these are the natural frequency, mass and damping of the TMD (Maurer Söhne, 2004). Optimisation formulae for the frequency and damping of the TMD for a structural system with no damping subject to harmonic excitation have been derived (Den Hartog, 1947). The optimal TMD frequency and damping (f_{opt} and ζ_{opt} respectively) are shown in Equations 2.12-2.13.

$$f_{opt} = f_{pri} \cdot \left(\frac{1}{1+\mu} \right) \tag{2.12}$$

$$\zeta_{opt} = \sqrt{\frac{3\mu}{8(1+\mu)}} \tag{2.13}$$

where f_{pri} is the frequency of the primary structure's mode to be controlled and μ is the mass ratio of the TMD relative to the primary structure.

These formulae have been extended to account for damped systems, systems subject to white noise and base excited systems (Fujino and Abé, 1993; Bakre and Jangid, 2007; Tsai and Lin, 1994; Warburton, 1982). However, this sort of vibration controller is not typically considered at the design stage of a floor; only once

a problematic floor has been identified.

One system for mitigation of human-induced vibrations that has been considered during the floor design is constrained layer damping (CLD). The ability of the visco-elastic material to increase damping in the primary structure is improved if the material is located close to the neutral axis and towards the supports; this subjects the material to the maximum shear strain (Willford et al., 2006). Design formulae for a variety of boundary conditions have been derived; some of these are summarised by Torvik (1980) where it is shown that the key design parameters for the increase in damping of the combined system are the shear modulus, length and thickness of the constrained layer. It is also important to note that the effective length of a vibrating beam is determined by the wavelength and hence the frequency of vibration. This means that the effectiveness of the constrained layer will differ for different modes of vibration (Torvik, 1980) . Some commercial constrained layer damping products have had their material properties incorporated directly into specific FE packages which can significantly assist the designer in the fine tuning stage. Potential increases in the modal damping due to the addition of Resotec, an example of a CLD system, are shown in Figure 2.7. It is important to note that there are more significant implications for the static design of beams that have the Resotec layer applied over 50% or more of the beam's length, which reduces the improvements in damping that can be achieved in practice (Willford et al., 2006).

Active Devices

With specific regards to AVC, as yet no procedure exists for structural engineers to design AVC into buildings for the mitigation of human-induced vibrations, predominantly due to the complexity of the non-autonomous system precluding both its inclusion into FE packages and the formulation of closed form solutions. Work by Hanagan et al. (2000) has gone some way towards achieving this goal. Here, an algorithm for determining optimal locations for actuators and sensors using

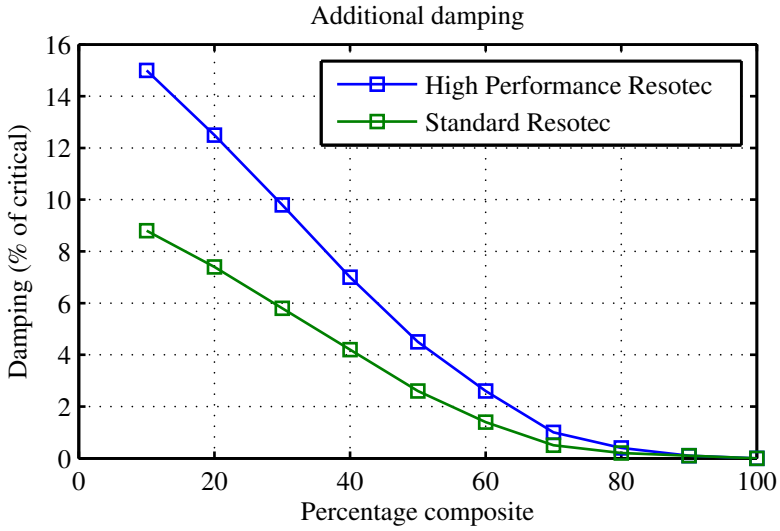

Figure 2.7: Typical increases in modal damping due to addition of CLD, after Willford et al. (2006)

data from an FE model was developed. This involved minimising a performance index based on the states of the structural model along with an exponential time-weighting function to ensure rapid disturbance rejection. However, it could be argued that the approach developed here is beyond the scope of most design engineers unless this were incorporated into specialist civil engineering design software. This work is based on the direct velocity feedback (DVF) controller which has been shown to be effective in a number of situations. However, there exist more robust and higher performing controllers suitable for mitigating floor vibrations so this work could be extended to utilise these. In addition, there are no indications as to how many actuators and sensors would be required to achieve a particular level of response reduction for a given size of floor: such response prediction is generally not available to civil engineers. It is possible that, for controllers based on the feedback of velocity states (such as DVF) the impact of AVC could be characterised by a pure increase in the level of damping for a structure. This would need to be linked to a typical zone of influence/effectiveness in order to determine parameters such as size and number of actuators suitable for a

preliminary design.

2.3 Active Control of Floors

2.3.1 Potential Benefits

There are numerous benefits that active control can provide over alternatives such as passive control. Compared with TMDs, much smaller masses can be used to add significant damping to a primary structure. Thus, AVC can be employed in situations with severe space limitations or when the strength of the structure acts as a limiting factor to implementing passive schemes (Preumont, 2002; Soong and Spencer, 2002; Hanagan, 1994). AVC also features the ability to target more than one mode of vibration simultaneously and can control much lower levels of vibration (Eyre and Cullington, 1985).

With AVC, variations in the response of the structure can be taken into account by the control system, such that more effective control can be enforced (Nyawako and Reynolds, 2007a). This variability can also be used to permit a degree of selectivity of control objectives, such as optimising human comfort at non-critical times and optimising structural integrity during severe dynamic loading. In addition, AVC tends to be relatively insensitive to the conditions of the site, or to ground motion, and can be applied in situations with multiple hazards (e.g. both seismic and wind excitation) (Soong and Spencer, 2002; Spencer and Soong, 1999).

2.3.2 Potential Problems

AVC is certainly not without its problems. The active control of vibrations is a relatively new area of research in the civil engineering community and as such there are a number of obstacles that must be overcome before the field can mature fully. As Soong and Spencer (2002) discuss, many of the challenges stem from the fact that this field is an integration of a number of diverse disciplines which

are not necessarily within the domain of traditional civil engineering, for example data processing and control theory.

There are also several difficulties faced when attempting to implement AVC in a civil engineering environment.

- First of all, the control system has added complexity due to: the magnitude of control forces which can operate over a very large scale; the non-linear behaviour of the system (e.g. stroke saturation on an actuator) and the uncertainties in the loading environments (Nyawako and Reynolds, 2007a; Soong and Spencer, 2002).
- Secondly, physically implementing the system has its own challenges: there is a limit on the number of sensors and actuators available for use; the actuators are typically large (though still much smaller than the masses used in a TMD), can have heavy power requirements and have complex dynamics (Soong and Spencer, 2002).
- On top of this, systems generally have a fail-safe requirement in a civil engineering application, although this is not as serious a problem in controlling floor vibrations as it is when controlling full structural seismic- or wind-induced motion, with the exception of highly sensitive equipment that could be damaged by excessive floor vibrations.
- Active control typically has higher operating and maintenance costs than passive control (Nyawako and Reynolds, 2007a).

2.3.3 Structural Modelling

For an effective control law to be designed it is important to create a model of the structure both for simulation purposes and for selection of appropriate controller parameters for different control laws. Generally it is not possible to solve the partial differential equations that accurately represent a distributed-parameter

system such as a floor so the system is discretised into a set of ordinary differential equations that are more readily solved with methods such as the finite element method. This discretisation could result in "spillover" due to higher order modes being neglected, though the effect is often minimal even for complex flexible structures (Hanagan, 1994). The problem of spillover truly occurs when the system is further reduced to a practical size for control implementation as it can be very difficult to realise a high-order controller that can perform in real-time (Du et al., 2008). Consequently, the significant spillover effects dramatically impact the effectiveness of the control law chosen (Hanagan, 1994). The approximations of spatial discretisation and modal truncation result in control laws that can never be *fully* realised. However, structural control differs from control theory in this respect because lower accuracy can be acceptable, providing the structural response is limited to a certain amplitude (Housner et al., 1996). Also, control laws have been repeatedly used to successfully improve the dynamics of real structures, even with these aforementioned problems. For example, it is common to place an actuator and sensor in the same location (a collocated setup) because this helps to reduce both control and observation spillover effects as well as significant phase lags introduced by non-collocated setups, as will be discussed in further detail in Section 2.3.5.

A completely different approach to forming a dynamic model of the structure is through the use of experimental modal analysis (EMA). By exciting the structure with a known excitation over a broad frequency range and measuring the resulting structural response it is possible to derive the frequency response functions (FRFs) of the structure, from which the modal properties (natural frequencies, damping, modal masses and mode shapes) can then be calculated. This is in contrast with the theoretical FE route which derives the modal properties purely from a description of the structure (mass, damping and stiffness matrices) (Ewins, 1984). The modal properties then permit the prediction of the response of the structure when it is subject to operational use. EMA has the distinct advantage over FE modelling

in that the dynamic properties of the structure are determined for how it is in real-life, as opposed to determining the properties of a theoretical model that for simplicity often excludes non-structural components (Smith et al., 2007). Obviously, the drawback of this method is that it can only be performed post-construction hence is of little use for pre-construction design of vibration controllers. Furthermore, for large structures it may be difficult to measure the response at sufficiently many locations which could lead to spatial aliasing (Setareh, 2010). The difficulties associated with modelling floors means that EMA is a very popular method for designing controllers for retrofit, for example Díaz and Reynolds (2010a); Nyawako (2009).

2.3.4 Control Laws

Control laws can be classified in many ways. In terms of the information that is processed by the controller, there are three different categories. These are (Soong and Spencer, 2002):

1. feedback (closed-loop), where the structural response is measured and used to calculate the control force;

2. feedforward (open-loop), where the excitation force is measured and used to calculate the control force, and

3. feedforward-feedback, where both the structural response and the excitation force are measured and used to calculate the control force.

When the excitation arises from moving machinery, measuring the forces can be quite feasible. However, in the case of human-induced vibrations this would require force plates under the entire floor which would be prohibitively expensive. For this reason, for the active control of human-induced vibrations the control laws are limited to those using feedback (closed-loop) (Hanagan, 1994). This feedback is one of the key elements to AVC; it is this element that allows the control law to

take account of variations in the structural response (and implicitly the excitation force) such that a more effective control force can be applied (Soong and Spencer, 2002). A typical AVC configuration is shown in Figure 2.8.

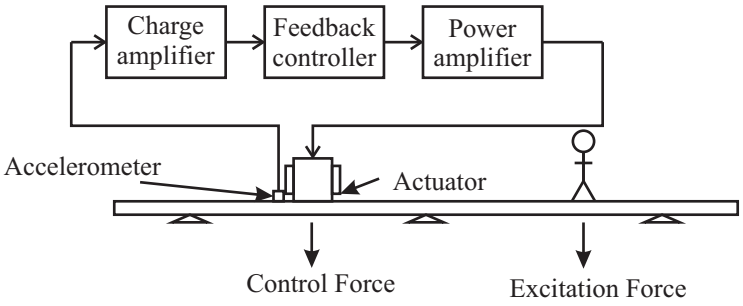

Figure 2.8: Typical AVC configuration, after Figure 13.12 in Preumont (2002)

Feedback based control laws typically fall into one of two categories: (1) direct-output feedback (DOFB) controllers, or (2) model-based (MB) controllers. In DOFB the sensor outputs are multiplied by a gain matrix to produce the actuator commands. Generally, methods based on this control law type require the feedback gain matrix to be 'tuned' numerically to achieve optimal closed-loop performance with regards to some criterion (e.g. robustness, disturbance rejection) (Hiramoto et al., 2000). It has been stated that a large number of sensors and actuators are required to allow for a precise control (Hanagan, 1994). However, later research has shown that good control can be achieved with a very small number of actuators and sensors in real floor structures (Díaz and Reynolds, 2010a; Nyawako, 2009; Hanagan and Murray, 1998). Model-based controllers on the other hand, use a state estimator to approximate the controlled mode states, upon which a gain matrix is applied to produce the actuator commands. This method requires higher processing power and an accurate model of the structure to accurately estimate the mode states in real-time (Hanagan, 1994). The DOFB method, which does not require a highly accurate model, is an attractive choice (Hanagan, 1994), however the difficulties associated with generating an accurate model should not preclude the use of model-based controllers.

To the author's knowledge there has been no investigation into a comparison between DOFB and model-based controllers with regards to implementation on civil engineering floor structures. However, most previous research in this field has focussed on DOFB controllers indicating a general preference for this controller type - probably due to their ease of implementation.

Direct Output Feedback (DOFB) Control Laws

Some of the DOFB control laws that have been previously investigated include Direct Velocity Feedback, Direct Velocity Feedback with Feed-through Term, Direct Acceleration Feedback, Compensated Acceleration Feedback and Response-Dependent Velocity Feedback. More elaborate details of these controllers are provided below.

Direct Velocity Feedback (DVF)

The DVF control law is one of the simplest control laws to implement which, in theory, implements pure viscous damping. The inputs to the actuators are the measured velocities multiplied directly by a gain matrix, as shown in Figure 2.9. Often accelerometers are used to measure the structural response, in which case

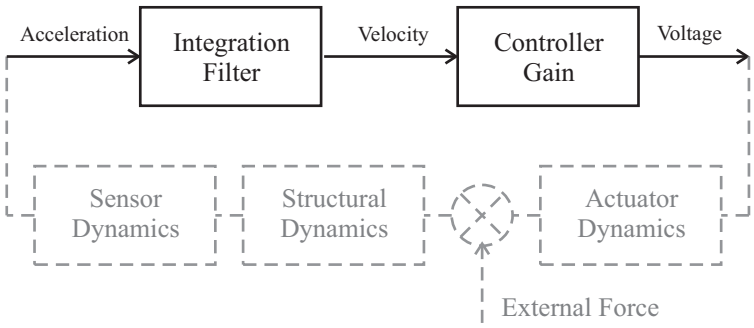

Figure 2.9: Direct Velocity Feedback Schematic

the outputs must be passed through some form of integrating element, i.e. numerical integration or an integration filter. The narrow restrictions of DVF result in a stabilising spillover effect, and in the absence of actuator and sensor dynamics

the collocated case is unconditionally stable (Hanagan, 1994); it has the property of interlacing poles and zeroes, as shown in Figure 2.10. When the dynamics of the system are represented as a rational partial differential equation, the poles of the system are the roots of the denominator and characterise the structure's natural frequencies and damping ratios, whilst the zeros are the roots of the numerator. These poles (and zeros) come in complex conjugate pairs, of the form:

$$\lambda_{1,2} = -\zeta\omega_n \pm \omega_n\sqrt{\zeta^2 - 1} \tag{2.14}$$

where, ζ is the damping ratio of the mode, ω_n is the circular natural frequency of the mode. These are shown in the complex domain on the Root Locus plot of Figure 2.10 for a system with 3 modes: the corresponding 3 pole pairs are shown as crosses, whilst the corresponding 3 zero pairs are shown as circles. As the feedback controller gain is increased the poles shift towards the zeros by the loci shown on the Root Locus diagram, and the resulting poles for a typical gain choice are represented by squares. It is observed that all 3 controlled pole pairs have higher damping than the uncontrolled pole pairs because they have moved away from the imaginary axis where the damping is zero. However, the control system and the structure do not behave as independent dynamic systems; there is a degree of interaction between the excitation and the structure as well as, to some extent, the sensors and the structure (Symans and Constantinou, 1999). So, when the actuator and sensor dynamics are considered, additional poles and zeros are introduced which dramatically affect the structure dynamics and eliminate this interlacing property for the collocated case (Díaz and Reynolds, 2010a), as shown in Figure 2.11. Here, it is observed that the loci for the poles introduced by the actuator dynamics move into the right half plane for some gain values, indicating that they would have negative damping and hence be unstable. Therefore, this places an upper limit on the range of stable feedback gains. In addition to this, it is usually the poles relating to the dynamics of the actuator that go unstable,

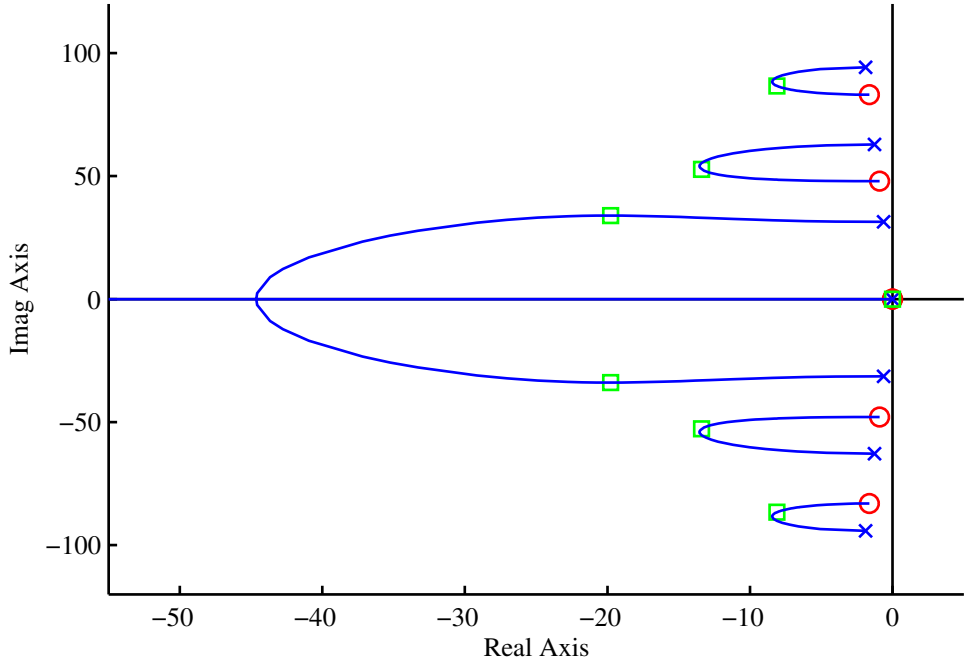

Figure 2.10: Root Locus for DVF with Interlacing Poles and Zeros

i.e. a low frequency instability, as shown in Figure 2.11. Although the gain is reduced to ensure stability, the damping ratio of the actuator itself will have been reduced which means that the force output (and hence stroke) at this frequency will be increased - potentially inducing stroke saturation as will be discussed later in Section 2.3.5. In order to avoid this, the feedback gain has to be decreased even further. Despite this limitation, the DVF control law has been used to successfully reduce the vibration response of structures. For example, Moutinho et al. (2007) use DVF to control the motion of a footbridge in Portugal. There are also several applications for problematic floor vibrations, such as the office floor and the chemistry laboratory floor as described by Hanagan et al. (2003).

Much work has been presented with DVF controller (Hanagan, 1994; Hanagan and Murray, 1997; 1998; Hanagan, 2005a; 2010). However, improvements to this controller can be achieved to enable greater performance. Also, in some structural implementations a single actuator/sensor pair will be insufficient to provide con-

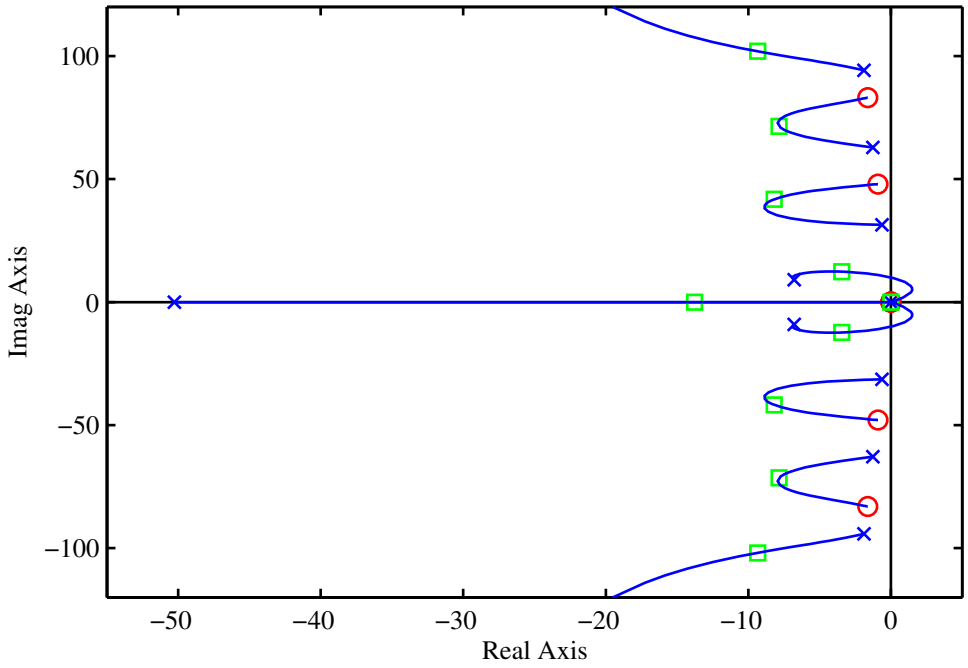

Figure 2.11: Root Locus for DVF with Actuator Dynamics

trol of the entire problematic floor area. In this case more complex control laws, potentially based on a structural model as in Section 2.3.4, may be required to robustly control multiple actuators and sensors. These require further investigation and implementations in real structures.

Single Input-Multiple Output Velocity Feedback

Some of the drawbacks of DVF have been improved upon by extending the range of inputs to the controller to include other measurements apart from the structural velocity. For example, Hanagan et al. (2003) utilise the actuator mass' velocity and displacement relative to the floor to derive the command voltage sent to a single actuator. These measurements were combined by the summation of fixed constant feedback gains applied to each signal. Results for this were mixed: a marginal improvement was noted on one test floor, whilst significant improvements were observed for another. Similarly, a controller based on the structural

velocity and structural acceleration is investigated by Nyawako et al. (2011). This study demonstrated the controller's ability to target higher frequency modes in addition to lower frequency modes.

Direct Velocity Feedback with Feed-through Term (DVF with FTT)

The introduction of a feed-through term, with schematic as shown in Figure 2.12, is investigated by Díaz and Reynolds (2009a). This feed-through term includes a

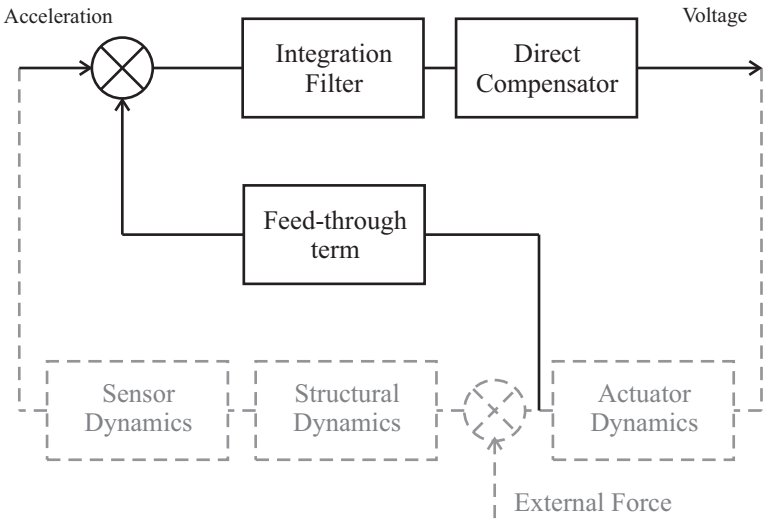

Figure 2.12: DVF with Feed-through term Schematic

small portion of the actuator force to the sensor signal which has the effect of introducing a pair of resonant system zeros at an arbitrary frequency (Aphale et al., 2007). This property is utilised by Díaz and Reynolds (2009a) to deal with problems introduced by the inclusion of actuator and sensor dynamics in a collocated system. The zeros are located between the poles for the first natural frequency of the structure and the poles for the natural frequency of the actuator, the frequency of which is generally chosen to be less than the first natural frequency of the structure. This re-introduces the property of interlacing poles and zeros when actuator dynamics are included which permits very high feedback gains without inducing limit-cycles in the actuator, as shown in Figure 2.13. This method is shown to

be robust with respect to stability and achieves excellent reductions in vibration response, as seen in Table 2.5.

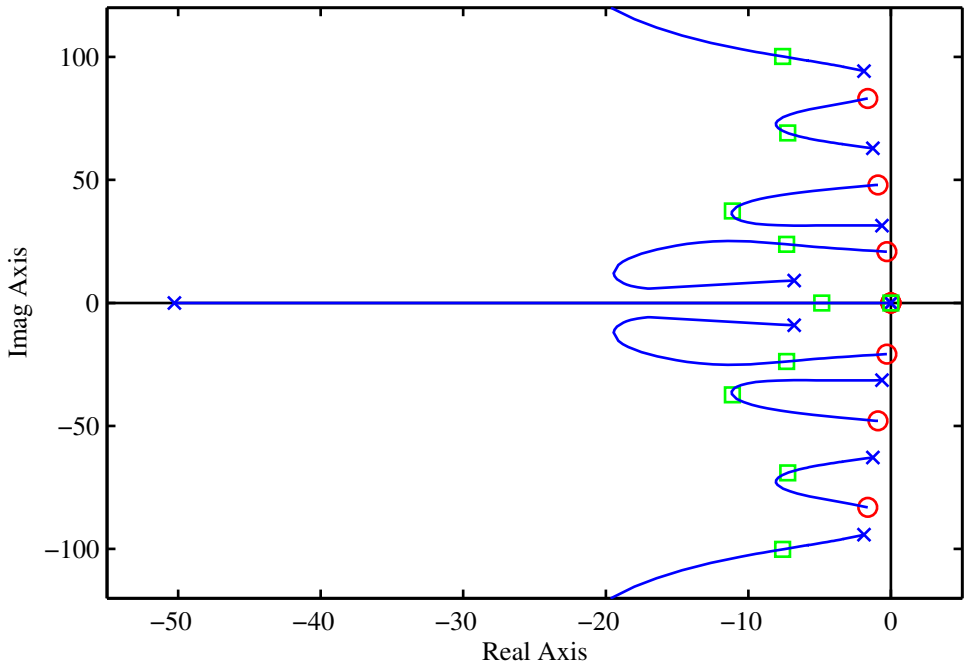

Figure 2.13: Root Locus for Typical DVF with FTT Controller

Direct Acceleration Feedback (DAF)

DAF uses the acceleration output from the sensors as the input to the gain matrix, as seen in Figure 2.14. This control law can be used in hybrid controllers to en-

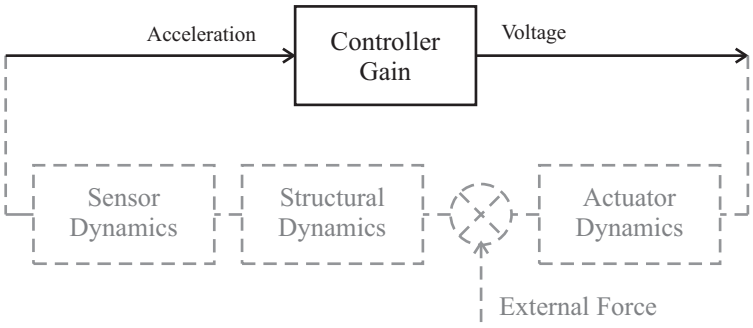

Figure 2.14: Direct Acceleration Feedback Schematic

hance the effectiveness of the passive component, especially when this is a TMD, because the motion of the TMD is a result of the acceleration of the structure (Nishimura et al., 1998; Mackriell et al., 1997). However, in AVC the effectiveness of DAF is observed to significantly depend on the frequency of the mode(s) to be controlled. This effect was investigated by Shahabpoor et al. (2010) and it was found that larger increases in damping could be achieved for higher frequency modes before instability occurs compared with lower frequency modes. For the actuator dynamics in this study, the cut-off between these higher and lower frequency modes was at about 7Hz. Furthermore, Díaz and Reynolds (2009b) conclude that DAF can provide better performance than DVF for floors that have a fundamental natural frequency higher than 6Hz. A DAF control law is also investigated by González Díaz and Gardonio (2007). The 90° phase shift that this controller has relative to DVF should, in theory, improve the stability margins. However, the transition between the actuator resonance and the first structural mode means that there is still a destabilising effect which places an upper limit on the implementable feedback gains. A typical root locus plot for DAF is shown in Figure 2.15. Here it is seen that the first mode is not controlled well, but higher frequency modes do show improvements to their level of damping.

Compensated Acceleration Feedback (CAF)

Similar to the DAF control law, CAF utilises acceleration measurements in the feedback mechanism. However, here a compensator is applied to the acceleration outputs, as seen in Figure 2.16. This introduces a phase-lag to account for the interaction between structure and actuator dynamics, such that the properties of high damping at the fundamental vibration mode and high stability margins are achieved (Díaz and Reynolds, 2010a). A phase-lead compensator, acting as a high-pass filter, is also included to prevent stroke saturation at low frequencies (Díaz and Reynolds, 2010a). Root locus methods are used in order to design the phase-lag compensator, while the properties of the phase-lead compensator are

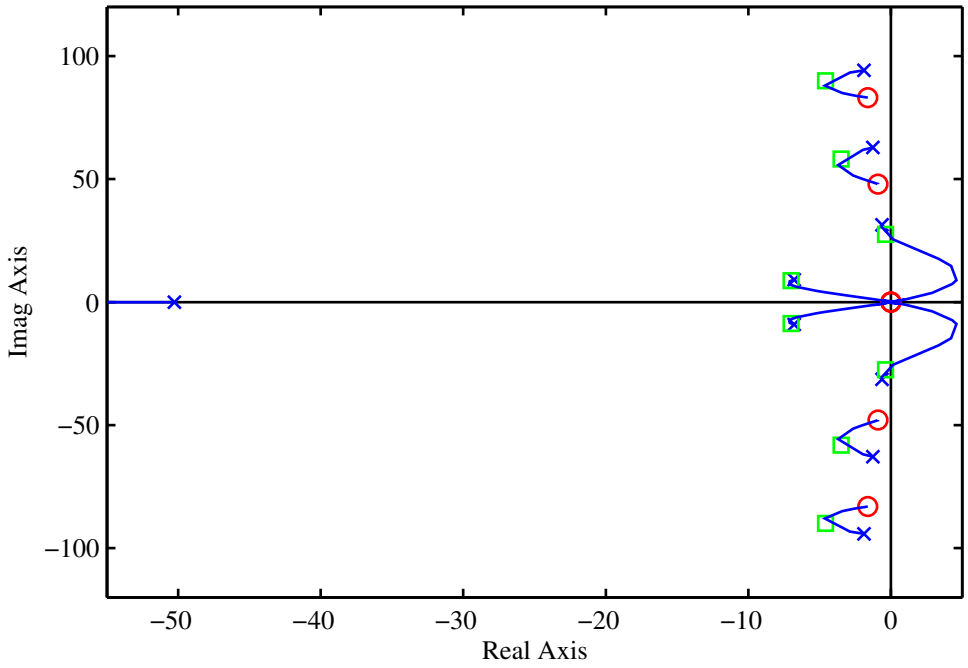

Figure 2.15: Root Locus for Typical DAF controller

calculated through a frequency domain analysis and optimisation study (Díaz and Reynolds, 2010a). A typical root locus plot is shown in Figure 2.17. Experimental results have shown that this control law can significantly reduce the level of vibration response in a real working environment (an office floor) - see Table 2.5.

Response-Dependent Velocity Feedback (RDVF)

The main idea behind the RDVF control law, shown in Figure 2.18 is to change the gain matrix that is applied to the velocity measurements, such that the maximum force output of the actuators is achieved for any velocity within a given range (Nyawako and Reynolds, 2009). That is, for low velocities a high gain matrix is used, while for high velocities a low gain matrix is used. A non-linear element is included such that once a minimum level of vibrations is detected the command signal to the actuators is zero, thus preventing the onset of limit cycles due to very high gains (Nyawako and Reynolds, 2009). The advantage of this control law over

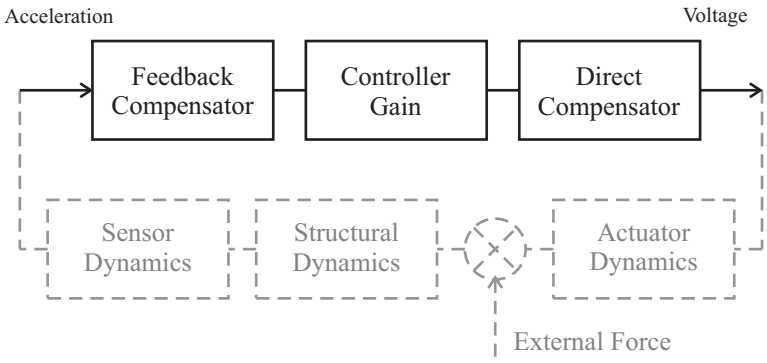

Figure 2.16: Compensated Acceleration Feedback Schematic

simple DVF is the automatic gain selection, whilst performance is very similar to DVF with tuned gain settings, as seen in Table 2.5. However, this controller is still the topic of active research and is in need of a thorough stability and performance analysis.

On-off controllers (bang-bang)

The schematic for these controllers is of a similar nature to that shown in Figure 2.18 in that the gain varies. However, here the gain varies in such a way that the command voltage signal is always in one of three states - maximum positive voltage, zero voltage or maximum negative voltage. A non-linear velocity feedback with dead-zone controller and a non-linear velocity feedback with a switching-off level controller are investigated by Díaz and Reynolds (2010b). Here, it is shown experimentally that the introduction of a dead-zone or a switching-off level to velocity feedback can avoid the appearance of limit cycles that are present in DVF with saturation. The width of dead-zone or switching-off level in the control laws tested is chosen as a function of the gains that are on the limit of stability. However, the relationship between settling time and dead-zone width or switching-off level is complex and results in wide-ranging performance, so should this controller be implemented in a real structure it would be prudent to investigate a range of widths or levels to achieve optimum performance.

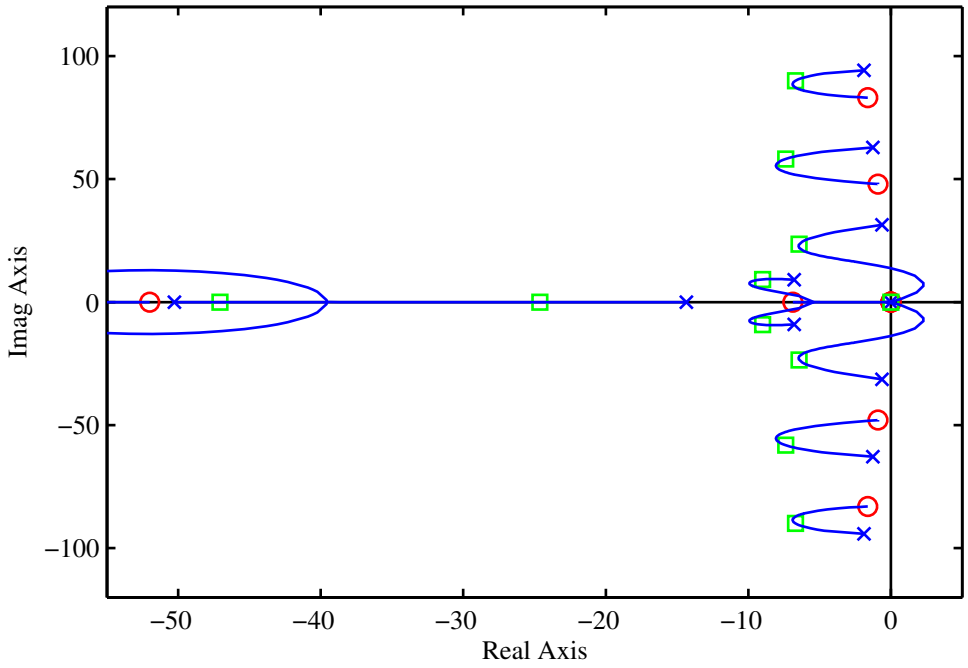

Figure 2.17: Root Locus for Typical CAF controller

Summary of experimental investigations

The results of several DOFB control law implementations are summarised in Table 2.5. Here, the maximum transient vibration value (MTVV) is used to characterise the response. This is equal to the maximum of the running 1s RMS of the frequency weighted structural acceleration.

Model-Based (MB) Control Laws

These control laws differ from the relatively simple DOFB laws in that they utilise an accurate model of the system to determine precise controller properties that meet specific design criteria. Examples of model-based controllers include the pole placement method, the linear quadratic regulator (LQR), the linear quadratic gaussian (LQG), independent modal space control (IMSC), $\mathcal{H}_\infty$ and $\mathcal{H}_2$ methods. These are discussed in some detail below.

There are now many examples of the use of these laws for active controllers in

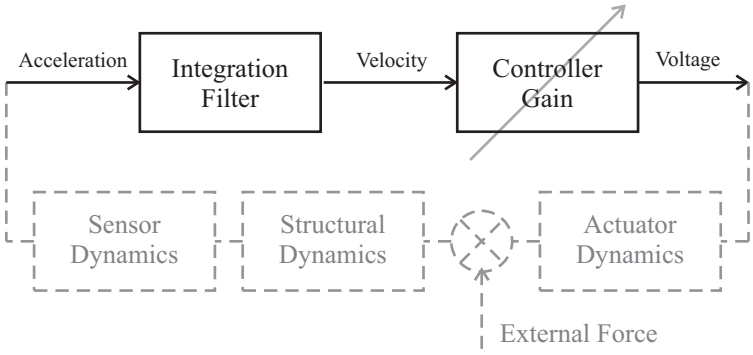

Figure 2.18: Response-dependent Velocity Feedback Schematic

structures for the reduction of the effects of seismic and wind loading (Wu et al., 2006; 1998; Suhardjo et al., 1992; Köse et al., 1996; Jabbari et al., 1995; Chase et al., 1999; Du et al., 2008; Lu et al., 2003; Dyke et al., 1996; Spencer et al., 1994) however applications for the control of human-induced floor vibrations remains extremely limited, though ongoing work is investigating their use for this application (Nyawako, 2009), hence their inclusion in this review.

Pole Placement

This method focuses on the location of the roots in the complex plane of the closed-loop transfer function. Usually the aim is to ensure that the dominant poles of a structural model are both far from the origin so that a fast transient response is achieved and away from the imaginary axis so that damping is improved, whilst maintaining stability in all other poles (Lurie and Enright, 2000). A model of the system must estimate the state dynamics when these are not directly measured; this can be performed with minimal loss of accuracy if the estimator dynamics are chosen such that their transient response is much faster than the system dynamics (Preumont, 2002). Pole placement methods are best suited for situations when the response is dominated by a small number of modes (Soong, 1988); unfortunately this situation rarely occurs for complicated civil engineering structures. Further, while this method benefits from relative simplicity it does suffer a number of

DOFB Control Law	Test Structure	Uncontrolled MTVV (m/s^2)	Controlled MTVV (m/s^2)	Reduction (%)	Source
DVF	Laboratory	0.130	0.054	59	[A]
DVF	Office Floor 1	0.058	0.017	70	[B]
DVF	Chem Lab Floor	0.038	0.009	75	[B]
CAF	Office Floor 2	0.031	0.010	68	[C]
CAF	Office Floor 2	0.033	0.016	52	[C]
DVF with FTT	Laboratory	0.168	0.007	96	[D]
RDVF	Laboratory	0.130	0.047	64	[A]

[A] Nyawako and Reynolds (2009)
[B] Hanagan and Murray (1998); Hanagan et al. (2003)
[C] Díaz and Reynolds (2010a)
[D] Díaz and Reynolds (2009a)

Table 2.5: Experimental Reduction in Vibration Response due to Several DOFB Controllers

drawbacks - namely, that a trial and error approach must be used to design the compensator and loop gains and there is no measure of how close the performance is to optimal (Lurie and Enright, 2000). Despite these drawbacks, pole placement techniques have been used for the control of ground-excited structures (Chang and Yu, 1998).

Optimal Control

One of the most popular methods for choosing optimal gains of a MB controller is the LQR method (Cao and Li, 2004; Stavroulakis et al., 2006). In this time-domain based method, the state feedback matrix is chosen such that a performance index

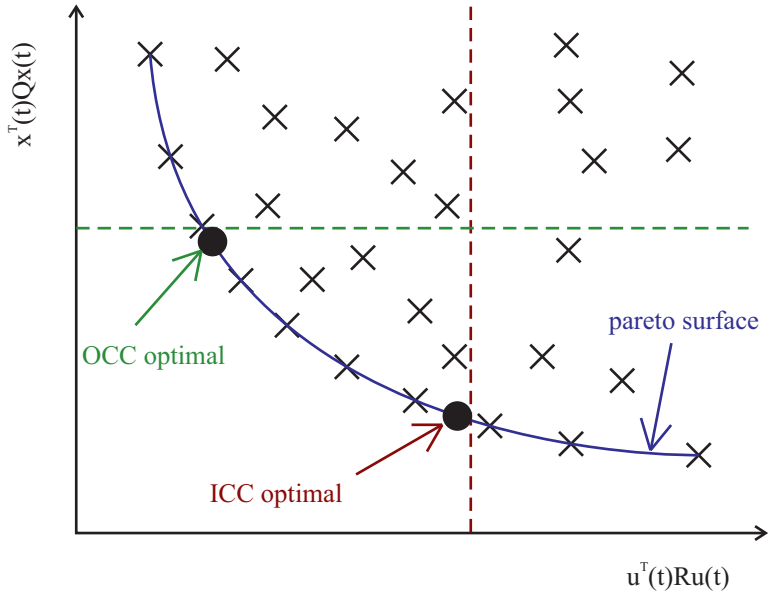

Figure 2.19: Pareto Surface for an Optimisation Problem with 2 Variables

(PI) is minimised, the typical form of which is shown in Equation 2.15:

$$J = \int_0^{t_f} \mathbf{x}^T(t)\mathbf{Q}\mathbf{x}(t) + \rho\mathbf{u}^T(t)\mathbf{R}\mathbf{u}(t)\,\mathrm{d}t \tag{2.15}$$

where $\mathbf{x}$,$\mathbf{u}$ are the system state and input variables respectively, $\mathbf{Q}$,$\mathbf{R}$ are the positive semi-definite and positive definite weighing matrices for $\mathbf{x}$,$\mathbf{u}$ respectively, and t_f is the time period considered. A scalar weighting factor, ρ, can be used to place relative importance between these (Preumont, 2002). The requirement for positive semi-definite $\mathbf{Q}$ and positive definite $\mathbf{R}$ ensures stability of the system which also means that the performance index, J, will be upward convex with a global minimum (Lynch and Law, 2002).

The range of feasible values for the weighting matrices means that no single solution exists for the multi-objective optimisation problem - instead, as shown in Figure 2.19, a set of Pareto optimal solutions exist (Park and Koh, 2004). Therefore there are numerous methods by which a single optimal solution can be chosen. The approach highlighted earlier is the use of a scalar weighting applied to the functions (ρ in Equation 2.15). Two further possible approaches are to constrain

either the input (input constrained control (ICC)) or the output (output constrained control (OCC)) to within a certain limit and minimise the other variable (Housner et al., 1997), as shown in Figure 2.19. The limits at which the variables are constrained is a subjective choice, for example Nyawako (2009) uses OCC with the threshold of human perception of vibration for the mode under consideration, as specified by BS6472:1992 (BSI, 1992) as the limit. Alternative methods include increasing $\mathbf{R}$ such that the largest expected transient does not saturate the actuator (though this could lead to a significantly oversized actuator) (Lurie and Enright, 2000) and using weighting matrices based on the system's kinetic and potential energy and the input energy (Alavinasab et al., 2006).

Finally, the use of goal-programming could be used to achieve the optimal solution - this is the solution that minimises the norm of some kind to the idealised goal (the best possible value for each function were it to be minimised independently) (Michalewicz and Fogel, 2004).

LQR controllers have linear feedback gains which permits a relatively simple analysis and implementation and they also possess good disturbance rejection and tracking (Stavroulakis et al., 2006). Further, there are guaranteed infinite gain margins and phase margins of 60°, assuming that all states are available and the inputs are deterministic (Skogestad and Postlethwaite, 2005). However, system uncertainties and actuator non-linearities are not incorporated into the performance index so the 'optimal' settings derived may not have the desired effect when implemented (Lurie and Enright, 2000).

LQR can also be applied to achieve optimal gains for a system derived in modal space. In IMSC each control force is a function of a single mode only which removes the coupling between degrees of freedom and permits the calculation of independent single degree of freedom (SDOF) equations for each controlled mode (Soong, 1988). This gives a substantial computational benefit especially when only a few modes are to be controlled. However, at least as many shakers

are required as the number of modes to be controlled. This is because physical coupling still exists for each mode so to control modes independently requires an invertible input matrix (Li et al., 2001). Modifications of IMSC that permit fewer shakers than modes to be controlled do exist - these are based on either a pseudo-inverse of the coordinate transformation from modal space to physical space, or an algorithm that switches between modes to be controlled (Hwang et al., 2006). The pseudo-inverse method is utilised by Li et al. (2001) for controlling multi-storey structures so that each storey can be controlled independently. IMSC was also extended by Park et al. (2004) and Park and Koh (2004) for the control of seismic-induced vibrations, who use fuzzy logic for the real-time determination of control gains and genetic algorithms for the determination of optimal gains.

One drawback with the LQR method is the dependence upon knowing the system states because in practice it can be difficult to directly measure these. The LQG method builds on the LQR by combining a Kalman filter with the LQR method to estimate the unknown states (Zhang and Roschke, 1999). The estimated plant is assumed to differ from the actual plant by the addition of Gaussian white noise (Lurie and Enright, 2000; Preumont, 2002) with disturbance signals also assumed to be Gaussian white noise.

This uncertainty gives a better closed-loop response at the crossover frequency (between the frequencies in disturbance rejection and those of sensor noise). LQG and variants thereof are a popular choice for the active control of seismic and wind induced vibrations of civil engineering structures where the assumption of white noise disturbance signals can be considered appropriate (Sheng et al., 2003; Lu et al., 1998; Abdel-Rohman, 1984; Zhang and Xu, 2001; Ho and Ma, 2007). As discussed in Section 2.2.1, human-induced vibrations predominantly occur at harmonics of a single frequency (or a range of single frequencies if a range of loading scenarios are considered), thus the suitability of LQG in this situation is compromised. Also, despite the good stability margins of both the LQR controller and the Kalman filter there are no guaranteed stability margins for the LQG controller, as

highlighted by Doyle (1978). Loop transfer recovery procedures can be utilised to approach the stability margins offered by LQR and Kalman filters, though the cancellation of plant zeros and the introduction of high gains can limit the practical use of these.

Robust Control

This class of control laws consider some degree of uncertainty in the structural model and/or the external disturbance. This is very important in civil engineering because an accurate dynamic model of the system is not often available, and the expected loading is stochastic in nature (Stavroulakis et al., 2006). Hence, robust control relates the two conflicting pressures of performance and stability in the presence of uncertainty in the system model as well as the exogenous inputs to which the model is subjected (Alkhatib and Golnaraghi, 2003; Smith and Chase, 1996).

Two of the key controllers in this category are the $\mathcal{H}_2$ and $\mathcal{H}_\infty$ controllers which are predominantly based in the frequency-domain (Balas et al., 2008; Lurie and Enright, 2000; Gu et al., 2005). The development of these controllers started from the work by Zames (1981) in the 1980's. The $\mathcal{H}_2$ norm essentially minimises the RMS power of the error signal from a generalised plant (Suhardjo et al., 1992), as shown in Equation 2.16

$$\|F_{wz}\|_2 \triangleq \left(\frac{1}{2\pi}\int_{-\infty}^{\infty} tr\left[F_{wz}(j\omega)F_{wz}(j\omega)^*\right]\,\mathrm{d}\omega\right)^{1/2} \tag{2.16}$$

where F_{wz} is the transfer function between the exogenous signals, w, and the error signal z, and $(\bullet)^*$ denotes the complex conjugate transpose of $(\bullet)$.

It is interesting to note that it is possible to define the error signal and represent the input signal in such a way that the LQG controller can be formulated from the general $\mathcal{H}_2$ formulation (Skogestad and Postlethwaite, 2005; Montazeri et al.,

2009).

There are multiple interpretations of the $\mathcal{H}_\infty$ norm, though they all surmount to the same controller. Firstly, the $\mathcal{H}_\infty$ norm can be described as the peak of the maximum singular value of $F(s)$, as seen in Equation 2.17. Secondly, from a time domain perspective, it can be described as the induced (worst-case) 2-norm, as seen in Equation 2.18 (Suhardjo et al., 1992; Skogestad and Postlethwaite, 2005; Gu et al., 2005; Wu et al., 2006).

$$\|F_{wz}\|_\infty \triangleq \sup_\omega \bar{\sigma}(F_{wz}(j\omega)) \tag{2.17}$$

$$\|F_{wz}\|_\infty \triangleq \sup_{w(t)\neq 0} \frac{\|z(t)\|_2}{\|w(t)\|_2} \tag{2.18}$$

where $\|\bullet\|_2 \triangleq \left(\int_0^\infty |\bullet(t)|^2 \, \mathrm{d}t\right)^{1/2}$ is the 2-norm of the vector signal $(\bullet)$, and $\bar{\sigma}(\bullet)$ represents the singular value of $(\bullet)$.

Generally the $\mathcal{H}_\infty$ controller is designed by specifying the frequency response of the disturbance rejection with weight functions that are calculated from the known disturbance spectral densities (Lurie and Enright, 2000). However, it is difficult to select the weights such that the controller provides a good trade-off between the conflicting objectives at crossover, leading to an overly conservative design (Skogestad and Postlethwaite, 2005). To deal with this a sub-optimal $\mathcal{H}_\infty$ controller can be designed which has properties similar to an $\mathcal{H}_2$ controller and facilitates a trade-off in this frequency range, or a less conservative design could be achieved through the use of μ-synthesis (Lurie and Enright, 2000; Montazeri et al., 2009).

$\mathcal{H}_\infty$ and variants thereof have been successfully utilised in the design of a variety of controllers, both for the reduction of seismic-induced vibrations and wind-induced vibrations in tall buildings (Wu et al., 2006; 1998; Suhardjo et al., 1992; Köse et al., 1996; Jabbari et al., 1995; Chase et al., 1999), but as previously stated, there are no recorded examples of this controller being utilised for the reduction

of human-induced vibrations in floors. Similarly, the $\mathcal{H}_2$ controller and variants have been used in similar applications (Du et al., 2008; Lu et al., 2003; Dyke et al., 1996; Spencer et al., 1994) but not for the mitigation of human-induced vibrations in floors.

Adaptive Control

In some cases the complexity and/or level of uncertainty in the structural system is so great that a fixed, robust, controller can not achieve the desired performance requirements; in this case an adaptive controller may be desirable (Casciati et al., 2012). This type of controller has adjustable parameters, often with initial values based on a fixed controller design, and a mechanism through which the parameters are adjusted (Housner et al., 1997). This process involves (Alkhatib and Golnaraghi, 2003; Housner et al., 1997):

- choosing a general structure for the controller with adjustable parameters,
- choosing a performance index,
- evaluating the performance of the controller in real-time, and
- adjusting the controller parameters in order to improve performance.

Adjustment of the parameters can be performed either directly from the error between the measured and desired outputs, or indirectly, i.e. using the error signal to update a model of the uncertain structure and basing the new controller parameters on this new model (Housner et al., 1997; Ioannou and Fidan, 2006). Unsurprisingly, the design of adaptive controllers is more involved than that for a fixed controller, in part because their use results in a non-linear time-varying system which has implications for stability. For example, Dewey and Jury (1965) presented an unstable adaptive controller whose gain varied within a range of gains that would have been asymptotically stable for a fixed controller on a linear time-

invariant system. However, this may be less of a problem for controlling floor structures because the variations in structural properties result from very infrequent modifications such as partition layout changes. This lends itself to a very slowly changing controller which is likely to exhibit linear properties on a small timescale, or even a gain scheduling controller where a range of fixed controllers are implemented, the choice of which depends on the operating conditions (Ioannou and Fidan, 2006).

2.3.5 Issues Associated with DOFB and MB Controllers

Actuator Issues

Typical AVC configurations used for floor vibrations have so far utilised commercially available actuators (Díaz et al., 2010; Nyawako and Reynolds, 2009; Hanagan, 1994). However, these are generally built with modal testing of structures in mind and so are not optimised for AVC. This means that they have a relatively large parasitic mass that does not assist with the generation of control forces and do not necessarily have the desirable dynamics properties for AVC. It is generally recommended to keep the natural frequency of the shaker well below the first natural frequency of the structure (Hanagan, 2005b; Elliott et al., 2001). However, a low natural frequency can lead to problematically high displacement of the actuator mass due to gravity which places a lower limit on the feasible shaker natural frequency. This can be overcome through the use of open-loop compensators (Rohlfing et al., 2011a) which alter the command output such that signals around the mechanical natural frequency are attenuated, whilst lower frequency components are amplified, thus appearing to reduce the natural frequency of the shaker.

So far, for the control laws discussed the actuators have been assumed to be linear devices. This is not the case. Two types of non-linearity are present for the proof-mass actuators typically used: force saturation and stroke saturation (Rohlfing et al., 2011b). Force saturation occurs when the current in the coil exceeds the

allowable limits, whilst stroke saturation occurs when the movement of the actuator mass exceeds the available displacement and hits the stops on the static component of the actuator. This can impart destabilising impulses into the structure and potentially permanently damage the actuator (Rohlfing et al., 2011a). Stroke saturation is generally only a problem at low frequencies because of the large displacements required to generate forces at these frequencies. Typical measures taken to avoid saturation therefore include using a command limiter or using a high pass filter to remove the low frequency components from the command signal. However, both these methods reduce the performance at higher frequencies. The command limiter restricts the maximum force that can be generated by capping the voltage at all frequencies and the high pass filter reduces the controllers ability to affect the first few modes of vibration (which are often the most important to control) because they are typically relatively close to the filter cut-off frequency and there are limits on how steep the filter's magnitude can roll off.

Controllability and Observability

Some of the most important aspects of active controller design are controllability and its duality observability. If a system is not controllable then there exists at least one mode of vibration that remains unchanged by the action of the actuator(s). Equivalently, if a system is not observable there exists at least one mode of vibration that remains undetected by the sensor(s) (Hespanha, 2007). This idea is illustrated in Figure 2.20.

The binary characteristics of the notions of controllability and observability can cause problems, particularly when directly applied to the placement of actuators and sensors, because a system can be considered completely controllable when an actuator is located an arbitrarily close distance to a location that results in an uncontrollable system (Hać and Liu, 1993). This leads to the controllability Gramian and the observability Gramian which give an indication of the degree of controllability and observability. For the dynamic system represented in state

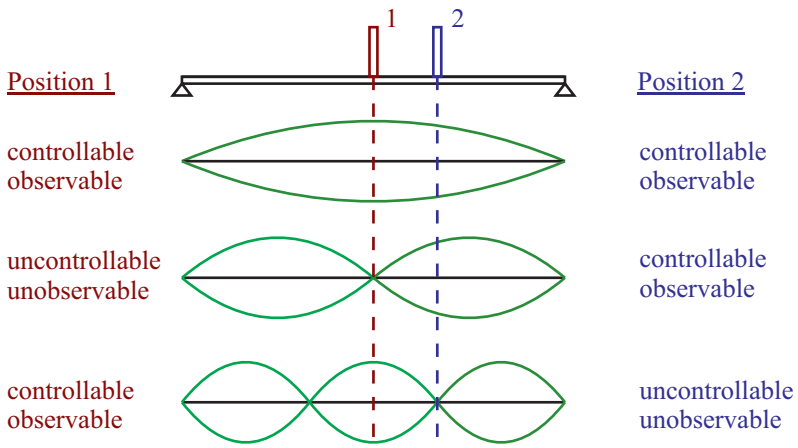

Figure 2.20: Controllability and Observability of a Simply Supported Beam

space as:

$$\dot{\mathbf{x}}(t) = \mathbf{A}\mathbf{x}(t) + \mathbf{B}\mathbf{u}(t) \tag{2.19}$$

$$\mathbf{y}(t) = \mathbf{C}\mathbf{x}(t) + \mathbf{D}\mathbf{u}(t) \tag{2.20}$$

where

$\mathbf{x}(t)$, $\mathbf{u}(t)$ and $\mathbf{y}(t)$ are the internal state vector, input vector and output vector respectively

$\mathbf{A}$, $\mathbf{B}$, $\mathbf{C}$, $\mathbf{D}$ are the state matrix, input matrix, output matrix and direct transmission matrix respectively,

the controllability Gramian (W_c) and the observability Gramian (W_o) are defined as (McFarlane and Glover, 1990)

$$W_c \triangleq \int_0^\infty e^{\mathbf{A}t}\mathbf{B}\mathbf{B}^* e^{\mathbf{A}^* t}\,\mathrm{d}t \tag{2.21}$$

$$W_o \triangleq \int_0^\infty e^{\mathbf{A}^* t}\mathbf{C}^*\mathbf{C} e^{\mathbf{A}t}\,\mathrm{d}t \tag{2.22}$$

where $(\cdot)^*$ denotes the complex conjugate transpose.

Optimal Placement of Actuators and Sensors

The optimal placement of actuators and sensors on a flexible floor is not a trivial decision and it is often the critical factor for the effectiveness of a control law (Alkhatib and Golnaraghi, 2003). Therefore, this is a crucial area for the effective implementation of AVC in real structures.

In general, it is not possible to compute both the optimal actuator/sensor locations and the optimal controller simultaneously when using a MB controller such as LQR or $\mathcal{H}_\infty$ since the controller can only be designed to meet closed loop specifications of stability and performance once the locations of actuators and sensors are fixed (Hiramoto et al., 2000). This means that a sequential design is generally used to find the optimum placement. DOFB controllers, despite their relative simplicity, often also require a sequential design (Lee et al., 1996). Here, actuator and sensor dynamics mean that even collocated actuator / sensor pairs are not unconditionally stable, so the feedback gain matrix must be tuned to fit the application.

Typical actuator/sensor location optimisation involves the maximisation of a performance index that is based on system eigenvalues or a controllability/observability index, subject to a set of constraints that ensure the design criteria are satisfied (Li et al., 2004). The performance index gives a quantitative measure of how close the current solution is to the utopian optimal solution.

Many algorithms consider the problem of actuator and sensor placement independently (Hać and Liu, 1993; Arbel, 1981; Hanagan et al., 2000; Wang and Wang, 2001; Bruant and Proslier, 2005). In this situation, a performance index is formulated based purely upon either the controllability Gramian or observability Gramian. Two different starting points have been considered during the formulation for optimal actuator placement:

1. minimise the control energy required to bring the system to a set position in a set time

2. maximise the energy transmitted to the structure for a given control input

It is interesting to note that both of these approaches have been shown to yield the same result - that some measure of the controllability Gramian be maximised (Bruant and Proslier, 2005). For the optimal sensor placement, the equivalent approach is to maximise the signal measured from the structure - though in reality it is often convenient to locate the actuators optimally and then ensure collocated sensors.

In the general case of a system with damping, the system response tends to zero as time increases so the minimum energy required to bring the response to rest through the action of the control system is actually zero. A finite time period is required to avoid this problem, as seen in the work by Hanagan et al. (2000) but this dependence upon an arbitrary time period is often an unwanted complication so generally the steady-state controllability Gramian is used instead (Hać and Liu, 1993).

Unfortunately, a performance index based purely upon maximising the controllability Gramian neglects the effect of individual modes - in this global measure it is possible to arrive at an "optimal" solution where one or more modes are actually uncontrollable (Hać and Liu, 1993). So, a performance index that also considers the controllability/observability of each mode is used, with a typical performance index shown in Equation 2.23

$$\text{PI} = \underbrace{\sum^{2m} \lambda_{C_i}}_{\text{global}} \cdot \underbrace{\sqrt[2m]{\prod^{2m} \lambda_{C_i}}}_{\text{local}} \tag{2.23}$$

where λ_{C_i} is the i-th eigenvalue of the controllability Gramian. This performance index shows a general trend of increasing towards areas where the most energy can be imparted into the structure, but drops off rapidly around areas where any mode becomes uncontrollable, as seen in Figure 2.21.

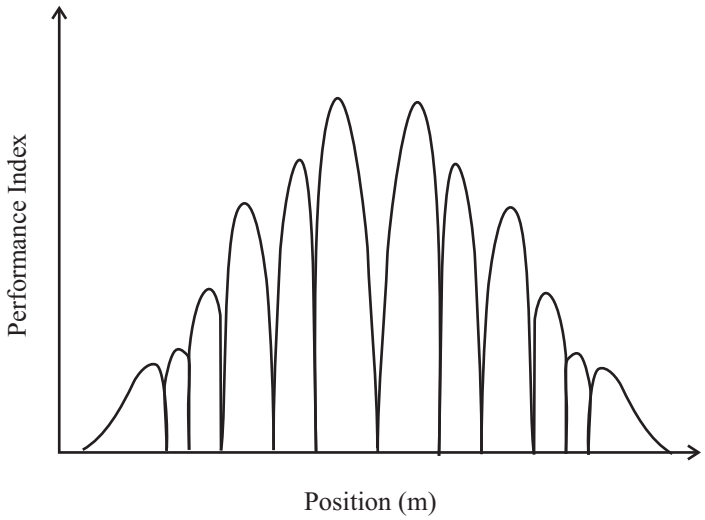

Figure 2.21: Performance index verses location of a force actuator for a simply supported beam with six modes, after Hać and Liu (1993)

One important drawback associated with this method is the dependence upon the choice of state variables - the difference in magnitude for velocity and displacement cause uneven weightings for the state variables in the optimisation function (Hanagan et al., 2000; Hać and Liu, 1993). A number of solutions exist for this problem. Firstly, the states 'modal velocity' and 'modal angular velocity' (i.e. modal displacement multiplied by natural frequency) should be used if possible and appropriate (Hać and Liu, 1993; Bruant and Proslier, 2005). Secondly, the states could be normalised by the range of expected values - so for floor vibrations this could be the limits provided by BS6841 (BSI, 1987) and ISO2631 (ISO, 1989). Another approach considered is to scale the state by the maximum value obtained if that state were specifically controlled by a single actuator (Bruant and Proslier, 2005). This results in a method that maximises the minimum degree of controllability and so aims to control every mode with equal weighting. This is similar to the approach used by Collet (2001) while investigating IMSC. While it is easy to see the appeal of controlling every mode equally well, one must remember the overall aim of reducing the level of vibrations and this method does not consider the fact that higher order modes tend to contribute less to the overall response.

So far the problem of spillover has not been discussed, but this consideration can be incorporated into the performance index by subtracting the equivalent performance index for the residual modes, as shown in Equation 2.24 (Hać and Liu, 1993; Bruant and Proslier, 2005; Hanagan et al., 2000):

$$\text{PI} = \left(\sum^{2m_c} \lambda_{C_i} \cdot \sqrt[2m_c]{\prod^{2m_c} \lambda_{C_i}} \right) - \gamma \left(\sum^{2m_r} \lambda_{C_i} \cdot \sqrt[2m_r]{\prod^{2m_r} \lambda_{C_i}} \right) \tag{2.24}$$

where $\gamma > 0$ is a scalar weighting through which the importance of minimising the effect of residual modes can be specified, m_c is the number of controlled modes and m_r is the number of residual modes.

It is also possible to form a performance index for the combined optimal placement of actuators and sensors (Schulz and Heimbold, 1983; Lee et al., 1996; Yang and Lee, 1993). These methods aim to minimise both the flexible system energy and the control energy and result in a performance index very similar to that used in LQR formulations. However, here the actuator and sensor locations are kept as variables.

2.4 Environmental and Economic Implications

2.4.1 Introduction

As previously discussed, improved design methods have led to the use of more slender floor elements in contemporary building structures. However, these floors can often fail to meet the limits imposed by vibration serviceability checks, despite satisfying ULS and deflection criteria. The use of AVC can significantly reduce the level of response in this situation and so has the potential to realise improvements in slenderness, and associated materials savings, whilst still adhering to vibration serviceability limits. This potential reduction in material use is desirable from both environmental and economical points of view. However, there

are costs associated with the installation and upkeep of an AVC system, whose relative importance must be quantified to evaluate the net impact of AVC over the whole life of the structure in which it is installed.

This section discusses the nature of the methods used to assess the environmental and economic impact of a structural system with specific considerations towards assessing the impact of an AVC system on a floor.

Environmental Assessment Methods

The increased awareness of environmental issues in recent years has resulted in a wealth of knowledge that is applicable to the investigation of the impact of AVC, though to date there exist no reported investigations into this specific area.

Broadly speaking, the environmental assessment methods can be classed as either (Chevalier and Le Téno, 1996):

- 'top-down' - these methods start from a list of environmental impacts, for which product-specific causal links are known, and work down to a list of requirements that the product should adhere to; and
- 'bottom-up' - these methods do not have a fixed definition of what an environmentally friendly product should be like; instead, they work from the material and energy flows of the building up to a quantified list of environmental impact indicators.

Top-down methods tend to rate the building with a score relative to a benchmark building and so permit the relative comparison of the environmental performance of buildings (Crawley and Aho, 1999), which makes them popular with design engineers. Unfortunately there has been no standardisation in this sector and so a large number of methods now exist. The most commonly used tools include: BREEAM (UK), ESCALE (France), EcoEffect (Sweden), ECOPROFILE (Norway), LEED (US) and GBTool (International) (Todd et al., 2001; Haapio and

Viitaniemi, 2008). A critical evaluation of these methods, and more, is provided by Haapio and Viitaniemi (2008).

However, problems exist with these top-down methods. The culmination of several environmental factors into a single score necessarily involves the subjective choice about the relative importance of several completely different factors, for which there is no scientific basis (BSI, 2006b). For example, some of the main issues considered by BREEAM include CO_2 emissions, energy efficiency, acoustic performance, public transport network connectivity, water re-use and recycling and flood risk (BRE, 2008). This can make it difficult for structural engineers to utilise these analyses to improve their designs through comparison with other buildings when there exist site-specific factors that are beyond a structural engineer's domain.

These issues are less of a problem for bottom-up methods which do not have a fixed definition of what an environmentally friendly product should be like (Chevalier and Le Téno, 1996). The two main methods are (Crawley and Aho, 1999):

- an environmental impact assessment (EIA) - which assesses the *actual* environmental impacts of an object located at a given site and in a given context; the object is considered as inherently site and context specific; and
- a life cycle assessment (LCA) - which assesses the non-site specific potential environmental impacts; the object is considered as a generic product that has a well defined purpose and life cycle.

A building can be considered to have both site specific properties and generic properties so the choice of an appropriate method is not a simple matter. When considering the impact of AVC on a building a general result is desired; that is, it should be as site-independent as possible so that a more generalised conclusion can be drawn - this favours the LCA approach. There are many examples in the

literature (Fay et al., 2000; Cole and Kernan, 1996; Junnila and Horvath, 2003; Li et al., 2010; Thormark, 2002) where an LCA has been adopted as the framework of choice for the identification of the environmental impacts of a building, predominantly because the nature of this analysis is more useful as a tool for designing generic improvements to buildings. The localised nature of an EIA is not desirable when evaluating the effect of AVC on a building and so is not considered further in this review.

2.4.2 Life Cycle Analysis

An LCA generally consists of 4 phases (BSI, 2006b):

1. **goal and scope definition**: where the purposes of the study and the system boundaries are defined
2. **life cycle inventory (LCI) analysis**: this is the stage when data is collected and calculations are performed to quantify material and energy inputs and outputs
3. **impact assessment**: when the significance of the potential environmental impacts are evaluated, based on the LCI analysis
4. **interpretation**: provides conclusions and recommendations.

Generally, the costs considered in an environmental LCA are the energy required to provide the desired product or service, or the carbon dioxide emitted during the same processes, though other factors such as emission of harmful substances and acidification are also sometimes considered (Junnila and Horvath, 2003).

There is no single agreed categorisation for the costs associated with the life of a building. However, one possible breakdown is shown in Figure 2.22. Here, the total costs are divided between (Dixit et al., 2010; Yohanis and Norton, 2002; Cole and Kernan, 1996):

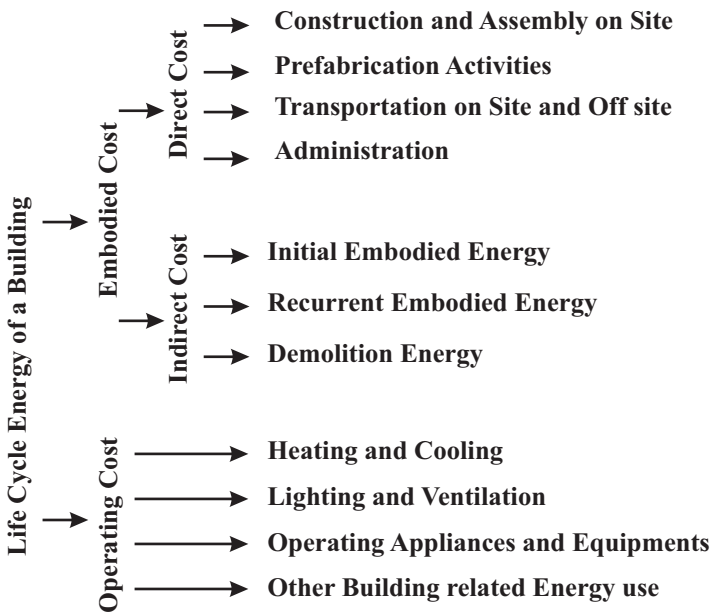

Figure 2.22: LCA Categorisation of Costs, after Dixit et al. (2010)

1. **embodied cost** - that associated with the building materials during all processes of production, construction, demolition and disposal; and

2. **operating cost** - that associated with the day-to-day use of a building, such as heating and cooling, ventilation, lighting and power for appliances.

The relationships of embodied cost and operating cost with respect to time are shown in Figure 2.23.

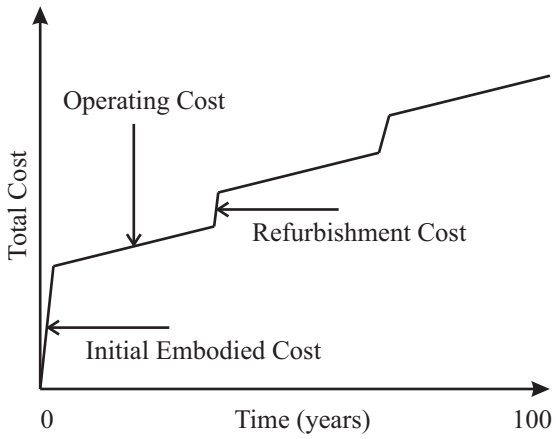

Figure 2.23: LCA over time, after Treloar et al. (2001b)

As previously mentioned, energy consumption is a commonly used cost in LCA studies. Here, the embodied and operating costs are referred to as embodied energy (EE) and operating energy (OE). Previous research has shown that in many situations, the embodied carbon is directly related to the embodied energy (Scheuer et al., 2003).

Designing AVC into a new structure would realise reductions in the embodied costs because less structural concrete and steel would need to be extracted, manufactured and transported to site. On the other hand, the operating costs would be increased due to the unavoidable ongoing maintenance of the AVC system and the electricity required for its operation.

Methods of Life Cycle Analysis

Process Analysis

In a process analysis the overall product system is subdivided into component unit processes to facilitate the identification of input and output flows such that (ideally) the energy or material entering the system is drawn from the environment with no prior human transformation (similarly for energy or materials exiting the system) (Horvath, 2004; BSI, 2006b;a; Li et al., 2010). The material and energy flows are then quantified such that the overall impact can be estimated. This method is quite accurate for the processes that are considered. However, the inclusion of *all* processes linked to the product would necessitate a prohibitively large system to analyse. For example, Buchanan and Honey (1994) perform a very thorough LCA, considering not only the energy required by the machines that make the product, but also the energy required to make those machines in the first place. Clearly this process of stepping further back from the end product cannot continue ad infinitum, so the system boundary is truncated such that "small" energy and material flows are neglected (BSI, 2006a). Problems arise because different studies truncate at different points, e.g. Scheuer et al. (2003) who only consider

the impacts from the actual processes themselves, citing relative insignificance as justification.

It has been shown that this truncation can lead to incompleteness in the products and processes considered as high as 50% and errors as high as 10% in the final estimate (Dixit et al., 2010; Lenzen, 2000). This limitation does not prevent the process-based LCA from being a very useful and frequently used method, indeed several databases exist that facilitate process based LCA by providing energy intensity coefficients - measures of the net energy inputs involved in the manufacture and transportation of construction materials, normalised with respect to material mass or material volume, for example Hammond and Jones (2008). This permits the calculation of the embodied energy as shown in Equation 2.25.

$$\begin{aligned} &\underset{\text{MJ}}{\text{Embodied Energy}} = \\ &\sum_{\text{kg}} (\text{Mass of Component} \times \underset{\text{MJ/kg}}{\text{Energy Intensity Coefficient}}) \end{aligned} \tag{2.25}$$

For example, Yohanis and Norton (2002) use a process-based LCA in their analysis of the OE and EE of a generic single-storey office building in the UK. To permit the comparison between different analyses the system boundary conditions are generally chosen to start and end at some combination of the following boundaries (Dixit et al., 2010):

1. cradle - prior to raw material extraction
2. gate - at the entrance of the construction site (i.e. all materials have been processed and transported)
3. grave - after demolition and waste disposal

It is imperative that researchers make the boundaries clear in their analysis so that comparisons can be accurately made.

Input-Output Analysis

An input-output analysis does not suffer from the same truncation errors that a process analysis does because of the fundamentally different approach to assessing the impact of material and energy flows. Here, economic input-output data, resource input data and environmental output data are combined to form environmental flows from one industrial sector to another (Treloar et al., 2001b). This is then used to assess the impact of the processes involved in the product system based on the cost of each process, as shown in Equation 2.26.

$$\underset{\text{MJ}}{\text{Embodied Energy}} = \sum_{\pounds}(\text{Cost of Product} \times \underset{\text{MJ}/\pounds}{\text{Energy Intensity Coefficient}}) \tag{2.26}$$

Essentially, the embodied energy is taken as a fraction of the total energy used by the industrial sector responsible for that product (Yohanis and Norton, 2002). This approach results in a much more complete analysis but suffers from assumptions of homogeneity and proportionality, errors and uncertainty of economic data and aggregation and grouping of sectors, which can lead to errors of up to 50% (Dixit et al., 2010). Furthermore, considering the case of AVC which is a highly specialist section within industry, these assumptions are even less likely to represent the true costs of installation.

2.4.3 Embodied Energy Analysis

The importance of embodied energy relative to operating energy has been the subject of much research over the years (Junnila and Horvath, 2003; Scheuer et al., 2003; Cole and Kernan, 1996; Yohanis and Norton, 2002). Many of these papers have found that the embodied energy and carbon associated with a building are much smaller than the respective operating energy and carbon, for example Edwards and Bennett (2003) state that the construction products account for 10-20% of the total building environmental impact. This has led researchers to conclude

that efforts should be made to improve the operation phase efficiency at the expense of initial construction cost.

As a result, there has been an increased number of energy efficient appliances and improved insulation materials being utilised in buildings (Dixit et al., 2010; Dimoudi and Tompa, 2008). For example, Kneifel (2010) noted that conventional energy efficiency measures can reduce energy use by 20-30% without significant alterations to the building design, and the OE of some buildings entered for the Green Building Challenge was reduced to such an extent that construction products contributed 50% of the total building impact (Edwards and Bennett, 2003). This is not an isolated case: a study by Thormark (2002) found that the embodied energy of low energy buildings in Sweden accounted for 40% of the total energy for a life span of 50 years, and a study by Yohanis and Norton (2002) found that the EE of a generic single-storey office building in the UK could account for 40% of the total energy for a life span of 25 years, though this life span could be considered shorter than a realistic situation.

A recent paper by Jones (2011) found that the very significant projected reductions in greenhouse gas emissions from electricity production (DECC, 2010) are rarely accounted for by current whole life carbon studies for buildings. For example, it was shown how neglecting this year-on-year improvement could lead to overestimates of the operational carbon by 50% and 95% for a typical new domestic building and a new primary school respectively. Whilst it is important to note that the reductions are based purely on pathways for the UK to meet its 2050 80% reductions targets, they nevertheless provide a useful insight into the effect of assuming static emissions from electricity production.

Furthermore, Li et al. (2010) note that the impact of the EE may be more significant than the OE because of the intensity of the tasks related to EE, which typically occur over a much shorter period than the life span of the building.

The aforementioned improvements in OE efficiencies have led to a shift in em-

phasis of research towards improving the EE of a building. However, the results from different EE analyses vary greatly (Buchanan and Honey, 1994). For example Dixit et al. (2010) found that of the commercial buildings they investigated, the mean EE was 9.19GJ/m^2 with a standard deviation of 5.4GJ/m^2, indicating large variability in the calculated EE values.

2.4.4 Importance of Structural Components

Floor structures are a major component of any building and as such generally constitute a significant portion of the EE of the structure. However, the degree of this contribution varies from study to study. Yohanis and Norton (2002) investigated a single-storey office building in the UK and found the flooring related to just 7% of the EE. However, Treloar et al. (2001a) considered five multi-storey office buildings in Melbourne, of size 3, 7, 15, 42 and 52 storeys, and found that the floors represented between 28% and 45% of the structural EE. Further to this, Dimoudi and Tompa (2008) investigated two contemporary office buildings in Greece and found that the floor slabs were 27% and 35% of the total EE. In this study, the authors noted that these buildings had large supporting frame elements due to strict standards for earthquake protection. These frame elements are made of reinforce concrete which has a high contribution to the EE and so reduces the percentage contribution from the floor slabs.

The EE of the floors has also been presented as normalised with respect to floor area. For example, Dimoudi and Tompa (2008) calculated the EE of a typical floor, consisting of 0.02m plaster, 0.18m reinforced concrete, 0.02m mortar and 0.025m ceramic tiles as 671MJ/m^2. Similarly, the ground floor, which varied only by the addition of 0.05m extruded polystyrene was calculated as 830MJ/m^2. In addition to this, Lawson (1996) calculated that a 200mm precast concrete tee beam with infill, suitable for upper floors (Aye et al., 1999), would have an EE of 602MJ/m^2 whilst a 200mm hollow core precast floor with concrete topping, suitable for ground floors, would have an EE of 900MJ/m^2. These figures relate

well with the data calculated by Dimoudi and Tompa (2008).

The possible reduction in floor materials brought about by the use of AVC could have a secondary effect and result in a decrease in the amount of materials needed for columns and foundations. These components also contribute significantly to the overall structural EE. For example, for the two case studies considered by Dimoudi and Tompa (2008) the columns and foundations contributed a total of 18% and 24% of the overall EE in each building respectively. Similarly, Yohanis and Norton (2002) report that the substructure alone contributed 17% of the EE for the office building studied.

2.4.5 Previous Investigations into Cost of Active Control

Gomez-Rivas et al. (2002) state that present-day (in 2002) costs for installation and maintenance of control systems are relatively low. Eight years later and there has been very limited uptake from the industrial market which would suggest that costs may still be an issue. Despite this, there exists no comprehensive review of the costs of AVC for suppressing human-induced vibrations in civil engineering floors.

The priorities regarding the decision variables for cost evaluation of whole-structure control from seismic- or wind-induced vibrations differ greatly from those for control of human-induced vibration in floors. For example, the risk of event occurrence is of paramount importance in a cost evaluation for seismic applications but less so for human-induced vibrations as there are relatively good estimates of the frequency of excitation available. Further to this, the risk of control system failure is also more severe in seismic- and wind-induced vibrations than it is for human-induced vibrations. This clearly has a great impact on the overall cost effectiveness of a given control system.

There are a small number of investigations into the costs associated with AVC in seismic or wind applications. In one such investigation by Wen and Shinozuka

(1998), it was found that the AVC system for seismic-induced vibrations of the building in their investigation was only cost effective in the extreme situation that the building life was long and the consequences of failure were large.

The cost-effectiveness of AVC has also been investigated by Wells (1998) for environmental loading of a 127m footbridge in London. In this particular situation the slenderness of the bridge was very important and it was found that a total of 54 tonnes of steel could be removed from the structure with the control system in place for the cost of the control system. Unfortunately budget constraints prevented the realisation of these potential benefits.

2.4.6 Methods for Evaluating the Cost of Active Control

The choice of whether to incorporate AVC into the design of a floor structure can be considered as an investment choice between:

1. Don't install AVC. This incurs standard initial construction costs but no further costs can be expected afterwards.

2. Do install AVC. This achieves reduced initial construction costs but additional initial AVC installation costs and costs for maintenance and running of equipment expected afterwards.

The relative magnitude of these costs will dictate which option is better over the life of the building, as shown in Figure 2.24. Here, option 1 is considered as the benchmark and the relative cost of option 2 considered against this.

Only a small portion of the overall project is considered here (that which is affected by the installation of the AVC system) which means that this particular problem differs from many standard investment problems, which the investment criteria are designed for use with. From Figure 2.24 it is observed that installing AVC generates all the income it will ever generate in Year 1, and from then on incurs costs - this is the opposite of a financial investment where an initial expen-

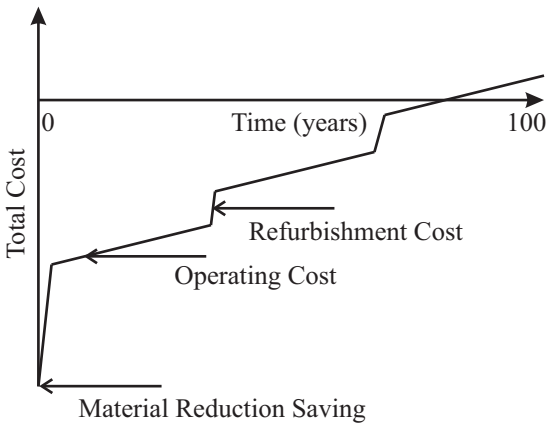

Figure 2.24: Projected Economic Costs over Life of Building

diture is offset by future income. In this closed case the "best" investment would be to invest for the shortest duration possible to avoid incurring significant costs, but clearly this is not desirable for a new building! For this reason, some evaluation figures commonly used in accountancy become less useful for understanding what is going on (e.g. the rate of return). Equally, there are some measures that have significant drawbacks in traditional accountancy but their use can be quite justified in this situation. For example, the payback period which is the time it takes to recoup the initial expenditure made on the project (Wright, 1973). The drawback of this method is that it ignores all cash flows after the payback period. However, when considering AVC installation, it is desirable that the payback period is *not* reached within the life of the building (else installing AVC is a poor investment). This means that only cash flows up to the payback period are of interest so that particular disadvantage is not a problem.

The payback method can be improved by accounting for the time value of money; this is the discounted payback method. It is well known that the present value of money is more than the future value (Wright, 1973; Mishan, 1988; Rogers, 2001). This is an important difference with an environmental assessment as the notion of discounting to account for the time value of costs tends not to be considered when calculating the energy consumed or CO_2 emitted as it would require a subjective weighting on the importance of these factors for future generations.

2.5 Concluding Remarks

This review has investigated the issues surrounding the inclusion of AVC into the design of new buildings as a means to increase performance for slender structures subject to human-induced vibration. The current guides for the design of floors from a vibration perspective were examined in Section 2.2 with the purpose of investigating ways in which AVC could be incorporated into the current design procedure. The optimisation procedure involved in the initial design of TMD's and similar passive devices was shown to be relatively simple and, by characterising the PVC as additional damping, permitted an intuitive process by which the response of the structure can be predicted. A method similar to this has yet to be realised for AVC, though significant progress towards this goal has been made. The relative complexity of actuator dynamics and the numerous control laws that exist are areas where further work is required in order to achieve simplified design guidance.

Section 2.3 considered the complexities of an AVC system, particularly discussing the different control laws, the issue of optimal actuator and sensor location and the current issues surround actuator technology. A number of approaches have been developed to manage some of the stability issues introduced by actuator dynamics, though this does not negate the necessary compromise needed between avoiding low frequency stroke saturation and performance of control of low frequency modes. So far, only DOFB controllers have been reported in literature for the mitigation of human-induced vibration in floors and while the performance of these controllers has been shown to be high, numerical tuning is often required to prevent stability issues. The use of model-based controllers, as used to mitigate seismic- and wind-induced vibrations in tall structures, is as yet relatively untested in this domain. However, this is likely to change as the trend of implementing more complicated controllers continues in the search for high performing robust controllers. This would allow greater control over problematic modes, but

extensive work is required to ensure that the controller remains effective even with the large model uncertainty that exists in floor structures, for example through the use of robust control techniques or adaptive control laws.

The final part to this review in Section 2.4 considered the environmental and economic impact of including AVC. Many advances have been made in the development of 'green' buildings. So far, these have focussed on improving the operating costs at the expense of embodied costs because this is where the biggest savings could be made. However, the embodied costs are becoming an increasingly important portion of the whole life-cycle cost of new buildings. As such there is a need for an assessment into the potential impact that incorporating AVC into new structures would have. LCA has been shown to be an effective method for the breakdown of factors that contribute to the overall environmental impact of a system and can be adapted to investigate AVC, in contrast with methods such as BREEAM which are more suitable for a comparative assessment of the overall environmental impact between a building and an arbitrary benchmark building. Current issues still surrounding the use of LCA are the appropriateness of the different analysis methods and the inconsistencies in embodied energy estimates. Any LCA of an AVC system would certainly have to take these aspects into consideration.

Chapter 3

A Comparison with Existing Technology

This chapter introduces a novel loading model that simulates the in-service loading within an office environment. This is utilised to compare the effectiveness of AVC with TMDs. The contents of this chapter are an adapted form of two conference papers, presented at the 5th World Conference of Structural Control and Health Monitoring (2010) and at SPIE Smart Structures/NDE (2012). Details of these papers are as follows:

M J Hudson and P Reynolds. Analytical and Experimental Evaluation of Active Vibration Control of an Office Floor Structure. In *Proceedings of 5th World Conference on Structural Control and Monitoring*, page 10047, Tokyo, 2010.

M J. Hudson, P Reynolds, and D S. Nyawako. Comparison of passive and active mass dampers for control of floor vibrations. In *Proceedings of SPIE 2012*, April 2012. doi: 10.1117/12.915956.

3.1 Introduction

Developments in recent years have allowed building engineers to design more slender elements in floor structures and still achieve ultimate limit state (ULS) requirements. However, these slender designs are more prone to excessive vibrations resulting from, for example, rotating machinery or pedestrians. When this leads to vibration serviceability requirements not being met, remediation techniques must be employed to deal with this. Typically, the problem is solved through the addition of supplementary concrete mass to the floor slab in order to increase the total mass of the dynamic system, or through the addition of columns and/or beams to increase the stiffness. The great expense and disruption caused by these methods have, in part, led to a need for alternative technologies. Two of these alternatives are tuned mass dampers (TMD), and active vibration control (AVC) with inertial mass actuators.

A TMD consists of a large mass attached to the main structure through a spring and a damping element. The mass, stiffness and damping values are chosen to target a particular mode of vibration such that the combination of the additional dynamic system and the original, problematic, mode results in two modes that have a lower overall response than the original mode.

TMDs have been used successfully to reduce the level of vibration in a large number of structures. However, with specific regards to TMD implementations on floors: Webster and Vaicaitis (1992) improved the response of a 16.8m long cantilevered steel/concrete composite floor by 60% through the use of four 850kg TMDs. These masses are equivalent to a mass ratio of 4.6% relative to the masses of the controlled structural modes. Hanagan et al. (2003) installed 14 liquid TMDs to control 2 structural modes in three 15.85m $\times$ 4.88m bays of an office floor. Setareh et al. (2006) demonstrated the use of Pendulum TMDs in two steel/concrete composite floors used as offices. Reductions of the vibration amplitude of 50% and 70% were recorded in each floor respectively. Importantly,

the second office floor utilised three TMDs, located at the centre of three separate bays, to control the dominant mode in each. Varela and Battista (2011) performed full-scale laboratory tests of multiple TMDs on a composite floor deck. Reductions of between 32% and 81% of the RMS acceleration were observed for the three different walking tests performed. There have also been several developments on a 'typical' TMD design in order to improve its performance and/or usability. For example, Chen et al. (2012) developed a TMD with a stiffness that could be adjusted by the addition of locking bolts to the coil mechanism used. Gad et al. (2012) developed a viscoelastic damper that was activated for very low levels of vibration (as would be expected in a floor environment) and had a sufficiently small height that it could fit between the floor slab and the false floor 150mm above. This was tested on a real office floor and achieved reductions in the peak structural acceleration of 40% in the bay tested.

The motion of the inertial actuators used in AVC generate a force that acts to reduce the response of the structure. This is achieved by measuring the structural response with accelerometers and using a given control law to generate a voltage signal that moves the inertial masses. This approach allows for a more broadband reduction in response with smaller, lighter, control units when compared with TMD technology. However, the technology is also more complicated and expensive than that of TMDs.

AVC has been used in several recent tests to improve the vibration performance of both bridges and floors. For example, Moutinho et al. (2007) implemented AVC on a stressed ribbon footbridge with two spans of 28m and 30m. Despite the actuators used not being optimal to control the structure having its first mode of vibration at 1Hz, a reduction of the peak response from 0.30m/s^2 to 0.19m/s^2 was achieved under walking excitation. This walking was tuned to match the problematic 4th vertical mode of vibration. Díaz et al. (2010) implemented AVC on the same footbridge that the TMD was implemented on by Casado et al. (2010) as described earlier. Here, reductions of 63% and 57% were achieved when the

structure was excited by walking at 1.75Hz and running at 3.5Hz respectively. Considering the case of floor structures, Hanagan and Murray (1998) successfully implemented AVC on a problematic office floor and a problematic laboratory floor. Reynolds et al. (2009) implemented AVC on a steel/concrete composite office floor. The bang-bang controller with a dead-zone nonlinearity was able to achieve a reduction of 49% of the maximum transient vibration value (MTVV) during walking tests tuned to the problematic mode of vibration, the MTVV being the maximum of the 1s running RMS of the structural acceleration. The same floor was controlled by Díaz and Reynolds (2010a) through the use of a compensated acceleration feedback controller. This achieved a 62% reduction in the MTVV when subject to walking tests. Further to this, in-service monitoring was conducted by Díaz and Reynolds (2010a) over a period of several days. Here it was found that the length of time spent above a response factor (defined in Equation 3.20) of 4 was reduced by 97% with active control.

This chapter investigates the advantages and disadvantages of each remediation method with regards to mitigating problematic human-induced floor vibrations in offices. A probabilistic force model is developed and used to simulate in-service loading on a finite element (FE) model of a typical office floor. The FE model and the force model are described in Section 3.2. Following from this, the design of each control technique is described in Section 3.4. The results of the analysis are described in Section 3.5 and conclusions are drawn in Section 3.6.

3.2 Description of Floor A

A typical office floor structure has been modelled using the FE software ANSYS (ANSYS, 2000), as shown in Figure 3.1. This is a composite structure of steel and concrete. A depth of 130mm has been used for the composite slab that spans between the long-span asymmetric cellular secondary beams. These are 748 $\times$ 152 / 210 $\times$ 72.2ACB and the short-span primary beams are 457 $\times$ 191 $\times$ 74UB. Full-height partitions and a lift shaft and staircase core have been added to make

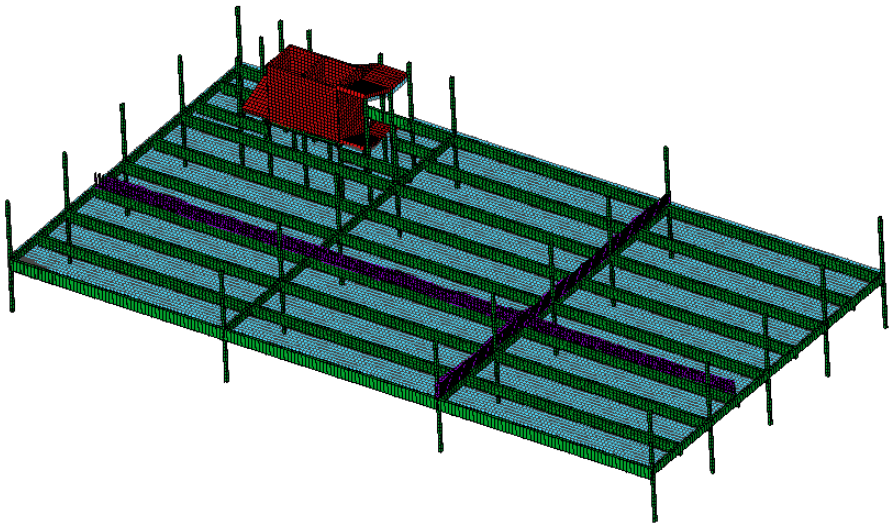

Figure 3.1: FE model of Floor A

the mode shapes more realistic by splitting up the very regular and global modes that would otherwise be expected from the bay layout in this structure. A modal analysis of this structure was performed and the results of this are shown in Figure 3.2.

The modal data for the first 25 modes of vibration were used to construct the state space model that represents this structure's dynamics. This corresponds to all modes with natural frequency less than 20Hz. This frequency cut off is higher than is recommended in the current guidance (Smith et al., 2007; Willford et al., 2006; Pavić and Willford, 2005). However, recent research (Živanović and Pavić, 2009) has questioned the suitability of this truncation, showing that even 'low frequency floors' such as this one can have a significant portion of the response attributed to the higher frequency modes. It was not possible to include more modes than this due to computational constraints. A damping ratio of 2% was assumed for all modes of vibration. In comparison with this assumed value, the SCI P354 guidelines (Smith et al., 2007) recommend using a value of 1.1% for bare floors and 3.0% for fully fitted out floors. Given the large areas of open-plan office space in this model, a damping ratio of 3.0% is unlikely to be achieved, so

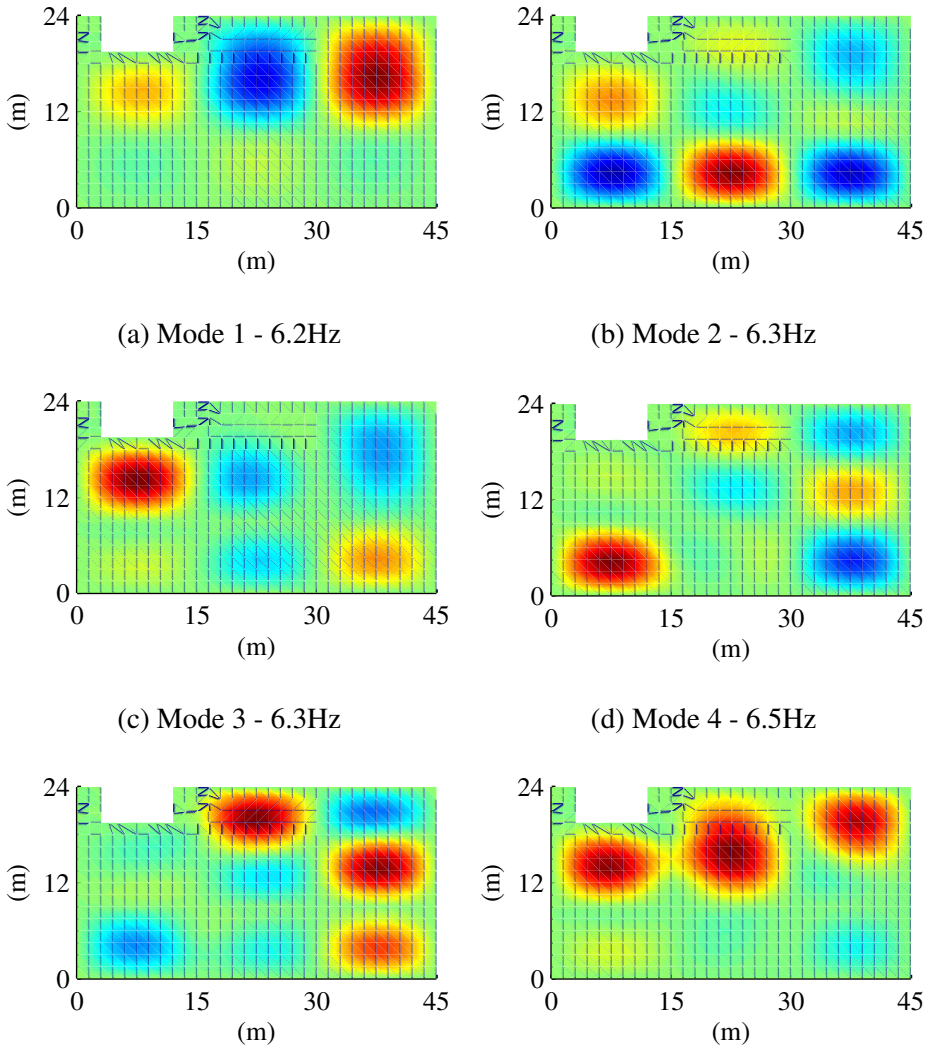

(a) Mode 1 - 6.2Hz

(b) Mode 2 - 6.3Hz

(c) Mode 3 - 6.3Hz

(d) Mode 4 - 6.5Hz

(e) Mode 5 - 6.6Hz

(f) Mode 6 - 6.9Hz

Figure 3.2: First six modes of Floor A

a more moderate 2.0% has been chosen.

3.3 Development of the Simulation Model

3.3.1 Plant Model

The natural frequencies, mode shapes and modal masses predicted by the FE model and damping ratios from experimental modal analysis (EMA) were used

to create a simulation model of the floor. This model is a transfer function relating the inputs (applied forces) to the outputs (accelerations). In this situation a modal plant (i.e. modal input to modal output) is used to facilitate using a roving applied force, as is discussed in Section 3.3.2.

First, it is useful to appreciate the origins of the plant transfer function. The real floor is a continuous system; however, this is approximated to a multiple degrees of freedom (MDOF) system by the FE software. In general, a multi-degree of freedom dynamic system, consisting of n nodes with one (vertical) degree of freedom per node, can be represented as:

$$\begin{bmatrix} m_{11} & m_{12} & \cdots & m_{1n} \\ m_{21} & m_{22} & \cdots & m_{2n} \\ \vdots & \vdots & \ddots & \vdots \\ m_{n1} & m_{n2} & \cdots & m_{nn} \end{bmatrix} \begin{Bmatrix} \ddot{y}_1(t) \\ \ddot{y}_2(t) \\ \vdots \\ \ddot{y}_n(t) \end{Bmatrix} + \begin{bmatrix} c_{11} & c_{12} & \cdots & c_{1n} \\ c_{21} & c_{22} & \cdots & c_{2n} \\ \vdots & \vdots & \ddots & \vdots \\ c_{n1} & c_{n2} & \cdots & c_{nn} \end{bmatrix} \begin{Bmatrix} \dot{y}_1(t) \\ \dot{y}_2(t) \\ \vdots \\ \dot{y}_n(t) \end{Bmatrix} + \begin{bmatrix} k_{11} & k_{12} & \cdots & k_{1n} \\ k_{21} & k_{22} & \cdots & k_{2n} \\ \vdots & \vdots & \ddots & \vdots \\ k_{n1} & k_{n2} & \cdots & k_{nn} \end{bmatrix} \begin{Bmatrix} y_1(t) \\ y_2(t) \\ \vdots \\ y_n(t) \end{Bmatrix} = \begin{Bmatrix} f_1(t) \\ f_2(t) \\ \vdots \\ f_n(t) \end{Bmatrix} \tag{3.1}$$

However, it is often easier to write this in the form of matrices:

$$[M]\{\ddot{Y}(t)\} + [C]\{\dot{Y}(t)\} + [K]\{Y(t)\} = \{F(t)\} \tag{3.2}$$

The deflection at a location, v, can be represented as a linear combination of the mode shapes at that location, ϕ_{vi}, and the modal amplitude $\eta_i(t)$, i.e.

$$y(v,t) = \sum_{i=1}^{m} \phi_{vi}\eta_i(t) \tag{3.3}$$

where m is the number of modes. For the displacement at n locations this results

in:

$$\begin{Bmatrix} y_1(t) \\ y_2(t) \\ \vdots \\ y_n(t) \end{Bmatrix} = \begin{bmatrix} \{\phi_{11} & \phi_{12} & \cdots & \phi_{1m}\} \\ \{\phi_{21} & \phi_{22} & \cdots & \phi_{2m}\} \\ & & \vdots & \\ \{\phi_{n1} & \phi_{n2} & \cdots & \phi_{nm}\} \end{bmatrix} \begin{Bmatrix} \eta_1(t) \\ \eta_2(t) \\ \vdots \\ \eta_m(t) \end{Bmatrix} \tag{3.4}$$

Defining

$$[\Phi] = \begin{bmatrix} \{\phi_{11} & \phi_{12} & \cdots & \phi_{1m}\} \\ \{\phi_{21} & \phi_{22} & \cdots & \phi_{2m}\} \\ & & \vdots & \\ \{\phi_{n1} & \phi_{n2} & \cdots & \phi_{nm}\} \end{bmatrix} \tag{3.5}$$

we arrive at

$$\begin{aligned} \{Y(t)\} &= [\Phi]\{H(t)\} \\ \{\dot{Y}(t)\} &= [\Phi]\{\dot{H}(t)\} \\ \{\ddot{Y}(t)\} &= [\Phi]\{\ddot{H}(t)\} \end{aligned} \tag{3.6}$$

which represents the conversion between physical responses and modal responses. Substituting Equation 3.6 into Equation 3.2 and premultiplying by $[\Phi]^T$ yields:

$$[\Phi]^T[M][\Phi]\{\ddot{H}(t)\} + [\Phi]^T[C][\Phi]\{\dot{H}(t)\} + [\Phi]^T[K][\Phi]\{H(t)\} = [\Phi]^T\{F(t)\} \tag{3.7}$$

This can be simplified by assuming orthogonality of mode shapes and proportional damping to

$$[M_m]\{\ddot{H}(t)\} + [C_m]\{\dot{H}(t)\} + [K_m]\{H(t)\} = \{F_m(t)\} \tag{3.8}$$

where

$$[M_m] = [\Phi]^T[M][\Phi] = \begin{bmatrix} m_1 & 0 & \cdots & 0 \\ 0 & m_2 & \cdots & 0 \\ \vdots & \vdots & \ddots & \vdots \\ 0 & 0 & \cdots & m_m \end{bmatrix} \tag{3.9}$$

and

$$[C_m] = [\Phi]^T[C][\Phi] = \begin{bmatrix} c_1 & 0 & \cdots & 0 \\ 0 & c_2 & \cdots & 0 \\ \vdots & \vdots & \ddots & \vdots \\ 0 & 0 & \cdots & c_m \end{bmatrix} \tag{3.10}$$

and

$$[K_m] = [\Phi]^T[K][\Phi] = \begin{bmatrix} k_1 & 0 & \cdots & 0 \\ 0 & k_2 & \cdots & 0 \\ \vdots & \vdots & \ddots & \vdots \\ 0 & 0 & \cdots & k_m \end{bmatrix} \tag{3.11}$$

and

$$\{F_M(t)\} = [\Phi]^T\{F(t)\} \tag{3.12}$$

where m_i, c_i and k_i are the modal mass damping and stiffness for each mode. The MDOF system has therefore become de-coupled into m independent single degree of freedom (SDOF) systems. Therefore, by substituting $c_i = 2m_i\omega_{n_i}\zeta_i$ and

$k_i = m_i\omega_{n_i}^2$, Equation 3.8 can be rewritten as:

$$\{\ddot{H}(t)\} + [C^*]\{\dot{H}(t)\} + [K^*]\{H(t)\} = \{F_M(t)\} \tag{3.13}$$

where

$$\begin{aligned}[C^*] &= [M_m]^{-1}[C_m] \\ &= \begin{bmatrix} 2\zeta_1\omega_{n_1} & 0 & \cdots & 0 \\ 0 & 2\zeta_2\omega_{n_2} & \cdots & 0 \\ \vdots & \vdots & \ddots & \vdots \\ 0 & 0 & \cdots & 2\zeta_m\omega_{n_m} \end{bmatrix}\end{aligned} \tag{3.14}$$

and

$$\begin{aligned}[K^*] &= [M_m]^{-1}[K_m] \\ &= \begin{bmatrix} \omega_{n_1}^2 & 0 & \cdots & 0 \\ 0 & \omega_{n_2}^2 & \cdots & 0 \\ \vdots & \vdots & \ddots & \vdots \\ 0 & 0 & \cdots & \omega_{n_m}^2 \end{bmatrix}\end{aligned} \tag{3.15}$$

where ζ_i is the damping ratio for mode i and ω_{n_i} is the natural frequency of mode i. At this point it is worth noting that the MDOF system has been fully described using only the modal mass, damping, frequencies and mode shapes, all of which are either outputs from the FE model or (in the case of damping) estimated.

This second order differential equation can be represented in state space form as a first order differential equation. For a linear time-invariant (LTI) system the state space equations are of the general form

$$\begin{aligned}\dot{\mathbf{x}}(t) &= \mathbf{A}\mathbf{x}(t) + \mathbf{B}\mathbf{u}(t) \\ \mathbf{y}(t) &= \mathbf{C}\mathbf{x}(t) + \mathbf{D}\mathbf{u}(t)\end{aligned} \tag{3.16}$$

where

$\mathbf{x}(t)$, $\mathbf{u}(t)$ and $\mathbf{y}(t)$ are the internal state vector, input vector and output vector respectively

$\mathbf{A}$, $\mathbf{B}$, $\mathbf{C}$, $\mathbf{D}$ are the state matrix, input matrix, output matrix and direct transmission matrix respectively,

For the dynamic system in this work, the state space equation is derived by rearranging Equation 3.8 for $\{\ddot{H}(t)\}$ and using the state vector

$$\mathbf{x}(t) = \left\{ \begin{array}{c} H(t) \\ \dot{H}(t) \end{array} \right\} \tag{3.17}$$

When the modal velocity, $\dot{H}$ is chosen as the output, this yields

$$\begin{aligned} \left\{ \begin{array}{c} \dot{H}(t) \\ \ddot{H}(t) \end{array} \right\} &= \left[\begin{array}{cc} 0 & I \\ -K^* & -C^* \end{array} \right] \left\{ \begin{array}{c} H(t) \\ \dot{H}(t) \end{array} \right\} + \left[\begin{array}{c} 0 \\ I \end{array} \right] F_M(t) \\ \mathbf{y}(t) &= \left[\begin{array}{cc} 0 & I \end{array} \right] \left\{ \begin{array}{c} H(t) \\ \dot{H}(t) \end{array} \right\} + [0] F_M(t) \end{aligned} \tag{3.18}$$

This state space system was transformed to transfer function form and multiplied by the Laplace operator 's' to finally produce the modal equation for the plant. The output of this modal plant is then converted back to physical accelerations through Equation 3.6, as is shown in Figure 3.3. This demonstrates the general procedure used for simulations, namely that:

- the output from the modal structural model is converted to physical accelerations;
- the physical accelerations corresponding to the locations of the control systems are isolated and used to calculate the physical force imparted by each control system;

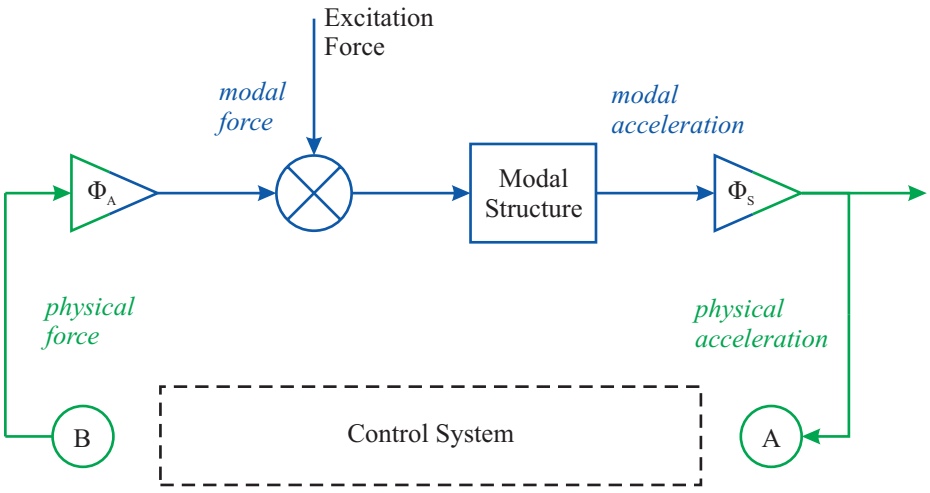

Figure 3.3: Block Diagram of Simulation Model

- the physical control forces are converted to modal control forces;
- and finally the modal control forces are summed with the modal excitation force to get the resultant modal force which is applied as the input to the modal structural model.

3.3.2 Input Force

In order to assess the vibration serviceability of the floor with all control configurations it was decided to simulate typical in-service loading using a probabilistic force model (Živanović et al., 2007). Here, multiple pedestrians were simulated simultaneously with their walking path determined by random start and end points. Rather than a simple linear path from start to end, the route taken by each pedestrian is based around a set of predefined 'corridors' that aim to simulate the walking paths in an office environment more closely. Naturally, the choice of desk layout is a subjective choice so the results of this analysis are one of infinitely many possibilities. However, a sensible choice of corridor paths can provide a solution that is representative of what could be expected in a real office environment. The choice of corridors used in these scenarios are shown in Figure 3.4a and an example of typical walking paths is shown in Figure 3.4b.

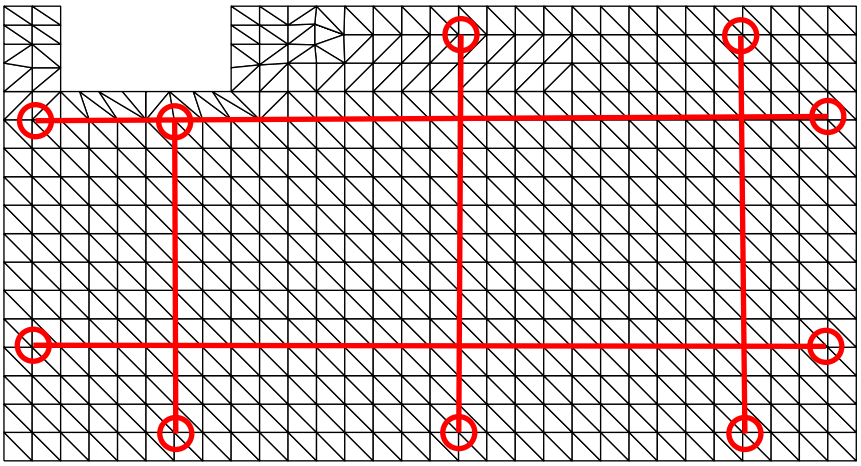

(a) Corridors

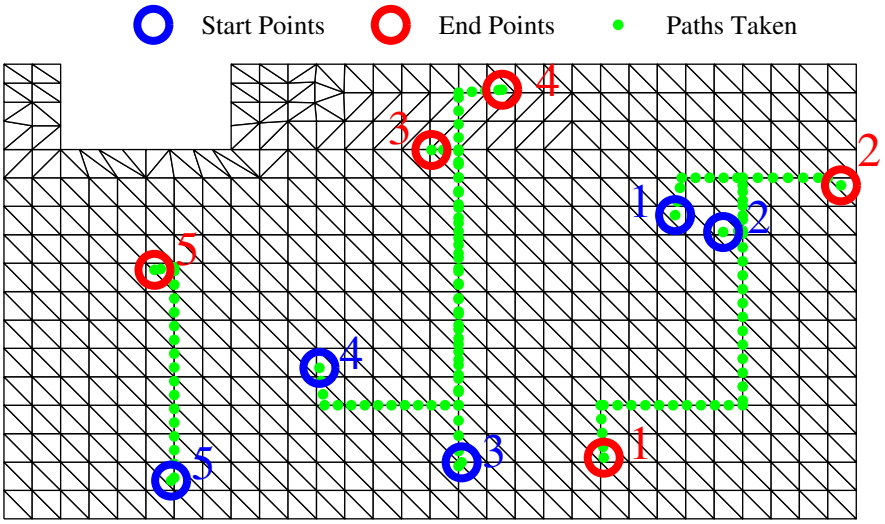

(b) Typical walking paths

Figure 3.4: Examples of Simulation Method Used

A more comprehensive discussion of this force model is provided in Section 4.4.3 where the number of people walking per minute is calibrated to match experimental results. However, the key parameters are also discussed here.

There are several parameters that define the nature of the walking force time history that have a variable value in this probabilistic analysis, all of which are cho-

sen independently for each pedestrian. The walking frequency and stride length are both set as normal distributions with mean values of 1.87Hz and 0.71m and standard deviations of 0.186Hz and 0.071m respectively (Živanović et al., 2007). The weight of each pedestrian is also set as a normal distribution: here, the mean weight was set as 76.7kg and standard deviation of 19.4kg which is based on NHS statistics for the UK (NHS Information Centre, 2010). The number of people starting to walk on the structure was set to be 5 every minute for a 1000m^2 office area. This was based on the results in Section 4.4.3 as discussed earlier. The start times themselves were distributed evenly throughout the entire time history. However, it is important to note that the end times for each pedestrian's route are determined by the walking frequency, stride length and total distance to travel (i.e. start and end point locations), and as such the number of people walking at any time will vary. One hour of walking was simulated but, for simplicity of data manipulation, this was divided up into six analyses lasting 10 minutes each. Whilst the start and end of each smaller analysis will be slightly different from the equivalent time in one long analysis, the effect is minimal when compared with the overall time history. It is important to note that the same walking time history was used for each subsequent analysis once it had been randomly generated for the first run - this was done to allow for a true comparison between the control configurations.

The force applied to the structure varied both spatially and temporally. To account for this, the contribution to each mode due to the force at a given moment in time was calculated; that is the walking force-time history was converted into a modal force-time history. This is then the input used in the simulation model, as can be seen in Figure 3.3 which is the reason why the model of the structure is a *modal* plant model.

3.3.3 Response calculation

The acceleration response of the structure subject to the walking excitation is calculated at a grid of points through the structure for each control configura-

tion. Recall that the same input force is used in each configuration so it is only the control that affects the structural response. The structural response was then weighted using the W_b frequency weighting (BSI, 2008) for vertical accelerations and based on this the running root mean square (RMS) was calculated. The most recent British standard (BSI, 2008) recommends the use of the vibration dose value (VDV) for evaluation of structural response. However, in addition to this, the Response (R) factor is also a useful measure of the vibration level. The formulations for these are described in Equations 3.19 and 3.20.

$$\text{VDV} = \left(\int_0^{T_t} {a_w}^4(t) dt \right)^{0.25} \tag{3.19}$$

where:

VDV is the Vibration Dose Value, m/s$^{1.75}$

$a_w(t)$ is the frequency weighted acceleration response of the structure in the time domain, m/s^2

T_t is the total time period, s

$$\text{R} = \max_t \left(\left(\int_{t-T/2}^{t+T/2} {a_w}^2(t) dt \right)^{0.5} \right) \times \frac{1}{0.005} \tag{3.20}$$

where:

R is the Response factor

T is the period used for the running RMS, s

When calculating the VDV it is usual to compare the value to that covered over a 16 hour day and the recommended acceptability limits proposed in design guides, for example as shown in Table 3.1. In order to convert the VDVs calculated in the simulations here with the VDV ranges in the guidance, the calculated VDVs must

be multiplied by a scaling factor given by Equation 3.21.

$$\text{VDV Scaling Factor} = \left(\frac{16 \times 60 \times 60}{T_t}\right)^{0.25} \tag{3.21}$$

Table 3.1: Range of VDV values that might cause adverse comments in offices (BSI, 2008)

Place and time	Low probability of adverse comment	Adverse comment possible	Adverse comment probable
Office building, 16h day	0.4 to 0.8	0.8 to 1.6	1.6 to 3.2

In addition, BSI (1992) recommends a maximum R factor for offices subject to continuous vibration (16h day, 8h night) as 4. It should be noted that BSI (2008) dropped the use of R factor in favour of the VDV limit, though in practice the R factor is still a commonly used vibration serviceability criterion as indicated by its inclusion in modern design guidance documents, such as Willford and Young (2006), Smith et al. (2007) and Pavić and Willford (2005). Most of these guidance documents recommend using a R factor limit of 4 in accordance with (BSI, 1992). However, Smith et al. (2007) recommends that for "busy offices" a more relaxed limit of 8 be used instead. This doubling of acceptable response significantly increases the probability of adverse comment. Indeed, recent research by Reynolds and Pavić (2011) into a rather lively floor that had attracted complaints from occupants found the average R factor over several days' monitoring was 7.83: only just below the limit recommended by Smith et al. (2007).

3.4 Vibration Controller Design

3.4.1 Tuned Mass Damper

A general schematic for the TMD control system is shown in Figure 3.5. Given that the structure has many modes of vibration within the frequency band excitable

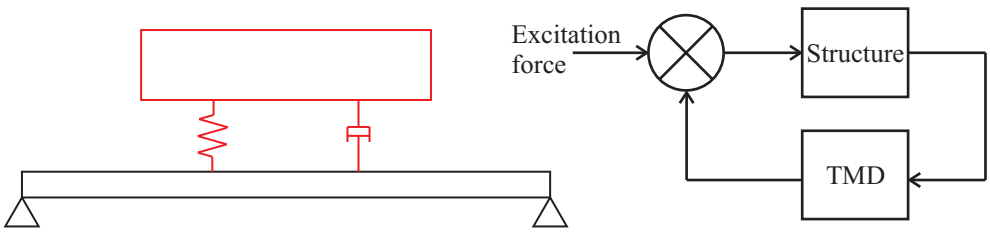

Figure 3.5: TMD Schematic

by human walking, multiple TMDs are required to successfully reduce the structural response over the entire structure. The parameters to optimise here are the mass, stiffness and damping of each TMD utilised. The mass of the TMD effectively relates to the performance: the higher the TMD mass the more reduction in response can be achieved. However, there are obvious physical limits on the practical size and weight of TMDs, therefore generally the maximum feasible size TMD is chosen.

With regards to the frequency and damping characteristics of the TMD, these parameters are chosen independently for each TMD and through the use of Den Hartog's formulae, as shown in Equations 3.22 and 3.23.

$$f_{opt} = \frac{1}{1+\mu} \tag{3.22}$$

$$\zeta_{opt} = \sqrt{\frac{3\mu}{8(1+\mu)}} \tag{3.23}$$

where:

f_{opt} is the optimum TMD frequency ratio, relative to the modal frequency it is tuned to

μ is the mass ratio: the mass of the TMD relative to the modal mass

ζ_{opt} is the optimum TMD damping ratio.

In order to simulate the effect of the TMD on the system, a model must be derived to equate the output from the structure, namely the structural acceleration, to the

force that is applied to the structure as a result of the movement of the TMD. This is derived below.

The equation of motion for a TMD of mass m_T, damping c_T and stiffness k_T is:

$$m_T\ddot{y_T}(t) + c_T(\dot{y_T}(t) - \dot{y}(t)) + k_T(y_T(t) - y(t)) = 0 \tag{3.24}$$

where $y_T(t)$ and $y(t)$ are the displacement of the TMD and the base structure respectively. This can be rearranged to give:

$$m_T\ddot{y_T}(t) + c_T\dot{y_T}(t) + k_T y_T(t) = c_T\dot{y}(t) + k_T y(t) \tag{3.25}$$

Applying the Laplace transform s with zero initial conditions assumed gives:

$$m_T\mathcal{Y}_\mathcal{T}s^2 + c_T\mathcal{Y}_\mathcal{T}s + k_T\mathcal{Y}_\mathcal{T} = c_T\mathcal{Y}s + k_T\mathcal{Y} \tag{3.26}$$

Collecting like terms and rearranging gives:

$$\frac{\mathcal{Y}_\mathcal{T}}{\mathcal{Y}} = \frac{c_T s + k_T}{m_T s^2 + c_T s + k_T} \tag{3.27}$$

Dividing through by m_T and using the relationships $c_T = 2\zeta\omega_n m_T$ and $k_T = m_T\omega_n^2$ gives:

$$\frac{\mathcal{Y}_\mathcal{T}}{\mathcal{Y}} = \frac{2\zeta\omega_n s + \omega_n^2}{s^2 + 2\zeta\omega_n s + \omega_n^2} \tag{3.28}$$

Now, to derive a relationship between the acceleration of the structure, A, and the force imparted by the TMD onto the structure, F, we have:

$$\frac{F}{A} = \frac{m_T\mathcal{Y}_\mathcal{T}s^2}{\mathcal{Y}s^2} = \frac{m_T\mathcal{Y}_\mathcal{T}}{\mathcal{Y}} = \frac{m_T(2\zeta\omega_n s + \omega_n^2)}{s^2 + 2\zeta\omega_n s + \omega_n^2} \tag{3.29}$$

It should be noted that, for simplicity, the properties of the TMD are assumed to be linear. One of the problems cited with TMDs is that the damping elements used often restrict movement of the mass at low amplitudes; meaning that a minimum

level of vibration is required to activate the TMD (Eyre and Cullington, 1985). These simulations do not account for this as it is difficult to quantify at exactly what vibration level the friction will be overcome and so are therefore potentially slightly optimistic with regards to TMD performance for low response levels.

3.4.2 Active Vibration Control

A general schematic for the AVC control system is shown in Figure 3.6. This does not go into the detail of Figure 3.3 which includes conversion between physical and modal space. However, it can be seen that the 'Control System' represented between points A and B in Figure 3.3 is represented by the 'Actuator' and 'Control Law' blocks of Figure 3.6.

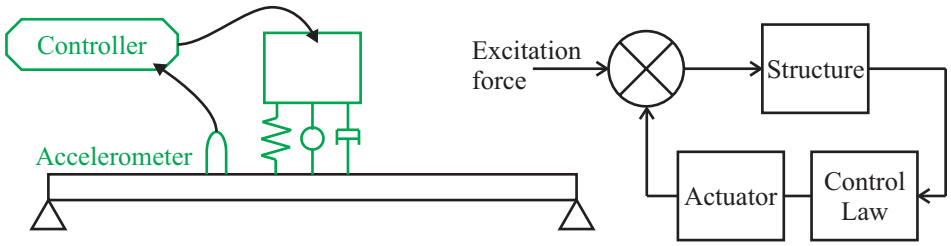

Figure 3.6: AVC Schematic

Specifically, this controller is detailed in Figure 3.7. The active control configu-

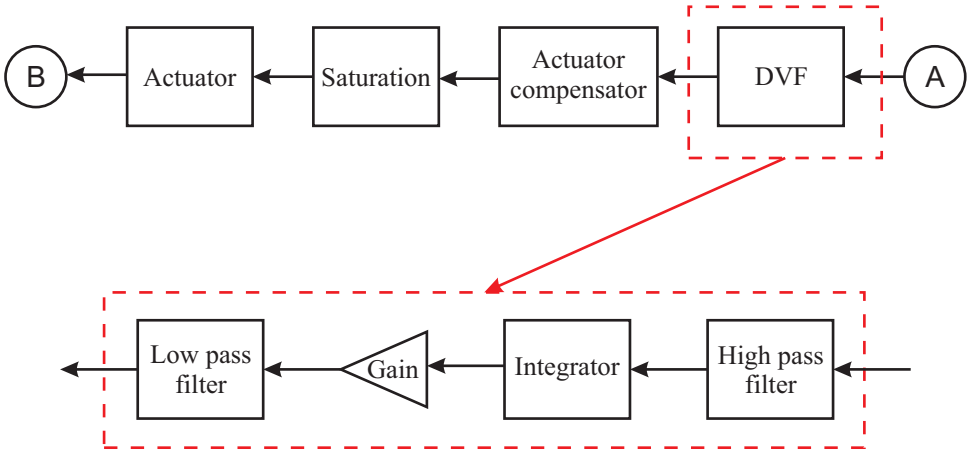

Figure 3.7: Schematic for AVC controller

ration consists of several collocated actuator and sensor pairs which act indepen-

dently to reduce the response at each location; thus resulting in a decentralised multiple input-multiple output (MIMO) controller, as shown in Figure 3.8. The

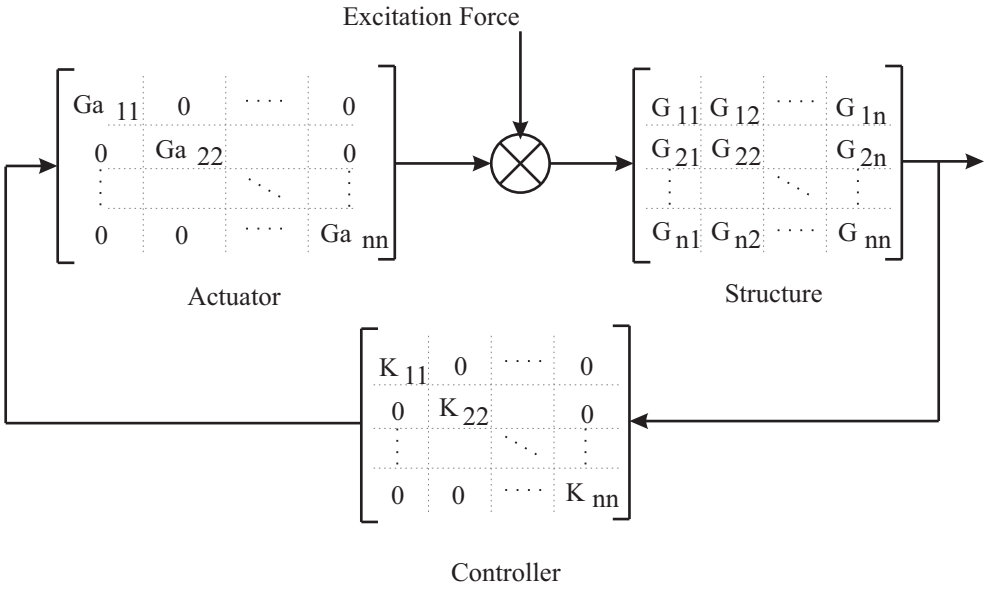

Figure 3.8: Decentralised AVC configuration

feedback gain for each control loop was initially chosen by considering the actuator/sensor pair in isolation and aiming to maximise the gain with the constraints of minimum gain margin being 2.0 and minimum phase margin being 30°. However, the structural system does not act independently at each control location; a force applied at one location will have a finite influence on the structural response at another location for every mode that has non-zero components at both locations. This can have the effect of reducing the stability margins. Therefore the feedback gain for all controller loops was reduced by the same percentage until the initial desired stability criteria were achieved.

The actuators used in the experiments were Model 400 electrodynamic shakers manufactured by APS Dynamics. These apply a force to the structure through the acceleration of an inertial mass that is attached to the shaker armature. The acceleration of the mass is caused by the force produced when a current-carrying coil moves in a magnetic field (Preumont, 2002). The actuator properties can be modelled by a third order transfer function for the force applied to the structure,

given an applied voltage:

$$G_a(s) = \frac{F}{V} = \frac{-\psi s^2}{s^2 + 2\zeta_a \omega_a s + \omega_a^2} \cdot \frac{1}{s + \varepsilon} \tag{3.30}$$

where $\psi = 15000$N/V is the force-voltage characteristic for the shaker, $\zeta_a = 0.6$ is the damping ratio for the shaker $\omega_a = 11.31$rad/s is the natural frequency of the shaker and $\varepsilon = 8 \times 2\pi$ is a lag term introduced by driving the actuators in voltage mode.

The control law used is a direct output feedback controller based on direct velocity feedback (DVF). Collocated actuator/sensor pairs are used with this control law to significantly improve stability, and independent controllers have been designed for each actuator/sensor pair which results in a decentralised MIMO controller. The inputs to the controller are the acceleration from each accelerometer. These are passed through a 2$^{\text{nd}}$ order high pass Butterworth filter with a 1Hz frequency cut off to remove very low frequency components. An integrator then converts this filtered acceleration into a filtered velocity. The dynamics of the shaker as it comes in its purchased state are not ideal for this control implementation, so are modified through the use of a compensator. The work by Díaz et al. (2012a) investigates actuator compensators and provides some recommendations for suitable actuator properties that reduce low frequency stroke saturation and instability. A compensator was therefore designed to achieve effective actuator dynamics of a natural frequency of 1.3Hz and a damping ratio of 0.7. Additionally, the low pass component of the actuator is shifted from 20Hz to 50Hz. The design of this compensator was through pole-zero cancellation of the measured undesirable actuator dynamics. This effect this compensator has is demonstrated in Figure 3.9. It is important to note the differing scales on the horizontal and vertical axes as this has the effect of disguising the increased damping associated with the new complex poles compared with a graph with equal axes. The original poles of the actuator are wiped out through the choice of zeros in the compensator and new poles are

applied as the poles of the compensator. This has an important effect on the actuator dynamics, as seen in Figure 3.10. The magnitude plots demonstrate how a

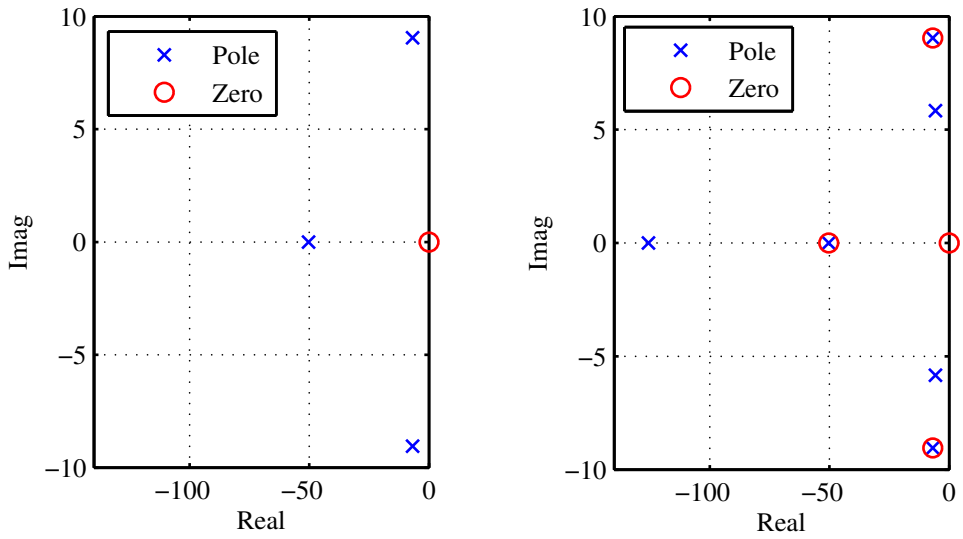

(a) Actuator Only (b) Actuator + Compensator

Figure 3.9: Pole Zero plots for Actuator and Compensator

larger force, relative to the peak force at low frequency, is achieved with the compensator which helps to increase performance at these frequencies. Alternatively, it could be thought of increasing stability for a given level of performance because the actuator will have a reduced force output (and hence stroke) at lower frequencies which can often be a problem when the finite dimensions of the actuator are taken into consideration. Additionally, the reduced roll off at higher frequencies means that there is a reduced additional phase lag between 4 and 10Hz which is an important frequency band for control. This means that the control law implemented will be more effective in this region. A 1^{st} order low-pass Butterworth filter with a 50Hz frequency cut off was used to restrict the control effort to the frequency range of interest. The feedback gain was chosen specifically for each individual feedback loop such that the gain margin and phase margins were at least 2 and 30° respectively. However, the interactions between each controller need to be considered also. These can act to destabilise the controller and so the gener-

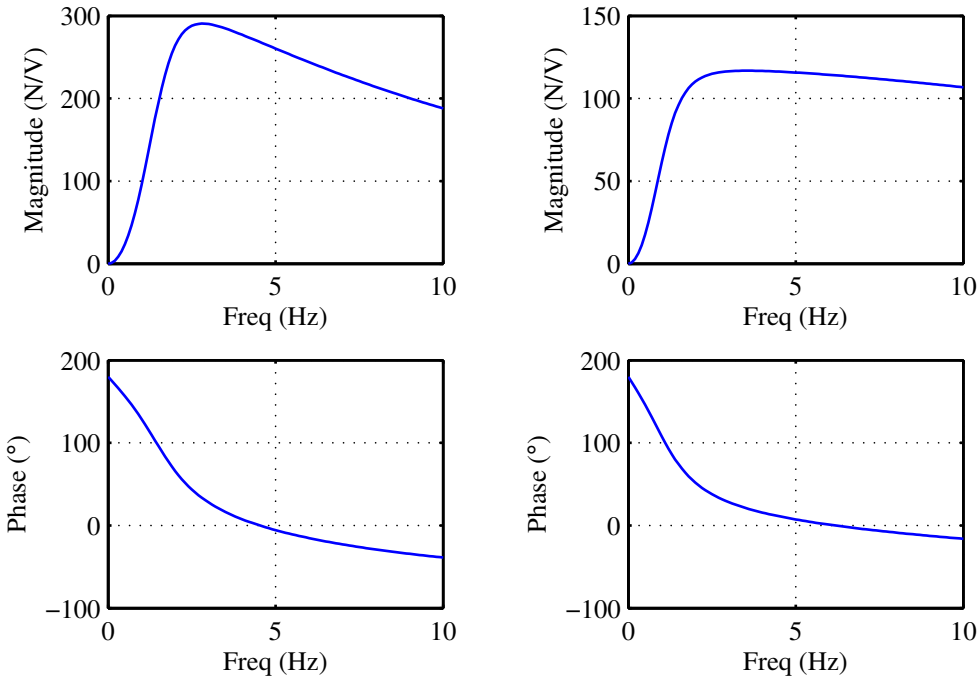

(a) Actuator Only (b) Actuator + Compensator

Figure 3.10: Bode plots for Actuator Dynamics

alised Nyquist criterion was used to assess the stability of the global controller. Here, the gains for each controller were then equally scaled to achieve the same gain and phase margin. Finally, the non-linearities of the actuators, namely force and stroke saturation, must be considered. For this reason, the output command voltages that drive each actuator are passed through a saturation non-linearity at 2V.

3.5 Results

A number of control configurations were simulated. These include the base case with no control at all, 3 TMD configurations and 1 AVC configuration.

3.5.1 Uncontrolled

The response of the structure with no control is presented first in Figure 3.11. Here, the maximum R factor for a 1s RMS period has been shown and a non-linear colour scheme has been used to emphasise the boundary for R=4 which is considered the upper limit for R factors for a high quality office environment.

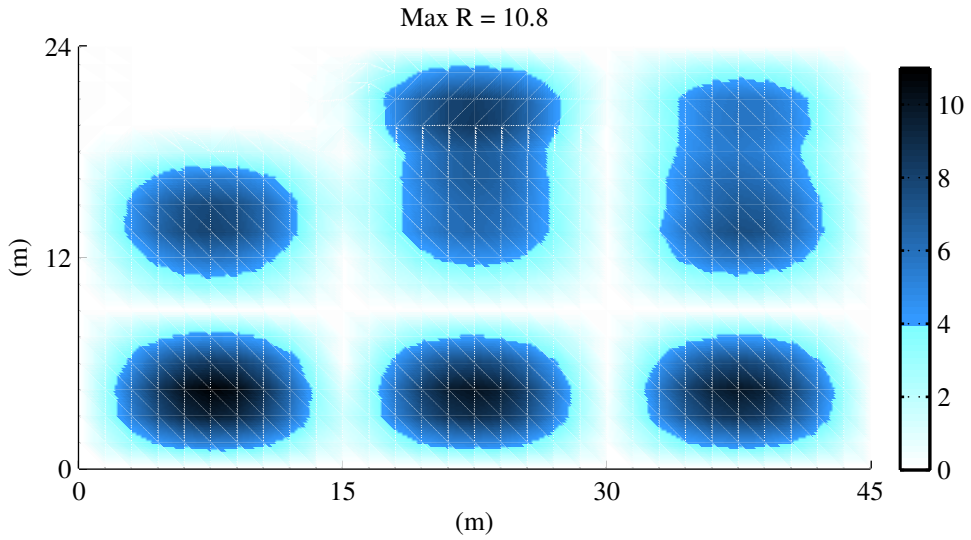

Figure 3.11: Contour of response of structure with no control

3.5.2 TMD configuration

The response is high in a number of locations. As such, multiple TMDs are required to reduce the response at all these high-response locations. Preliminary investigations indicate that the first 9 modes (with a frequency range of 5.6Hz to 10.5Hz) need to be controlled for the response to be reduced sufficiently. Therefore, by assigning one TMD to each mode of vibration, the minimum number of TMDs required is 9. The locations of the TMDs were chosen to be the antinodes of each mode they were tuned to, in order to maximise their effectiveness. However, by examining Figure 3.2 it is apparent that the antinode for Mode 2 coincides with the antinode for Mode 7. In order to simulate a physically realisable system

Table 3.2: Range of TMD masses for various mass ratios

Mass Ratio	Range of TMD masses, kg	Total Mass of all TMDs, kg
1%	220 - 420	3066
2%	440 - 840	6132
3%	660 - 1260	9198

the TMD for mode 2 was relocated to $(37.5, 4.5)$ which it can be seen is nearly an antinode also. In addition to this, the TMD for mode 9 had to be relocated to $(37.5, 21.0)$. This is because when it was located at the antinode of Mode 9 $(37.5, 12.0)$ a particularly high response was observed in the $(37.5, 21.0)$ region. Moving the TMD to this location did not reciprocate the problem at $(37.5, 12.0)$. The final TMD locations are shown by the red crosses in Figure 3.14.

It is not apparent what mass ratio will achieve the required reductions in response. Table 3.2 shows the range of expected TMD masses based on the modal masses of the first 9 modes for various mass ratios. The performance of each TMD system with the proposed mass ratios is shown by the point accelerance frequency response function (FRF) in Figure 3.12.

The results shown in Figure 3.12 show that as the mass of the TMD increases, so too does the reduction in response at the frequency that the TMD is tuned to: at this location the TMD is tuned to the second mode at 6.50Hz. The FRF at 8-9Hz does not decrease in a similar fashion; in fact, the peak is actually higher for the larger TMD mass. This is because of the effect from nearby TMDs causing a detrimental effect in the response at this location - with the significance of this degradation increasing with the increasing TMD mass. This point is demonstrated in Figure 3.13. Here, the first three lines show the uncontrolled case and the cases for a single TMD tuned to the second mode at 6.50Hz at $(37.5, 4.5)$ with mass ratio of 1% and 3%. Here it is seen that the peak due to the 6.50Hz mode is increasingly reduced with TMD mass, and the response of the higher frequency modes are also slightly decreased due to the damping elements within the TMD. Importantly, the response at the antiresonance at about 8.5Hz remains low for both cases. The

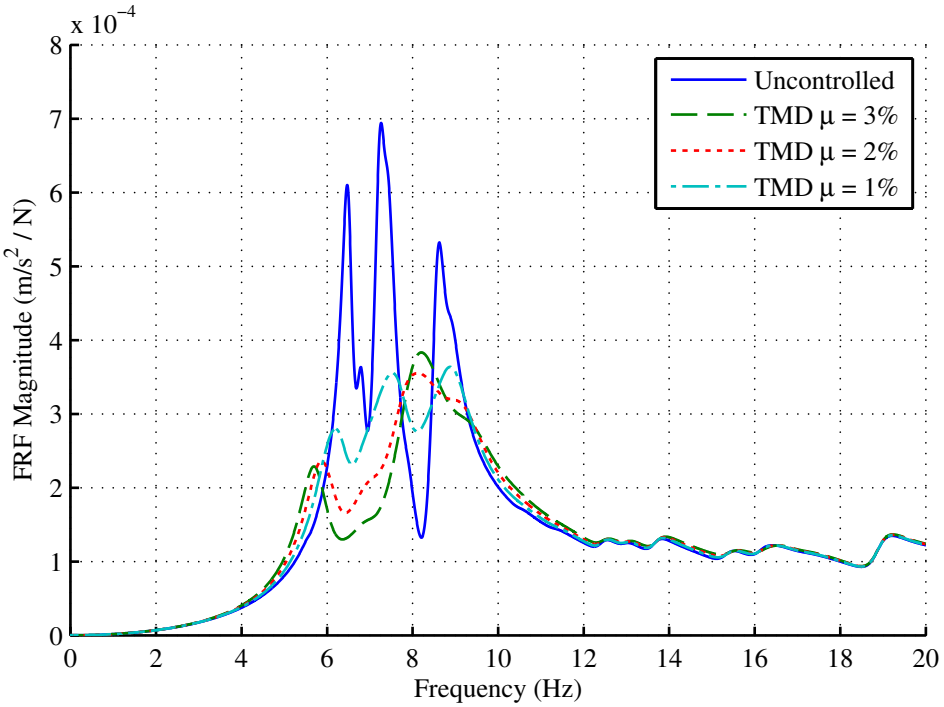

Figure 3.12: Point accelerance FRF at $(37.5, 4.5)$ with varying mass ratio for all TMDs

fourth line shows a point mobility FRF with all other TMDs present (with a mass ratio of 3%) but the TMD at $(37.5, 4.5)$ missing. Here, the antiresonance has been removed and the higher response has been introduced. This is purely due to the influence of nearby TMDs.

It should also be noted that the addition of nearly 10t to the superstructure is a significant amount and careful consideration must be paid to the ULS capacity of the structure.

The response of the structure was simulated using all three TMD configurations. The results for a mass ratio of 3% are presented in Figure 3.14.

3.5.3 AVC configuration

Eight actuator/sensor pairs were chosen for the AVC configuration that could achieve a reduced response over the entire structure, with locations indicated by

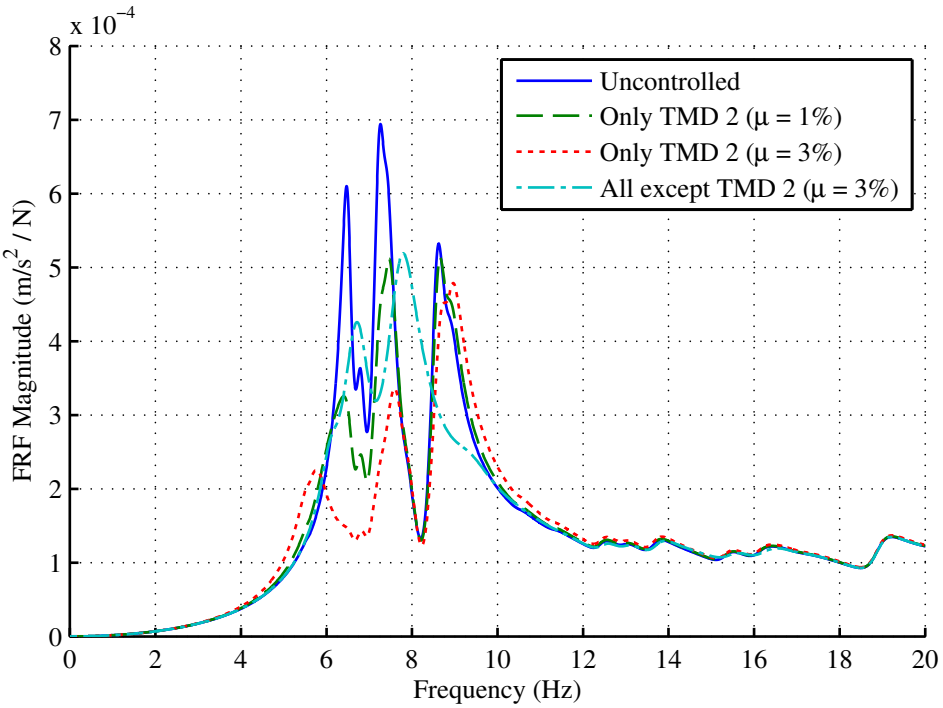

Figure 3.13: Point accelerance FRF at $(37.5, 4.5)$ with various configurations of TMD

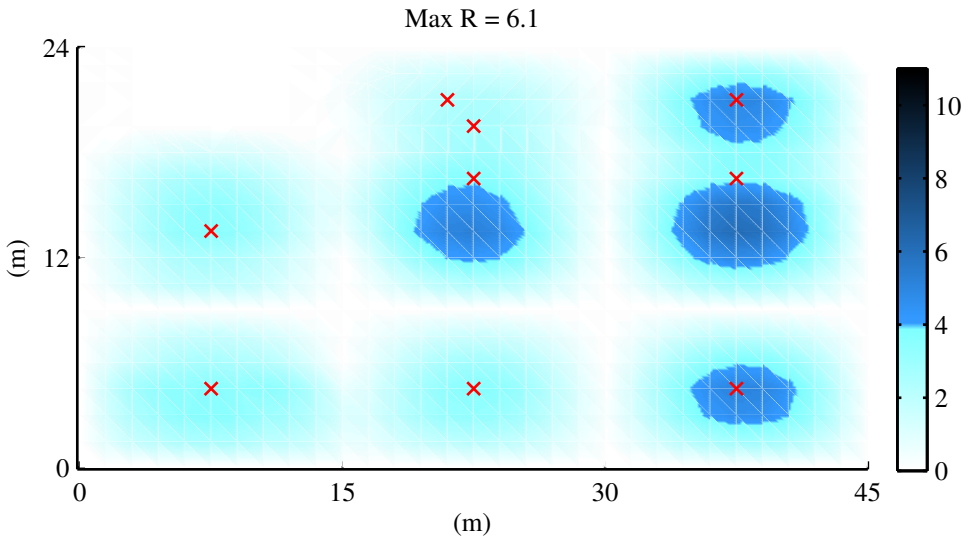

Figure 3.14: Contour of response of structure with 9 TMD's, each with mass ratio 3%

the green crosses in Figure 3.16. This number was arrived at by steadily increasing the number of actuators and sensors, combined with manual optimisation of their locations, until the response was satisfactorily decreased throughout the floor area. The initial locations of these actuator sensor pairs were chosen through examination of where the response was high and with consideration of the mode shapes that cause such a response. Because of this the locations for the AVC units are slightly different from those used in the TMD configuration (where the location was chosen based on the antinode of the mode to be controlled). For a comparison, the point accelerance FRF for the actuator/sensor pair located at $(37.5, 3.8)$ is shown in Figure 3.15 which is a relatively close location to the accelerance FRF plotted in Figure 3.12 for the TMD configurations.

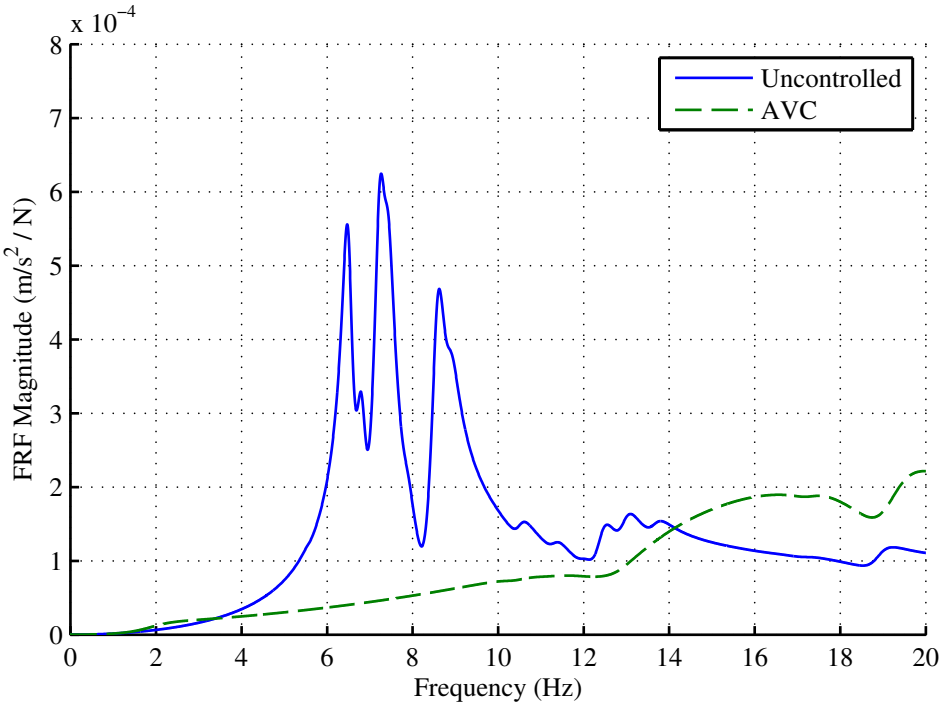

Figure 3.15: Point accelerance FRF at $(37.5, 3.8)$ with all AVC units active

The point accelerance FRF shown in Figure 3.15 has a much lower magnitude in the 5-12Hz region than all TMD configurations shown in Figure 3.12. This is expected given the broadband controller implemented for AVC which attenuates the response at all frequencies in a given frequency range, rather than targeting

just one mode of vibration. It is apparent that the response above about 14Hz is actually increased slightly with AVC. This is caused by the low-pass filter at 50Hz. Pure velocity feedback utilises a pure integrator on the acceleration signal, that is it has a -90° phase angle. However, to avoid the controller attempting to attenuate high frequency noise which could cause high frequency instability and a degradation of performance, a low-pass filter is introduced. This has the effect of introducing phase lag at frequencies lower than the cut-off frequency for the filter, which in itself degrades the performance of the AVC units. However, this is not a problem for the AVC controller because this frequency range is not easily excitable by pedestrian walking, and what excitement does occur is far offset by the improvements in response at the lower frequencies. Indeed, the resulting contour plot of maximum Response factor shown in Figure 3.16 demonstrates this effectiveness quite clearly.

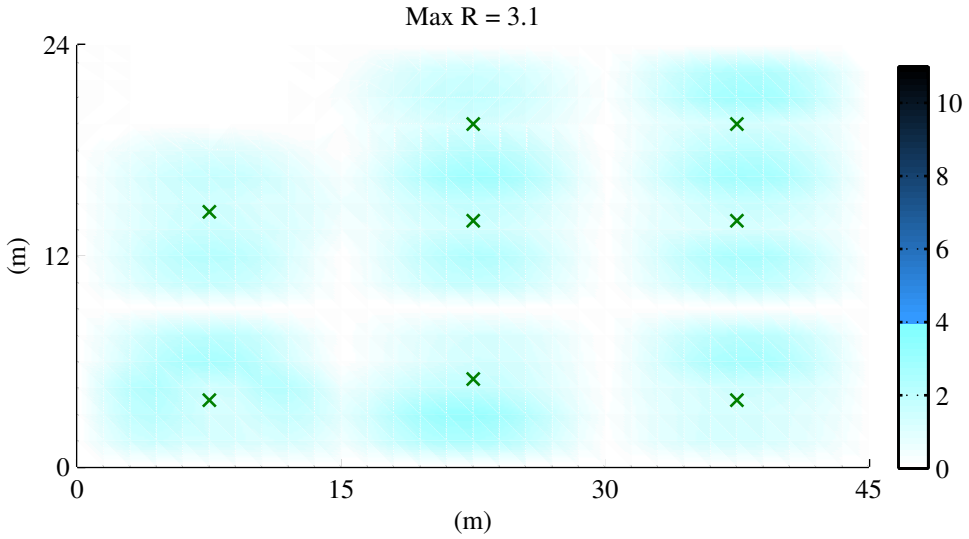

Figure 3.16: Contour of response of structure with 8 AVC actuators

The probabilistic nature of the analyses performed here has allowed a long time duration (1 hour) to be simulated. This means that it is possible to calculate, not only the maximum response achieved, but the probability that a particular response level will be exceeded. This approach is used here to simulate what

R factor equates to a 10% chance of being exceeded, or in other words, a 90% chance that the response of the structure will be below that R factor. This is very useful information about the response of a floor because it can be argued that it is more representative of the typical response actually felt by occupants.

In addition to this, the RMS period used to calculate the R factor can have a significant effect on the final value. Therefore, in this study two values have been used to allow for a clear comparison: 1 second and 10 seconds.

Therefore, the results of each control configuration have been processed to calculate the maximum across all locations of: VDV scaled for a 16hour day; R factor with 1s RMS period and 10s RMS period which 100% of measured responses are lower than; and R factor with 1s RMS period and 10s RMS period which 90% of measured responses are lower than. These results are summarised in Table 3.3. Note, that for indicative purposes the equivalent mass ratio for the AVC configuration has been included. This is calculated by equating the TMD mass for a given mass ratio to the active mass in AVC; this is therefore effectively an average mass ratio.

Table 3.3: Results summary for all control configurations

Controller	Max VDV, $m/s^{1.75}$	R factor (1s RMS)		R factor (10s RMS)	
		100% P	90% P	100% P	90% P
No Control	0.21	10.8	2.4	7.1	2.3
AVC ($\mu \equiv 0.08\%$)	0.06	3.1	0.6	1.8	0.6
TMD ($\mu = 1\%$)	0.13	5.9	1.5	4.0	1.4
TMD ($\mu = 2\%$)	0.12	5.4	1.2	3.9	1.1
TMD ($\mu = 3\%$)	0.11	6.1	1.1	4.2	1.0

It is interesting to observe that in this situation increasing the TMD mass did not lead to a reduction in the maximum response measured in the structure. This links back to the problem discussed earlier where the 9th TMD had to be moved because its initial inclusion caused a higher response elsewhere. Despite this, the response is generally lower, as indicated by the 90% R figures. Further to this, the

area of the building that contains a higher response is reduced by including larger TMD masses.

3.6 Conclusions

The high response of an office floor has been reduced through the use of two mechanical devices that add damping to the structure - TMDs and AVC. The benefits of using each technology have been shown. For this particular floor, nine TMDs were able to significantly reduce the response of the structure such that the highest response over the entire structure was reduced by between 38% and 45% for a mass ratio of 1%, depending on the measure used (e.g. VDV, 90% probability for R factor etc.). This is improved to 41% to 56% by using larger TMDs with a mass ratio of 3%. For the AVC configuration: eight actuators were able to reduce the response even further - by between 71% and 75%.

It has also been shown that the effect that TMDs have on locations other than their point of attachment to the primary structure can actually cause a higher response than the uncontrolled case if care is not taken. It should be noted that this effect, though not demonstrated here, also can occur for AVC.

AVC's ability to target multiple modes of vibration simultaneously allows for very large reductions in response over the entire frequency range of interest. However, the issues of observability and controllability mean that multiple actuators are still required for AVC to fully control all modes of interest in the structure. This idea leads to a possible improvement to AVC implementations in future, through the use of a larger number of smaller and cheaper actuators, distributed throughout the structure.

Chapter 4

Structural Design Implications

The work in this chapter builds on the groundwork developed in Chapter 3 through further analysis of active control implementations. Here, the number of actuators required to control a particular floor area is considered through investigation of two typical floor structures. The effect that these different structural design configurations have is studied, with the aim of finding structural properties that lead to improvements in the performance of active control. This work is presented as an adapted form of a paper submitted to the journal Structural Control and Health Monitoring. Details of this paper are as follows:

> M J Hudson and P Reynolds. Implications of structural design on the effectiveness of AVC of floor structures. *Structural Control and Health Monitoring*, In Review, 2013a.

4.1 Introduction

There have been significant improvements in the design and construction of new office buildings in recent years. This has enabled the creation of more slender structures that meet ultimate limit state requirements. However this, combined with the trend for open-plan office layouts, results in floors that are more prone to excessive vibrations resulting from human excitation (Middleton and Brownjohn, 2010; Ebrahimpour and Seek, 2005; Pavic et al., 2008; Živanović and Pavić, 2009). When this problem arises it is usually mitigated through the addition of extra mass to the floor or by stiffening the framing members, for example by installing additional columns (Hanagan, 1994; Smith et al., 2007; Setareh and Hanson, 1992a). This is done in an effort to reduce the amplitude of vibration within the frequency range that can be excited by human loading. However, both these solutions inherently detract from the benefits of the more slender structural form utilised in the first place.

One alternative technology currently being developed for use in civil structures is active vibration control (AVC). This technology can achieve significant reductions in the response of a structure whilst maintaining a slender structural form. AVC involves the use of one or more sensors, typically accelerometers, that monitor the response of the structure at key locations. These response measurements are processed in real time by a controller which generates a control voltage that drives one or more actuators. These impart a force onto the structure in an attempt to reduce the vibrations monitored.

One of the simplest, yet effective, control laws is direct velocity feedback (DVF). This controller has the effect of introducing additional damping into the system for a broad range of modes and, in the absence of actuator dynamics, is unconditionally stable (Hanagan, 1994; Hanagan et al., 2003). However, actuator dynamics are unavoidable and have a destabilising effect on the controller, which must be taken into account via reduction of feedback gain or use of suitable compensators

(Hudson and Reynolds, 2012). Nevertheless, DVF has been used by Hanagan et al. (2003) to achieve response reductions of 70% and 75% on an office floor and a chemistry lab floor respectively.

There are a number of variations on DVF that have been developed. For example, compensated acceleration feedback was developed by Díaz and Reynolds (2010a) and uses phase lag and phase lead compensators on the acceleration response signal to retain the property of high damping of the first structural mode and high stability margins. This was implemented on an office floor and achieved reductions in the structural response of 68% and 52% for the two pacing rates used for excitation.

Response-dependent velocity feedback was developed by Nyawako and Reynolds (2009) as a non-linear controller that implemented velocity feedback, but with a feedback gain that varies depending on the level of response. Additionally, Díaz and Reynolds (2009a) introduced DVF with a feed-through term. This has been shown to be highly effective at reducing the response of a laboratory test structure to human-induced vibrations: 96% reductions were achieved.

These previous investigations have focussed on the reductions that AVC can achieve at a single point; generally a single actuator/sensor pair are used and located at the same position. Whilst this is a crucial measure of the AVC performance, it is likely that excessive vibrations are a problem over a relatively wide area not just at a single location, so it is also important to consider how far from the location of the AVC unit this reduction in response is achieved. This directly relates to the number of AVC units that would be required to successfully control a given floor area.

When considering the effectiveness of AVC in terms of its global mitigation performance then controllability and observability of modes is of crucial importance. This means that in order to control a mode that is causing a high dynamic response, the mode shape amplitude of that mode must be non-zero (and preferably large)

at the control location. The mode shapes are clearly dependent upon the structural design. As further advances are made with AVC of floor structures there is a real possibility of designing a slender structure that requires AVC to meet vibration serviceability limits. In this scenario it would be possible to design the structure in a way that optimised the effectiveness of AVC. This chapter therefore investigates the effect that different 'typical' designs have on the effectiveness of AVC. Two case studies are investigated: both are real structures with observed vibration serviceability issues. In order for these simulations to be representative of what would be expected within an office, the force model introduced in Chapter 3 is calibrated and verified using experimentally acquired data. The layout of this chapter is as follows: the design of the AVC controller used in the studies is discussed in Section 4.2 and the development of the two models used to represent the structures is discussed in Section 4.3. Following from this, the methodology used to assess the structural response is discussed in Section 4.4. This includes the calibration and verification of the force model. Finally, results are provided in Section 4.5 and conclusions are drawn in Section 4.6.

4.2 Details of Controller Utilised

A direct output feedback controller was used in this study; this was a decentralised form of DVF. Details of this controller are provided in Section 3.4.2 but there are minor modifications to the specific control law used and so details are also provided here. The general schematic for the controller used is shown in Figure 4.1.

Accelerometers are used to detect the structural response, so this acceleration must be integrated to provide a velocity signal. A 2nd order high-pass filter at 1Hz is used to remove low frequency components. These filter properties were chosen as a compromise between minimising the destabilising effect of low frequency components and minimising the effect on both actuator dynamics and the lowest modes of vibration. Additionally, a 2nd order low-pass filter at 50Hz is included

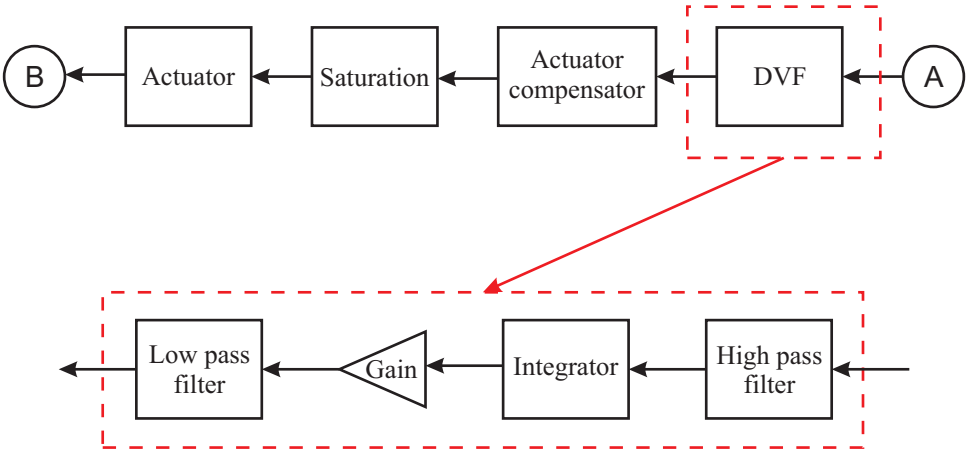

Figure 4.1: Schematic for AVC controller

to reduce sensitivity to noise and prevent the controller from attempting to control very high frequency modes that do not contribute significantly to the perceived structural response.

Whilst DVF is unconditionally stable in the absence of actuator dynamics (Hanagan, 1994) there is a limit on the maximum stabilising gain when the finite actuator dynamics are considered. The actuators used in this study are the APS Dynamics Model 400 electrodynamic shakers. It has been demonstrated (Díaz et al., 2012a) that there is a trade off between stroke saturation, stability and vibration attenuation for the natural frequency and critical damping ratio of the actuator dynamics. A compensator has been designed to modify the actuator command signal such that the physical properties of the shaker are effectively modified to desired properties. These properties are selected as having a natural frequency of 1Hz and a critical damping ratio of 0.7. This aims to minimise stroke saturation by reducing the magnitude of the command signal at the frequencies corresponding to the structure's quasi-static response to the first harmonic of walking. This could otherwise result in displacements much larger than those needed for the control of the structural modes and lead to stroke saturation. The compensator achieves these changes in characteristic properties through pole-zero cancellation of the existing actuator dynamics. Whilst this approach is not robust for the control of

structures (Preumont, 2002) the dynamics of the actuators can be determined with confidence and so can be modified in this way.

The active control configuration consists of several collocated actuator and sensor pairs which act independently to reduce the response at each location; thus resulting in a decentralised multiple input-multiple output controller, as shown in Figure 4.2. As discussed in Section 3.4.2, the constant negative feedback gain for

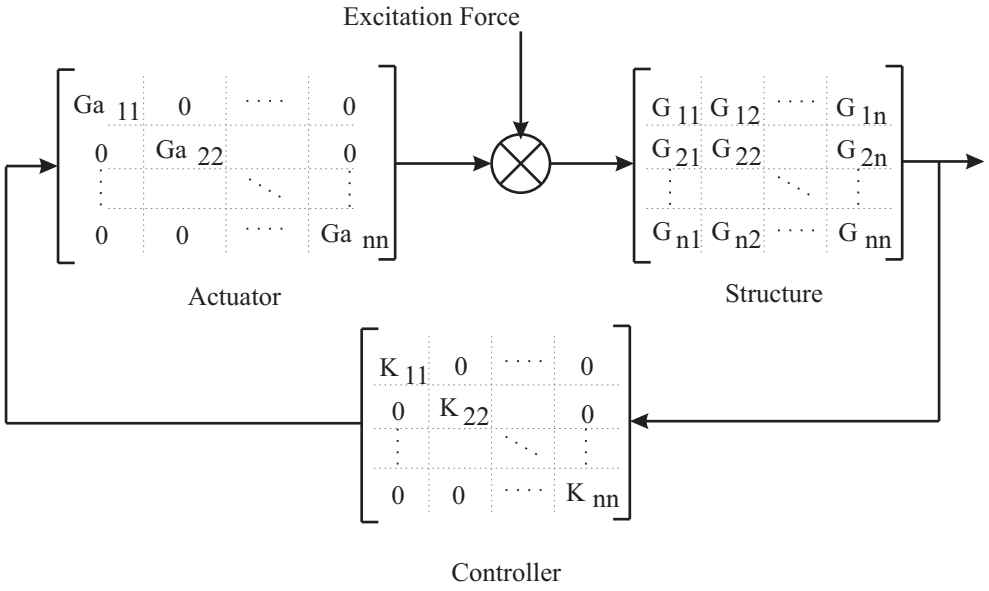

Figure 4.2: Decentralised AVC configuration

each control loop was initially chosen by considering the actuator/sensor pair in isolation and aiming to maximise the gain with the constraints of minimum gain margin being 2.0 and minimum phase margin being 30°. However, the structural system does not act independently at each control location; a force applied at one location will have a finite influence on the structural response at another location for every mode that has non-zero components at both locations. This can have the effect of reducing the stability margins. Therefore the feedback gain for all controller loops was reduced by the same percentage until the initial desired stability criteria were achieved.

In addition to these linear components (or assumed linearity in the case of actuator dynamics) the control law also contains non-linear elements: the command volt-

age to each actuator that is generated by the controller described above is passed through a saturation non-linearity. This acts as a further precautionary step to avoid both stroke and force saturation in the actuators.

4.3 Development of Finite Element Models

Finite element (FE) models of two floor structures were created. These floors were chosen because they are both of typical design, but illustrate different modal properties. Specifically, Floor B has small narrow bays whilst Floor C has more square, larger bays and this leads to quite distinct mode shapes. Experimentally determined modal properties were available for these two floors so the FE models were updated to better match reality before simulations were performed. Additionally, the author has experience of designing and implementing AVC on both of these structures so they are deemed ideal for further analysis. The development of the two FE models are discussed in the following sections.

4.3.1 Floor B

Floor B is the first floor of a relatively new office building in the UK. The details of this floor are provided here, though they have been previously described by Hudson and Reynolds (2010). This steel/concrete composite structure has steel primary beams at 6m spacings, steel secondary beams at 3m spacings and steel columns located around a 6m $\times$ 12m grid, as shown in Figure 4.3. A normal-weight concrete slab upon steel decking spans between the secondary beams. Construction drawings of the floor were used to determine the sizes of the structural elements. Details around irregular geometric details vary (e.g. around lift-shaft core), but typically: the primary beams are 792 $\times$ 191 \ 229 $\times$ 101ACB; the secondary beams are 254 $\times$ 146 $\times$ 31UB; and the columns are 254 $\times$ 254 $\times$ 73UC. The asymmetric cellular beams are constructed from two Tee sections: the upper Tee from a 457 $\times$ 191 $\times$ 89UB and the lower Tee from a 610 $\times$ 229 $\times$ 113UB; voids of diameter 550mm are cut at 750c/c. Photographs taken on-

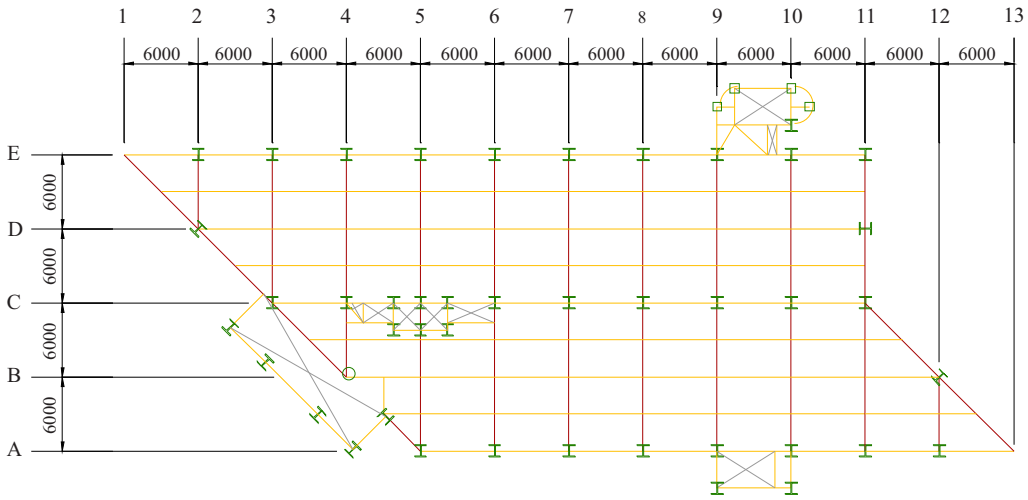

Figure 4.3: Structural layout for Floor B

site have provided an estimate for the concrete slab as being 130mm deep, with 60mm trapezoidal decking. The Young's Modulus of this normal weight concrete was assumed to be 38GPa (Smith et al., 2007; Pavić and Willford, 2005).

The FE software ANSYS was used to develop a model of the floor. SHELL63 elements were used to model the composite concrete slab; the orthotropic properties were modelled by assuming constant element thickness but using a proportionally smaller Young's Modulus in the weaker direction. The steel beams and columns were modelled using the 3D beam element BEAM188, whilst the slabs were modelled using SHELL63 elements which have both bending and membrane capabilities. The composite action between the steel beams and the composite slab was modelled by applying a vertical offset to the beams.

The columns were assumed to be fully fixed one storey above and below the floor under consideration. 10% of the assumed design imposed load and 100% of an assumed dead load due to services, false flooring etc. was applied as additional mass to the concrete slab elements, as is recommended in modern guidance (Smith et al., 2007).

The modal properties of this structure were determined experimentally using multiple reference excitation and a roving accelerometer configuration, as described

by Reynolds et al. (2009), with the test grid as indicated in Figure 4.4. Curve fitting of the frequency response function (FRF) was used to approximate the modal properties up to 9Hz beyond which point it became difficult to fit modes accurately.

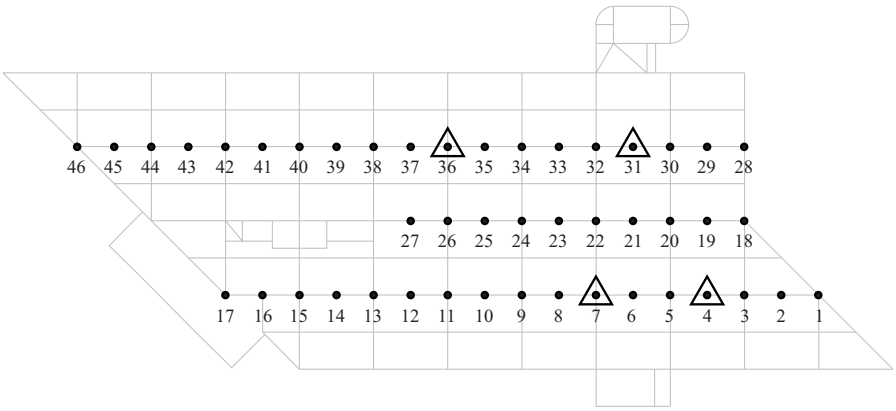

Figure 4.4: Test point locations for experimental modal test on Floor B. Location of excitation actuators shown by triangles

The experimental data were compared with preliminary modal analysis results from the finite element model and a number of adjustments were made to the original model to better reflect the dynamics of the real structure. The two free corners at A13 and E1 in Figure 4.3 resulted in highly responsive localised modes in the FE model which were not detected in the experimental data. Although the location of the actuators would not have excited these localised modes, the fact that the tenants have no complaints about these areas would suggest that these modes are being suppressed, possibly due to some form of restraint being provided by the external cladding. For this reason additional columns were added at these locations; the effect that these had on the other modes was found to be not significant.

Further to this, the natural frequencies of the mode shapes tended to be too high. This indicates that there was either too much stiffness modelled or not sufficient mass. In order to investigate this issue the connections between the primary beams and the columns were modified from their fully fixed state and set to a pinned con-

nection. This modification results in modal properties that correlate better with the measured data. Unfortunately, no construction details of the connections are available to verify that this loss of stiffness is the cause of the frequency discrepancy.

Finally, the real structure has a section containing small meeting rooms that are partitioned off from the rest of the open-plan office. As a result of this, the experimental data observed much lower mode shape amplitudes in this region when compared with other areas of the floor. Partitions were therefore modelled in this area in the FE model by using 100mm wide isotropic SHELL63 elements with a Young's Modulus of 30MPa.

A modal analysis of the FE model yielded many modes because of the relatively flexible partition walls that were included in the analysis. Model reduction was performed in order to include as many structural modes as possible whilst still having a computationally feasible problem to solve. This was performed by removing all modes whose maximum mode shape amplitude on the floor slab was less than 10% of the overall maximum mode shape amplitude, i.e. all modes with localised partition bending only were removed. The overall effect on the system's FRFs at four key locations was found to be negligible, therefore the model reduction was considered satisfactory.

Some of the key structural modes from the updated FE modal analysis are compared with their equivalent modes from experimental modal analysis (EMA) in Figure 4.5. It should be noted that the curve fitting procedure used to fit the experimental modes generated (slightly) complex modes. For comparison purposes these modes were normalised with respect to the angle of the point with the largest mode shape amplitude. The higher frequency FE modes tended to differ more in terms of their mode shape compared with the experimentally determined mode shapes. It was observed that a single experimental mode was split into several closely spaced FE modes. However, the net effect on the system is expected to be approximately the same, as demonstrated by the FRFs shown in Figure 4.6. In

order to generate this FRF plot a level of damping had to be assumed for each FE mode. The values chosen were based upon matching the point accelerance FRFs at the four locations used for the experimental modal testing. The results of this are that all modes have 3% damping except for the mode at 7.85Hz which had an assumed level of 5% in order to better match the measured FRFs.

4.3.2 Floor C

Floor C is the second floor of a recently re-developed office building, also in the UK. This steel/concrete composite structure has a less regular geometry than Floor B. However, it is loosely based on steel primary beams at 13m spacings, steel secondary beams at 3m spacings and steel columns on a 13m $\times$ 9m grid, as shown in Figure 4.7. A lightweight concrete slab on steel decking spans between the long-span secondary beams. Construction drawings of the floor were again used to determine the sizes of the structural elements. Typically, the primary beams in this structure are PG500 $\times$ 200 $\times$ 241; the secondary beams are PG500 $\times$ 160 $\times$ 94; and whilst many column types are used, the columns supporting the centre of the floor are 356 $\times$ 356 $\times$ 287UC. The Fabsec cellular beams used have voids of diameter 330mm cut for services. The concrete slab is 130mm deep and is supported by Holorib decking. The Young's Modulus of the light weight concrete was initially assumed to be 38GPa; the same value as used in Floor B. A similar modelling technique was used for this floor, namely that BEAM188 elements were used for the steel beams and columns and SHELL63 elements for the orthotropic slab.

The modal properties of this structure were also determined experimentally using multiple reference excitation and a roving accelerometer configuration using the test grid shown in Figure 4.8. FRF curve fitting was used to approximate the modal properties up to 11Hz beyond which point it became difficult to fit modes accurately.

The FE model was updated following comparison between experimental modal

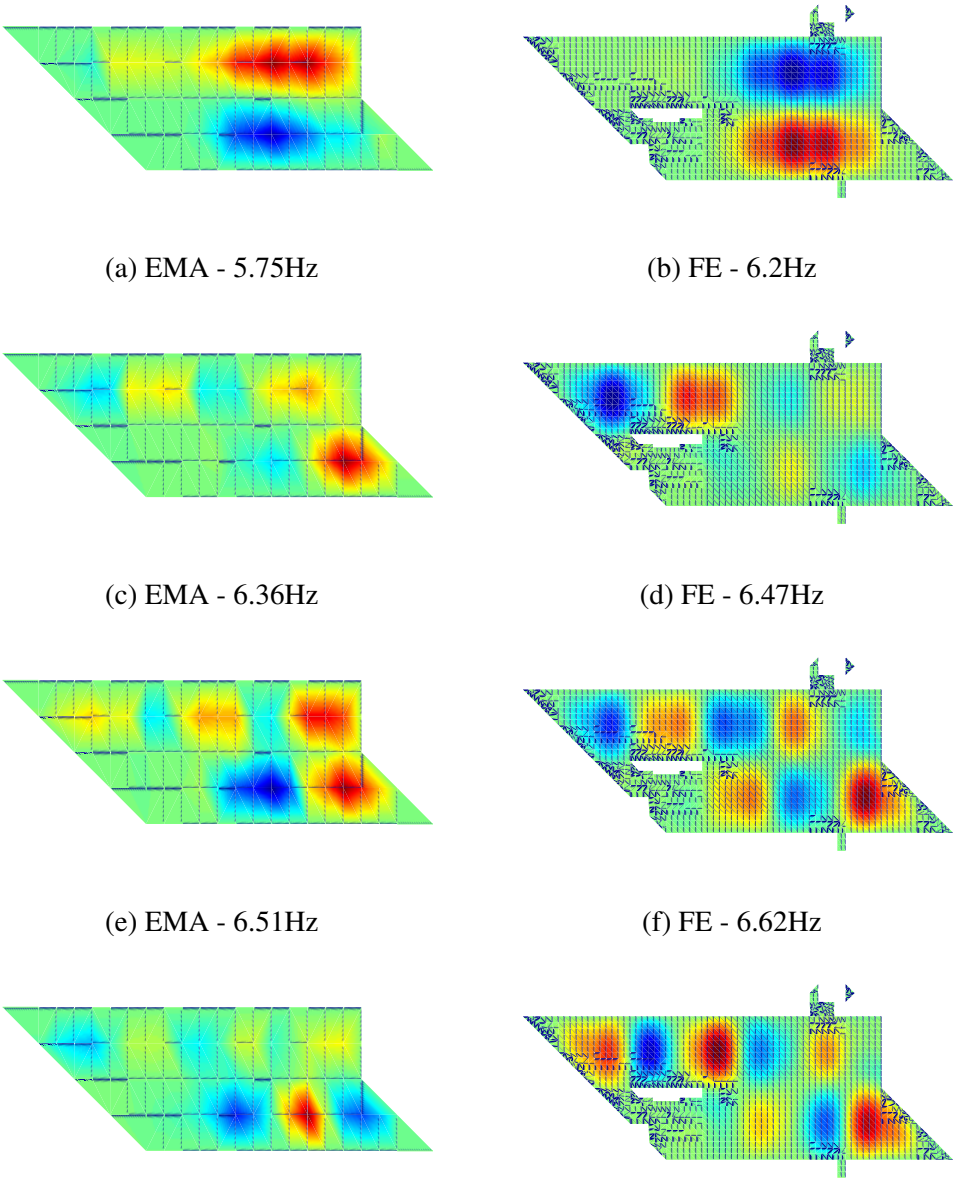

(a) EMA - 5.75Hz

(b) FE - 6.2Hz

(c) EMA - 6.36Hz

(d) FE - 6.47Hz

(e) EMA - 6.51Hz

(f) FE - 6.62Hz

(g) EMA - 6.95Hz

(h) FE - 6.89Hz

Figure 4.5: Comparison between simulated and measured mode shapes for Floor B

properties and FE modal properties. The natural frequency of the modes were slightly too high so it was decided that the use of lightweight concrete may require a slightly lower Young's Modulus to be used. Therefore, the original value was reduced by 20% to 30.4GPa.

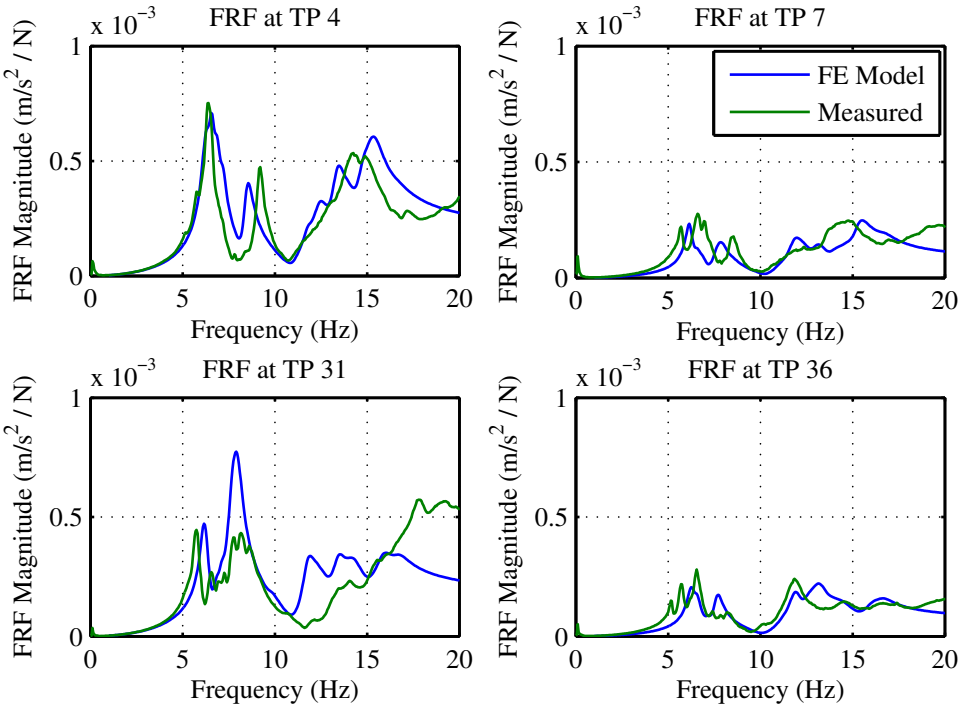

Figure 4.6: Comparison of experimentally determined FRFs and those from the updated FE model at 4 test points (TPs) on Floor B

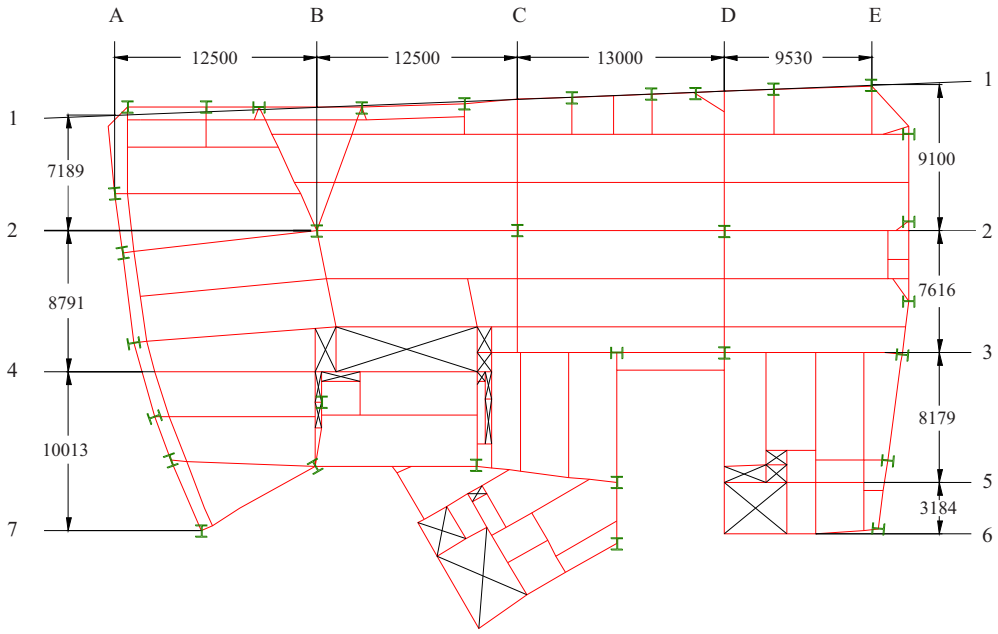

Figure 4.7: Structural layout for Floor C

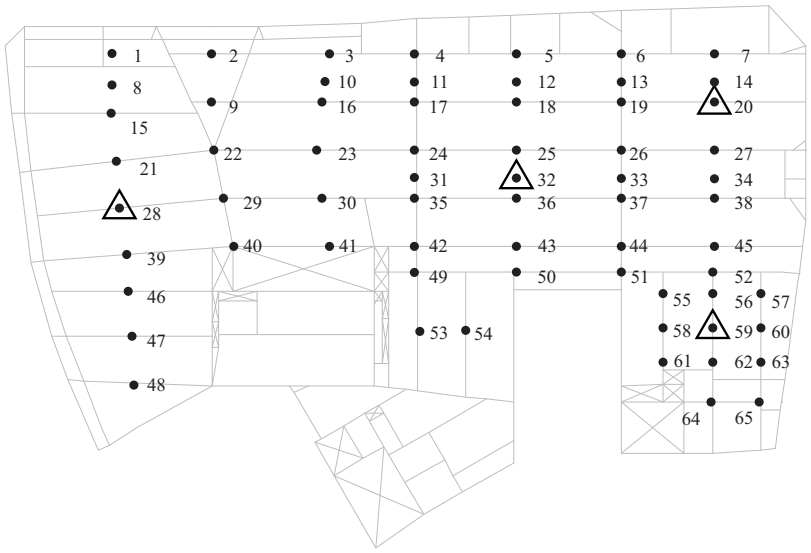

Figure 4.8: Test point locations for experimental modal test on Floor C. Location of excitation actuators shown by triangles

Also, in the real structure there is a small office in the corner, between gridpoints D5 and E5 on Figure 4.7, separated from the rest of the office by a glass partition. This appeared to have the effect of stiffening the bay in this area such that the magnitude of the mode shapes around this region was reduced, as compared with the results in the FE model. Therefore, this partition was added to the FE model, modelled as a glass plate 4mm thick. The full Young's Modulus of glass was not used to model these partitions because the partitions appeared to be connected to the false ceiling and hence would lose significant stiffness. Numerical updating was performed and a final value of 5GPa was chosen to match the experimental data.

Modal reduction was also required to eliminate the partition modes that did not contribute significantly to the dynamic response of the floor. The same methodology was used here as was described earlier for Floor B.

Some of the key structural modes are compared with their equivalent experimentally determined modes in Figures 4.9 and 4.10.

A level of damping had to be assumed for each mode. The value chosen was

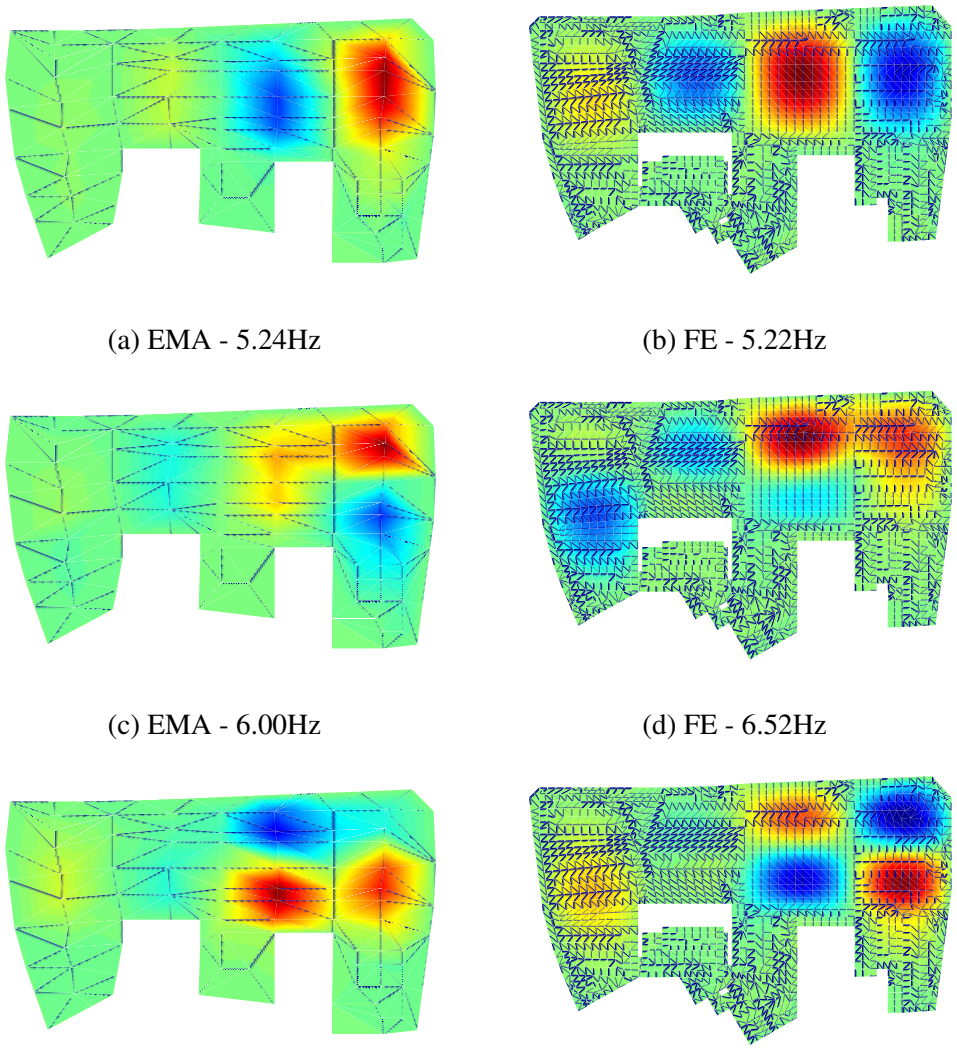

(a) EMA - 5.24Hz

(b) FE - 5.22Hz

(c) EMA - 6.00Hz

(d) FE - 6.52Hz

(e) EMA - 6.53Hz

(f) FE - 6.36Hz

Figure 4.9: Comparison between simulated and measured mode shapes for Floor C (1)

based upon matching the point accelerance FRFs at the four locations used for the experimental modal testing. The results of this with an assumed level of damping of 3% for all modes is presented in Figure 4.11. It is apparent that the FE FRF does not match as well with the measured FRF for this floor when compared with the equivalent comparison for Floor B. One reason for this is the difference in frequencies for the higher frequency modes, although the mode shapes for these

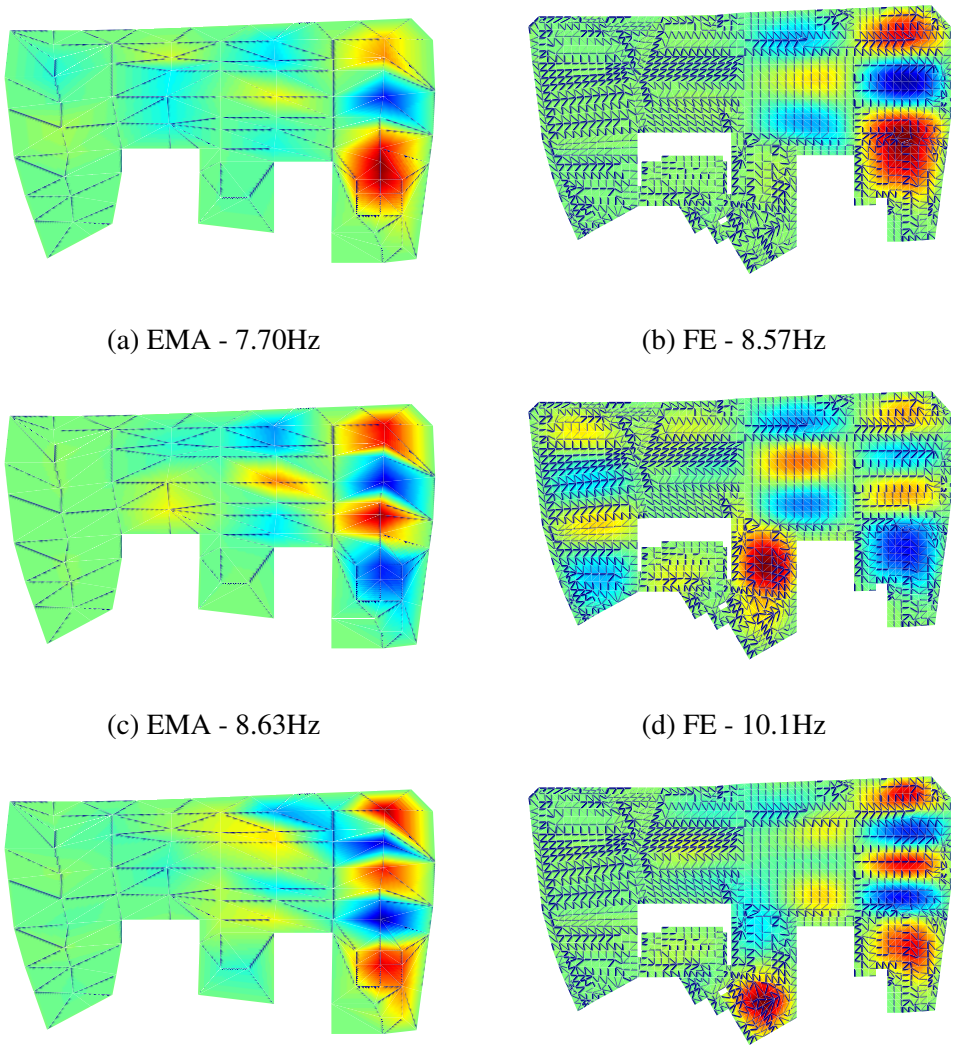

(a) EMA - 7.70Hz

(b) FE - 8.57Hz

(c) EMA - 8.63Hz

(d) FE - 10.1Hz

(e) EMA - 11.1Hz

(f) FE - 12.9Hz

Figure 4.10: Comparison between simulated and measured mode shapes for Floor C (2)

modes appear very accurate. Interestingly, this is the opposite situation compared with Floor B where the modal frequencies matched well but the mode shapes themselves were split and so did not match as well. This demonstrates some of the difficulties associated with modelling civil floor structures.

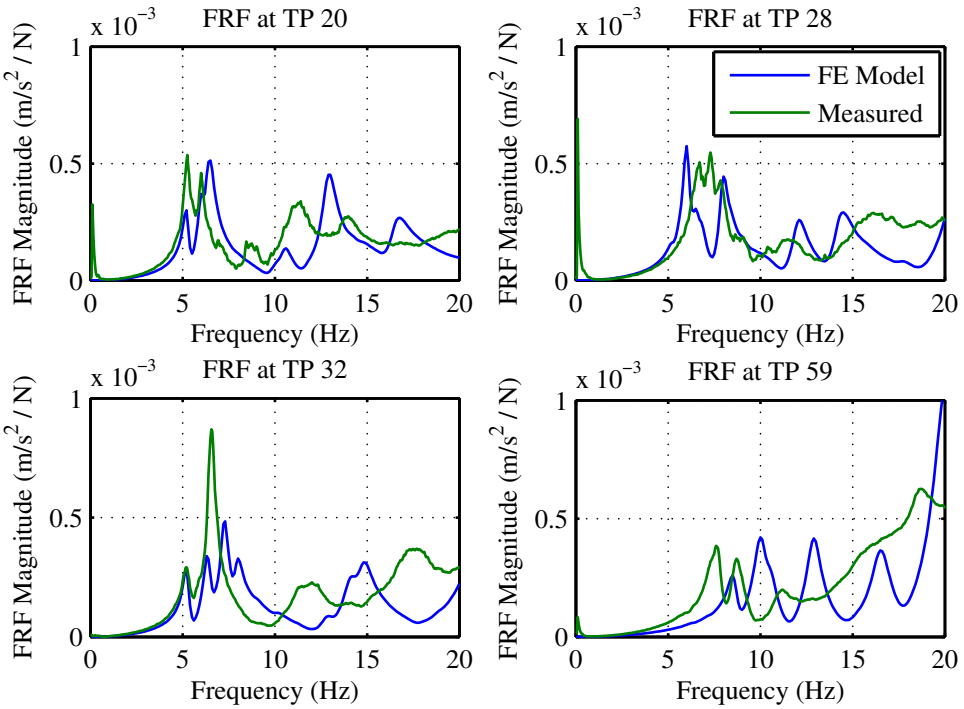

Figure 4.11: Comparison of experimentally determined FRFs and those from the updated FE model at 4 locations on Floor C

4.4 Methodology for Assessing Structural Response

4.4.1 Modal model

The modal properties derived from the FE floor models were utilised to generate the standard equations of motion. For Floor B, 92 structural modes were considered for these analyses (equating to all modes under 16Hz), whilst for Floor C 113 modes were considered (equating to all modes under 30Hz). The reason for the difference in frequency ranges is due simply to the inherent nature of the floors' designs. As many modes as was computationally feasible were chosen for the analyses. This is despite the first natural frequency of each floor being less than 10Hz and hence classified as a "low frequency floor" by many modern guidelines (Smith et al., 2007; Willford and Young, 2006; Pavić and Willford, 2005). The frequency cut-offs suggested by these guidelines is much lower than the uppermost frequencies considered here. However, research is starting to indicate (Živanović

and Pavić, 2009) that ignoring the higher frequency components of the response can lead to significant inaccuracies. A modal model of the structure was then created as discussed in Section 3.3.1.

4.4.2 Response post-processing

The response of the structure is evaluated by its acceleration. Each acceleration time history is filtered using the W_b frequency weighting, in accordance with BSI (2008), to account for the variation in the human perception of vibrations in the vertical direction, over the frequency band of interest. The Response (R) factor was calculated, as described by Equation 4.1.

$$R = \max_t \left(\left(\int_{t-T/2}^{t+T/2} {a_w}^2(t)dt \right)^{0.5} \right) \times \frac{1}{0.005} \tag{4.1}$$

where:

R is the Response factor

T is the period used for the running root mean square (RMS), s

As noted in Section 3.3.3, the more recent standards have dropped the use of R factor in favour of the vibration dose value (VDV) limit, though in practice the R factor is still a commonly used vibration serviceability criterion as indicated by its inclusion in modern design guidance documents. The latest standard that used the R factor, which is cited in many of the design guides (Willford and Young, 2006; Smith et al., 2007; Pavić and Willford, 2005) recommends a maximum R factor for offices subject to continuous vibration (16h day, 8h night) as 4.

4.4.3 Force model

The structural response of each floor was then determined by simulating multiple pedestrian loading. The loading chosen aimed to simulate a typical office envi-

ronment as accurately as possible.

In order to do this a number of assumptions had to be made. Firstly, it was assumed that the occupants would have an equal probability of walking to and from any location within the floor plan, i.e. "popular" areas such as the meeting rooms are not accounted for. It was also assumed that the pedestrians aimed to walk along pre-defined corridors as opposed to a straight line route, thus taking into account obstacles such as desks and walls. Naturally, considering this from a design perspective it is not possible to evaluate every possible desk arrangement to arrive at the worst case scenario. However, in these existing structures it is possible to use the existing desk layouts to generate walking paths. The optimal route for each path was chosen to be the one that minimised the number of corridors traversed. Where multiple routes have the same number of corridors (a likely scenario when a grid of overlapping corridors is used) the path with the shortest distance is chosen.

The force function used for each pedestrian is based on the probabilistic model developed by Živanović et al. (2007). This uses a normal distribution to represent step frequency and step length in order to generate time domain representation of the first 5 harmonics and subharmonics of walking. The force model in this chapter extends upon this model slightly in that the weight of each pedestrian is also represented by a normal distribution - the details for which are derived from NHS 2009 trend data (NHS Information Centre, 2010). This distribution is defined by a mean of 76.7kg and a standard deviation of 19.42kg.

Calibrating the force model

The start time density for the pedestrians, that is the rate at which new pedestrians start to walk along their route for a given floor size, was calibrated using experimental data from two days of in-service response monitoring from Floor B. These data were recorded on Friday 11 November 2010 and Monday 15 November 2010 from 7am to 7pm on each day. This is the most active 12 hour period in the day

and so was deemed most appropriate for comparing with the responses from the simulated walking. The response was measured at two locations simultaneously, as indicated in Figure 4.12.

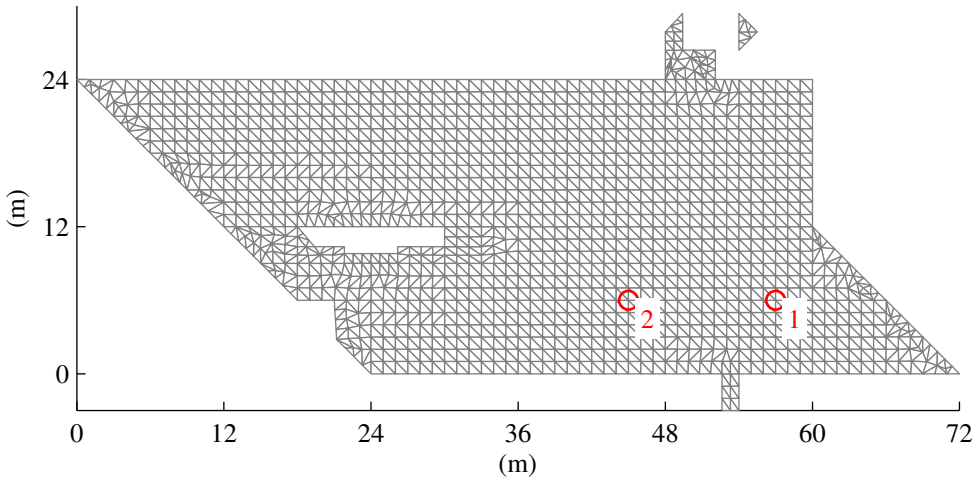

Figure 4.12: Locations of accelerometers for experimental in-service monitoring

With regards to the force model, it was assumed that the interval between pedestrian start times was equally distributed throughout. However, the random route length and walking speed mean that the number of active pedestrians on the structure at any time varies throughout the analysis. Two hours of data were simulated and the response calculated at the same two locations as used in the experimental tests. A value of six people per minute has been used for the 1224m^2 floor plan of Floor B. This force model was applied to the FE model of Floor B for a total duration of two hours. For ease of computation and numerical data handling the simulation was divided into six runs lasting 20 minutes each. Whilst this does mean that the force time history will be slightly different at the start and end of each block when compared with a single continuous run, the net effect is expected to be minimal on the overall time history. The choice of corridors for these simulations are shown in Figure 4.13, and an example of typical routes for pedestrians walking along these corridors is shown in Figure 4.14. These corridors were cho-

sen based on the actual desk arrangement and door locations within the office so that the corridors were as similar as possible.

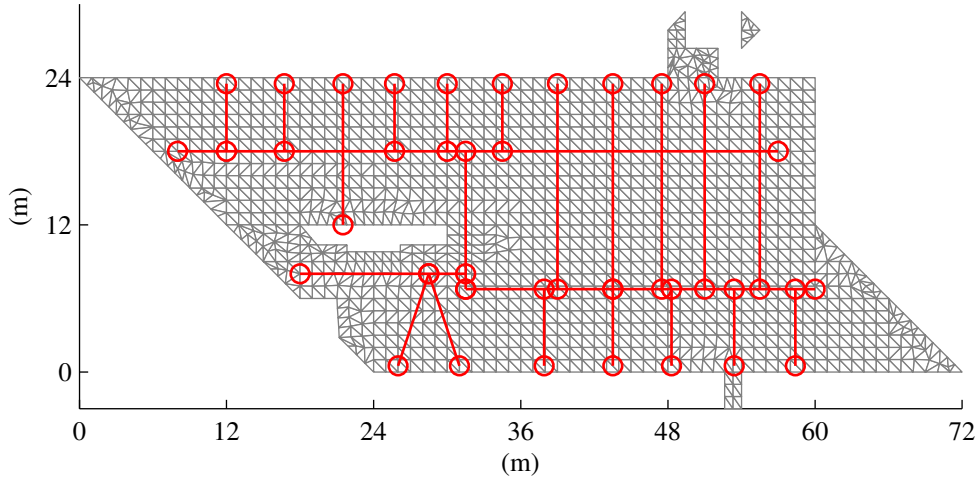

Figure 4.13: Corridors used in walking simulations

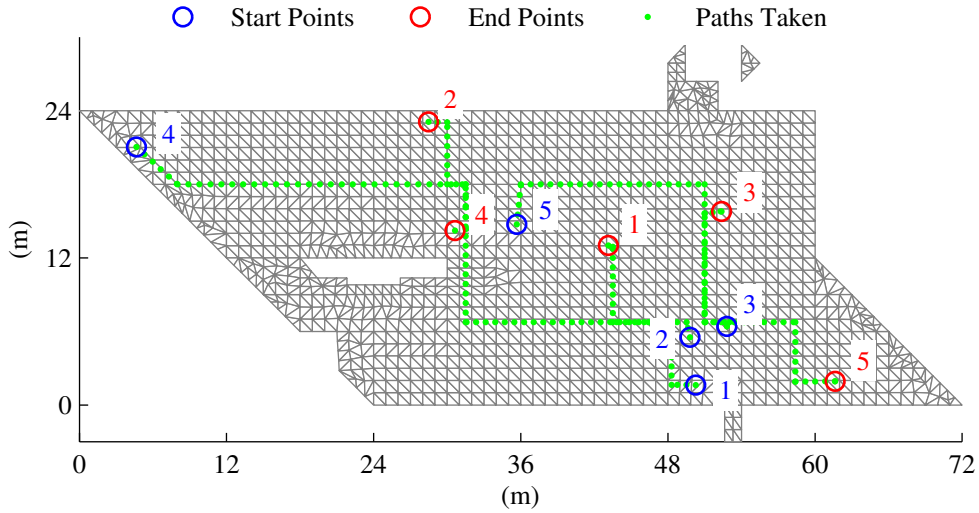

Figure 4.14: Example routes taken by five pedestrians

In order to compare the resultant time histories, the 1-second running RMS of the W_b frequency weighted acceleration was calculated and used to evaluate the proportion of time spent at a particular response level for each point. The resultant

probability distribution (PD) and cumulative distribution function (CDF) (being the integral of the PD with respect to the response level) for both the simulated data and the two days' experimental data are shown in Figure 4.15.

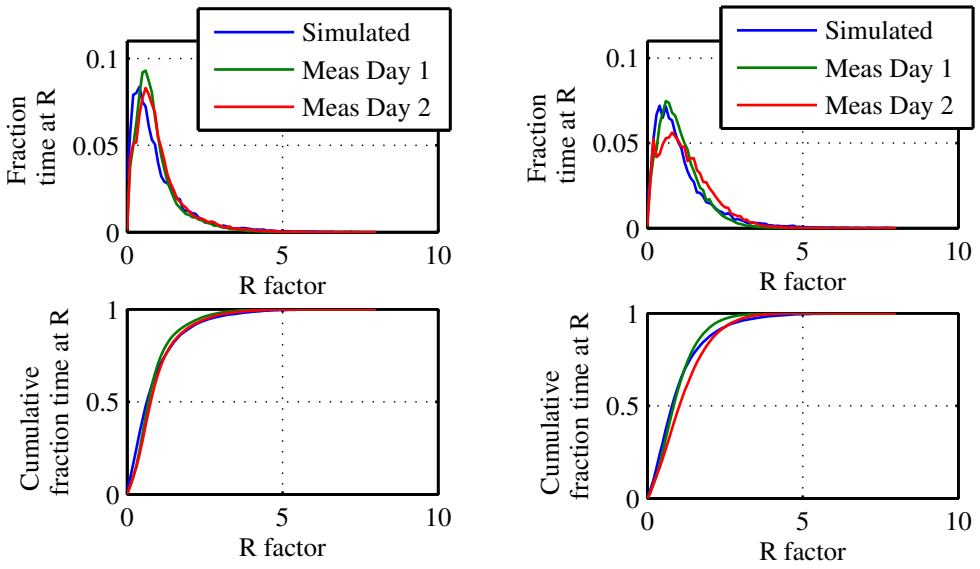

(a) Location 1 (b) Location 2

Figure 4.15: Comparison between simulated and measured responses

It is observed that the simulated trace is similar to the experimental trace for this start time density. Generally, the simulation trace falls between the inter daily variation in the PD and CDF curves for each of the two experimental days with nominally identical in-service loading. However, it is worth discussing some of the differences that do exist between the two. Firstly, the simulated PD for each location appears to peak at a lower response level. This corresponds to a very low level of excitation (less than R=1 which indicates the vibrations are not perceptible to humans). The reason for this could be that other sources of excitation exist in reality, e.g. car traffic, wind, machinery. These have been ignored in the simulations because it is assumed that their contribution to the overall response is small and because their potentially non-stationary nature would be overly complicated to include in the analysis. However, these excitation sources could raise the response slightly at the low levels of response considered here.

Finally, a large number of random variables are utilised in this study so it is important that the simulation runs for long enough such that the results are representative of the underlying statistical processes. So, the PD and CDF curves for each of the 20 minute runs is shown in Figure 4.16 along with the overall PD and CDF curves. The variation observed is relatively small which indicates that the simulation duration chosen is sufficient.

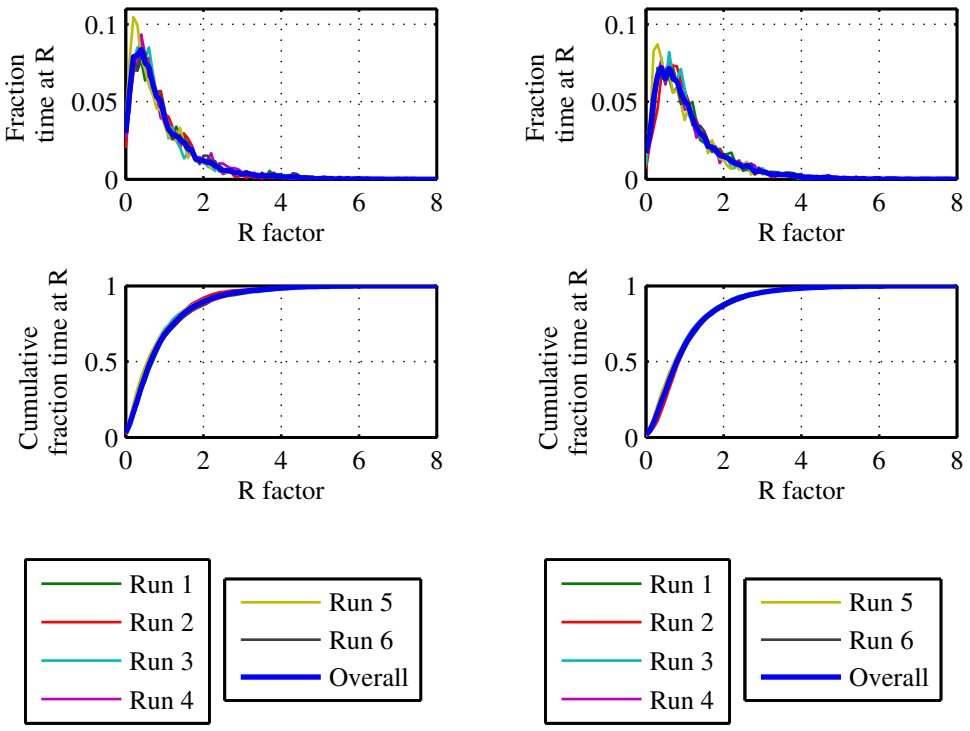

(a) Location 1 (b) Location 2

Figure 4.16: Verification that average PD and CDF curves are representative

Verifying the force model

Walking was also simulated on Floor C. This floor also had its response when subject to in-service walking loads experimentally measured at two locations, as shown in Figure 4.17; the data from this were used to verify the walking model used. This walking model utilised the same number of pedestrians per minute as was used in the walking model for Floor B. This was because the floor areas

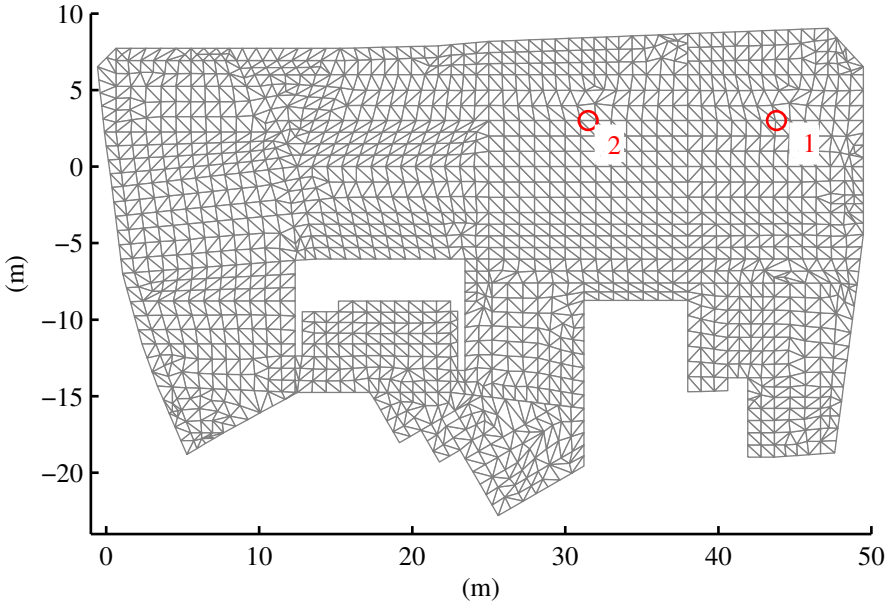

Figure 4.17: Locations for response measurement during in-service loading on Floor C

are approximately the same (namely, 1224m^2 for Floor B and 1137m^2 for Floor C). The walking paths were regenerated using the corridor patterns shown in Figure 4.18. Once again, these corridors were chosen based on the desk arrangement and door locations as used in the office during the experimental configuration. The response at the two locations shown in Figure 4.17 was measured and the probability distribution and cumulative probability distribution were calculated for the 1s running RMS. These are shown in Figure 4.19 along with the experimentally measured PD and CDF curves. The simulated and experimental data match very well, although the response at TP18 is slightly reduced in the measured data and this reduction in response is not replicated in the simulations.

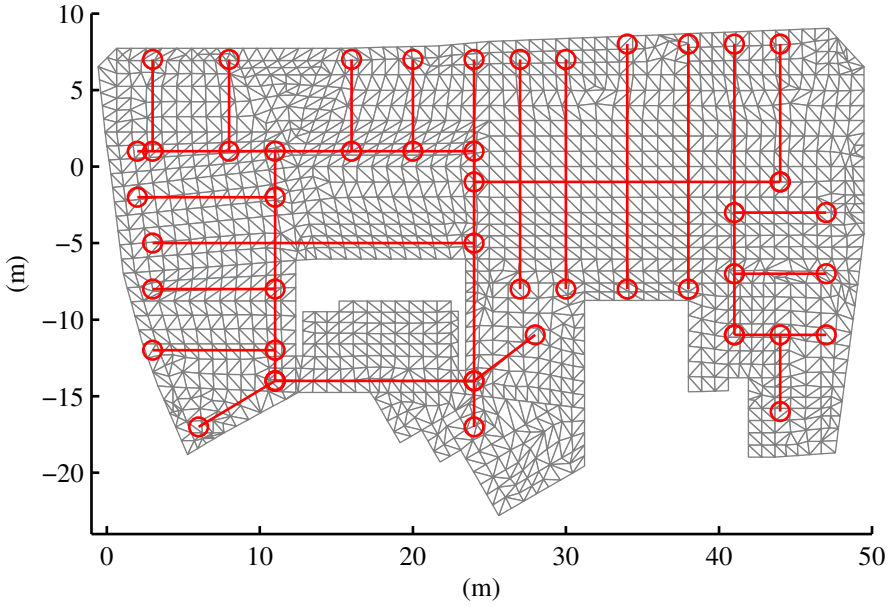

Figure 4.18: Corridors used for walking simulations on Floor C

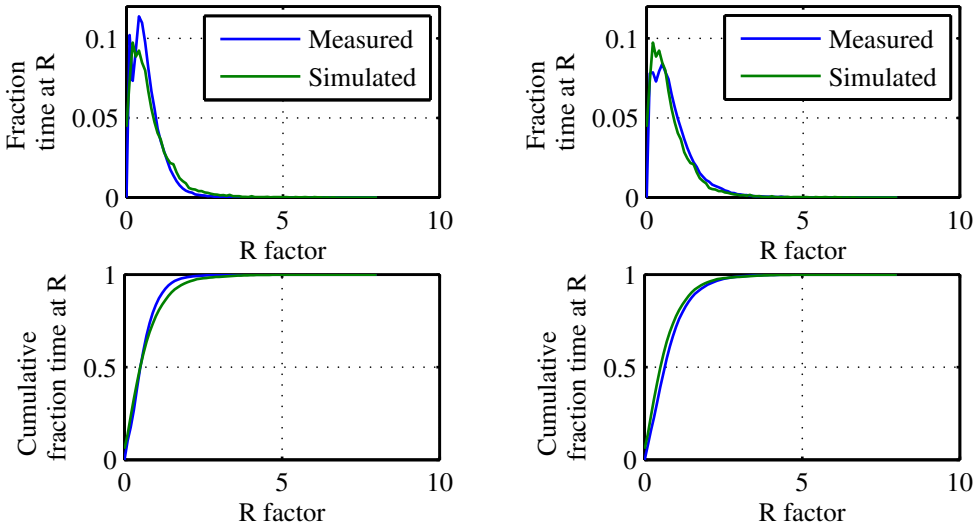

(a) Location 1 (b) Location 2

Figure 4.19: Comparison of simulated PD and CDF with measured data for two locations on Floor C

4.5 Results

4.5.1 Floor B

Uncontrolled

Walking was simulated on Floor B as described in Section 4.4.3. However this time instead of considering two key points, the response at every node in the structure was simulated so that a contour plot of the response across the structure could be determined. By doing this the areas of high response can easily be determined and, in subsequent tests, compared with the reductions made possible through the use of AVC. The results for the uncontrolled case are shown in Figure 4.20. Note

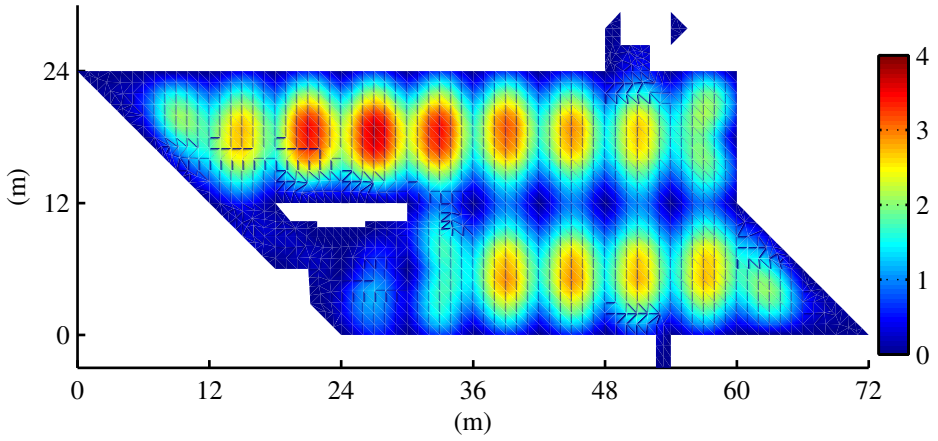

Figure 4.20: Contour plot of uncontrolled response for Floor B

that this plot does not show the absolute maximum response achieved at each point, rather the response that has a 5% chance of being exceeded. This measure has been chosen because it is believed by the authors to give a better representation of the typical structural response, particularly given the stochastic excitation force applied. Unfortunately, there is no available guidance as to what level of response is acceptable when considering the 5% exceedence level, so the aim of this work is to investigate how easy it is to reduce the structural response in areas where the response is particularly high. Figure 4.20 shows that the response is generally

high at the centre of each 12m $\times$ 6m panel and that a significant number of bays have this high level of response. Interestingly, the highest response is located in the $(x, y) = (27, 15)$ region whereas the occupants noted the most problematic area as being in the $(x, y) = (57, 6)$ region. There are many possible reasons for this observed difference. Firstly, in Figure 4.6 it is observed that the response at TP31 is noticeably higher at approximately 8Hz in the FE model compared with the EMA results. The mode shapes in Figure 4.5 indicate that the FE modes tend to be of a more global nature than those measured, which is likely to be the cause of this observed difference. A possible reason for the FE model having more global mode shapes is the presence of unmodelled non-structural features that exist at $(x, y) = (27, 15)$ in the real structure. Further to this, the pedestrians were assumed to have equal probability of starting at any location within the structure. However, in the real structure there is a main entrance to the office located at $(x, y) = (30, 6)$ which will attract more traffic and some of the people walking to/from this region would excite modes that extend to the problematic area. Despite this difference, the results are believed to be a good representation of the typical structural response.

Controlled

Following from this, the same excitation force was used to simulate the response of the structure with active control at several locations. Control locations were chosen based on both the uncontrolled response levels in Figure 4.20 and on the mode shapes to try and maximise the effectiveness of AVC on all modes of vibration. Three different configurations were examined: configuration 1 consists of 4 control actuators at intuitively optimal locations; configuration 2 consists of 5 control actuators located such that different bays are controlled when compared with configuration 1; finally configuration 3 consists of 8 control actuators located to control all problematic bays. The actual locations of the actuators for each configuration are indicated with green crosses in the contour plots of response shown

in Figures 4.21-4.23.

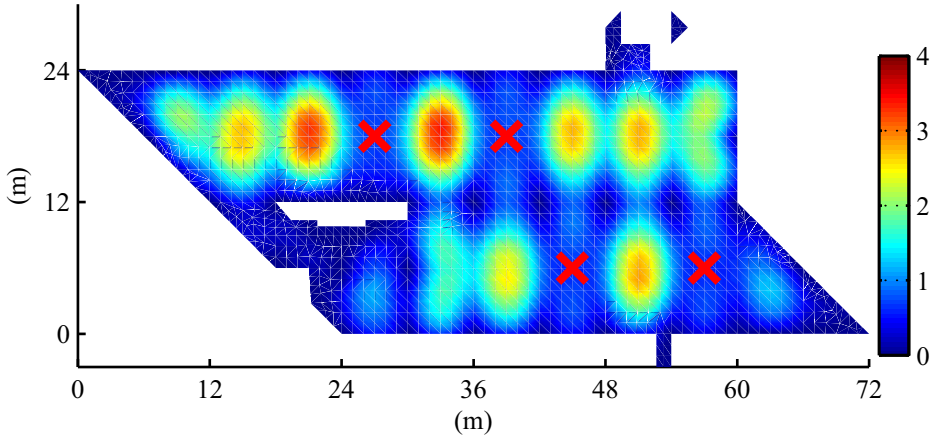

Figure 4.21: Contour plots of controlled structural response with AVC Configuration 1

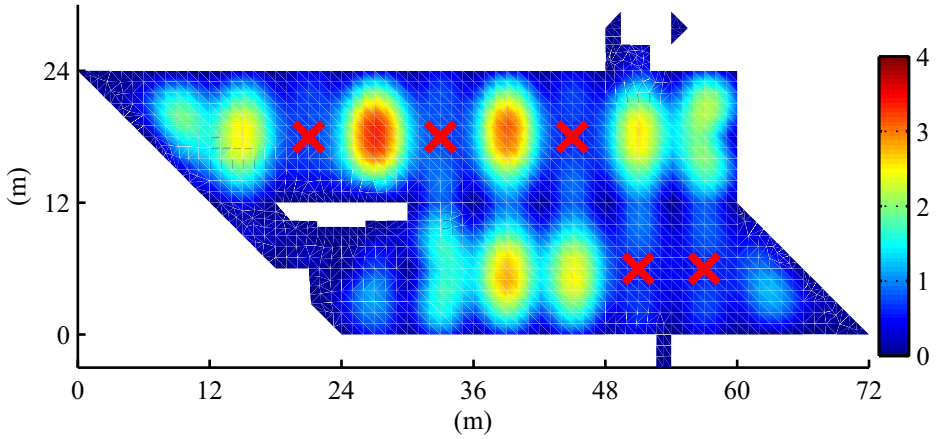

Figure 4.22: Contour plots of controlled structural response with AVC Configuration 2

The performance of the AVC system can be evaluated by considering the transfer function plot of the open and closed loop systems. It is not feasible to present this for all locations so this has been performed for just 3 locations for Floor B: these are at $(x, y) = (45, 6)$, $(51, 6)$ and $(57, 6)$, i.e. the three locations on the bottom bays as shown in Figure 4.23. The transfer function plots for inputs and outputs at these three locations are shown in Figure 4.24. The performance at low frequencies (less than 10Hz) is very good at all locations. It is evident that the

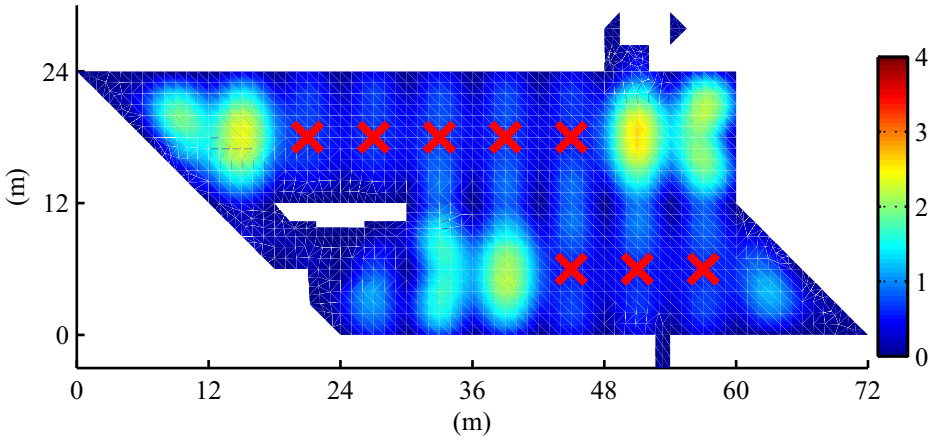

Figure 4.23: Contour plots of controlled structural response with AVC Configuration 3

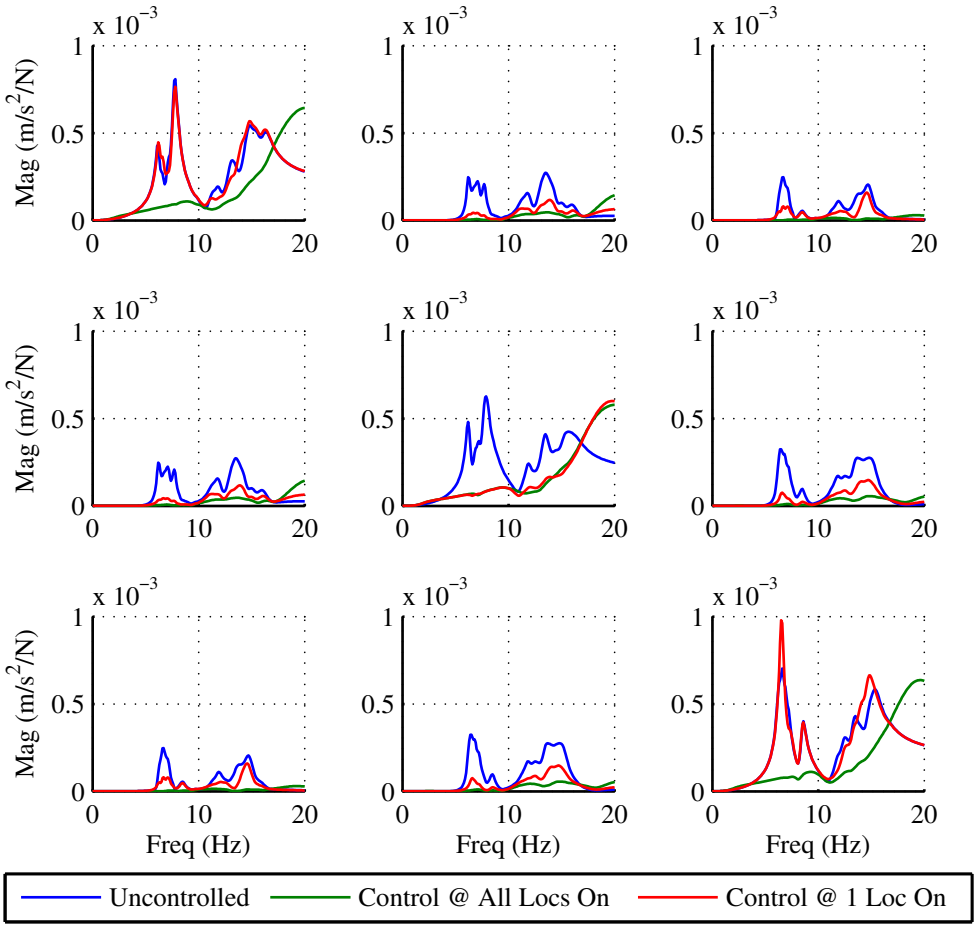

Figure 4.24: Transfer function plots for three locations on Floor B

performance at higher frequencies (typically greater than about 18Hz) is actually worse with control - i.e. energy is being shifted to these higher frequencies. This is generally not a problem because the higher frequency modes are not as easily excited by human excitation which contains most excitation energy at relatively low frequencies (Živanović et al., 2007). Therefore, the performance benefits by decreasing the low frequency response typically far outweigh the increase at the higher frequencies. However, care must be taken to ensure that the gain is not increased to such an extent that the system becomes unstable at this frequency region.

The results in Figures 4.21-4.23 clearly show the effect AVC has upon the global structural response. Each panel that contains an actuator has a highly attenuated structural response. However, this attenuation does not extend beyond the boundaries of each panel. This is because the response at each location is a result of the combination of many modes of vibration, each localised over a different portion of the structure. Each actuator will control the modes at its location very well, hence the high attenuation in that panel. However these modes are only some of the modes that contribute to the response in adjacent bays. This idea is best presented by considering the transfer function plots for the controlled system similar to that previously described but with only one actuator active. This is shown by the red lines in Figure 4.24 where the second actuator, at $(x, y) = (51, 6)$ is active.

Here it can be seen that the collocated response for the second actuator is significantly reduced, as are the off-diagonal terms related to actuator 2. This shows that the modes that have a non-zero amplitude at position two are successfully controlled. However, the collocated responses away from point 2 are not significantly reduced, and in fact for point 3 are increased. This is because of the contribution from other modes that are not controllable from position 2.

Considering Figures 4.21 and 4.22 it is apparent that the various configurations of AVC with actuators in alternate bays is insufficient to successfully control all

modes of vibration; it is not until an actuator is placed in each panel, as shown in Figure 4.23, that a high level of attenuation is observed in all bays.

Finally, it is interesting to consider the effectiveness of each actuator by examining the reduction in response for the controlled case compared with the uncontrolled. This is presented as the reduction in R factor from the uncontrolled case for AVC configuration 1 in Figure 4.25. Here it becomes apparent that the reduction in response is isolated to each panel individually.

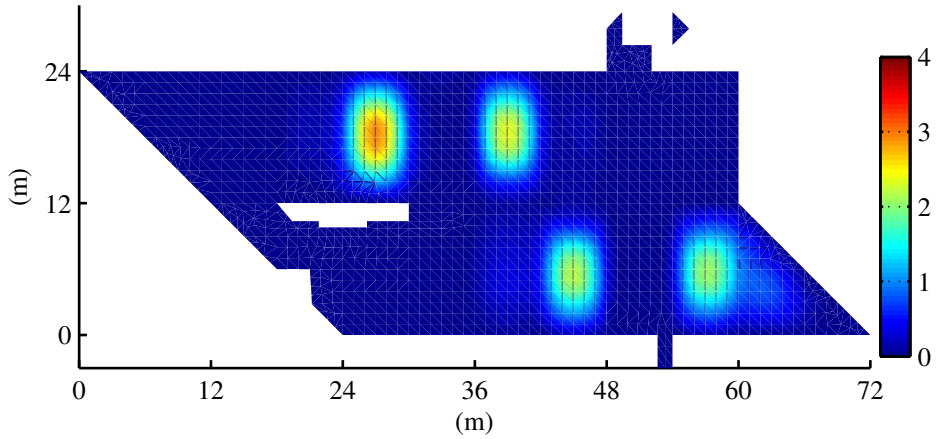

Figure 4.25: Reduction in response for AVC configuration 1 on Floor B

4.5.2 Floor C

Uncontrolled

Walking was also simulated on Floor C. The 5% exceedence contour plot of the response was calculated for the uncontrolled case, as shown in Figure 4.26 using the same method described in Section 4.5.1. This plot indicates that the response is of similar level to Floor B. The response is generally slightly lower for this structure but has the similarity that the response is highest around the middle of each panel. However, it is important to note that the structural arrangement of this structure means that each panel is much larger compared with the bays in Floor B.

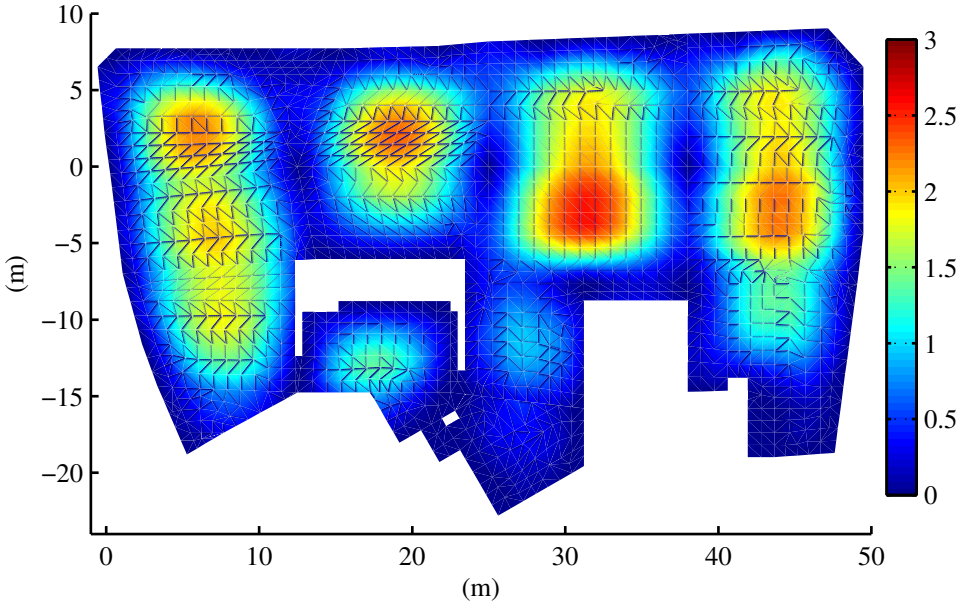

Figure 4.26: Contour of response with 5% probability of exceedence for uncontrolled Floor C

Controlled

Following from the uncontrolled simulations an AVC system was designed to reduce the response of the floor. Four control locations were chosen based on the areas of high response in the uncontrolled case and the mode shapes. These locations are shown in Figure 4.27. Recall that the structural arrangement of Floor B meant that the effect of each control unit was localised to each panel. Therefore, it is interesting to observe how localised the AVC system effects are in this floor. This is demonstrated for the control units located at $(x, y) = (43.8, -3)$, $(31.5, -3)$ and $(18.8, 3)$ in Figure 4.28 (referred to as locations 1, 2 and 3 respectively) where the transfer function plots of the uncontrolled, fully controlled and partly controlled (one unit active) are shown. Here it can be seen that the fully controlled case achieves very significant reductions in the response at each location. However, when only one actuator is active the reduction is still localised to each panel. However, the bays are larger in this case and the control is therefore likely to be effective over a larger physical area. Furthermore,

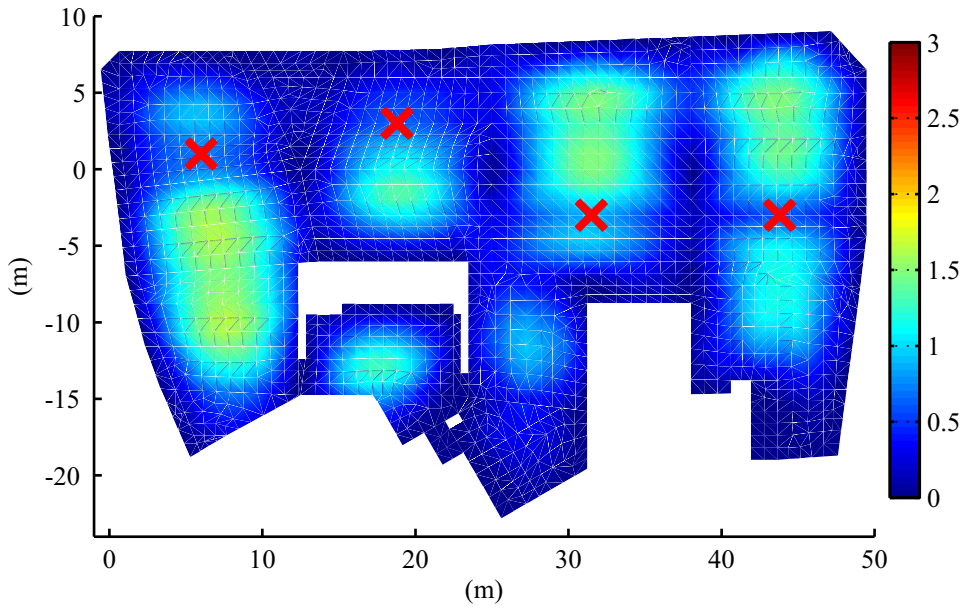

Figure 4.27: Contour of response with 5% probability of exceedence for controlled Floor C

it can be seen that there is an appreciable reduction in the response for location 3 in this partly controlled case. By examining the cross-accelerance FRFs it is clear that the mode that contributes significantly to the high response at location 3 is controllable at location 2, and therefore the control has the effect of reducing the response at this location. This is achieved because the mode shapes are more global in nature and so the control can have an appreciable effect at a large distance away. This effect is not observed for more modes than it is because the minimum number of actuators have been used which means that the overlap of controlled modes will be at a minimum - hence, the effect of having more global mode shapes is that fewer actuators are needed.

Walking was once again simulated on the floor and the response measured at all locations such that a contour plot of the 5% exceedence could be generated. This is shown in Figure 4.27. Here it can be seen that the response is significantly reduced across the entire floor structure using only four actuators. The effectiveness of each actuator is shown in Figure 4.29 as the reduction in R factor from the uncontrolled case. This confirms the previous results, namely that the vibra-

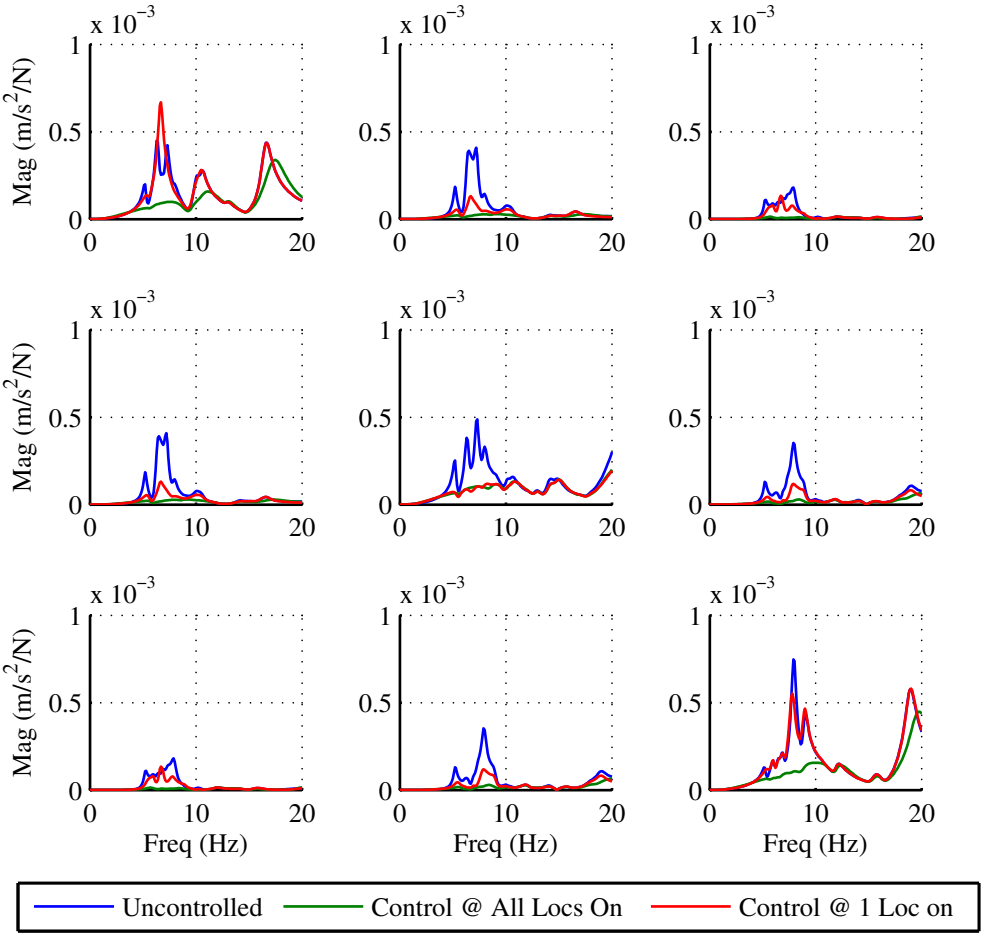

Figure 4.28: Transfer function plots for three locations on Floor C

tion mitigation is still localised to around the actuator. However, the larger size of the bays and the more global mode shapes mean that the area controlled is increased. There is a slight extension of this effectiveness into nearby bays and this contributes to a small reduction in response here too.

4.6 Conclusions

The walking simulation model, first described in Chapter 3, was calibrated and verified in this Chapter. This extends upon the probabilistic force model by Živanović et al. (2007) in order to simulate multiple pedestrians walking to and from random locations within a floor area. The simulations were applied to finite

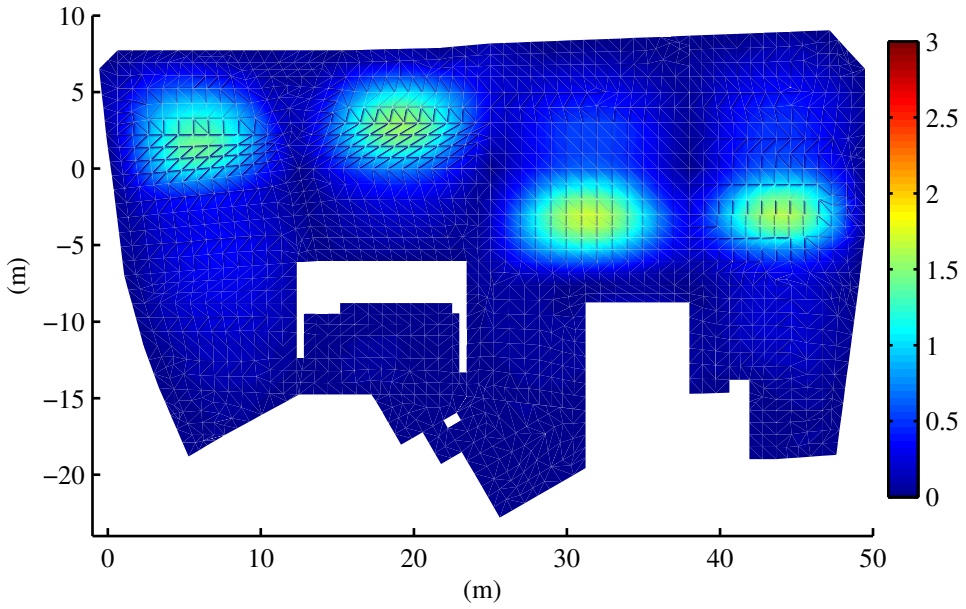

Figure 4.29: Reduction in response with AVC on Floor C

element models of two structures: one structure was used to calibrate the number of people walking whilst the other was used to verify these results. A close correlation with measured data was found on both floors which demonstrates the great potential this method has for predicting the response of structures with a loading more similar to that of typical in-service loading.

A decentralised controller was also simulated on each floor. Contour plots of the response in both the uncontrolled and controlled scenarios showed how the control effectiveness varied throughout each structure. Floor B required a relatively large number of actuators because the effectiveness of each was quite localised to the panel in which it was located. On the other hand, Floor C required fewer actuators to control a similar floor area. This is because the size of each panel was larger and so the effect of AVC was also spread over a larger area. Additionally, the mode shapes are global in such a way that control can be extended slightly to areas outside the panel. The actuators were located such that the minimum number were needed to control the floor area, and this means that redundancy between the actuators is minimised. This indicates that a rule of thumb for the number of

actuators required to control a floor area is based on the number of bays, rather than on the number of modes as is often the case in traditional control applications.

The increasing number of modern floor structures suffering from excessive vibration problems means that the inclusion of AVC at the design stage is becoming a possibility. The implications of this work are that in this scenario it could be beneficial to design a floor to be more flexible and have larger bays in order to improve the effectiveness of AVC and hence reduce the number of required actuators. Whilst this could have the effect of increasing the response of the structure in the uncontrolled case, when the control is active the response will be significantly reduced.

Chapter 5

Control Laws from the Power Demand Perspective

The work in this Chapter investigates the trade off between performance of AVC and the power demand required. Here, research considers if there are any potential improvements that could be made to the power demand of active control without compromising on the perceived response of the structure. The work presented is an adapted form of a conference paper presented at IMAC XXXI (2013). Details of this paper are as follows:

> M J Hudson, P Reynolds, and D Nyawako. Power requirements for active control of floor vibrations. In *Proceedings of IMAC XXXI*, California, 2013. Society for Experimental Mechanics.

5.1 Introduction

There have been numerous papers in recent years examining the use of active vibration control (AVC) for the mitigation of annoying vibrations in floor structures (Hanagan, 1994; Nyawako, 2009; Díaz and Reynolds, 2010a; 2009a). These have been shown to be very effective at reducing the vibration responses of the floors. However, when real floor structures are observed to require vibration mitigation, it is generally only passive technologies such as tuned mass dampers (TMDs) that are utilised; very rarely is AVC considered as it is still at a relatively new stage for this application.

Whilst AVC is a fairly well developed technology in other fields, e.g. aeronautics, space and marine, its use for the mitigation of floor vibrations is still emerging. This is one of the reasons why the hardware associated with it is typically expensive. In addition to this, AVC has on-going costs associated with running the active devices. Over the life of a building this could amount to substantial electricity costs. The research in this chapter investigates the issue of on-going electricity costs from the perspective of controller design.

Much research into AVC for floors has focussed on the use of direct output feedback (DOFB) controllers. For example, direct velocity feedback (DVF) has been the basis of much research (Hanagan, 1994; Hanagan and Murray, 1998; Hanagan, 2005a). Here, the structural acceleration from the accelerometers is integrated and a constant gain applied to the resulting velocity. In the absence of actuator dynamics this acts to increase the structural damping. However, actuator dynamics have a destabilising effect for high feedback gains. Developments from DVF have included: response dependent velocity feedback (RDVF) (Nyawako and Reynolds, 2009); compensated acceleration feedback (CAF) (Díaz and Reynolds, 2010a); DVF with a feedthrough term (Díaz and Reynolds, 2009a) and On-Off nonlinear control (Díaz and Reynolds, 2010b). These developments all utilise the key benefit of DVF, namely that the structural damping is effectively enhanced, but offer

some improvement. For example, RDVF effectively employs an automatic gain selection for DVF, whilst CAF and DVF with a feedthrough term deal with some of the instability issues brought about through the dynamics of the actuators. The On-Off nonlinear control aims to eliminate stability issues that can arise through non-optimal feedback gain choice when using DVF.

Alongside these developments, model-based (MB) controllers are being investigated for this application; research in this field for the application of floor vibrations is on-going however literature in this area is much less common. For example, an LQR (Linear Quadratic Regulator) controller was examined by Nyawako (2009) which used the threshold of human perception of vibrations and output constrained control for the optimisation procedure. Further to this, independent modal space control (IMSC) and Pole-Placement technologies have been investigated by Nyawako et al. (2012) to isolate individual problematic modes in an attempt to reduce spillover instability and improve robust performance.

There are two aspects from the currently developed control laws that have potential to facilitate savings in power requirements for AVC of floor vibrations. Firstly, there is the possibility of using a model-based controller that utilises known structural dynamics to control specific modes of vibration. For example, IMSC provides a framework through which one can control low frequency modes that are more likely to be problematic whilst leaving higher frequency modes uncontrolled. In theory, this could allow the controller to reduce the energy used for control purposes whilst still achieving vibration mitigation performance for critical structural modes of vibration. Secondly, the use of a switching-off rule as used in the on-off control could be utilised. This would allow the actuator to become inactive during periods of low structural response and only be active when the response exceeded a particular threshold. This chapter investigates these two ideas through experimental research performed on a laboratory slab structure. Additionally, the use of a switching-off rule is further investigated through simulations with realistic in-service loading on a finite element (FE) model of a floor.

The development of the control algorithms is discussed in Section 5.2. Following from this, the experimental investigation is discussed in Section 5.3 and the further investigation into the switching-off rule is discussed in Section 5.4. Finally, conclusions are drawn in Section 5.5.

5.2 Active Controllers

5.2.1 Direct Output Feedback Design

The direct output feedback controller used in this study is a modified form of DVF. Here, the acceleration signal from the accelerometer is passed through a 2nd order high-pass filter at 1Hz to remove low frequency components before being integrated to yield a velocity signal. A 1st order low-pass filter is also included at 50Hz to avoid the actuator attempting to control very high frequency modes and noise. Finally, an actuator compensator is included to artificially reduce the natural frequency and increase the damping ratio of the actuator. The feedback gain is chosen such that a gain margin of 2 and a phase margin of 30° are achieved. A saturation non-linearity at 2V is included in the command signal in order to reduce the chance of stroke saturation occurring at low frequencies and to avoid force saturation. In addition to this, for some of the tests a switching-off rule has been incorporated to deactivate the actuator when the root mean square (RMS) of a previous block of data is below a threshold value. The general schematic which is used for both the DOFB controller and the MB controller is presented in Figure 5.1, whilst the schematic for this DOFB controller is shown in Figure 5.2.

5.2.2 Model Based Design

The model based controller used in this study is an IMSC design, as described by (Nyawako et al., 2012). The active control configuration is very similar to that described in this study. It was demonstrated that one actuator and two accelerometers can control the first mode of vibration whilst leaving the second mode un-

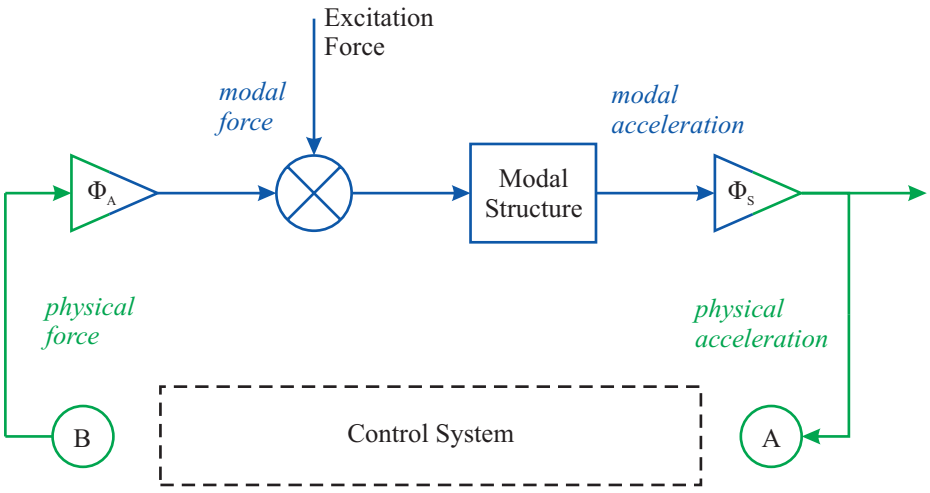

Figure 5.1: General AVC Schematic

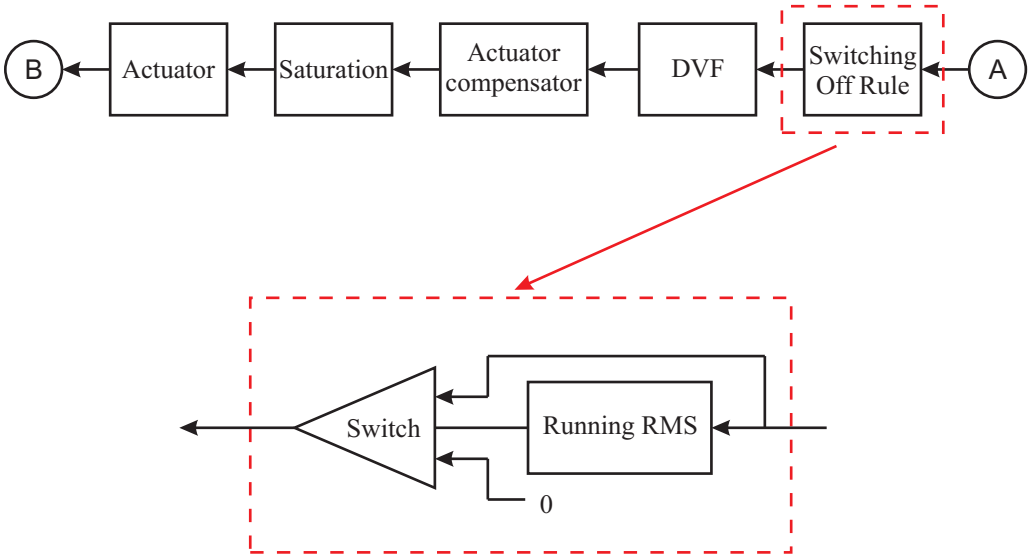

Figure 5.2: Control architecture for the DVF controller

attenuated. Here, the simple dynamics of the structure are utilised to simplify the design process. The structural mode shapes' orthogonality condition is utilised, resulting in the actuator being located at one third span and the two accelerometers at third and two-third spans respectively. In this way, the accelerometers and actuators are located at nodal points for modes 3-6, as shown in Figure 5.4 and the phase of the second mode differs by exactly 180° between the two accelerometers. This means that the acceleration signal from each accelerometer can be combined and the resultant signal will only feedback to control the first mode of vibration.

The controller schematic is shown in Figure 5.3.

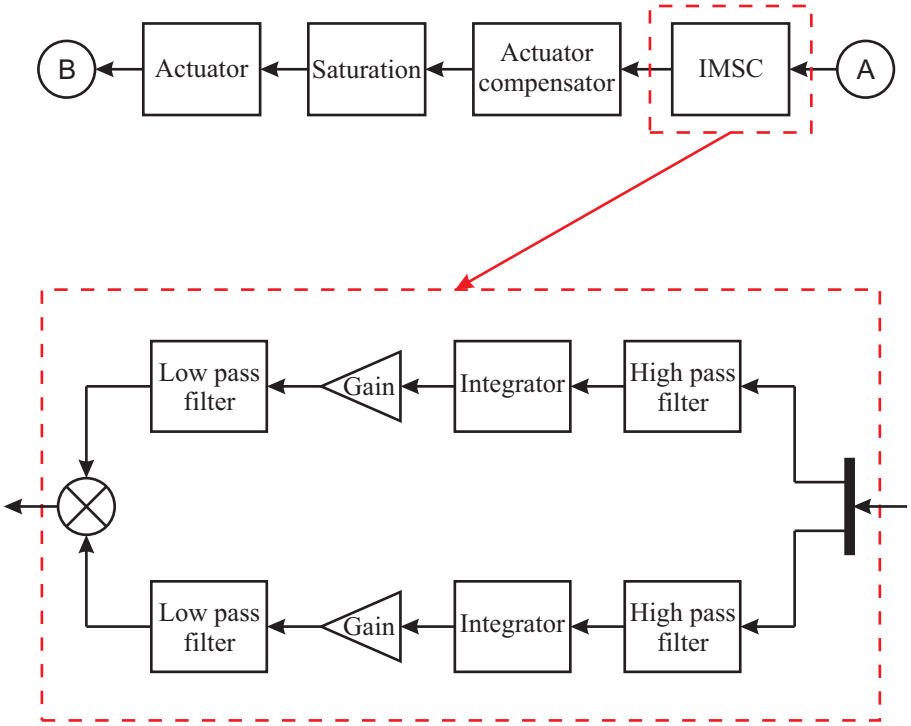

Figure 5.3: Controller design for IMSC

5.3 Experimental Investigation - Floor D

5.3.1 System Description for Floor D

Modal properties

The structure used for this testing is a laboratory slab strip at the University of Sheffield. This is a 11.2m $\times$ 2.0m $\times$ 0.275m reinforced concrete slab spanning 10.8m between knife edge supports. The modal properties of this structure were determined through a forced vibration test using one APS dynamics model 400 shaker located 2.9m from the support and 0.2m from the long edge of the slab, and 21 Honeywell QA accelerometers located on an irregular 3 $\times$ 7 grid throughout the structure. This irregular grid was chosen to capture as many modes as possible within the frequency band of interest. The data were processed in ME'scope and

modal parameters identified using global curve fitting with the Ortho Polynomial method. The resulting mode shapes are shown in Figure 5.4 and modal parameters in Table 5.1.

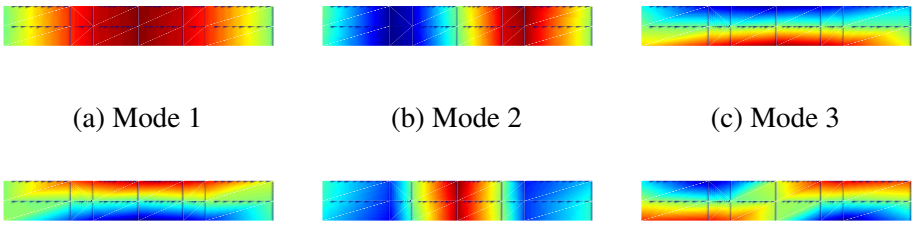

(a) Mode 1 (b) Mode 2 (c) Mode 3

(d) Mode 4 (e) Mode 5 (f) Mode 6

Figure 5.4: First six modes of vibration of slab strip

Mode Number	Natural Frequency / Hz	Damping Ratio / %	Modal Mass / kg
1	4.6	2.2	6010
2	16.8	0.5	6010
3	26.1	1.2	3540
4	28.7	1.1	21250
5	37.7	1.2	7310
6	51.4	2.3	2600

Table 5.1: Modal properties for first six modes of vibration of slab strip

The modal mass estimated for the fourth mode of vibration is very large. Indeed, this is larger than the total mass of the structure itself and so cannot be physically correct. This mode of vibration is very close, both in terms of frequency and mode shape, to the third mode of vibration which makes it difficult to approximate accurately. This mode splitting has occurred because the support conditions are not perfectly simply supported there is a gap between support and structure at one of the corners (Reynolds, 2000). The increased modal mass will reduce the simulated response of the fourth mode. However, the modal mass for the third mode of vibration is a much more realistic value and it is believed that the net effect will be a response spectrum similar to reality.

Walking force

The aim of this chapter is to determine and compare the typical power demand from the active control system due to walking excitation. However, to allow for accurate comparisons the excitation must be repeatable and human walking is not: there is both intra- and inter-person variability with walking excitation (Živanović et al., 2007). Therefore, it was decided that the excitation would be provided by another inertial mass actuator generating a force representative of walking. This was done by converting a walking force time history into a command voltage such that when this was used to drive the actuator a force representative of walking was generated.

The force time history for a pedestrian walking at around 2.2Hz to 2.3Hz was measured using an instrumented treadmill (Racic, 2009). This frequency of walking has a second harmonic that will excite the first structural mode of vibration. However, it is very difficult to generate the component corresponding to the first harmonic of this walking because of the stroke limits of the inertial mass actuator. As this frequency component is not the primary cause of the structural response, it was deemed justifiable to remove this component from the time history through the use of an 8th order high-pass Butterworth filter at 3Hz. It is worth noting that a high order filter, such as this, significantly modifies the phase of the signal. However, it has been shown that the phases between walking harmonics are random (Živanović et al., 2007) so this additional phase contribution was not considered a problem.

The actuator was driven in current mode so that the dynamics did not include the third order lag term that is introduced by running in voltage mode. This meant that the inverse was physically realisable because the numerator and denominator coefficients were of the same order. However, the inverse of the actuator dynamics were modified with the use of a 2nd order high-pass Butterworth filter at 0.5Hz to avoid magnification of low frequency components, as shown in Figure 5.5.

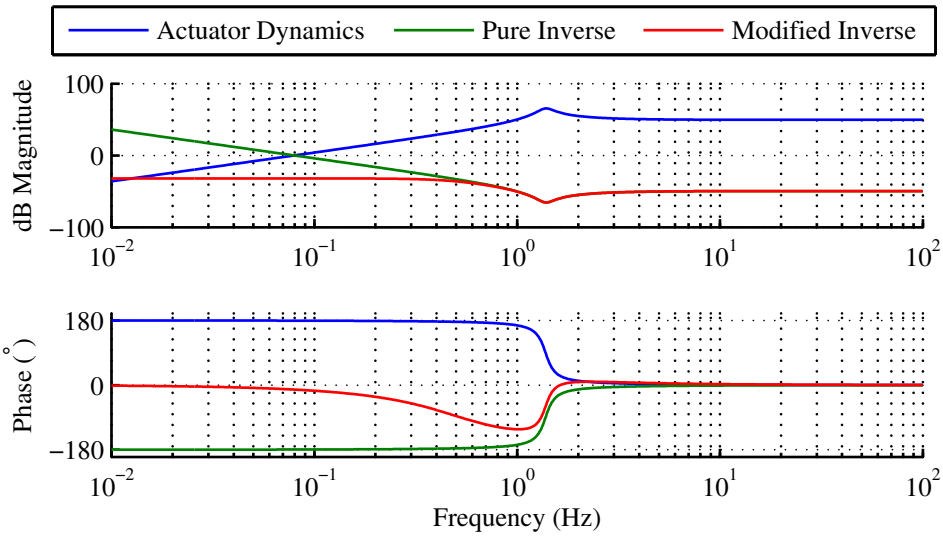

Figure 5.5: Original and modified inverse of actuator dynamics

The net effect of all the filtering on the walking time history is shown in Figure 5.6a. Here, the original force time history after filtering at 3Hz is shown along with the force measured from the actuator when simulating this force time history. A close correlation is observed between the experimental force and the filtered treadmill data, with the exception that the amplitude of the sharp peaks are slightly reduced for the actuator force. A closer examination into the frequency content of these two forces indicates that this can be considered negligible. A fast fourier transform of similar time history segments of each force was calculated and these are presented in Figure 5.6b. It is apparent from Figure 5.6b that above about 2Hz, the original treadmill force, the filtered treadmill force and the force from the actuator are almost identical. There is a slight peak in the actuator force which corresponds with the resonant peak of the actuator in current mode at 1.38Hz. However, this peak is minimal and does not contribute significantly to the response of the structure so is not problematic.

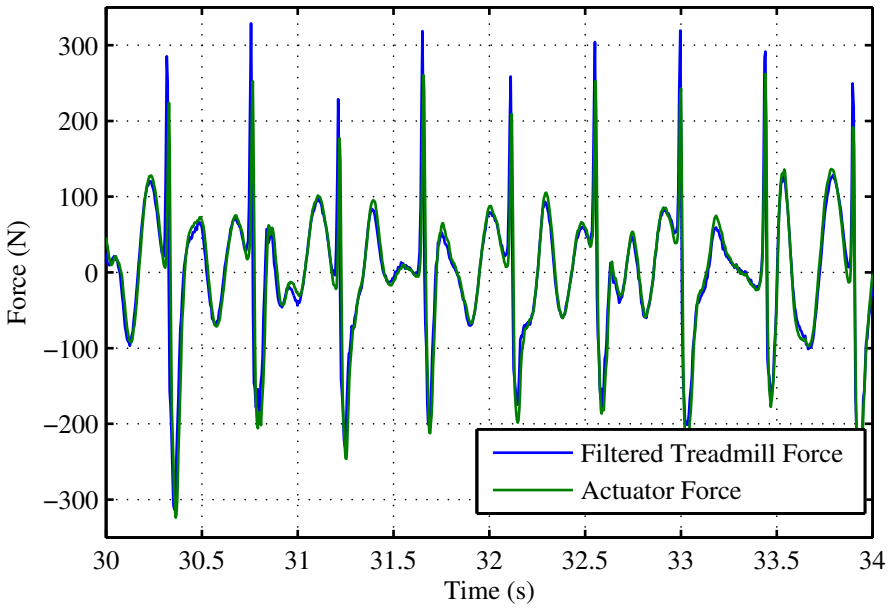

(a) Measured and theoretical walking time history

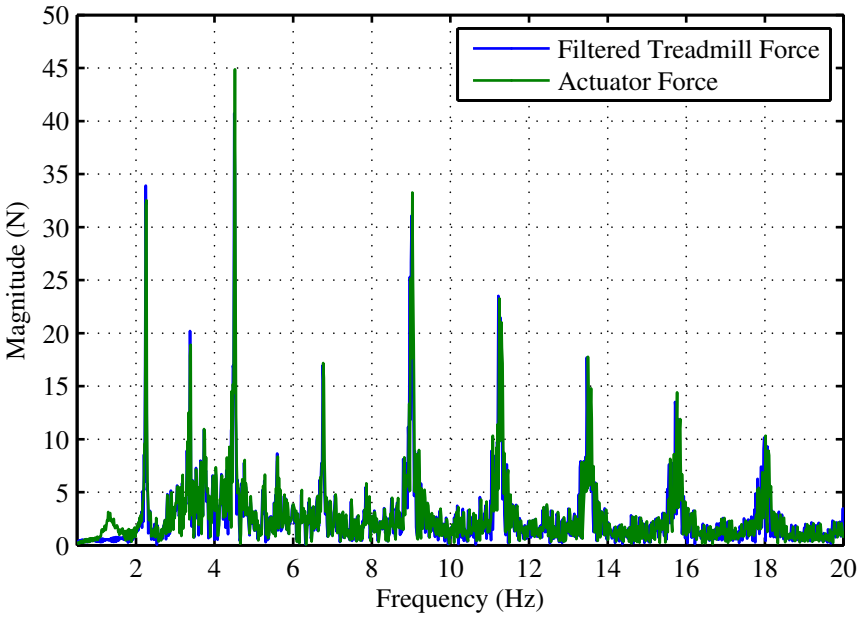

(b) Frequency content of measured and resynthesised forces

5.3.2 Results for Floor D

The power demand of the actuator and amplifier was measured through the use of a custom built power meter. This device samples the mains voltage and current

supply at 2.8kHz to calculate the average power over 5 mains cycles (0.1 seconds). The power meter was used to monitor the APS Electrodynamics model 124 EP extended power amplifier when this was used to drive the APS Electrodynamics model 400 shakers with attached reaction masses. Monitoring the power at this point accounts for all losses within the amplifier and actuator circuit and therefore is indicative of the amount of electricity the device is drawing from the grid.

Both controller types were configured on the laboratory slab structure as described in Section 5.2, and frequency response function (FRF) measurements were taken to validate the controllers were performing as expected. The results of this are shown in Figure 5.7. Here it is observed that DVF successfully reduces the magnitude of response for both modes, whilst IMSC reduces the response for mode 1, but does not reduce the response of mode 2. In fact, a slight increase in the response is noted for mode 2. It is believed that this is due to the assumption that the shape function at the location of both accelerometers is exactly equal and opposite for mode 2. However, slight differences could be expected in reality which may result in the slight deterioration in response at this frequency.

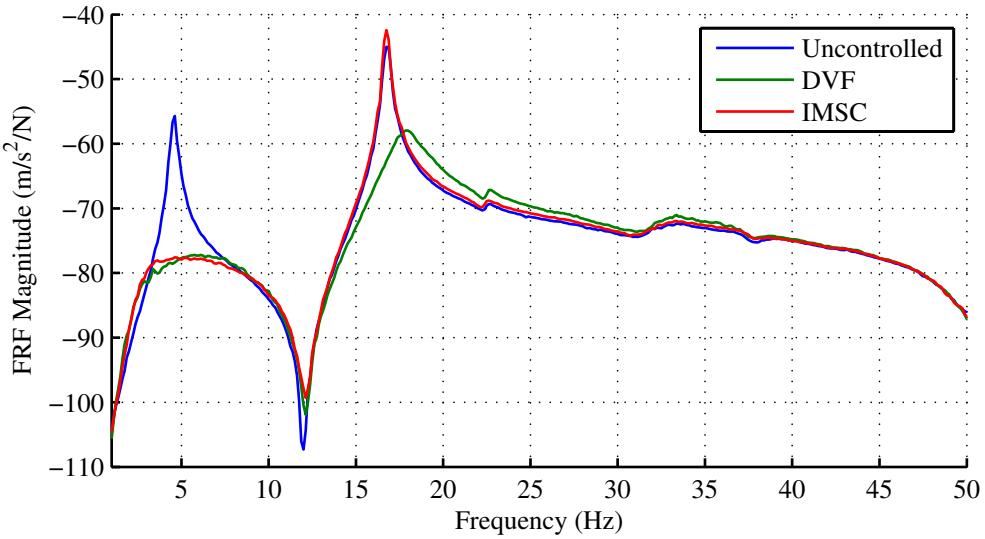

Figure 5.7: FRFs for DVF and IMSC controllers

As previously stated, the aim of this work is to investigate the power demand of

AVC for human-induced floor vibrations. Therefore, two different walking time histories were synthesised using the actuator: one at around 2.25Hz to achieve resonance with the first mode of vibration through the second harmonic of the walking force, and one at 2.5Hz to impart as much energy into the system at higher frequencies as is realistic. The idea behind this second time history is that the impulses due to each footfall will significantly excite the second mode of vibration and so the difference between DVF and the IMSC controller (which controls the first mode but does not control the second mode) should become apparent. In addition to these forces, real walking was conducted on the slab strip for comparative purposes. This set of walking types was applied to the structure with 1) no control, 2) control using DVF controller, and 3) control using IMSC controller. Note that the gain for both DVF and IMSC had to be reduced to 80% of the original value for the case of the real walking excitation in order to avoid stroke saturation from the quasi-static structural response to the 2.25Hz component of the force.

Typical time histories for the acceleration response and the power demand are shown in Figure 5.8, whilst the maximum response measured and average power for each of the experiments is shown in Figure 5.9. The maximum response is characterised by the R factor which is the maximum of the one second running RMS of the W_b frequency weighted acceleration signal, normalised by 0.005m/s^2. These results show that both controllers reduce the maximum R factor recorded for all walking excitation types, as should be expected. However, it is particularly interesting to note the results for the 2.25Hz excitation which aimed to target the first mode of vibration. Here, IMSC does not reduce the response of the structure as much as DVF despite the FRFs in Figure 5.7 showing the magnitude of response for the first mode to be approximately equal for these two controllers. This is because this excitation also has significant higher frequency components that excited the second mode of vibration. Considering the power demand, it is important to note that the amplifiers were left running but had no command voltage

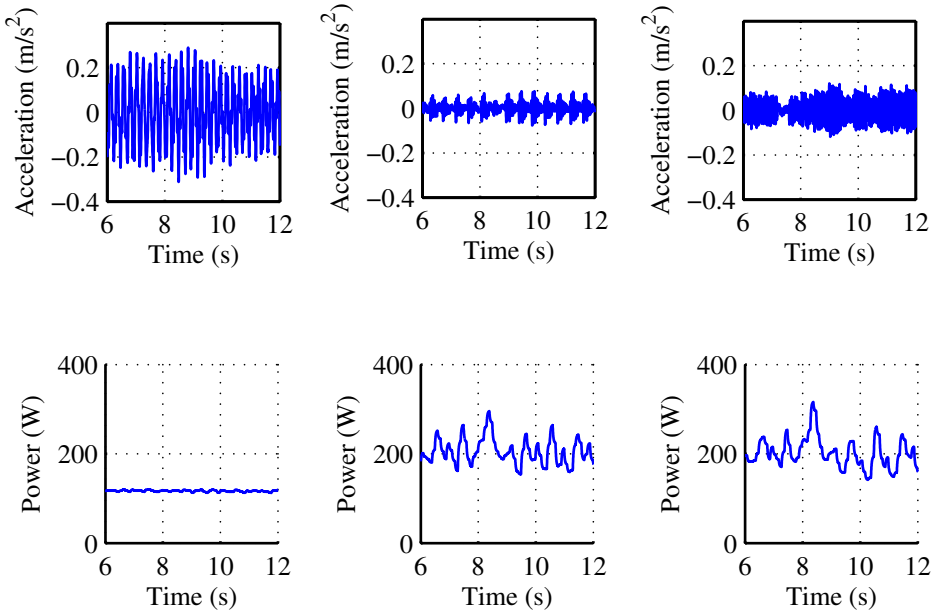

(a) Uncontrolled (b) DVF (c) IMSC

Figure 5.8: Acceleration and average power measured for 2.25Hz synthesised walking excitation

applied to them for the uncontrolled case. This is the reason why all uncontrolled cases reported an average power of 114W - these are the overhead required for the amplifier to run itself. A marginal improvement in the power demand for IMSC over DVF was observed for all three excitation types. However, the response of the structure is significantly higher with IMSC.

Variations in DVF Feedback Gain

In order to explore this area further, the feedback gain of the DVF controller was systematically decreased and the experiment repeated. The resulting changes to the controlled structure's FRF are presented in Figure 5.10, and the results for these controllers subject to the walking excitation are shown in Figure 5.11

It is apparent that by varying the feedback gain for DVF we have arrived at a set of controllers that all lie closer to the utopian goal of zero response for zero power

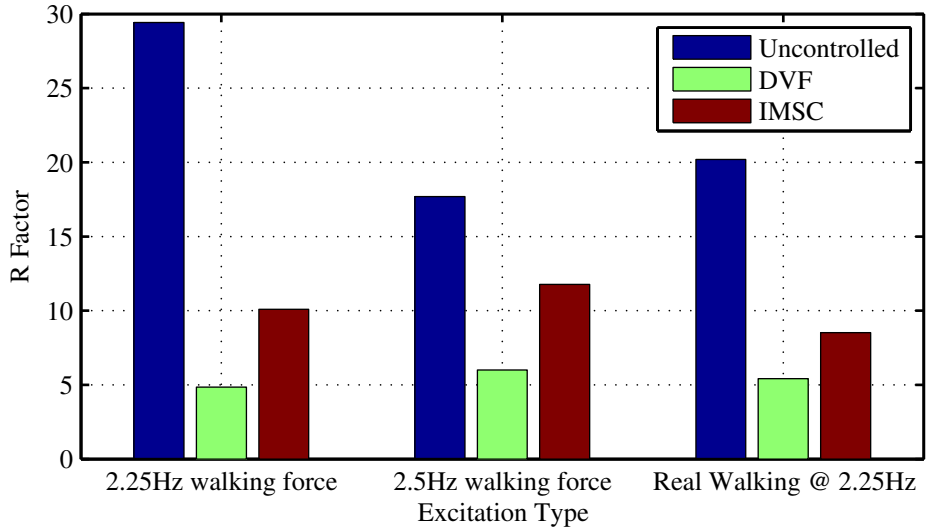

(a) Response

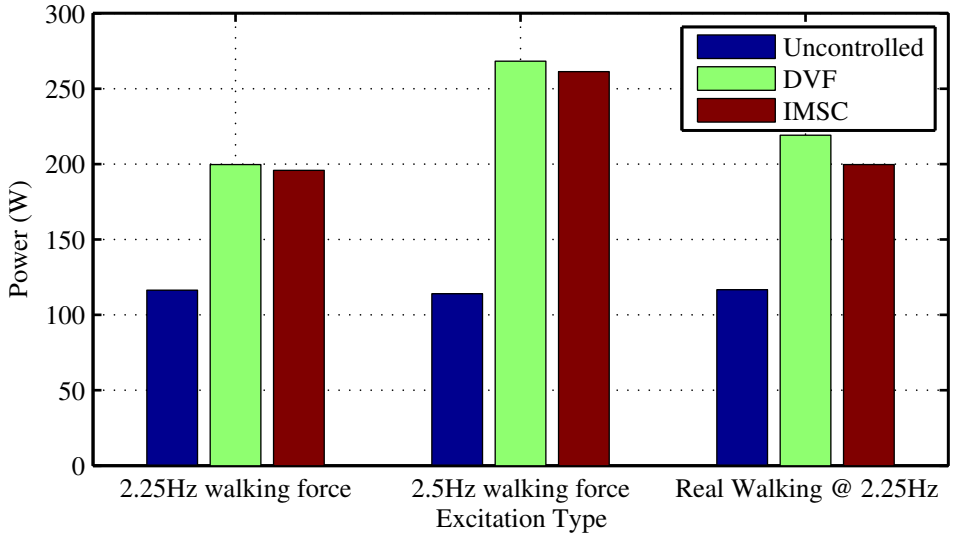

(b) Power

Figure 5.9: Maximum Response factor and average power measured for various types of excitation

demand than the IMSC controller. This means that for this structure the DVF controller is the preferred choice and this is due to the significant contribution to the structural acceleration from the second mode of vibration. It is crucial to note that this does not mean that DVF is "better" than IMSC or other model-based controllers; it means that there is no benefit in designing a model-based controller

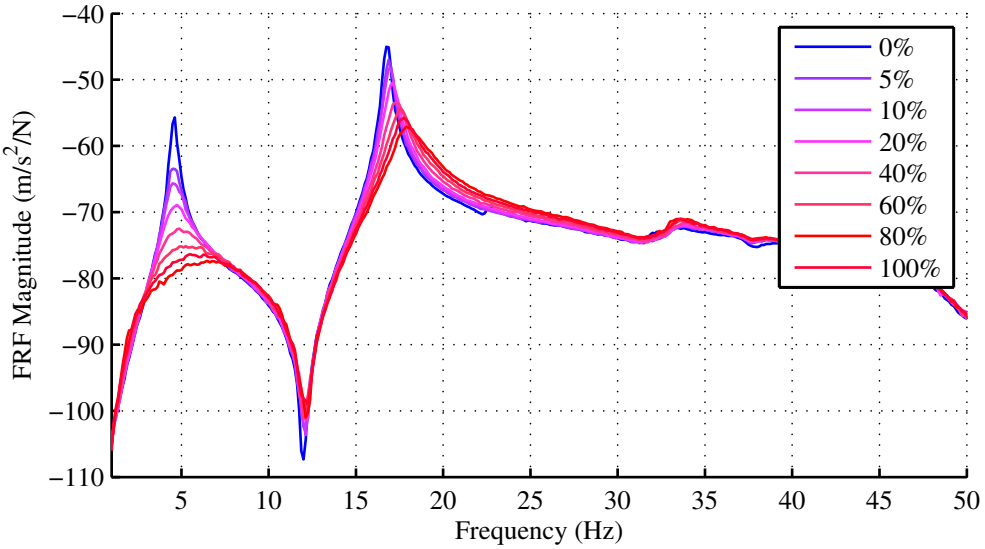

Figure 5.10: FRFs for uncontrolled structure and DVF with gains varying from 5% to 100% of optimal

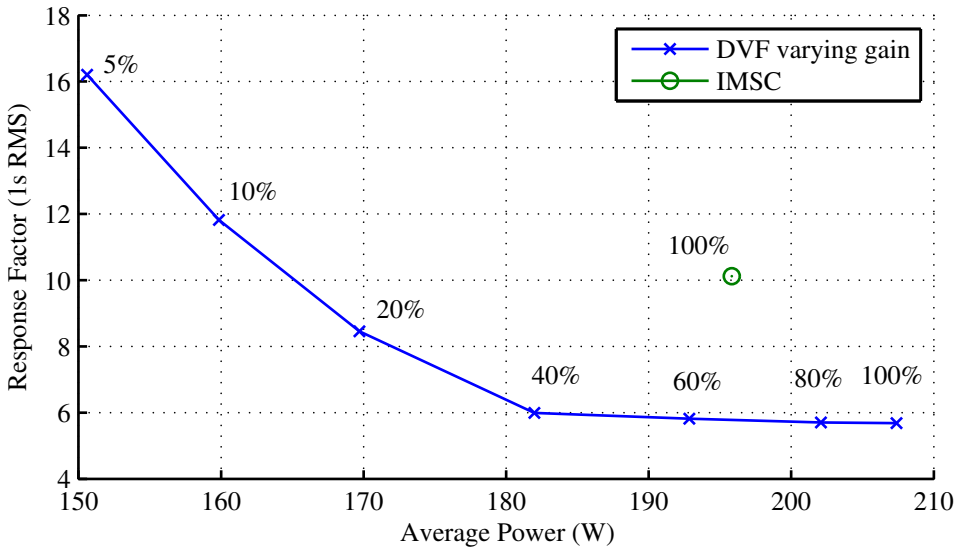

Figure 5.11: Average power and maximum R factor for various feedback gains (as indicated by % of optimal) of DVF and IMSC

to intentionally not control higher frequency modes (within a range excitable by human walking) with the idea of reducing power consumption because little power saving is made and the structural response can be significantly higher.

Use of a Switching-Off Rule

The effect of using a switching-off rule is considered next. The idea here is to prevent the actuator from working when the response of the structure is below a threshold, such that power savings can be made whilst keeping the large responses low. The nature of the excitation/structural system in this study is such that high response levels are achieved and maintained for the entire test duration. This means that the switching-off rule must be set relatively high so that its effect can be seen. A range of different thresholds were chosen, namely from R=4 to R=8 (with frequency weightings applied assuming the response is dominated by the first mode of vibration). In addition to this, a range of time periods used to calculate the RMS response were considered - 1s, 0.5s and 0.25s. A 2nd order high pass filter at 1Hz was used to remove low frequency components of the measured acceleration before the RMS block was calculated. The differences in both vibration response and average power are very small for the controllers tested. This means that the results are more strongly influenced by both external excitation and variance in the amplifier overhead. Therefore, to improve reliability of the experiments, each test was repeated several times and averages of the results were taken. These averaged results from all the tests with the switching-off rule for DVF are shown in Figure 5.12 where they are compared with the results for varying the gain in DVF. Here it is seen that by using a high threshold, i.e. a higher level of response is permitted before the actuator turns on, the maximum response is increased and the average power is decreased. This effect is observed for all RMS block sizes. However, when compared with a simple linear decrease in the gain for DVF it is seen that reducing the gain is a more effective solution for this situation; the average power required for a certain level of response is high when using a switching-off rule. The reason for this can be found by examining the time history of the power demand and structural response, as shown in Figure 5.13. The threshold for the switching-off rule in the controller shown in Figure 5.13 is at an RMS acceleration of $0.042 m/s^2$ which approximately equates to an R factor of 8.

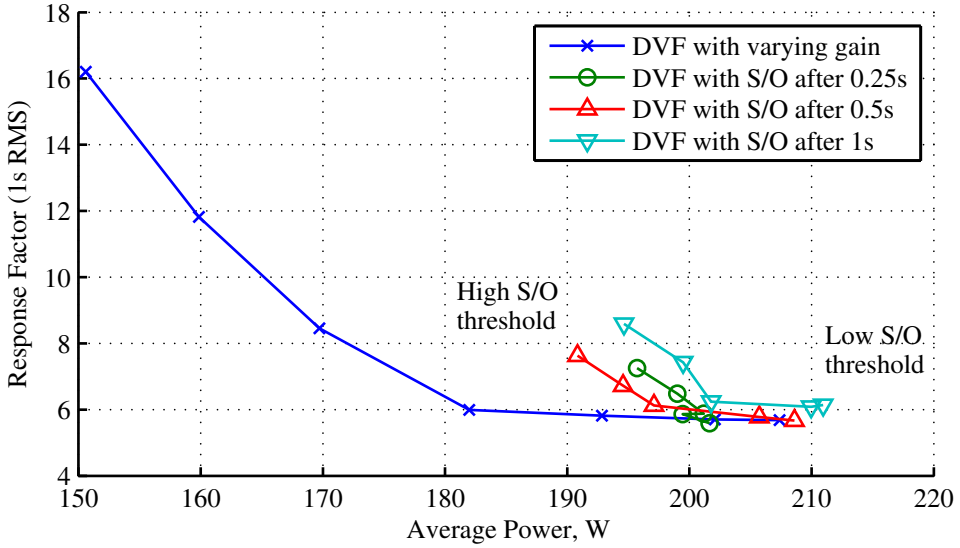

Figure 5.12: Comparing effect on response and power of varying DVF gain with varying switching-off parameters

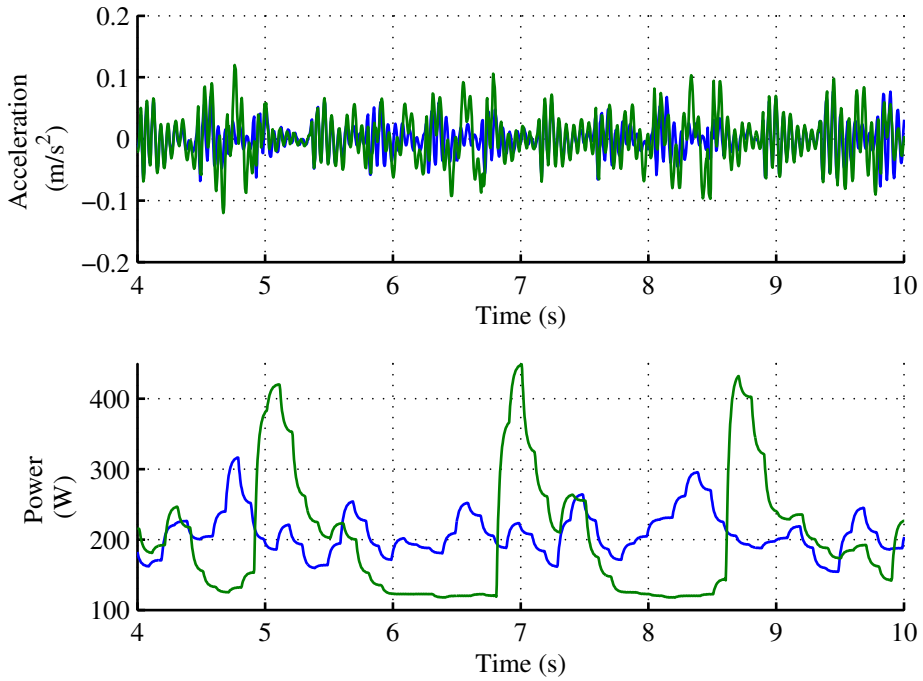

Figure 5.13: Time history for AVC power demand and structural response without a switching-off rule and with

The power demand for the switching-off controller rises rapidly to a high level as soon as the threshold is exceeded. As the response reduces below the threshold the controller switches off. However the continuous excitation will cause an increase in the response. This means that at the instant in time when the response increases above the threshold again, the controller will have to work harder to reduce the response than if it had been working all the time. In addition to this, the delay introduced by having to wait one second to determine the RMS of the acceleration means that the response could actually be higher than the threshold. Evidence of this is seen in Figure 5.13 where the same threshold values are used for each block size, but the response factor measured is lower for the smaller blocks. The continuous nature of the excitation used in these tests meant that the response alternated between being under and over the switching-off threshold relatively rapidly. This increases the proportion of power spikes relative to the total duration. As Figure 5.13 shows, the power demand is low when the response is below threshold, high immediately after the response exceeds the threshold, and approximately the same as the controller without a switching-off rule once the response has exceeded the threshold for a short duration. Therefore, the effectiveness of using a switching-off controller is dependent on the ratio of low to high levels of response.

Finally, a relatively simple deadzone was considered. This is effectively a special case of the switching-off rule where the block size for calculating the RMS of the acceleration is one sample. Thresholds varying from R=1 to R=8 were considered (with the same assumption of frequency weighting being for the first mode of vibration as in previous tests). The results of this are shown in Figure 5.14. Here, again the compromise between increase in response and reduction in power is observed as the deadzone threshold changes. However, all the solutions lie further from the utopian goal compared with simply changing the DVF gain.

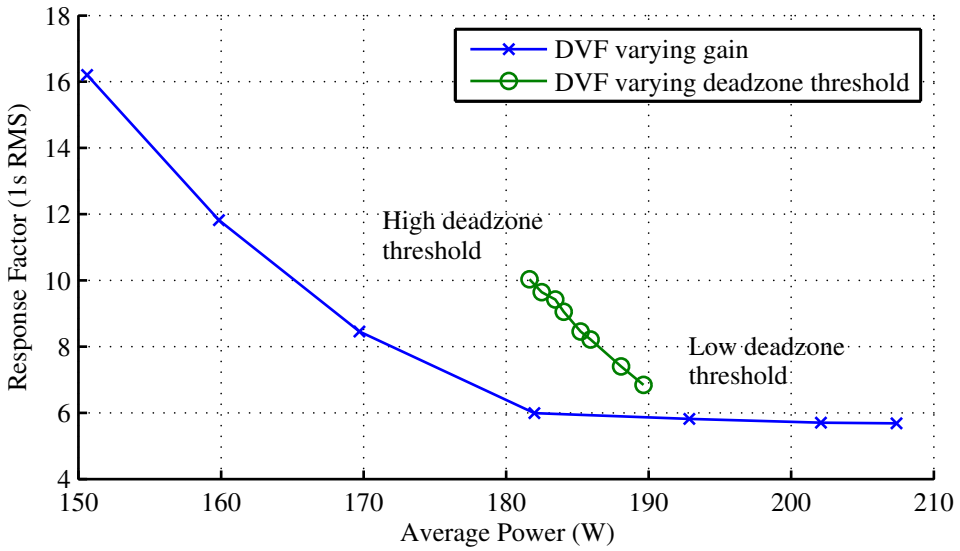

Figure 5.14: Comparing effect on response and power of varying DVF gain with varying deadzone threshold

5.4 Numerical Investigation - Floor A

Additional simulations were performed using the switching-off rule to further investigate the possible effectiveness of this control law. This involved simulating typical office loading onto a model of a real structure rather than using the continuous excitation from just a single pedestrian as considered in Section 5.3.2. This loading has longer periods of relative quiet and so has the potential to demonstrate the benefits of using a switching-off rule more effectively. It is important to note one of the limitations with this method: namely, that the office loading (as validated in Section 4.4.3) does not have any constant noise applied to it to simulate the small effects of non-pedestrian excitation (e.g. internal machinery, transmitted external vibrations etc.). This means that depending on how long each pedestrians route is there could be times when there is absolutely no excitation. In this situation, both a linear DVF controller and a DVF controller with a switching-off rule would generate 0.0V command voltage. However, it is expected that this situation would arise relatively infrequently, especially compared with the situation where pedestrian excitation occurs a significant distance from a particular actuator

and so would generate a small structural response at that location. In this latter situation the two controllers would generate different command voltages.

5.4.1 System Description for Floor A

The structure chosen for this investigation was the 130mm structural variation of Floor A, as described in Section 3.2. This is a composite structure of steel and concrete. A depth of 130mm has been used for the composite slab that spans between the long-span asymmetric cellular secondary beams. These are 748 $\times$ 152 / 210 $\times$ 72.2ACB and the short-span primary beams are 457 $\times$ 191 $\times$ 74UB. Full-height partitions and a lift shaft and staircase core have been added to make the mode shapes more realistic by splitting up the very regular and global modes that would otherwise be expected from the bay layout in this structure. The in-service office loading used as the excitation in this analysis is discussed in Section 6.5.2. As in previous studies the same excitation was applied for each controller type, though this excitation itself was randomly generated.

A baseline level of power demand for a given maximum structural response was derived by varying the feedback gain of a linear DVF controller from 0% to 100% of the desired maximum gain.

The switching-off rule has two key parameters that define its operation: the threshold that the calculated RMS of the structural response must reach before control is activated from the 'off' state, and the time period over which the RMS of the response is calculated. Both of these parameters were varied during the tests. The response threshold was varied through R=1, R=2 and R=3, whilst the RMS time was varied through 0.2s, 0.5s, 1s, 2s and 5s. Whilst these parameters were varied, a constant value of T=1s and R=1 were used for each variable respectively.

Additionally, a 'quiet' office environment was also simulated which had two people starting every minute rather than five. This was done to investigate how the reduced loading in this scenario affected the efficiency of the switching-off rule.

5.4.2 Results for Floor A

The results from these simulations are demonstrated in Figure 5.15. Here, each point represents a single simulation run, characterised by the average power demand during that test (using the correlation between drive voltage as derived in Section 6.5.1) and the response of the most responsive location on the floor.

Firstly, considering the power demand with respect to the absolute maximum response, as shown in Figure 5.15a, the use of the switching-off rule does appear to be beneficial with respect to the use of DVF for some choices of switching-off parameters. However, it should be noted that the differences are relatively small. To investigate this further it is interesting to compare selected time history samples from similar runs.

Figure 5.16 shows the structural response at the position of the first actuator (at $x = 7.5$m, $y = 4.6$m) and the power demand for this actuator too. Note, that this does *not* show the location or indeed necessarily the same run as that which generated the maximum response - it was deemed more appropriate to compare the same test run and location each time regardless of the results summary. DVF with a gain of 60% of maximum and a switching-off rule with RMS duration 1s and threshold value R=1 are the blue and green lines respectively. The DVF controller continuously attempts to reduce the structural response whilst the switching-off rule only does this when the RMS of the response exceeds the threshold value. The calculation of the RMS of the response necessarily incurs a delay in the time it takes for the controller to become active again, meaning that the response may have actually exceeded the threshold value by the time the controller turns on. This is evident in Figure 5.16b where the response for the switching-off rule exceeds the threshold and then is controlled.

These two runs have similar maximum responses but the average power requirements for the switching-off rule are lower. When the power demand rises, the switching-off rule power demand rises to a higher level than the DVF rule. This

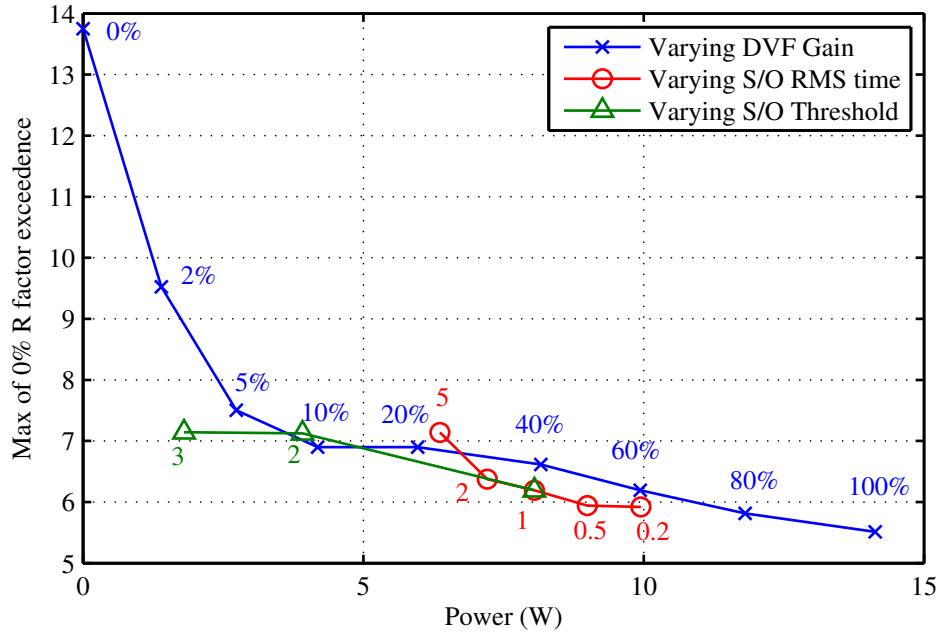

(a) RMS 0% exceedence

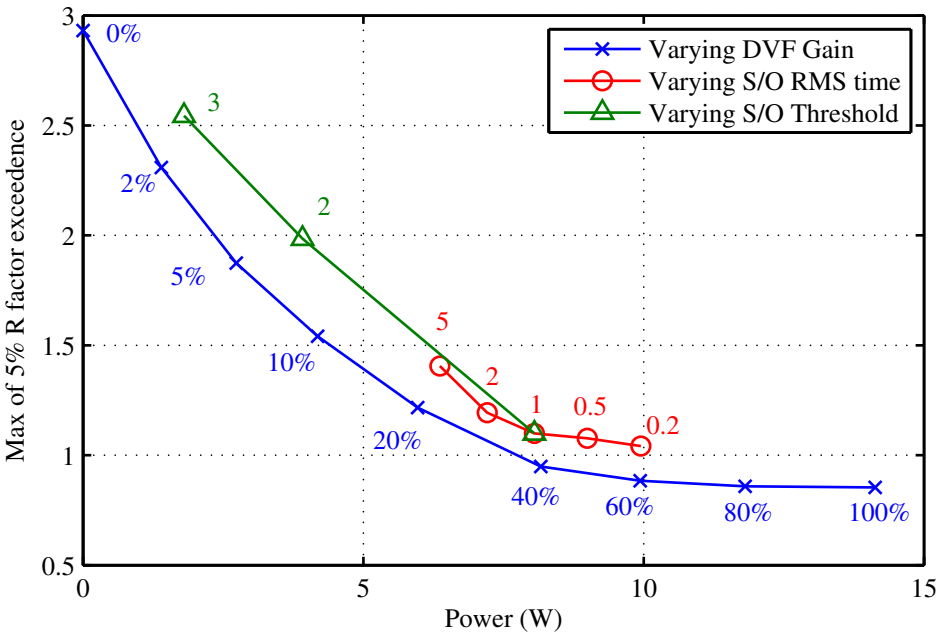

(b) RMS 5% exceedence

Figure 5.15: Summary of power demand results for various controllers under normal office loading

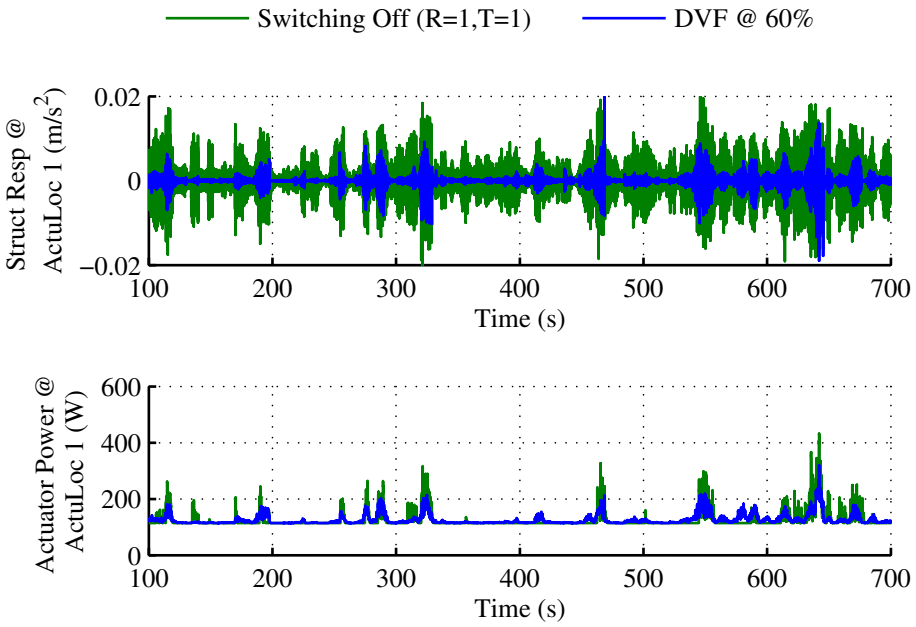

(a) Time History

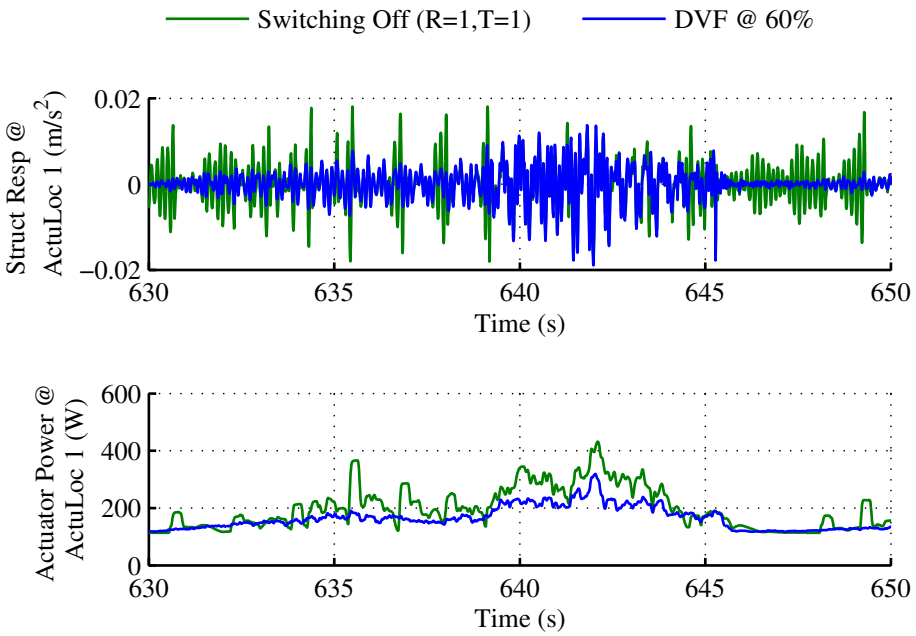

(b) Zoomed in Time History

Figure 5.16: Time history for structural response and actuator power demand for one run with Switching-Off rule and DVF at 60%

is especially evident in the zoomed in view (Figure 5.16b). However, it should be noted that the difference in power is relatively small, as will be highlighted later. The key difference between these simulations is the structural response. As noted earlier, this is *not* the time history which shows the overall maximum response. However, in this run the maximum recorded response is a transient phenomenon and is approximately the same for these two runs, but the response at other times is consistently lower for DVF compared with the switching-off rule. This is because the response is relatively low so the switching-off rule is in an inactive state. This saves power and compensates for the fact that when there is a higher response the switching-off rule has an increased power demand.

Following from this, it is interesting to compare these results with two other cases that have similar responses - DVF with a gain of 5% and a switching-off rule with RMS duration 1s and threshold value R=2 as shown in Figure 5.17.

In this comparison it is evident that the structural response is generally higher for both scenarios; this is expected given the lower DVF gain and the increased threshold for the switching-off rule. However, in this scenario the two controllers effectively achieve the same level of response all the time. This results in a 5% exceedence response which is similar for the two controllers. However, there is a significant difference between the power demand for these controllers. The DVF controller has a low power demand all the time, even during periods of relatively high excitation, as seen in Figure 5.17b. This is because the gain is so low that the actuator effort is minimal. However, the switching-off rule has a gain of 100% so when the structural response does exceed the threshold the power demand is very high. Looking closer at the time history of the structural response, it is apparent that the switching-off rule reduces the response in small bursts, using lots of power as soon as the response exceeds the threshold and reducing the response to near zero and hence turning off the controller. The response then increases because the excitation is still present and the pattern repeats. In this situation, the small gain that is present for the DVF controller is sufficient to keep the response to

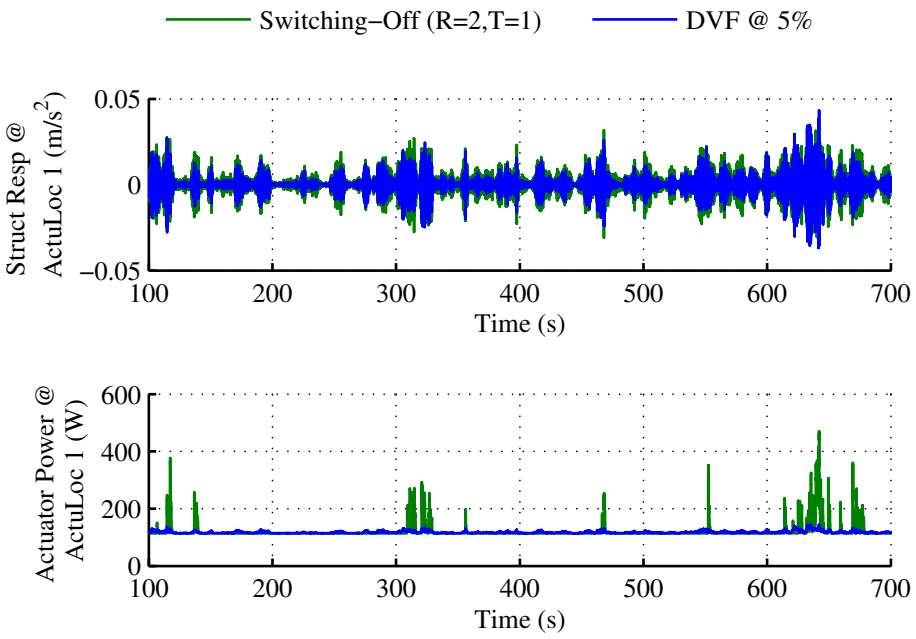

(a) Time History

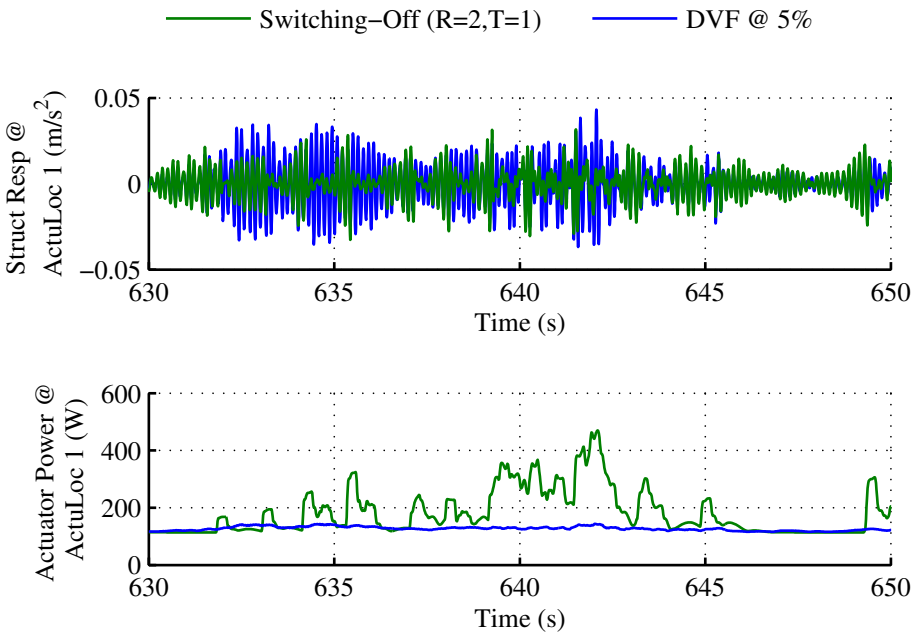

(b) Zoomed in Time History

Figure 5.17: Time history for structural response and actuator power demand for one run with Switching-Off rule and DVF at 5%

approximately the same level as this threshold, whilst operating continuously it has a much smaller power demand. As the power demand at other times is very similar between the two controllers - the net effect is that the switching-off rule achieves the same level of response but at a greater power cost.

As mentioned earlier, a 'quiet' office environment was also simulated to investigate how this would affect the efficiency of the switching-off rule. This was done by decreasing the number of pedestrians starting to walk on the structure from five people per minute to two people per minute. The average power and structural response were measured in a similar way to that for the 'normal' office environment and the results are presented in Figure 5.18.

The results from these simulations are similar to those for the 'normal' office environment shown in Figure 5.15, particularly for the 5% exceedence case. It is clear from Figure 5.18 that both the maximum response and the 5% exceedence response are lower in the quieter office and so too are the power requirements - which makes sense given the reduced applied load. This means that the period of time when the switching-off rule is in the inactive state compared with the standard DVF controller is increased. The maximum response for all switching-off rules is above the thresholds used, so is similar to (though understandably slightly higher because of the time delays involved in calculating the RMS of the response) the case with DVF with 100% gain. This explains why the switching off rule appears more beneficial for the 0% exceedence response measurement. In contrast, the DVF controller works in the same manner as for the 'normal' office environment - namely, the actuator effort is low but continuous. This keeps the general response low and because the gain is low, so too is the power requirement. The switching-off rules with a threshold of R=1 successfully keep the response below this value, but the high gains they use when they are active means that the power requirements are high.

The results from these simulations match well with the experimental results pre-

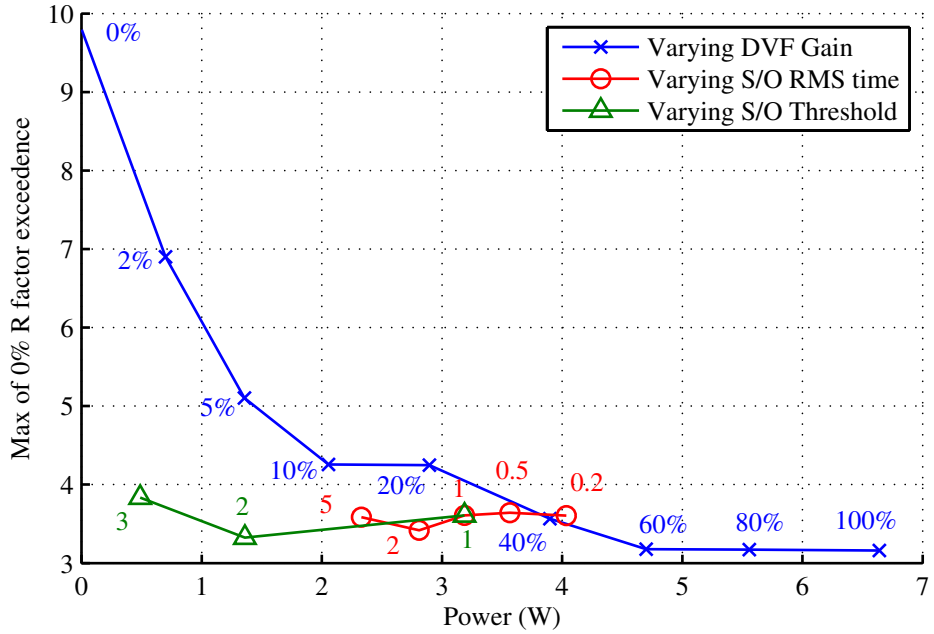

(a) RMS 0% exceedence

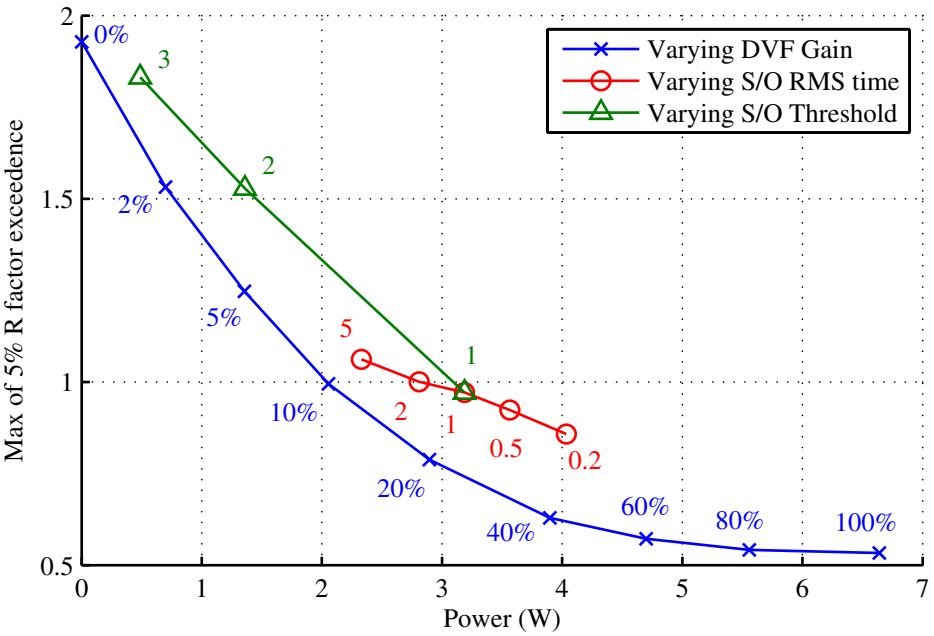

(b) RMS 5% exceedence

Figure 5.18: Summary of power demand results for various controllers under 'quiet' office loading

sented in Section 5.3. The same general relationship between average power and response factor was observed for the varying gains with DVF. Additionally, the use of the switching-off rule also matches well - in the experimental case with continuous excitation the switching-off rule does not perform as well because there are no significant quiet periods for it to improve its average power.

One feature common to all these results is the non-linear relationship between the power demand and the structural response. Diminishing returns are observed for higher gains with respect to the reduction in response for a given increase in power. Considering this from another perspective, this non-linearity can be utilised to facilitate savings in power demand for a relatively small increase in the structural response. As observed in Figures 5.15 and 5.18 this applies both to the absolute maximum and to the 5% exceedence response.

Additionally, it is interesting to compare the FRF plots for the controllers with these varying gains at actuator location 1. These are shown in Figure 5.19.

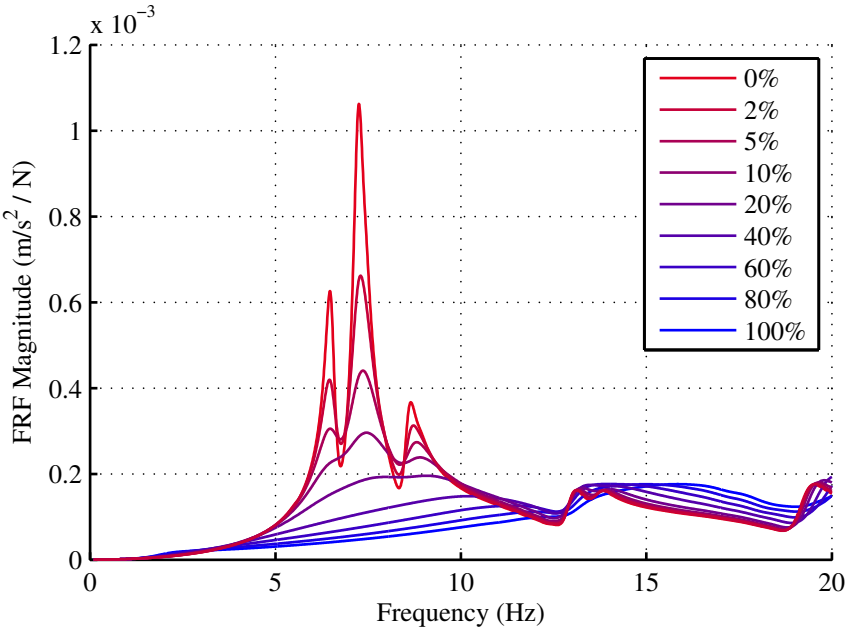

Figure 5.19: FRF magnitude plots for structure at actuator location 1 for a variety of DVF gains

Although the 5% and 0% exceedence responses are much more complicated than the FRF magnitude at a single location, a similar diminishing returns in the response reduction is observed for increasing gains. This mirrors the diminishing returns seen for the 5% and 0% exceedence responses. Indeed, when the root locus plot for this controller, as shown in Figure 5.20, is examined the reason for this becomes evident.

Here, the mode at about 7.3Hz has very significant additional levels of damping introduced as the feedback gain increases. This is highlighted in Figure 5.21 which plots the damping for this mode for various feedback gains.

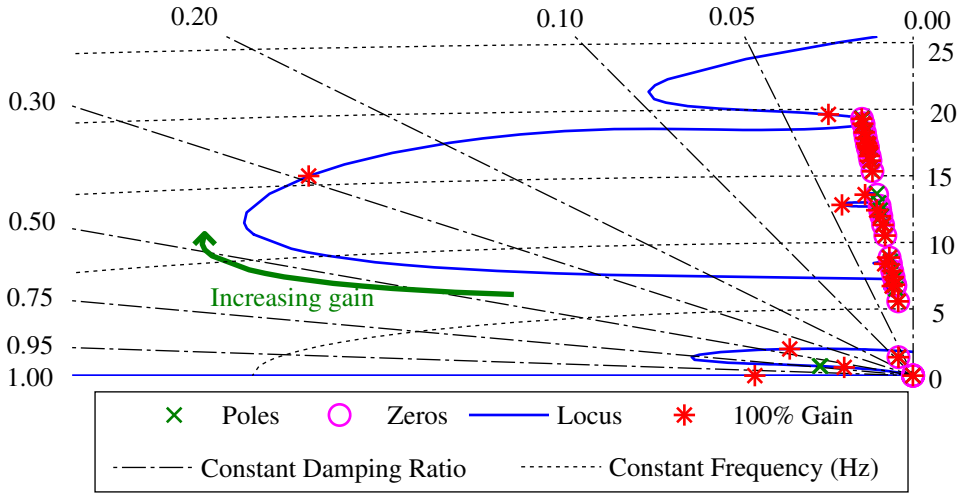

Figure 5.20: Root locus plot for controller design at location 1

For gains below about 0.45 of the design gain the damping increases rapidly. However, this reaches a peak at about 0.5 of the design gain and then steadily decreases up to the design gain. However, although the damping is decreasing with increased feedback gain, this does not mean that the response is also increasing; it is believed that these gain levels corresponds to the beginning of the formation of a nodal point at this location which is how further improvements in the response at this location are achieved (Preumont, 2002). Recall that the feedback gain was chosen to meet specific stability margins with the understanding that the response will decrease with increased feedback gain up to this point. This is indeed ob-

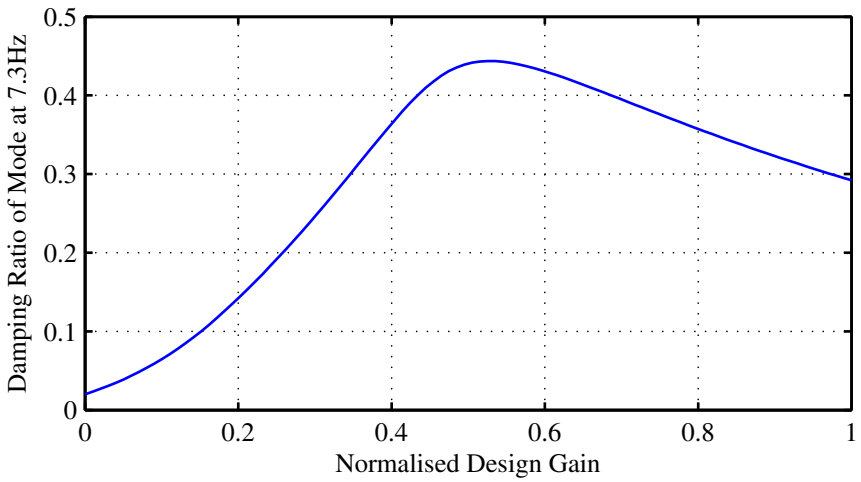

Figure 5.21: Variation in damping ratio with respect to feedback gain

served in both the FRF plot of Figure 5.10 and the response plots of Figures 5.15 and 5.18. It is possible that with this decrease in damping the response is actually increased at other locations. Therefore, there could be an improved control design based on global response minimisation using maximisation of damping. Naturally, when there are many modes of vibration in a specific band of interest then there is some degree of subjectivity as to how the optimum damping values for each mode are combined. Additionally, it should be noted that the poles relating to the other two peaks observed in the bode plot of Figure 5.19 in the 5 to 10Hz region also have increases in damping for increased feedback gain, but the levels of damping introduced are much smaller and so are not visible in the root locus plot of Figure 5.20.

This has potentially significant benefits: a reduced gain increases the stability margins of the system and reduces the possibility of stroke saturation which can both damage the actuators and can also potentially destabilise the system. Furthermore, it may be possible to extend this to utilise smaller, cheaper, actuators given that the force capacity can be reduced without significant increasing the response. As one of the key costs associated with active control is the initial cost of the actuators this could have significant benefits.

5.5 Conclusions

The power requirements of various active control configurations have been investigated. A repeatable walking force has been generated by inertial actuators, which facilitates direct comparisons between controller types for the same excitation input.

It immediately became apparent that there is a high power demand from these actuators when the force output from the actuator is zero. These overheads contribute a significant portion of the total average power demand from the shakers: the largest average power recorded was about 270W indicating that, for these tests, at *best* the overheads accounted for 40% of the total and typically they accounted for the majority of the power consumption. Future work should certainly investigate the use of improved actuation technology that has much lower overheads. Work to this effect is actually already in progress - preliminary results show that the overhead power of an inverter used to replace the current amplifiers for a new actuator technology, as discussed in Section 6.5.3 are approximately 24W. This is a significant improvement on the APS Dynamics amplifiers and with this level of overhead the relatively small changes in power exhibited by the differing control laws will become much more important.

With regards to specific controllers tested, it was observed that no significant power savings were made by using IMSC to intentionally not control the second vertical mode of vibration, when compared with a simple DVF controller. Indeed, the marginal power savings made are far outweighed by the increase in response despite the relatively high frequency of this mode.

For this excitation type the most effective way to reduce the power requirements of the controller are to use a simple DVF controller with a reduced feedback gain. Although the use of a switching-off rule did achieve power savings, the structural response was higher than DVF for any given average power requirement. However, other excitation types may not result in the same conclusion: the ef-

fectiveness of the switching-off rule is dependent on the proportion of time the controller switches from inactive to active resulting in large transient increases in power demand. The use of a deadzone (i.e. a switching-off rule with block size of one) was similarly not as effective as a simple reduction in feedback gain for DVF.

The non-linear relationship between response reduction and power demand has the potential to realise some further improvements to AVC installations; by using a reduced feedback gain it is possible to make power savings and also decrease the possibility of stroke saturation. This in turn means that smaller actuators could be used which may permit significantly decreased installation costs.

Chapter 6

A Life Cycle Analysis

Whilst Chapter 3 demonstrated the significant reductions in response that can be achieved with active control, the costs of doing so were not considered at all. These are investigated in this Chapter by studying what the economical and environmental costs of an active control implementation would be over the entire life of a building. The contents of this chapter are an adapted form of a paper submitted to the ASCE Journal of Structural Engineering. Details of this paper are as follows:

> M J Hudson and P Reynolds. A Life Cycle Analysis of an Office Floor With Active Vibration Control. *ASCE Journal of Structural Engineering*, In Review, 2013b.

6.1 Introduction

The vibration problems associated with many slender floor structures can be remediated through the use of active vibration control (AVC). AVC involves measuring the dynamic response of a structure, processing the acquired signals and then using these to derive force signals to be applied to the structure so that its response is reduced. This approach has numerous advantages over other vibration mitigation techniques such as structural redesign. For example, adding columns or props would likely be architecturally undesirable and adding concrete mass to the floor necessarily involves the use of much more material and is very disruptive during the remediation phase. Meanwhile, AVC has the advantage of being composed of a set of small units that can be distributed around the underside of a floor. Hence it is unobtrusive and does not require additional structural material. However, it does have the disadvantage of on-going running costs and because this technology is very new for this application it can be very expensive to set up initially.

Taking this use of AVC further, one might design a floor structure from the outset to incorporate AVC to ensure it meets its vibration serviceability limits. This makes it possible to create more slender structures which require fewer construction materials whilst still having low vibration levels. This concept of integrating AVC into the design of a structure has been researched previously for other applications of AVC. For example, Pil and Haruhiko (1996) present a recursive method for designing a mechatronic system with vibration control. Park and Koh (2004) use genetic algorithms to optimise the design of a ten-storey earthquake-excited building incorporating active tendon control where both the structural stiffness of each floor and the number and distribution of actuators were some of the design variables optimised. Additionally, Molter et al. (2012) present a methodology for designing the topology of a cantilever beam with AVC at specific locations, with the aim of reducing the tip displacement from the first two vibration modes. However, to the author's knowledge there exists no study into the incorporation

of AVC into the design of new floor structures and no consideration as to the potential advantages and disadvantages that this might have.

The choice to include AVC at the design stage is significantly different to the remediation case discussed previously because a deliberate decision would have been made with the knowledge that the structure would fail vibration serviceability without AVC. Therefore, there must be a solid rationale for making this choice. This chapter aims to investigate this issue by considering the advantages and disadvantage of utilising AVC in a typical floor structure's design. Here, both the environmental and the economic aspects are considered. This study takes the form of a life cycle analysis (LCA) of the floors, both with and without active control. The main factors considered are: 1) the construction material savings made possible through the use of AVC; 2) the additional initial cost of the AVC system and 3) the on-going costs of the AVC system for the lifetime of the building. All of the initial costs can be considered as 'embodied' costs, whilst all costs associated with the day to day usage of the building can be considered as 'operating' costs. The inclusion of AVC into a structure will reduce the embodied costs of a building through structural material savings, whilst increasing the operating costs through AVC's on-going electrical and maintenance costs. Therefore, to determine the potential benefits of including AVC from the design stage, the amount by which the embodied and operating costs change must be quantified.

The choice of controller used throughout this study is discussed in Section 6.2 and the test structure is described in Section 6.3. Next, all the factors that affect the embodied costs (both environmental and economic) are discussed in Section 6.4. Following from this, the operating costs are discussed in Section 6.5. Finally, the results are discussed in Section 6.6 and conclusions are drawn in Section 6.7.

6.2 Active Control Implementation

Previous research has investigated numerous controllers which aim to improve the performance of AVC, most of which of which are predominantly based on direct velocity feedback. The key idea behind this controller is to increase the structural damping by feeding back the structural velocity and applying a force proportional to this. The structural damping naturally present in floors is generally very low so this is a particularly attractive control law as very significant improvements in the response of the structure can be achieved (Hanagan, 1994; Díaz et al., 2012b; Díaz and Reynolds, 2009a; Nyawako and Reynolds, 2009). The controller used throughout this study is a modified form of Direct Velocity Feedback (DVF) and the schematic for this controller is shown in Figure 6.1. In practice, accelerometers

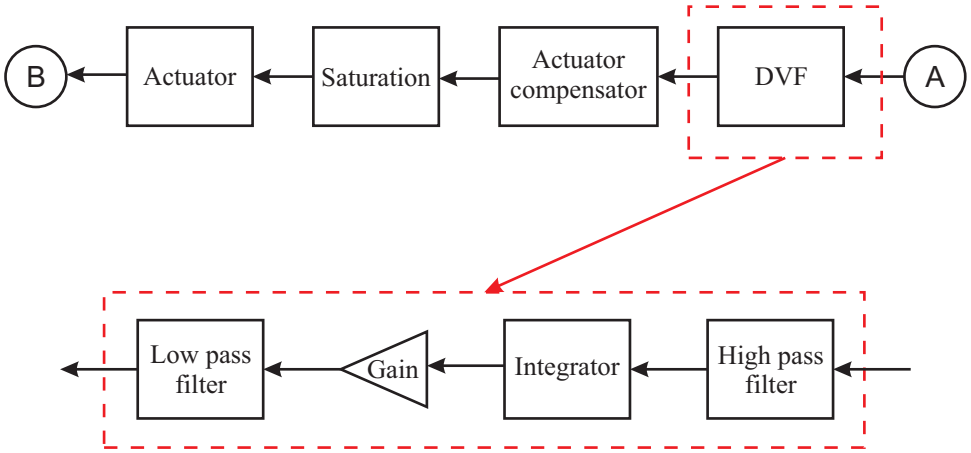

Figure 6.1: AVC schematic

are generally used to monitor the structural response, therefore the signal from these must be integrated to derive a velocity signal. However, a high pass filter must be incorporated to avoid low frequency amplification resulting from this integration, and conversely a low pass filter must be incorporated to avoid high frequency signals from noise on the signal line. Both of these filters are included in the controller, being represented as a 2nd order high pass filter with a cutoff frequency of 1Hz and a 2nd order low pass filter with a cutoff frequency of 50Hz respectively.

The inherent dynamics of the actuator are not ideally suited to the application of active control; in order to reduce the chance that the stroke of the actuator be exceeded a compensator was applied such that the dynamics of the actuator are effectively modified to have a natural frequency of 1Hz and a damping ratio of 0.7. This compensator works through pole-zero cancellation of the original actuator dynamics. Whilst this is generally not a recommended approach for the control of structures (Preumont, 2002) the dynamics of the actuators can be determined accurately and so this approach is considered sufficiently robust.

The signal from a single accelerometer is used to derive the command voltage that drives a corresponding single actuator. Large civil structure will require more than one actuator/sensor pair to control the entire structure sufficiently. The approach used here is to decentralise the DVF controller; that is, each actuator/sensor pair acts to reduce the response at its location based on information at that point only, as shown in Figure 6.2.

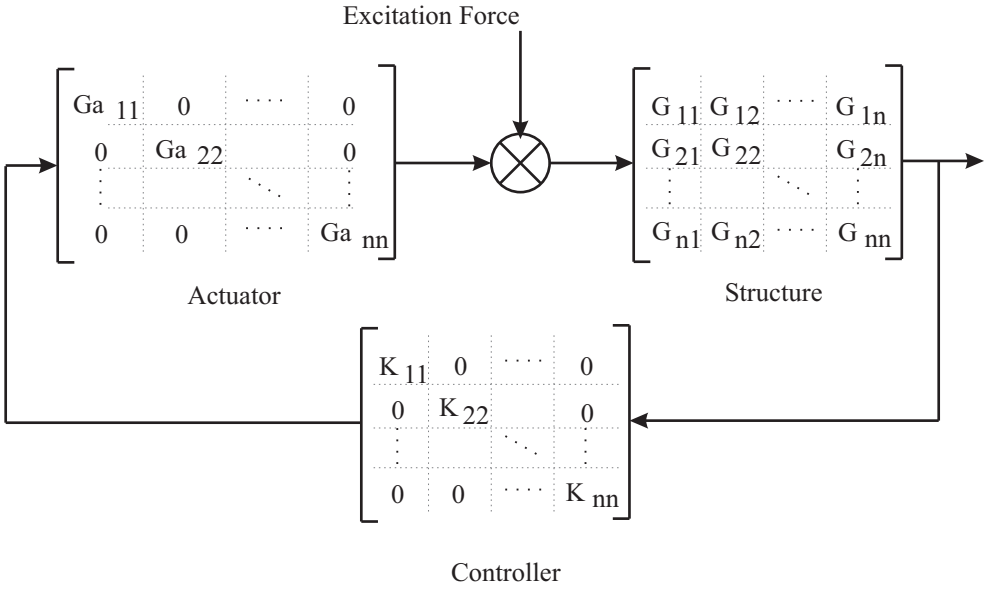

Figure 6.2: Decentralised AVC configuration

The feedback gain for each actuator/sensor pair was first chosen such that when the system was evaluated using the generalised Nyquist criterion, a gain margin of 2.0 and a phase margin of 30° were achieved. However, there will be some degree

of interaction between the different controllers wherever there are non-zero mode shape amplitudes at multiple actuator/sensor locations. This tends to have the effect of reducing the stability of the system so the phase and gain margins of the global system will be lower than those of each independent loop. To deal with this, the feedback gains applied for all control loops were decreased by the same proportion until the overall stability margins were 2.0 and 30° for gain and phase respectively. Note, that the non-linear trade-off between performance and power demand for the controller, as discussed in Chapter 5, was not utilised in this study for simplicity and because the power saving is relatively small compared with the power overheads. However, future work could incorporate this saving.

Finally, the command voltage is passed through a saturation nonlinearity before it is sent to the actuator amplifiers. This helps to prevent force saturation and acts as a further strategy to help reduce the possibility of stroke saturation. In the current study, this saturation voltage was set at 1V.

6.3 Description of Test Structure

For the purposes of this study a notional test structure was designed. This was a five-storey steel framed office building with a composite steel/concrete floor slab. The elevation along the long building wall is shown in Figure 6.3 and the layout of one of the floors is shown in Figure 6.4. The key areas of interest in this structure are the first to fourth floors where AVC is simulated; it is assumed that the ground floor would not have a vibration serviceability issue. The upper floors are assumed to be identical in construction. Details for this floor structure have been previously described in Hudson et al. (2011). The column grid used is 15m × 6m, with 6m long primary beams spanning between the columns and 15m long secondary beams spanning between the columns and primary beams at 3m spacings. The composite steel/concrete slab spans between the secondary beams and has an initial design depth of 130mm. This floor is a relatively slender structure with large panels and subsequently has modes that are easier to control

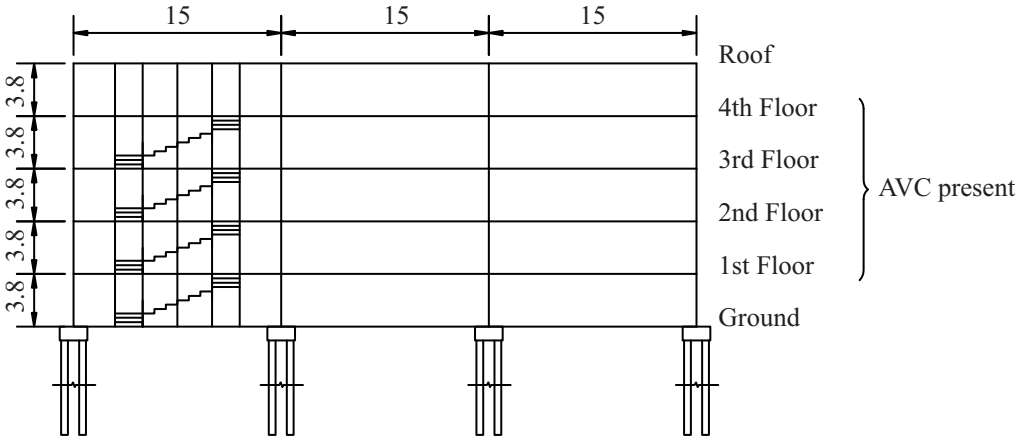

Figure 6.3: Test Structure Elevation

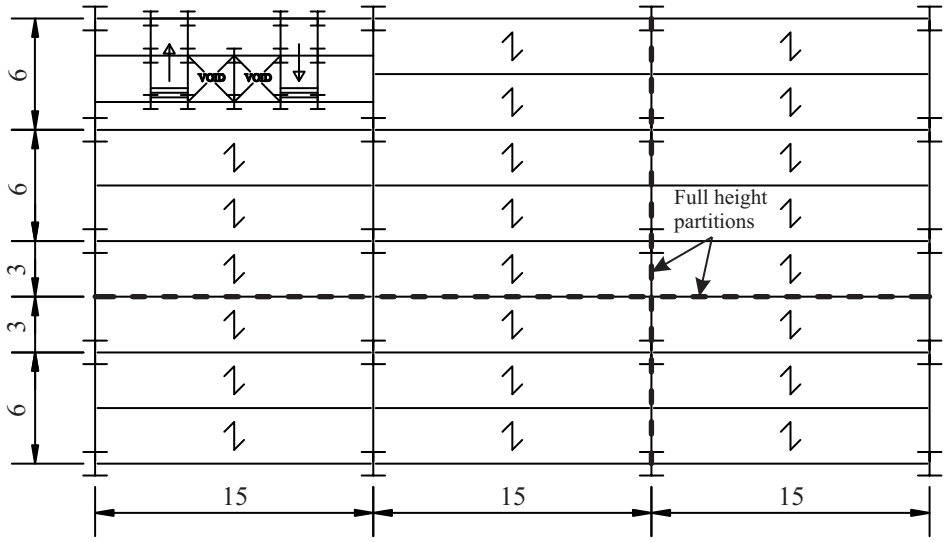

Figure 6.4: Structural Layout for Test Floor

with fewer actuators. Most structures have irregularities in the structural layout which tend to break up the very global modes of vibration and make them more localised. In order to simulate this a lift shaft and staircase have been included. Also, two full-height partitions have been modelled to break up this otherwise very large floor area. These are indicated by the thick dashed lines on Figure 6.4.

The member sizes for this structure were chosen to meet ultimate limit state (ULS) and deflection criteria when a 130mm slab depth was chosen. Asymmetric cellular beams were used as the long-span secondary beams because of the long distance

these relatively light members can span. These were sized at 748 $\times$ 152 $\setminus$ 210 $\times$ 72.2ACB, whilst the primary beams were sized at 457 $\times$ 191 $\times$ 74UB. In addition, columns were modelled from the floor below to the floor above the floor in question, fixed at each end. 305 $\times$ 305 $\times$ 198UC columns were chosen as these met ULS criteria for the calculated load on the lowest storey. The finite element model was created in ANSYS (ANSYS, 2000). All beams were modelled using the element type BEAM44 which is uniaxial with tension, compression, bending and torsion capabilities (ANSYS, 2000). In addition, this element type permits an offset to be supplied; this feature was utilised to model the composite action between these beams and the concrete slab as accurately as possible, in accordance with design recommendations (Smith et al., 2007). This slab was modelled using the orthotropic element SHELL63. A constant depth was used for each slab element but the Young's modulus was reduced in the weaker direction and the material density modified such that the properties of the profiled decking were incorporated (Smith et al., 2007). The depth of the slab was initially taken as 130mm but varied between each structural design, as is discussed in Section 6.4.1. Other standard modelling assumptions were included, namely that: all connections were assumed to be fully fixed; loading was taken to be 100% of dead load and 10% of imposed load; and the dynamic young's modulus of concrete was used (Pavić and Willford, 2005; Smith et al., 2007).

The staircase floor and lift shaft walls were modelled as concrete plates of thickness 300mm and 150mm respectively, and the partitions were modelled as per the methodology of Miskovic et al. (2009), thereby being 1m long vertical elements with axial stiffness only with magnitude 1.0×10^8N/m.

A modal analysis of the floor resulted in the mode shapes as shown in Figure 6.5. It is observed that these mode shapes are relatively localised, as intended by the addition of the lift shaft, staircase core and the partitions. A 2% level of damping for each mode was assumed. This was based on the fact that this is still a very open plan office layout and so there are fewer mechanisms through which damp-

ing could be added to the furnished structure. This value lies between the SCI guidance values Smith et al. (2007) which recommends 1.1% for bare floors and 3.0% for fully fitted out floors.

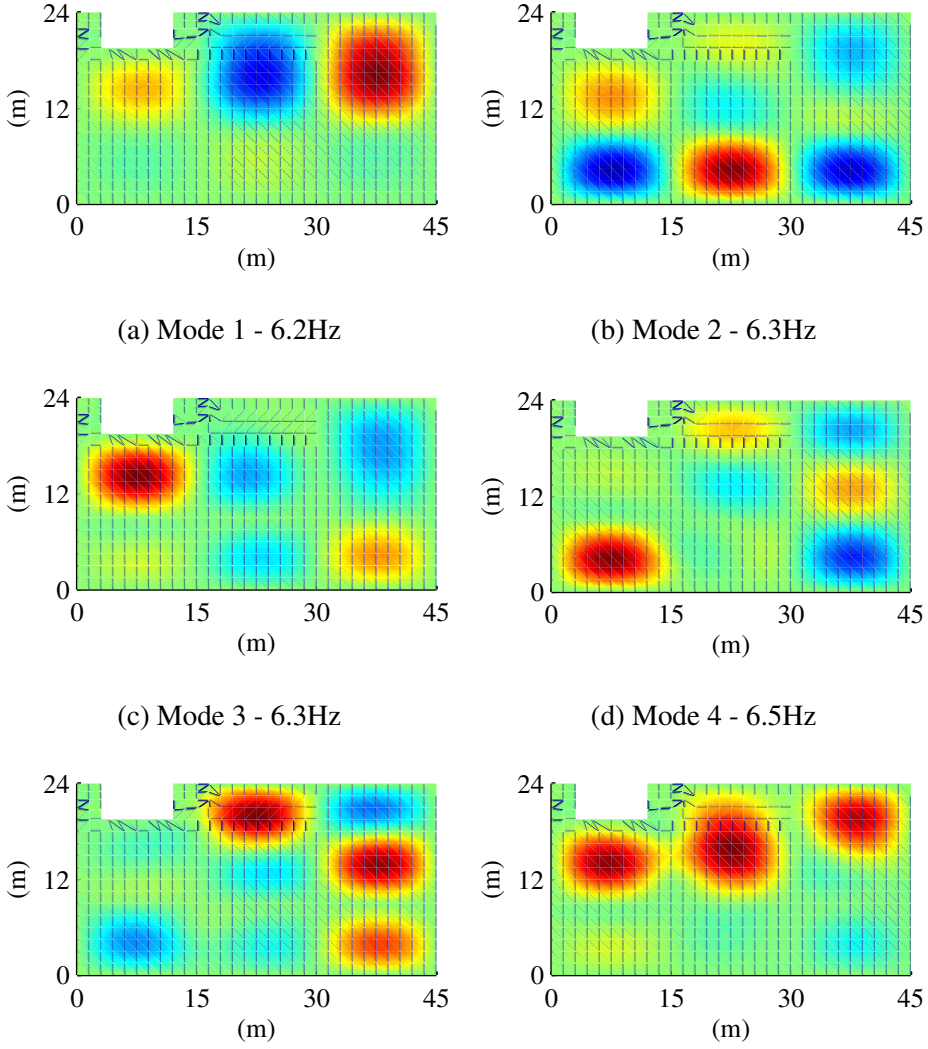

(a) Mode 1 - 6.2Hz

(b) Mode 2 - 6.3Hz

(c) Mode 3 - 6.3Hz

(d) Mode 4 - 6.5Hz

(e) Mode 5 - 6.6Hz

(f) Mode 6 - 6.9Hz

Figure 6.5: First six modes of test structure

6.4 Embodied costs

The embodied costs are those associated with the construction of the building. In this study, only the *changes* in embodied energy through the different struc-

tural design are considered, relative to a benchmark structure. This benchmark structure is taken to be the structure required to meet vibration serviceability limits without the use of active control. Following from this, more slender building designs are generated that utilise active control in order to meet the vibration serviceability requirements. These more slender structures can therefore be thought of as having negative embodied costs, relative to the benchmark structure because they have required fewer materials in their construction. In this study the depth of the floor slab is varied to make the floor structures more slender. However, this in turn can lead to decreased column and foundation sizes due to the reduced self weight of the structure. However, the inclusion of AVC will also incur a 'positive' embodied cost which reduces, to some extent, the benefits from material savings. The embodied costs considered in this study are financial, embodied energy (EE) and embodied carbon (EC). The EC in this study also includes the contributions from other greenhouse gases such as methane, carbon monoxide and dinitrogen monoxide in their equivalent CO_2 mass, often referred to as CO_2e.

6.4.1 Methodology for Determining Material Savings

It was decided that the dynamic response of the uncontrolled structure should not be evaluated using the methodology provided by Appendix G of the Post-Tensioned Concrete Floors Design Handbook (Pavić and Willford, 2005) or similar modern design guides because these methods cannot incorporate the feedback and nonlinear properties of AVC. Therefore, to be consistent with both uncontrolled and controlled analyses, the response of the structure had to be simulated using a different methodology.

The approach chosen was to simulate a person walking on the spot for a total of 20 steps at a grid of points throughout the structure. Ground reaction forces, measured from an instrumented treadmill (Racic, 2009) at a variety of walking paces, were utilised to simulate the walking. The pacing rates chosen increased in 0.05Hz increments from 1.5Hz to 2.5Hz. Where the desired pacing rate differed

slightly to the pacing rate of an available measurement, the closest match was scaled accordingly in the time domain to represent this more accurately.

The response at each location was calculated for a range of pacing frequencies and from these the worst case response was calculated. The acceleration response was then weighted by the W_b filter from BSI (2008) to account for the human body's frequency dependent sensitivity to vibrations, and this weighted acceleration was then used to calculate the response factor, R. This was calculated as the maximum value of the running 1s root mean square (RMS) of the weighted acceleration response, normalised by $0.005 m/s^2$. The calculated response factor for each point in the structure was compared with recommended limits. For a quiet office environment this is taken to be a response factor of 4 (BSI, 1992). It should be noted that more recent standards (BSI, 2008) no longer use this response factor to determine the vibration serviceability limit of a floor, instead preferring the vibration dose value (VDV). However, this is not easily calculated for the excitation type considered here because of the VDVs dependence on duration. Therefore for simplicity the response factor is used as the determining response measurement of the floor.

The depth of the slab was sequentially increased from its initial depth and the response recalculated for the entire floor area in each new structure. This was repeated until the response for the uncontrolled state met vibration serviceability limits and this depth of slab was taken as the reference floor against which other designs have some material savings.

The locations for applying AVC were determined by considering the points of the uncontrolled structure that had a high response, in addition to considering the configuration of the mode shapes in order to increase controllability and observability from each controller. The response calculations were repeated for the more slender structures with AVC. Consequently, the potential material savings on each floor were thus calculated from the difference between the minimum slab depth that met vibration serviceability limits in the uncontrolled state and the slab depth

for the controlled floors. There are also material savings that can be realised in the columns and supporting substructure due to the reduced dead load from each floor. Therefore, the columns, piles and pile caps were designed for each structure and the corresponding material savings calculated.

6.4.2 Material Savings on the Test Floor

The response of the floor was determined using the methodology described in Section 6.4.1. This was performed for the initial design with a slab depth of 130mm for all modes up to 20Hz (the first 25 modes). In addition to this, the responses from two other models were calculated. These had increased slab depths of 170mm and 210mm in an attempt to reduce the vibration response in the uncontrolled conditions. The mode shapes for these structures are not presented because they are very similar to those shown in Figure 6.5. Interestingly, the fundamental natural frequency of the structures does not decrease significantly despite the additional mass; actually a slight increase of 0.1Hz is observed for the most extreme case. This is because the concrete slab acts compositely with the steel beams so an increase in concrete depth also results in an increase in stiffness which acts to increase the natural frequencies. The simulations for these structures also included modes of vibration up to 20Hz, equating to the first 22 and 20 modes respectively for the structures with a 170mm and 210mm slab depth.

The resultant response data for all three structures are represented in Figures 6.6-6.8 as contour plots of the maximum response achieved at each location regardless of excitation frequency. Note that a nonlinear colour scheme has been employed here to highlight the areas of the floor that exceed the response factor limit of R=4.

The response for the structure with a 130mm slab depth is much greater than R=4 in six large areas and the absolute maximum response is 10.6. As the slab depth increases to 170mm and 210mm the response is indeed reduced, with absolute maximum responses being 7.0 and 5.4 respectively. All of these maxima are

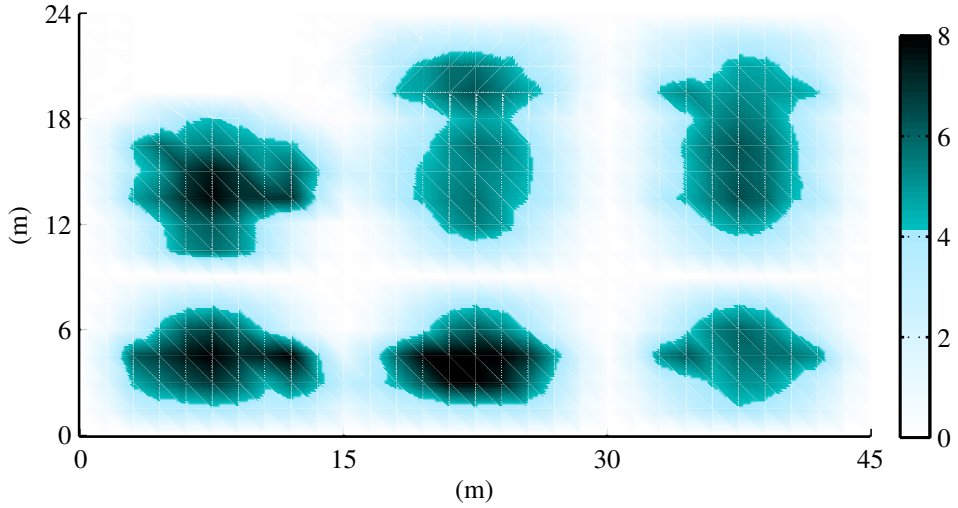

Figure 6.6: Uncontrolled response for 130mm slab depth

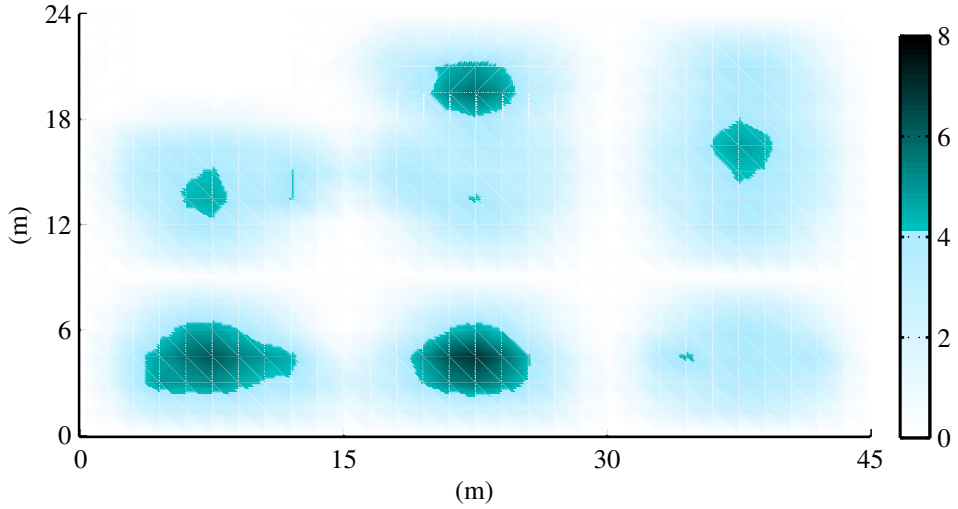

Figure 6.7: Uncontrolled response for 170mm slab depth

greater than the limit of R=4. However, the 210mm structure does not exceed this limit in many locations - it is only two small areas where the response is large. This point is demonstrated by examining the percentage of the floor that fails to meet the vibration serviceability limits, as shown in Table 6.1.

It was decided that the relatively small area of the floor that exceeded the limit

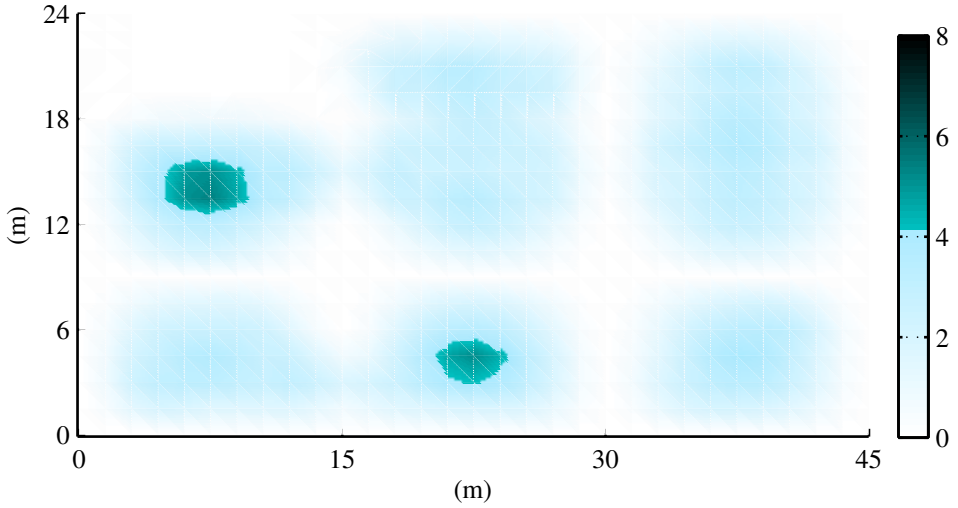

Figure 6.8: Uncontrolled response for 210mm slab depth

Table 6.1: Response Summary for Floor B Structural Options

Slab Depth (mm)	Maximum R Factor		Percentage of Floor with R>4	
	Uncontrolled	Controlled	Uncontrolled	Controlled
130	10.62	5.51	29.55	3.46
170	6.95	4.74	7.4	0.87
210	5.37	n/a	1.95	n/a

for the 210mm structure would not be likely to attract complaints from tenants on this floor, so this was deemed an acceptable structure in terms of the vibration serviceability limits. Therefore, having computed the benchmark structure (the uncontrolled structure with a 210mm deep slab), the next part of the investigation was to calculate the response of the other two structures (with slab depths of 130mm and 170mm) with control to bring them in line with the vibration serviceability limits. The minimum number of actuators/sensors required to achieve this were chosen, with their locations based on both areas of high response and the mode shapes in order to maximise controllability and observability. The locations chosen are shown in Figures 6.9-6.10.

The response of the controlled structure was calculated in the same way as for the uncontrolled structure, and the results of this analysis are provided in Figures 6.9-

6.10. The effect that AVC has on the structural response is quite apparent in

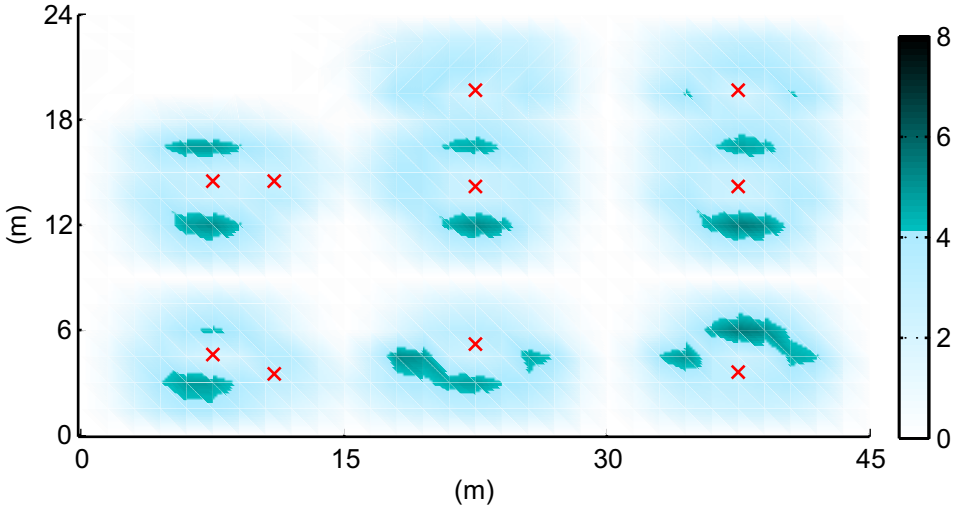

Figure 6.9: Controlled response for 130mm slab depth

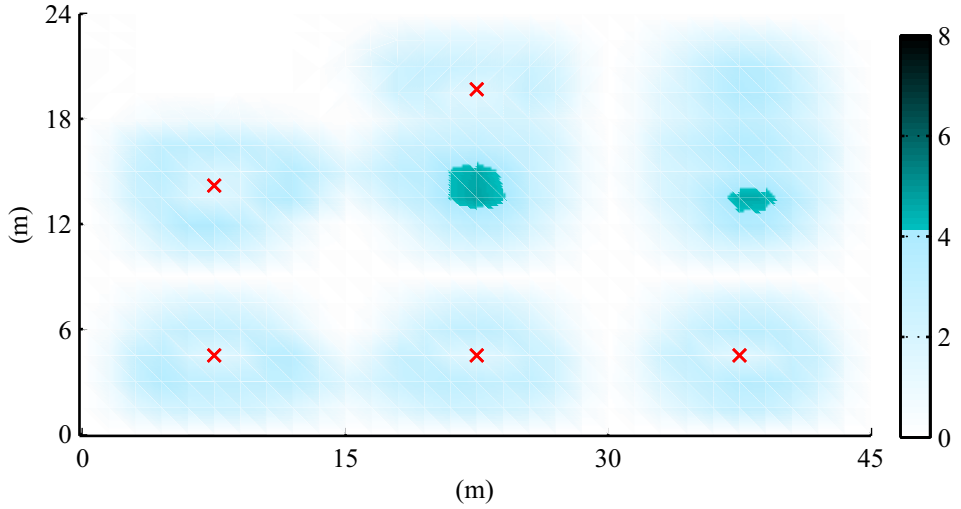

Figure 6.10: Uncontrolled response for 170mm slab depth

these contour plots. The areas of high response in the uncontrolled case have been effectively eliminated and it is only the regions further from the actuators where the response is slightly higher than R=4. The control law shown for the 130mm structure involves ten actuators/sensors. However, it is worth noting that when only six actuators/sensors are used for this slab most of the areas of high response are satisfactorily reduced, but there are several small areas of response that exceed

the limit of R=4 and which in total cover 7.47% of the floor area. This was deemed too high to be acceptable so additional actuators were required for this structure. It is possible that with an improved controller design these additional actuators may not be necessary.

A total of five actuators were required to bring the response of the 170mm structure to within vibration serviceability limits. It is interesting to note that one of the locations for these actuators in is in area where the response of the uncontrolled structure was less than R=4. This is because each control loop was designed to reduce the response for its single location only; not using any information about other locations. The reason for this is possibly best explained through reference to Figure 6.2. If one considers the case where $n = 2$ and $K_{22} = G_{a_{22}} = 0$ then the structural responses, a_1 and a_2 are given by Equations 6.1 and 6.2,

$$a_1 = G_{11}(f_1 + G_{a_{11}} K_{11} a_1) + G_{12} f_2 \tag{6.1}$$

$$a_2 = G_{21}(f_1 + G_{a_{11}} K_{11} a_1) + G_{22} f_2 \tag{6.2}$$

where G is the structural dynamics, f is the excitation force, G_a is the actuator dynamics, K is the feedback compensator, and the subscripts refer to degrees of freedom. K_{11} is designed to reduce a_1 by considering G_{11}, i.e. Equation 6.1, but it also has an effect on a_2 through G_{21}, i.e. Equation 6.2. The zeros of G_{21} will differ to those of the collocated G_{11} system, so there is no guarantee that the beneficial effects of K_{11} will also apply to a_2. In order to avoid this problem, either K_{11} must be designed using information about point 2 or K_{22} and $G_{a_{22}}$ must be non-zero (i.e. another actuator/sensor pair is included) and designed to reduce the response of G_{22}. Here, the latter option is chosen for simplicity.

The results of this study revealed three possible design options: an uncontrolled structure with slab depth of 210mm and two controlled structures with slab depths of 130mm and 170mm. This demonstrates that significant material savings can be realised through the use of AVC: in this study, savings of 80mm and 40mm off the

slab depth were made. For the floor plan of these structures this equated to total volumes of 86.4m^3 and 43.2m^3 respectively.

The equivalent EE and EC for this concrete were calculated by multiplying the mass of the concrete by coefficients from the database provided by Hammond and Jones (2008). Here, it is assumed that the additional concrete from the base case of 130mm is the same concrete as is used for the rest of the concrete slab - i.e. only one layer of concrete is formed. Although this additional concrete would not have any structural requirements, it is unlikely that a separation would be used in practice. Therefore, reinforced concrete of strength 25/30MPa with 110kg rebar per m^3 concrete was assumed, and this has EE and EC coefficients 1.92MJ/kg and 0.198kgCO_2e/kg. The low embodied energy of this material means that transportation could become significant. The data provided in the ICE database (Hammond and Jones, 2008) is from cradle to gate, i.e. it does not include the EE required for getting from the production gates to the site. In 2007 the average transportation distance by road for ready-mix concrete was 8.3km (Quarry Products Association, 2008), and the EE and EC of road freight transport were calculated as 0.668MJ/tkm and 0.05kgCO_2/tkm (Spielmann et al., 2007). This results in an increase of less than 1% for both EE and EC coefficients. However, there is much greater error in the uncertainty of the original data itself. For this reason, the transportation from factory gate to site was not considered. The price of concrete is variable, so in this study an assumed value of £150/m^3 was used. The changes in embodied energy, carbon and price for the floor slabs in each of the two structures considered in this study are shown in Table 6.4.

6.4.3 Other Structural Material Savings

This section considers the secondary effects resulting from a decrease in the slab depth; namely that the reduced self weight of the building can yield reductions in the column, pile and pile cap sizes. The sizes of these sections were determined through a simplified design process with further details provided below.

The column sizes used in Section 6.3 were not changed for each of the different structures because the extra stiffening contribution from the relatively small change in column stiffness would have a negligible effect on the response of the floor. However, the section size is critical for determining material savings so a load take down was calculated to determine the column sizes for each structure considered. For simplicity, it was assumed that the roof was of the same construction type as the most slender of the office floors' design, with a constant slab depth of 130mm and the minimum imposed load for a roof with access of 1.5kN/m^2. The columns were assumed to have pin connections so were checked for axial compressive strength and buckling only in accordance with BSI (2010). Considering one of the internal columns, it was found that 305 $\times$ 305 $\times$ 198UC columns were required for the 210mm and 170mm slab depth structures. However, for the 130mm structure, the reduced size of 305 $\times$ 305 $\times$ 158UC was appropriate. This was assumed to apply equally to all columns, regardless of location within the structure. The EE and EC coefficients for steel sections were set at 21.50MJ/kg and 1.53kgCO_2e/kg (Hammond and Jones, 2008) whilst the price of steel was set at £1.1/kg (Tata Steel, 2012).

The design of the piles requires knowledge of the soil conditions. The building in this study is not based on an existing structure so no soil conditions were available; therefore "typical" values were assumed. These are shown in Table 6.2. The piles were assumed to be bored and were checked for axial capacity only (Curtin et al., 2006). For the soil conditions assumed, it was calculated that for the 210mm, 170mm and 130mm slab depths, the required pile depths were 27m, 25m and 23m respectively for 4 piles of 500mm diameter per column. The same price and EE / EC coefficients were assumed for this substructure concrete as were used in Section 6.4.2.

The pile caps were designed by calculating the depth of cap required to meet the local shear and bending shear checks (Curtin et al., 2006). The plan dimensions of the pile caps were calculated using a 100mm cover to the edge of the pile and

Table 6.2: Assumed soil conditions

Depth (m)	Soil type
0 to 5	Fill material. Negligible contribution to axial capacity of pile
5 to 10	Sand and gravel. Assume angle of friction 30°
10 to 15	Stiff clay. Assume strength of 150kN/m^2
15 to 30	Very stiff clay. Assume strength of 300kN/m^2

a spacing between piles of 1.5 times the pile diameter. For the piles calculated earlier, it was therefore calculated that the structures with 210mm, 170mm and 130mm slab depths required pile caps of depth 1.1m, 1.0m and 0.9m respectively with width and breadth 2.0m.

The changes in embodied energy, carbon and price for these structural components are shown in Table 6.4.

6.4.4 The Initial Cost of AVC

The AVC system can be broken down into three key components: the sensors that detect the motion of the structure; the controller which processes these signals; and the actuator which delivers the controlling force. Previous studies into the use of AVC for floors (Hanagan, 2005a; Díaz and Reynolds, 2010a; Hudson and Reynolds, 2010) have used commercially available equipment that is not tailored specifically towards an AVC implementation. Naturally, this has the benefits of flexibility of use. However, it is not the most efficient way to install AVC and significant savings can be made by using bespoke equipment. Therefore, the initial cost was calculated based on an actuator, controller and accelerometer that are tailored for this purpose.

A significant proportion of the cost, both environmentally and economically, of an AVC installation is expected to come from the actuator. Drawings were used for a new actuator that was designed at the University of Sheffield and, as of Autumn 2012, is currently being built. These drawings permitted a detailed bill of quantities to be constructed, and from this the total embodied energy was calcu-

lated. The full bill of quantities for the AVC components is shown in Table 6.3. Several assumptions had to be made to derive the EE and EC of the AVC system from the available data sources. A detailed list of these assumptions is provided in Appendix A.

Table 6.3: Bill of Quantities for AVC components

Part Name	**Mass (kg)**	**Cost (£)**	**EE (MJ)**	**EC (kg CO_2e)**
Steel lamination	2.15	390.00	70.7	5.9
Bottom plate	3.10	183.50	480.4	28.4
Top plate	3.10	186.50	480.4	28.4
PM[a] Back Iron	4.59	322.50	92.3	6.7
Guideway	1.72	297.00	97.5	11.2
Shaft	4.00	151.00	80.4	5.8
Flange	0.23	158.00	4.6	0.3
Shell	5.49	501.00	311.1	35.8
End Strip	1.25	450.00	71.0	8.2
Connection board	15.12	390.00	857.4	98.6
Lateral board	0.12	92.00	18.9	1.1
Strip for encoder	0.21	40.00	32.9	1.9
Cheek end plate	0.02	40.00	1.4	0.1
Permanent magnets	1.84	2800.00	69.6	13.8
PM assembly	0.00	350.00	0.0	0.0
Copper wire	1.50	810.00	214.5	11.1
Bearings	4.20	467.20	651.0	34.6
Encoder	0.31	900.00	61.7	3.7
Controller (and amplifier)	2.10	900.00	451.7	27.7
Springs	0.25	60.00	14.2	1.6
Mounting plate	7.05	35.00	141.6	10.3
Embedded controller	0.50	200.00	107.5	6.6
Accelerometer	0.15	500.00	252.9	15.7
Signal conditioner	0.50	50.00	8.5	0.4
Misc cables	0.50	50.00	13.0	0.6
Total	60.00	10323.70	4585.1	358.4

[a] PM denotes Permanent Magnet

The total embodied energy, carbon and price for the actuators used in each of the structures is shown in Table 6.4.

Table 6.4: Total changes relative to benchmark structure

Structure	Criterion	Total changes relative to benchmark structure					
		Slab	Piles	Pile Caps	Columns	AVC	Total
130mm	Mass (tonnes)	-829	-151	-38	-15	2	-1031
	Energy (GJ)	-1593	-290	-74	-327	183	-2099
	CO_2e (tonnes)	-164	-30	-8	-23	14	-211
	Cost (£1000)	-52	-9	-2	-17	413	333
170mm	Mass (tonnes)	-415	-75	-19	0	1	-508
	Energy (GJ)	-796	-145	-37	0	92	-886
	CO_2e (tonnes)	-82	-15	-4	0	7	-94
	Cost (£1000)	-26	-5	-1	0	206	175

6.5 Operating costs

The operational costs are those associated with the ongoing usage of the building. There were two calculation stages necessary to determine the electrical costs of the control unit and hence the operational costs. Firstly the probable usage of the actuators during in-service loading must be calculated; and secondly the power requirements of each control unit must be determined. The electrical costs of the accelerometers and controller unit itself are considered to be negligible for the purposes of this calculation, therefore the latter procedure simplifies to one of calculating the power demand of the actuators. Although it was possible to base the embodied costs on actuators that were optimised for AVC, as these are not available for testing yet it was not possible to do the same for the operating costs. Therefore, all the costs calculated in this section are based on the current actuator technology. As with the embodied costs, the factors considered in this study are financial price, operational energy (OE) and operational carbon (OC).

6.5.1 Power requirement of actuators

The power requirements of each actuator was determined experimentally using a specially constructed power monitor that provides the instantaneous power draw at the point of the mains supply. This device samples the mains voltage and current supply at 2.8kHz and calculates the average power over 5 mains cycles. This

method of calculating the power has the advantage that all inefficiencies within the amplifier and actuator are accounted for hence the environmental and economic cost to the user are easily calculated. However, this method does not guarantee that a simple relationship between the power demand and a parameter such as the command voltage could be derived.

The actuator and amplifier used in this study are the APS Electrodynamics model 400 shakers with attached reaction masses and the APS Electrodynamics model 124 EP extended power amplifier respectively. Two types of signal were used to drive the actuator in voltage mode: a harmonic signal for a range of voltages (0.1V to 1V) and a range of frequencies (2Hz to 50Hz), and a random signal for a range of voltages (0.1V to 2V) up to 100Hz. The use of two signal types helps to ensure the derived relationship is valid for the full range of operation for the shakers.

The power drawn by, command voltage to and current output from the amplifier were recorded. The average power was calculated for each test and was compared with the average value of the running RMS (with a 0.25s RMS period) of the current output. The result of this was found to be a linear relationship as shown in Figure 6.11a. Log-log axes were used because of the large range of the acquired data.

Note, that this is an approximation: by using the current measurement only this is assuming the voltage across the actuator component is perfectly in phase with the current in order to calculate the real power. In reality, this will not be the case because of the inductance within the actuator coils, hence the approximation derives the apparent power - this differs to the real power by the power factor, which will vary depending on what position the armature is. However, it can be seen in Figure 6.11a that the empirical fitting is approximately correct for the load cases considered.

A 0.25s RMS period was used for calibration. A least squares line of best fit was

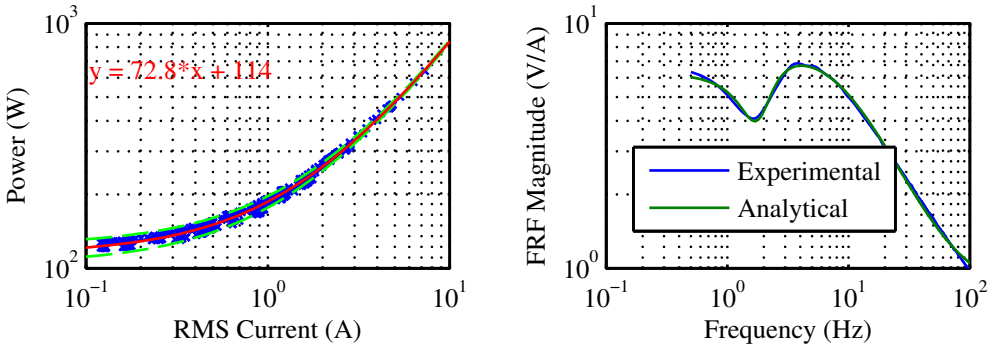

(a) Relationship between RMS current and average power

(b) Transfer function for command voltage to current output

Figure 6.11: Analytical prediction of power demand

then modelled to the data and the relationship was found to be:

$$\text{Power (W)} = 114 + 72.8 \times \text{RMS Current} \tag{6.3}$$

This line of best fit has an R-squared value of 0.995, indicating that 99.5% of the variation in power was predicted by the linear relationship. A lower and upper bound on the linear fit have been calculated based on the value of the residuals, and these are shown in Equations 6.4 and 6.5.

$$\text{Lower-bound Power (W)} = 104 + 72.8 \times \text{RMS Current} \tag{6.4}$$

$$\text{Upper-bound Power (W)} = 124 + 72.8 \times \text{RMS Current} \tag{6.5}$$

These are useful to give an idea of the magnitude of the error in the curve fitting and are shown in Figure 6.11a, though because the axes are logarithmically scaled they appear as curves rather than straight lines. As stated earlier it is preferable to derive a relationship between the command voltage and the power demand. To this end, a transfer function between the command voltage and current output was experimentally found and a transfer function model was fitted to this data, as shown in Figure 6.11b.

This transfer function can be utilised with the linear relationship derived in Equa-

tion 6.3 in order to arrive at the power requirement for a given command voltage time history.

This relationship was verified experimentally to ensure the methodology chosen yielded accurate power predictions for typical voltage time histories that are used in active control - not just the harmonic and random signals used during the identification stages. Therefore, a simple DVF controller was implemented on the simply supported slab strip at the University of Sheffield. The actuator and sensor were both placed at one third span in order to control the first and second modes of vibration (at 4.5Hz and 16.8Hz respectively), as shown in Figure 6.12.

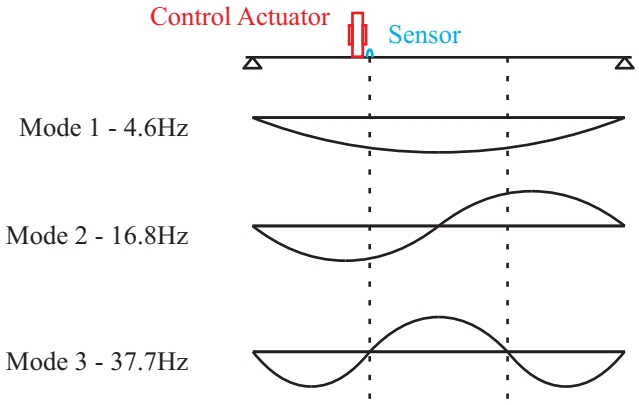

Figure 6.12: Controller on experimental slab strip to verify power predictions

Walking excitation was provided at 2.25Hz by walking across the structure and back again. The power demand of the actuator was measured using the custom-built power meter described earlier and the command voltage to the actuator was recorded. The voltage time history was used to calculate the power demand using Equation 6.3 and the transfer function shown in Figure 6.11b. The resulting simulated power and experimentally measured power are compared in Figure 6.13.

The simulated power tracks the general trend of the measured power very well. However, small transient peaks and troughs are not simulated as well, as shown at 22.5s and 22.8s in Figure 6.13. This is not a major problem for the present work because for long durations these peaks and troughs will average out. Indeed, for

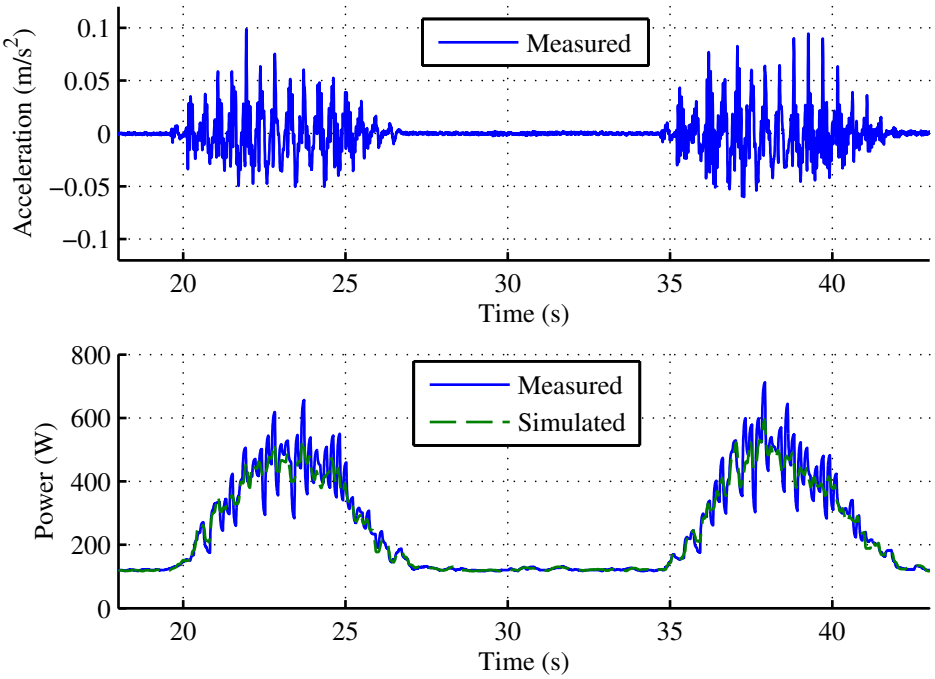

Figure 6.13: Comparison of simulated and experimentally measured power for active control

the time history shown the average powers for the measured and simulated time histories are 249W and 243W respectively, an error of approximately 2.5%.

6.5.2 Probable Actuator Usage

The probable usage of the actuators must be determined through simulation of a realistic in-service load applied to the structures. Therefore, a probabilistic force model is used to simulate many pedestrians walking between randomly generated start and end points. This is the same force model that was developed in Section 4.4.3. Key details are reproduced here.

An equal distribution of start and end points was assumed. However, the pedestrians were not modelled as walking directly between the points: instead a series of corridors were decided apriori and the pedestrians walked preferentially along these. This aimed to simulate obstacles such as desks and walls in a real office environment. The optimal route along the corridors was chosen as the one that

traversed the fewest number of corridors, and when this yielded multiple options the shortest distance from those options was chosen. The results from the validation of this force model in Section 4.4.3 indicate that a suitable distribution of start times is equally distributed at 6 people per minute for every $1000m^2$ floor area.

The force function that was applied to each person was based on the probabilistic model developed by Živanović et al. (2007). Here, the stride length and walking frequency are represented as normal distributions with means of 0.71m and 1.87Hz and standard deviations of 0.071m and 0.186Hz respectively. In addition, the pedestrian weight is assumed to be represented by a normal distribution, defined by a mean of 76.7kg and a standard deviation of 19.52kg.

This loading was applied to the structure over a two hour period whilst active control was simulated (split into 6 $\times$ 20 minute periods for ease of numerical processing). The command voltage for the actuators was recorded; this voltage time history was then combined with the results from Section 6.5.1 to derive the power demand of the actuators over time.

The average power demand over this period was calculated which thus allows the total annual electrical energy to be calculated. This was used to calculate the annual OE, OC and operating economic cost. There is great uncertainty over future electricity prices, so for simplicity it was assumed that electricity prices will rise each year by the same amount and that this is equal to the prevailing interest rate. This means that the present value of any future electricity charges will be equal to the starting year price. It is beyond the scope of this work to predict more detailed changes in future electricity prices. A fixed price of £0.12/kWh$_{\text{grid}}$ was assumed which was the average variable unit price for the UK in 2011.

Similarly, a static value for the OE coefficient was used. This is because the OE depends on the efficiency of the power generation network and it is beyond the scope of this work to predict how this will change over time. Therefore, a value of 9.96MJ/kWh$_{\text{grid}}$ was used throughout. The derivation for this value is shown in

Appendix A.

However, the OC was calculated using the predictions in Jones (2011). This uses the framework provided by the 2050 pathways analysis from the Department for Energy and Climate Change (DECC) (DECC, 2010) to predict how the OC of electricity will vary as the UK strives towards improving the carbon intensity of energy. The resultant changes in OC coefficient are shown in Figure 6.14. Beyond this time frame, the OC coefficient was assumed to remain constant at the 2050 level.

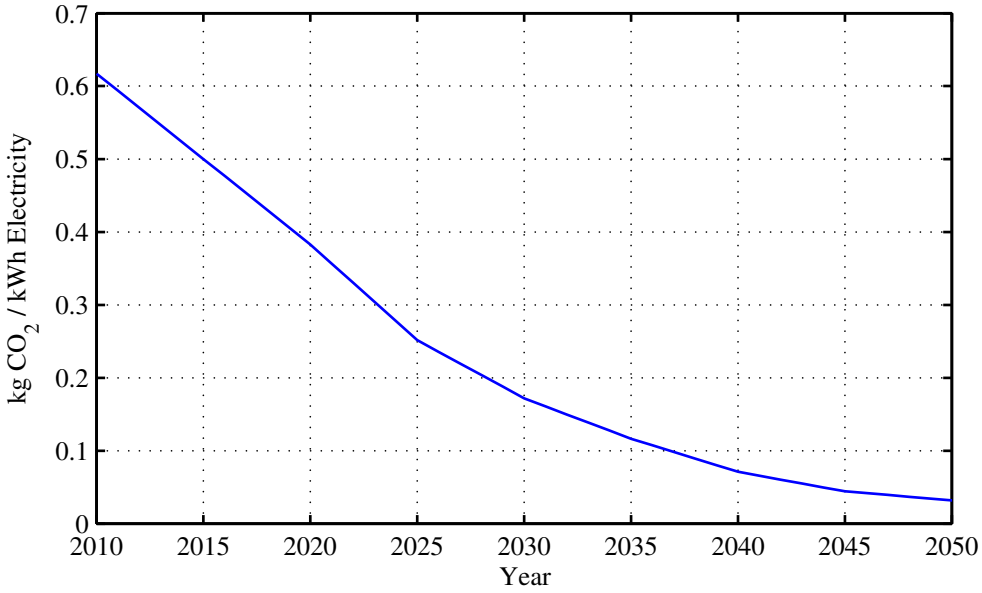

Figure 6.14: Changes to the Operating Carbon of Electricity, from Jones (2011)

6.5.3 Results for Test Structure

The methodology described in Section 6.5.2 was applied to each of the controlled structures. The power demand to each actuator was recorded and processed to determine the operating costs of AVC on these structures. A small portion of a typical run on the 130mm structure is shown in Figure 6.15, whilst the cumulative distribution functions for each actuator's power for all runs are shown in Figure 6.16a for the 130mm structure and Figure 6.16b for the 170mm structure.

Based on these results, the average power for all actuators was then calculated as 128W and 137W for the 130mm and 170mm structure respectively. It is interesting to observe that this average power is not much higher than the overhead power of 114W which demonstrates one of the disadvantages of the current actuator technology and the benefits that can be achieved by reducing these high overheads.

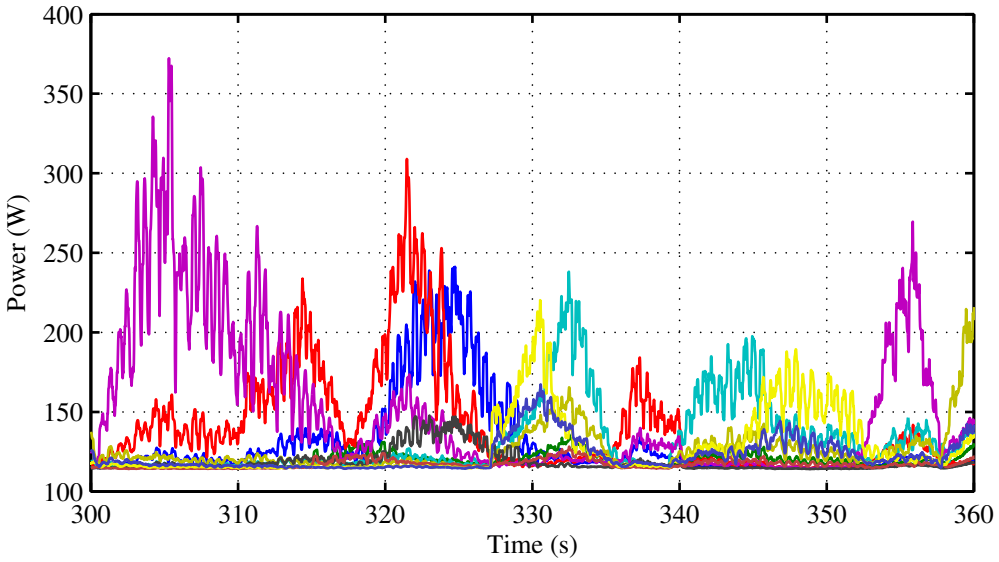

Figure 6.15: Time history of actuator power for one run on 130mm slab structure

The annual operational costs of running the actuators in each structure were calculated based on a 12 hour working day for 5 days a week and 52 weeks a year using the energy, carbon and price coefficients described in Section 6.5.2. This was performed for three cases - 1) with the currently available actuator technology, 2) with an ideal case where the overheads for running the actuators were zero, and 3) a realistic goal where, the overheads have been reduced to 24W. This value of 24W was derived by measuring the overhead power demand for an inverter which will be used in future work using linear motor technology in place of the currently available actuators. At the time of writing this new technology was not in a fully usable state hence the reason why the previous simulations are based on data from

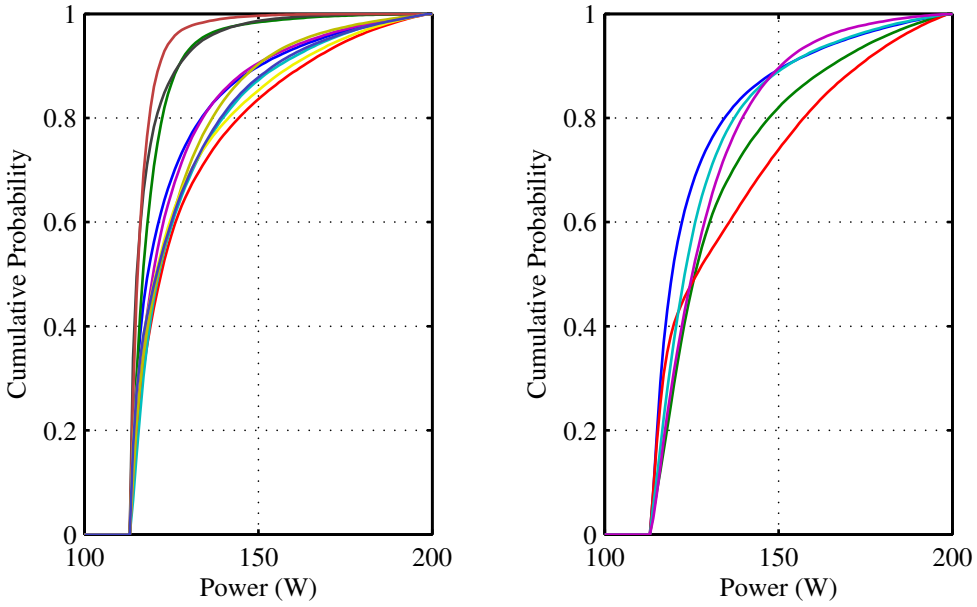

(a) Cumulative distribution function for actuator power on 130mm slab structure

(b) Cumulative distribution function for actuator power on 170mm slab structure

Figure 6.16: Typical power demand characteristics for AVC

the existing amplifiers. It is expected that the efficiency in converting electrical power to mechanical power will be similar, if not better, with the new technology so it is deemed appropriate to use the same power demand approximation as for the old technology, but with the different, measured, overhead power demand. These results were combined with the embodied costs from Section 6.4 and then the whole life costing shown in Figures 6.17-6.19.

By their very nature, the operational costs run for as long as the building is in use, so there comes a point at which the benefits of installing AVC no longer outweigh the associated costs: this is the payback period and has been calculated for the two structures, as shown in Table 6.5.

The high initial cost of the actuators results in a higher cost than the savings made through reduced construction materials before operating costs are even considered. However, this is an unrealistic comparison because the costs are based on those for the prototype actuator. In order to investigate the potential benefits that

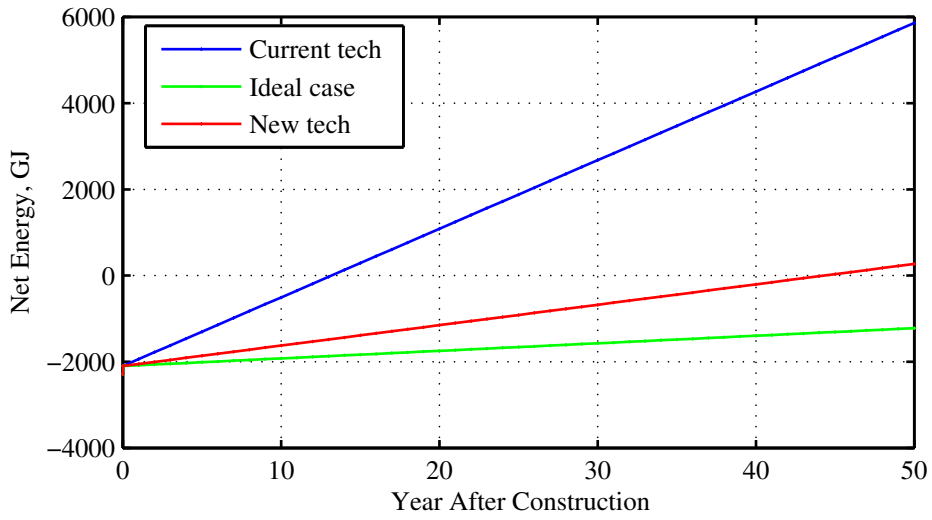

(a) Whole life energy use for 130mm Structure

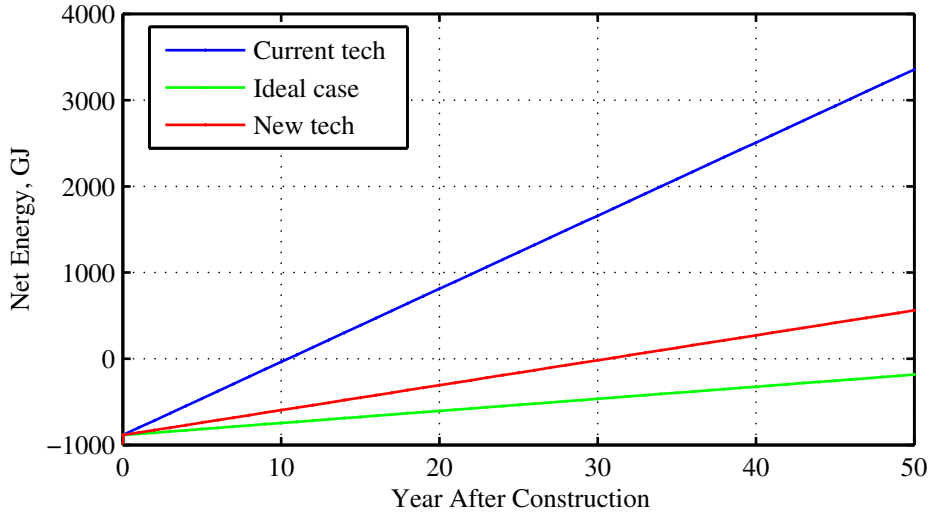

(b) Whole life energy use for 170mm Structure

Figure 6.17: Whole life energy for both controlled structures

mass production could bring by reducing the cost of the actuators, a further study was conducted to investigate how the payback period varied with actuator cost. The results of this are shown in Figure 6.20. It is evident that the cost of the actuators has to reduce by a significant amount (to less than 20% of the prototype cost or about £2000) before the benefits of using AVC are seen beyond year 0.

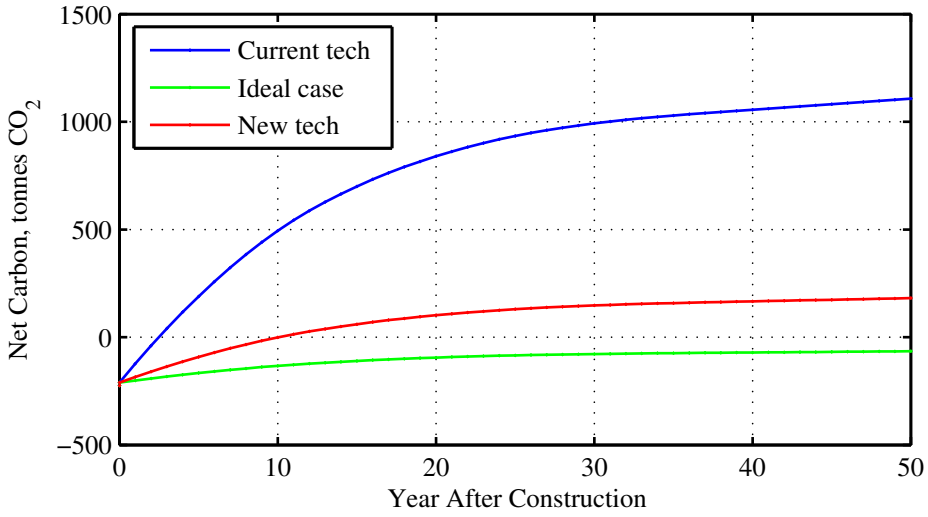

(a) Whole life CO_2e for 130mm Structure

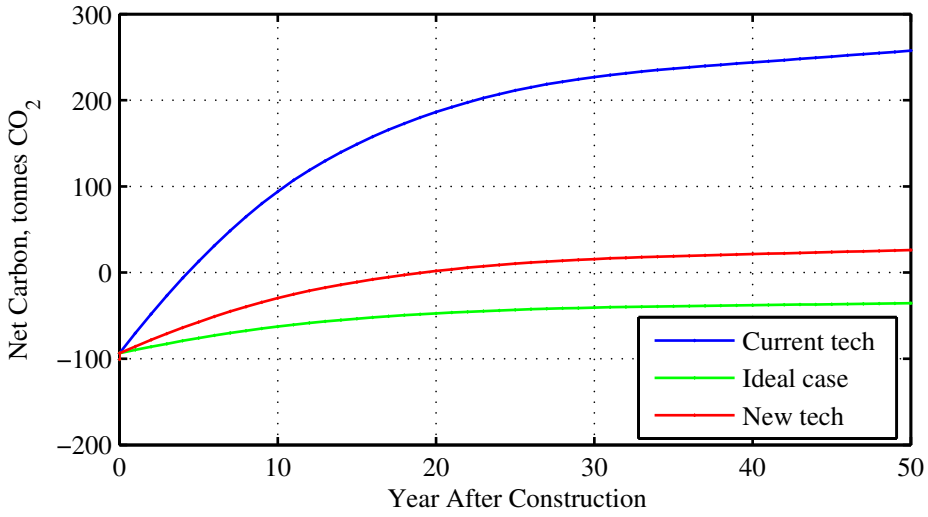

(b) Whole life CO_2e use for 170mm Structure

Figure 6.18: Whole life carbon for both controlled structures

However, for there to be a saving beyond 50 years then the cost must be reduced to 12% and 6% for the 130mm and 170mm structures respectively.

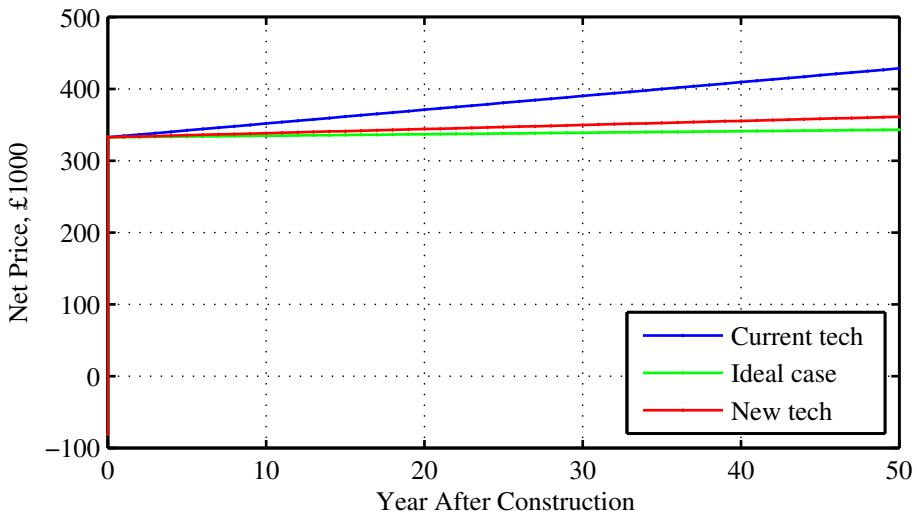

(a) Whole life financial cost use for 130mm Structure

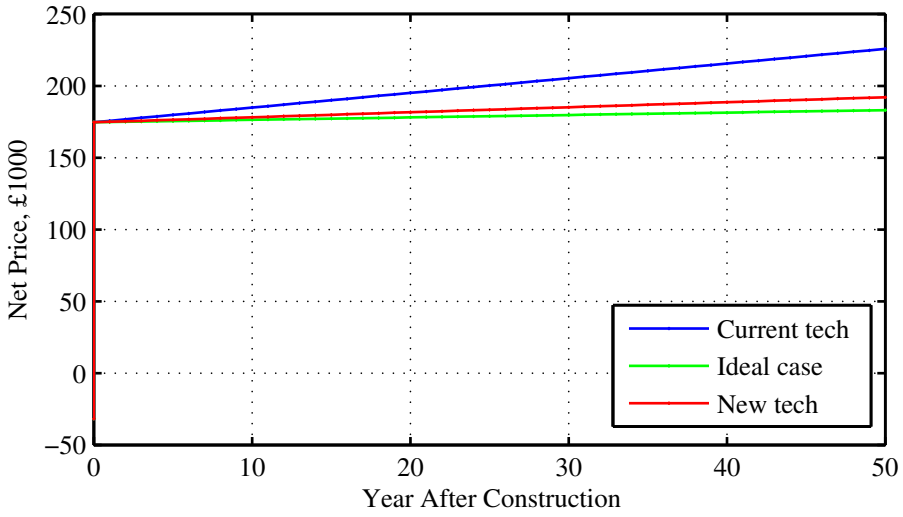

(b) Whole life financial cost use for 170mm Structure

Figure 6.19: Whole life cost for both controlled structures

6.6 Discussion

Some of the results presented in this Chapter are clearly case specific, e.g. the soil conditions which determine pile size and the structural configuration used for the floor and for the piles. Although this means that the results cannot be directly applied to similar structures, this Chapter was intended to show a typical example of

Table 6.5: Payback period for AVC using the 'new tech' scenario

Criterion	Payback period (years)	
	130mm	170mm Slab
Energy	47	33
CO_2e	13	22
Cost	0	0

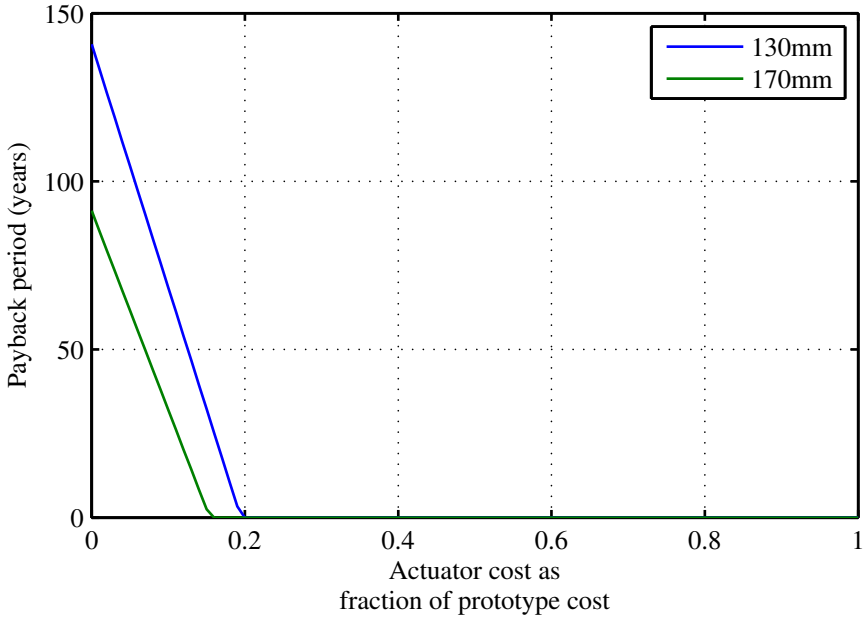

Figure 6.20: Payback period for varying actuator initial cost

the methodology discussed earlier in this chapter and to demonstrate some of the consequences of this design choice which would be useful information for further studies. Also, it should be noted that the results from this LCA are limited because they do not include the contributions from maintenance of the AVC system and any changes to the thermal mass of the building which could significantly affect the cooling / heating costs associated with running the building. However, there are some generalised points that present themselves in this work and are discussed here.

One of the most critical factors in determining how feasible an AVC installation would be, in terms of economic or environmental benefits, is the number of actuators required to bring the response of the uncontrolled structure to a satisfactory

level. In the present study, ten actuators were required for the most slender structure whilst five were required in the less slender structure. The decentralised modified DVF controller used in this study is not likely to be the optimal controller for this floor because of possibility of increasing the structural response at locations away from an actuator. Indeed, only six actuators were required to bring most of the floor's response to an acceptable level. However, additional areas near to the actuators necessitated four more actuators for satisfactory control. It is possible that a multiple input-multiple output (MIMO) controller could improve upon this by utilising information from other locations. The actuators themselves are the most expensive components of an AVC installation so the possibility of using more sensors than actuators to improve the response of the structure would also appear to be a sensible option. The problem with this is the need for a robust controller which can operate well even when the structural properties are modified slightly, for example by adding or removing non-structural partitions, so this is still an area of active research.

The initial financial cost of AVC is clearly too high at present, as can be seen in Table 6.4. This in itself is significantly higher than all the financial benefits derived from material savings and so results in a payback period of 0 years for both the structures considered. Over 90% of the initial economic and environmental costs associated with AVC are due to the actuators. However, it is important to note that the price used for these is that for a prototype actuator and as such the price can be expected to fall once this technology becomes more readily accepted and the actuators enter mass production. The embodied energy and carbon of the actuators is also significant, though much less than the equivalent savings made through material savings, as seen in Table 6.4. The main contributor to the EE and EC in the actuators is the use of aluminium and stainless steel. These are required for their light weight and durability respectively, so there is not much that can be done to avoid these besides sourcing alternative materials with similar properties. It is perhaps surprising that the embodied energy and carbon of the rare earth magnets

is relatively low despite their high financial cost, as seen in Table 6.3. The coefficients used here were derived through the approximation that their manufacture is similar to the manufacture of iron sinter and neodymium oxide, as discussed in Appendix A. There will be some truncation errors in these coefficients, for example no contribution to land transformation was accounted for, and the manufacturing process of Neodymium magnets will likely involve further processing than the approximation assumes. However, the magnets account for such a small portion of the total EE/EC for the actuators, that an increase in this coefficient of 100% would only increase the total AVC EE/EC coefficient by about 1.5% so the results from this study are not deemed sensitive to this uncertainty.

With regards to the material savings made, the largest contributor to these is the concrete slab, primarily because this is where the most material can be saved. However, the large EE/EC coefficients for steel mean that a relatively small saving here can equate to a significant EE/EC saving, as can be seen by the savings in column sizes for the 130mm floor. In the cases considered here, only changes in slab depth were considered. However, it is possible that beam size reductions could also be realised, in which case the EE/EC savings could be significantly increased.

The derived relationship between the command voltage and the power demand for the present actuators appears to represent reality well for the type of usage expected with a linear controller on a floor as shown in Figure 6.13. There does appear to be a degree of 'smoothing' in the simulated power (i.e. the second by second variance is less than that measured), but the average power represents reality well which is the important factor in this study.

The biggest factor contributing to the operational cost of the actuators is the overhead associated with running the amplifiers. This constant 114W power draw accounts for 89% and 83% of the actuator power demand for the two structures considered in this study. As discussed, new approaches are being investigated

to minimise this and preliminary results show that the inverter to be used with the new prototype actuators has much lower overheads of 24W. It is interesting to compare the power demand of AVC with those of other typical operating costs within buildings; these data are shown in Table 6.6. Here we can see that AVC has only a small contribution to the operating costs of a building even with the current overheads of 114W included: this is between 0.2% and 1.3% of total electricity for the structures studied.

Table 6.6: Typical Annual Energy Usage in Office Environments, after BRECSU (2000)

	Annual Energy Usage (kWh/m^2)	
	Standard air-conditioned office	Prestige air-conditioned office
Heating and hot water (gas/oil)	178	201
Cooling	31	41
Fans, pumps, controls	60	67
Humidification	18	23
Lighting	54	60
Office Equipment	31	32
Catering	6	24
Other	8	15
Computer room	18	105
Total Gas/Oil	178	210
Total Electricity	226	358
AVC (old amplifiers)	3.0 (130mm) or 1.6 (170mm)	
AVC (new amplifiers)	0.9 (130mm) or 0.5 (170mm)	

There is a relatively large degree of uncertainty regarding future electricity prices. The data presented in this chapter are assumed to increase constantly with inflation. Whilst this may be considered unlikely for the time period considered, it is considered beyond the scope of this chapter to predict changes in this value. This can therefore be considered as a ‘best possible case’ scenario for electricity prices. Meanwhile, the efficiency of electricity generation and distribution processes is assumed to remain constant throughout, although some improvements are likely to be seen in this area. However, the carbon associated with electricity

generation was modelled as decreasing in the future, in line with the UK's aim to reduce its carbon emissions. This means that a project that starts later will have a year by year reduction in the OC compared with the case studied here with a start date of 2012. The rapid changes in OC for electricity seen in these first few years could result in significant reductions to the OC of AVC in the first few years of operation.

The financial cost of running the actuators was relatively small compared with the other costs in the analysis, as seen in Figure 6.19a and 6.19b. For example, the cost of running the actuators over a 50 year period was calculated as being £14200 when the new amplifier overheads were used for the 130mm structure, whilst the total financial savings due to materials savings were about £78500. However, given that this is using inflation linked electricity prices the reality will likely be a higher cost. Additionally, the OE and OC for the actuators were very significant and resulted in a relatively short payback period for the structures that incorporated AVC, as seen in Table 6.5 and Figures 6.17a-6.17b and 6.18a-6.18b.

No maintenance costs for AVC have been included in this analysis. Given the infancy of this technology there is not much information available to determine how long an AVC system would last in continuous operation within an office floor, nor how much would then have to be replaced. It is worth noting that the payback periods in this study are all relatively low, so it is not expected that the inclusion of maintenance costs would significantly affect the results of this work.

At present, the payback period for all criteria is less than fifty years which could be considered a minimum design life. This means that, for the factors considered in the current case study and the current level of technology available, the installation of AVC is not justified by economic or environmental considerations alone. However, there are some significant factors that this study does not include because they are hard or impossible to quantify. For example, the cumulative effect of reducing the slab depth over many storeys could result in the possibility of

including an additional floor for a fixed building height. This would have great implications to the expected revenue of the building through the leasing of more floor space. In addition, AVC allows the creation and use of floors that would otherwise be impossible. This could be a key feature in prestigious buildings and it is possible that building owners would pay a small premium to have this luxury.

6.7 Conclusions

This work presents an initial life cycle analysis of the changes brought about by the incorporation of AVC into the design stage of an office building. Three buildings were considered in this analysis: a reference structure which required no AVC and had a slab depth of 210mm and two, more slender, variants with 170mm and 130mm slab depths but which utilised AVC to bring the response of the floor subject to human excitation to an acceptable level. The proposed methodology examines three factors: the financial cost, the total energy required and the total carbon dioxide (or equivalent for other greenhouse gases) emitted during both the initial construction phase and the operation phase over the building's lifetime.

It was found that the initial financial cost of AVC is too high at present. The result of this was that for the cases studied here the cost of installing AVC was greater than the cost of the materials saved, although the ensuing running costs of the AVC installation were relatively low. The EE and EC of the AVC installation were much smaller than the equivalent savings from material savings in both structures. In order to see some benefit of using AVC beyond the installation stage, the cost of the actuators would have to be reduced by 80% of the prototype cost for these case studies. However, the initial cost of the actuator installation in terms of energy and carbon was much smaller than the savings made through construction materials. The OE and OC are significant costs and resulted in payback periods of between 13 and 47 years, based on using the newer technology considered for the overhead of the amplifiers.

The methodology shown demonstrates that there are potential benefits to incorporating AVC into the design stage of floors based on economic or environmental principles. However, further research is required to significantly reduce both the initial and on-going costs of AVC before this can be realised. This will involve the development of improved actuators and amplifiers, along with improved control laws that control the floor more efficiently in terms of the power demand they require.

Chapter 7

Conclusions & Recommendations for Further Work

The goal of this thesis was to investigate the feasibility of incorporating active vibration control (AVC) to enable more slender floor structures. To investigate this, a number of key research aims were provided in Chapter 1. The research detailed in this thesis has worked towards meeting these aims, and as such a number of conclusions can be drawn. This Chapter draws concluding remarks based on the previously described work, and provides recommendations for where future work could be focussed.

7.1 Conclusions

A novel force model that simulates the in-service loading from an office environment has been developed. Following calibration using experimental data from one office floor, the force model generated responses that correlated well with the experimentally acquired response data from a second office floor. This force model provides the basis for many simulations used in this work in order to assess a more realistic response from the floor models.

It has been shown in the current work that both tuned mass dampers (TMDs) and AVC can effectively reduce the response of an entire floor structure. However, the total participating mass required to do this with TMDs was significantly higher than the AVC scenario: a total of 9198kg for TMDs compared with 240kg for AVC for the example floor structure considered. In addition to this, the level of reduction was significantly higher with AVC: a reduction of 71% to 75% for AVC compared with only 41% to 56% with TMDs. This demonstrates the key benefits of using AVC over TMDs, namely a larger reduction over the entire floor area for a smaller total active mass.

Although AVC has the advantage that it can target many modes of vibration simultaneously, it is inherently limited by controllability and observability issues. This means that there is still a requirement for multiple actuators to control the response over the entire floor area. The work in this thesis has demonstrated this

by simulating the response of the structure throughout the entire floor area rather than at just a single point. From this, a noticeable zone of influence was observed around each actuator, clearly showing the effect that the actuator has on reducing the response of the structure in a relatively localised area.

These controllability and observability issues meant that the two different structural floor designs considered in this work performed quite differently with AVC. It was found that the floor with larger panels and more global mode shapes was able to have its response reduced by a smaller number of AVC units than the structure with smaller, more rectangular bays. This is because when the size of each bay was larger, so too was the effect of AVC spread over a larger area. Additionally, for this structure the mode shapes were global in such a way that control was extended slightly to areas outside the controlled bays. The implications of this are that one could design a structure to be inherently more flexible and have larger bays; this would likely make the uncontrolled state actually worse, but because the structure is more controllable the net effect of combined structure and AVC would be more efficient. Furthermore, the results in this study indicate that a good rule of thumb for the number of decentralised AVC systems required to control a particular floor area is based on the number of significant bays, rather than the number of modes as is the case with traditional control theory.

The overheads associated with running the amplifiers for the actuators are very high for the off-the-shelf actuators used in the majority of AVC studies. However, different technologies exists, such as class D amplifiers or linear motor technology, which improve on this and the incorporation of these into actuator configurations is the focus of current research. Once this has been achieved then the relatively modest power savings made through the trade-off between performance and power demand, resulting from changes in the control law, will become more significant. Here, it was found that one of the most effective ways of reducing the power demand of a control law is to use a relatively simple controller such as direct velocity feedback (DVF) but to reduce the feedback gain. Although this

may appear obvious at first, the non-linear relationship between power demand and response reduction means that significant power savings can be made *without* a significant increase in the structural response as might be expected. The implications of this are that with reduced feedback gain, so too is the output force which means that smaller, cheaper actuators may be able to be used effectively, which would reduce the high initial costs as well as the on-going costs.

Alternative strategies such as using a model-based controller to target only particular modes of vibration did not decrease the power demand significantly but resulted in an increase in response compared with DVF. The switching-off rule was effective at reducing the power demand, but a simple decrease in gain for the DVF controller achieved a better average power to response ratio for most scenarios. This is because the switching-off rule utilised a high gain, so when the response was high so too was the power demand. In contrast, the DVF controller with a reduced gain achieved similar overall response reductions but on average the power demand was less because when the response was high the power demand was significantly less. This more than offset the relatively small saving in power made by the switching-off rule when the response was below the switching-off threshold.

An initial life cycle analysis has been performed which investigates the implications of incorporating AVC into a floor design. Here, it was found that the initial financial cost of AVC is too high at present. This analysis utilised the prototype cost for the actuator so is a worst case scenario; however, the financial cost of the AVC was significantly higher than the initial savings made through reduced construction materials usage and the cost of the AVC units would have to be reduced by 80% for these initial costs to equate. As this is a new technology it is expected that future research improvements and mass production will reduce these costs, although it is beyond the scope of this study to predict by how much.

Assuming that the cost issue is either resolved through future research or consid-

ered a reasonable cost to pay for the benefit of achieving a more slender structural form, then the environmental considerations will then become of some importance. Here, the initial environmental costs of installing AVC that were considered (CO_2e emissions and energy required) were found to be significantly lower than the savings made from reduced construction material usage. However, the operating energy and carbon costs were significant. This is partly due to the relatively high overhead costs associated with the amplifiers used in this work; that is, the electricity required before any command signal is sent to the actuators. When the currently available actuators' overheads are used, the overheads accounted for between 83% and 89% of the average power demand and resulted in even shorter payback periods. Additionally, no account of changes in the thermal mass of the building were considered, so heating and cooling costs for the building could be significantly increased through the use of a more slender structural form.

The payback period for all criteria in the life cycle analysis (when using the linear motor technology) is less than fifty years which could be considered a minimum design life. This would suggest that it is not currently economically or environmentally favourable to install AVC. However, there are other potential factors that this study does not include because they are difficult or impossible to quantify. For example, the cumulative effect of reducing the slab depth over many storeys could result in the possibility of including an additional floor for a fixed building height. This would have great implications to the expected revenue of the building through the leasing of more floor space.

In addition, it should be noted that the conclusions from this environmental assessment are applicable only for the case studied here. The scale by which the various factors differ (e.g. AVC installation cost compared with construction materials savings) have allowed some generalisations to be made, but this is still only a sample size of one so care should be taken when considering the implications of this study for other floor designs.

7.2 Recommendations for Further Work

One of the key areas where further research is required is the combined structural and control system design. In this work, general conclusions were drawn based on observability and controllability. However, it is expected that further insights could be sought through further work. One approach to this could be to use a genetic algorithm (or similar optimisation technique) to evaluate different designs from the perspective of minimising material costs, number of actuators and overall response, with the constraints that the solution must be a structurally viable option. The outcomes from this could provide the necessary insights into which design approaches are best at achieving the optimal combined system.

Additionally, there is currently no guidance for structural engineers considering active control for floor control. Therefore, further work is required to develop guidelines for structural engineers to advise on when AVC is suitable and how a building should be best designed to incorporate AVC. This might also be supplemented with specialist design software to enable practising structural engineers to evaluate the beneficial effects of active vibration control.

As was mentioned earlier, improvements in actuator cost and overheads are fundamental requirements to widespread adoption of this technology. The author is aware of current research investigating this issue. However, a commercially attractive/viable option may not be available until even more developments are made. In addition to this, the methodology developed in this paper should be applied to a variety of different floor structures. The conclusions drawn from this study are heavily dependent on the number of actuators required as this dictates both the initial cost and the on-going costs of AVC. Therefore, different floors with different AVC requirements will yield different payback periods for the criteria chosen.

For simplicity, changes to the thermal mass of the building and the maintenance costs of the AVC system have not been considered in the initial life cycle analysis. Both of these should be quantified as accurately as possible and then included in

the life cycle analysis to yield more accurate payback period predictions.

Additional factors should be considered in the environmental assessment. Although CO_2e and energy are two of the most popular criteria, these are not the only contributing factors. Alternatives such as resource consumption, air pollution, water pollution etc. are arguably equally important but could have very different life cycle characteristics to the factors studied here.

There is great potential for the development of smaller actuators that could be more easily distributed throughout the structure. This would help significantly with the issue of controllability and observability of modes, and as suggested by the results in Chapter 5, each smaller actuator may be able to achieve similar response reductions to the larger ones currently used. However, further work is required to validate this claim.

A lot of the work in this thesis is based on simulations and it is important to verify the conclusions of this work through experimentation. One key experiment that should be investigated is implementing many AVC units within a floor and monitoring the response all over, rather than just at the point of control. Although it is understood that there are practical limitations to this, i.e. the availability of suitable structures, and the expense of setting up the monitoring system, the potential benefits that could be derived through this work are significant.

References

Mohamed Abdel-Rohman. Active Control of Tall Buildings Against Stochastic Wind Forces. *Journal of Wind Engineering and Industrial Aerodynamics*, 17: 251–264, 1984.

A. Alavinasab, H. Moharrami, and A. Khajepour. Active Control of Structures Using Energy-based LQR Method. *Computer-Aided Civil and Infrastructure Engineering*, 21:605–611, 2006.

Rabih Alkhatib and M. F. Golnaraghi. Active Structural Vibration Control: A Review. *The Shock and Vibration Digest*, 35(5):367–383, 2003.

Julian M Allwood. Transitions to material efficiency in the UK steel economy. *Philosophical transactions. Series A, Mathematical, physical, and engineering sciences*, 371(1986):20110577, March 2013. ISSN 1364-503X. doi: 10.1098/rsta.2011.0577.

Hans-jörg Althaus, Mike Chudacoff, Roland Hischier, Niels Jungbluth, Maggie Osses, and Alex Primas. Life Cycle Inventories of Chemicals. ecoinvent report No. 8, v2.0. Technical Report 8, Swiss Centre for Life Cycle Inventories, Dubendorf, Switzerland, 2007.

ANSYS. Release 11.0 Documentation for ANSYS, 2000.

Sumeet S Aphale, Andrew J Fleming, and S O Reza Moheimani. Integral resonant control of collocated smart structures. *Smart Materials and Structures*, 16(2): 439–446, 2007. ISSN 0964-1726. doi: 10.1088/0964-1726/16/2/023.

Ami Arbel. Controllability Measures and Actuator Placement in Oscillatory Systems. *International Journal of Control*, 33(3):565–574, 1981.

Lu Aye, Nick Bamford, Bill Charters, and Jon Robinson. COBRA 1999 Optimising embodied energy in commercial office development. Technical report, RICS Research Foundation, Melbourne, 1999.

H. Bachmann. Case Studies of Structures with Man-Induced Vibrations. *Journal of Structural Engineering*, 118(3):631–647, March 1992.

N R Baddoo, A W Morrow, J C Taylor, and CIM Steel. *C-EC3 - concise Eurocode 3 for the design of steel buildings in the United Kingdom : based on DD ENV 1993-1-1: 1992 Eurocode 3 design of steel structures: Part 1.1 general rules and rules for buildings with reference to the UK National Application Documen*. Steel Construction Institute, Ascot, 1st edition, 1993.

S. V. Bakre and R. S. Jangid. Optimum parameters of tuned mass damper for damped main system. *Structural Control and Health Monitoring*, 14(3):448–470, 2007. doi: 10.1002/stc.166.

Gary Balas, Richard Chiang, Andy Packard, and Michael Safonov. Robust Control Toolbox 3: Getting Started Guide. Technical report, The Mathworks, Inc., 2008.

BRE. BREEAM Scheme Document Offices 2008 - SD5055. Technical report, Hertfordshire, 2008.

BRECSU. Energy Consumption Guide 19: Energy use in offices. Technical report, Building Research Energy Conservation Support Unit, Watford, UK, 2000.

J. M. W. Brownjohn and C. J. Middleton. Procedures for Vibration Serviceability Assessment of High-Frequency Floors. *Engineering Structures*, 30(6):1548–1559, 2008.

I Bruant and L Proslier. Optimal Location of Actuators and Sensors in Active Vibration Control. *Journal of Intelligent Material Systems and Structures*, 16 (3):197–206, 2005. ISSN 1045-389X. doi: 10.1177/1045389X05047989.

BSI. Guide to Measurement and evaluation of human exposure to whole-body mechanical vibration and repeated shock - BS 6841:1987. Technical report, 1987.

BSI. Loadings for Buildings - Part 3: Code of practice for imposed roof loads - BS 6399-3:1988. Technical report, 1988.

BSI. Guide to Evaluation of Human Exposure to Vibration in Buildings (1Hz to 80Hz) - BS 6472:1992. Technical report, 1992.

BSI. Loading for Buildings - Part 1: Code of practice for dead and imposed loads - BS 6399-1:1996. Technical report, 1996.

BSI. Structural use of concrete - Part 1: Code of practice for design and construction - BS 8110-1:1997. Technical report, 1997.

BSI. Environmental Management - Life Cycle Assessment - Requirements and Guidelines - BS EN ISO 14040:2006. Technical report, 2006a.

BSI. Environmental Management - Life Cycle Assessment - Principles and Framework - BS EN ISO 14040:2006. Technical report, 2006b.

BSI. Guide to Evaluation of Human Exposure to Vibration in Buildings - Part 1: Vibration Sources other than blasting - BS 6472-1:2008. Technical report, 2008.

BSI. Eurocode 3 : Design of steel structures - BS EN 1993-1-1:2005. Technical Report April, 2010.

Andrew H. Buchanan and Brian G. Honey. Energy and carbon dioxide implications of building construction. *Energy and Buildings*, 20:205–217, 1994.

H. Cao and Q. S. Li. New control strategies for active tuned mass damper systems. *Computers & Structures*, 82(27):2341–2350, October 2004. ISSN 0045-7949. doi: 10.1016/j.compstruc.2004.05.010.

C. M. Casado, J. de Sebastián, I. M. Díaz, and A. Poncela. Vibration Serviceability assessment and passive vibration control of a lively footbridge. In *Proceedings of the 5th World Conference on Structural Control and Monitoring (5WCSCM)*, page 249, Tokyo, 2010.

F. Casciati, J. Rodellar, and U. Yildirim. Active and semi-active control of structures - theory and applications: A review of recent advances. *Journal of Intelligent Material Systems and Structures*, May 2012. ISSN 1045-389X. doi: 10.1177/1045389X12445029.

Chih-Chen Chang and Lung-On Yu. A simple optimal pole location technique for structural control. *Engineering Structures*, 20(9):792–804, 1998.

J. G. Chase, S. E. Breneman, and H. A. Smith. Robust H infinity static output feedback control with actuator saturation. *Journal of Engineering Mechanics*, 125(2):225–233, 1999.

Xin Chen, Youliang Ding, Ai-qun Li, Zhiqiang Zhang, and Peng Sun. Investigations on serviceability control of long-span structures under human-induced excitation. *Earthquake Engineering and Engineering Vibration*, 11(1):57–71, March 2012. ISSN 1671-3664. doi: 10.1007/s11803-012-0098-0.

J. L. Chevalier and J. F. Le Téno. Requirements for an LCA-based Model for the Evaluation of the Environmental Quality of Building Products. *Building and Environment*, 31(5):487–491, 1996.

Mischa Classen, Hans-jörg Althaus, Silvio Blaser, Matthias Tuchschmid, Niels Jungbluth, G Doka, M Faist Emmeneger, and W Scharnhorst. Life Cycle Inventories of Metals. Final report ecoinvent data v2.1, No 10. Technical Report 10, Swiss Centre for Life Cycle Inventories, Dubendorf, Siwtizerland, 2009.

Raymond J. Cole and Paul C. Kernan. Life-cycle energy use in office buildings. *Building and Environment*, 31(4):307–317, 1996.

M. Collet. Shape Optimization of Piezoelectric Sensors Dealing with Spill-Over Instability. *IEEE Transactions on Control Systems Technology*, 9(4):654–662, 2001.

Drury Crawley and Iliari Aho. Building environmental assessment methods: applications and development trends. *Building Research & Information*, 27(4/5): 300–308, 1999. ISSN 0961-3218. doi: 10.1080/096132199369417.

CSA. Guide for floor vibrations - CSA Standard CAN 3-S16 1-M 89. Steel Structures for Buildings - Limit state design, Appendix G. Technical report, Canadian Standards Association, Toronto, 1989.

W. G. Curtin, G. Shaw, G. I. Parkinson, and J. M. Golding. *Structural Foundation Designers' Manual*. Blackwell Publishing, Singapore, 2nd edition, 2006. ISBN 13:978-1-4051-3044-8.

Hilda Dahlsten. *Life Cycle Assessment of Electricity from Wave Power*. Masters dissertation, Swedish University of Agricultural Sciences, 2009.

B Davis and T. M Murray. Slender monumental stair vibration serviceability. *Journal of Architectural Engineering*, 15(4):111–121, 2009.

DECC. 2050 Pathways Analysis - URN 10D/764. Technical report, Department of Energy and Climate Change (DECC), July 2010.

J. P. Den Hartog. *Mechanical Vibrations*. McGraw-Hill Book Company, 1947. ISBN 9781443725361.

A. Dewey and E. Jury. A note on Aizerman's conjecture. *IEEE Transactions on Automatic Control*, 10(4):482– 483, October 1965. ISSN 0018-9286. doi: 10.1109/TAC.1965.1098190.

I. M. Díaz, C. M. Casado, and J. de Sebastián. Active vibration control study of an in-service footbridge using an inertial proof-mass actuator. In *5th World Conference on Structural Control and Monitoring*, page 10074, Tokyo, 2010.

I M. Díaz, E Pereira, M J Hudson, and P Reynolds. Enhancing active vibration control of pedestrian structures using inertial actuators with local feedback control. *Engineering Structures*, 41:157–166, 2012a.

Ivan M. Díaz and P. Reynolds. Robust saturated control of human-induced floor vibrations via a proof-mass actuator. In *Smart Materials and Structures*, volume 18, page 125024, Porto, 2009a.

Ivan M. Díaz and P. Reynolds. Performance of SISO active control strategies for floor vibrations. In *IV ECCOMAS Thematic Conference, Smart Structures and Materials*, Porto, 2009b.

Ivan M. Díaz and Paul Reynolds. Acceleration feedback control of human-induced floor vibrations. *Engineering Structures*, 32(1):163–173, 2010a. ISSN 0141-0296. doi: 10.1016/j.engstruct.2009.09.003.

Iván M. Díaz and Paul Reynolds. On-off nonlinear active control of floor vibrations. *Mechanical Systems and Signal Processing*, 24:1711–1726, 2010b. ISSN 0888-3270. doi: 10.1016/j.ymssp.2010.02.011.

Iván M. Díaz, Emiliano Pereira, and Paul Reynolds. Integral resonant control scheme for cancelling human-induced vibrations in light-weight pedestrian structures. *Structural Control and Health Monitoring*, 19(1):55–69, February 2012b. ISSN 15452255. doi: 10.1002/stc.423.

A. Dimoudi and C. Tompa. Energy and environmental indicators related to construction of office buildings. *Resources, Conservation and Recycling*, 53(1-2): 86–95, 2008.

Manish Kumar Dixit, José L. Fernández-Solís, Sarel Lavy, and Charles H. Culp. Identification of parameters for embodied energy measurement: A literature review. *Energy and Buildings*, 42(8):1238–1247, August 2010. ISSN 03787788. doi: 10.1016/j.enbuild.2010.02.016.

J. Doyle. Guaranteed margins for LQG regulators. *IEEE Transactions on Automatic Control*, 23(4):756–757, 1978.

Haiping Du, Nong Zhang, and Hung Nguyen. Mixed H2/H infinity control of tall buildings with reduced-order modelling technique. *Structural Control and Health Monitoring*, 15(1):64–89, 2008. ISSN 15452255. doi: 10.1002/stc.207.

S. J. Dyke, B. F. Spencer, P. Quast, M. K. Sain, D. C. Kaspari Jr, and T. T. Soong. Acceleration feedback control of MDOF structures. *Journal of Engineering Mechanics*, 122(9):907–918, 1996.

Arya Ebrahimpour and Ronald L. Seek. A Review of Vibration Serviceability Criteria for Floor Structures. *Computers & Structures*, 83(28-30):2488–2494, 2005.

Suzy Edwards and Philip Bennett. Construction products and life-cycle thinking. *UNEP Industry and Environment*, Apr-Sep:57–61, 2003.

Emad El-Dardiry, Endah Wahyuni, Tianjian Ji, and Brian R. Ellis. Improving FE models of a long-span flat concrete floor using natural frequency measurements. *Computers & Structures*, 80(27-30):2145–2156, November 2002. ISSN 0045-7949. doi: 10.1016/S0045-7949(02)00264-X.

S. J. Elliott, M. Serrand, and P. Gardonio. Feedback Stability Limits for Active Isolation Systems with Reactive and Inertial Actuators. *Journal of Vibra-*

tion and Acoustics, 123(2):250–261, 2001. ISSN 07393717. doi: 10.1115/1.1350822.

B. R. Ellis. Serviceability evaluation of floor vibration induced by walking loads. *The Structural Engineer*, 79(21):30–36, 2001.

D. J. Ewins. *Modal Testing: Theory and Practice*. Research Studies Press Ltd, Letchworth, England, 1984.

R. Eyre and D. W. Cullington. Experience with vibration absorbers on footbridges - Research Report 18. Technical report, Transport and Road Research laboratory, 1985.

Roger Fay, Graham Treloar, and Usha Iyer-Raniga. Life-cycle energy analysis of buildings: a case study. *Building Research & Information*, 28(1):31–41, 2000. ISSN 0961-3218. doi: 10.1080/096132100369073.

Markus Feldmann and Christoph Heinemeyer. Vibration Design of Floors: Guideline - RFS2-CT-2007-00033. Technical report, Institut und Lehrstuhl fur Stahlbau Leichtmetallbau, 2007.

Markus Feldmann, Christoph Heinemeyer, Chr Butz, E Caetano, A Cunha, F Galanti, A Goldack, O Hechler, S Hicks, A Keil, M Lukic, R Obiala, M Schlaich, G Sedlacek, A Smith, and P Waarts. Design of floor structures for human induced vibrations. Technical report, JRC-ECCS, Italy, 2009.

R Fisher. Does the handling of iron sinter present a potential health hazard from the release of respirable crystalline silica? Technical report, The Iron Platform, 2010.

Y. Fujino and M. Abé. Design formulas for tuned mass dampers based on a perturbation technique. *Earthquake Engineering & Structural Dynamics*, 22:833–854, 1993.

Emad Gad, Tuan Nguyen, Ibrahim Saidi, John Wilson, and Nick Haritos. Reduction of Excessive Floor Vibration Using a New Viscoelastic Damper. In *EACS 2012 - 5th European Conference on Strutural Control*, number June, pages 1–8, 2012.

Alberto Gomez-Rivas, Weining Feng, and George Pincus. Engineering Technology Laboratory for Structural Control of Structures. In *Proceedings of the 2002 American Socity for Engineering Education Annual Conference and Exposition, vol 1825*, volume 1825, 2002.

C González Díaz and P Gardonio. Feedback control laws for proof-mass electrodynamic actuators. *Smart Materials and Structures*, 16(5):1766–1783, October 2007. ISSN 0964-1726. doi: 10.1088/0964-1726/16/5/031.

C.G. Gordon. Generic criteria for vibration-sensitive equipment. In *Proceedings of the SPIE*, pages 71–85, 1991.

M. J. Griffin. A Comparison Of Standardized Methods For Predicting The Hazards Of Whole-Body Vibration And Repeated Shocks. *Journal of Sound and Vibration*, 215(4):883–914, August 1998. ISSN 0022-460X. doi: 10.1006/jsvi.1998.1600.

D.-W. Gu, P.Hr. Petkov, and M.M. Konstantinov. *Robust control design with MATLAB*, volume 14 of *Advanced Textbooks in Control and Signal Processing*. Springer, London, 1st edition, 2005.

Timothy G Gutowski, Sahil Sahni, Julian M Allwood, Michael F Ashby, and Ernst Worrell. The energy required to produce materials: constraints on energy-intensity improvements, parameters of demand. *Philosophical transactions. Series A, Mathematical, physical, and engineering sciences*, 371(1986): 20120003, March 2013. ISSN 1364-503X. doi: 10.1098/rsta.2012.0003.

A. Haapio and P. Viitaniemi. A critical review of building environmental assessment tools. *Environmental impact assessment review*, 28(7):469–482, 2008.

A Hać and L Liu. Sensor and Actuator Location in Motion Control of Flexible Structures. *Journal of Sound and Vibration*, 167(2):239–261, 1993.

G. P. Hammond and C. I. Jones. Embodied energy and carbon in construction materials. *Proceedings of Institution of Civil Engineers : Energy (in press)*, 161(2):87–98, 2008.

Linda. M. Hanagan. *Active Control of Floor Vibrations*. Phd thesis, Polytechnic Institute and State University, Virginia, December 1994.

Linda. M. Hanagan. Walking-Induced Floor Vibration Case Studies. *Journal of Architectural Engineering*, 11(1):14–18, March 2005a.

Linda. M. Hanagan. Active floor vibration system, Patent Specification 6874748, 2005b.

Linda. M. Hanagan. Practical Implications of Optimizing an Active Floor Vibration Controller. In *Proceedings of the IMAC-XXVIII*, Jacksonville, Florida USA, 2010. Society for Experimental Mechanics Inc.

Linda. M. Hanagan and Thomas. M. Murray. Active Control Approach for Reducing Floor Vibrations. *Journal of Structural Engineering*, 123(11):1497–1505, November 1997.

Linda. M. Hanagan and Thomas. M. Murray. Experimental Implementation of Active Control to Reduce Annoying Floor Vibrations. *AISC Engineering Journal*, 35(4):123–127, 1998.

Linda. M. Hanagan, Ernest. C. Kulasekere, Kirthi. S. Walgama, and Kamal Premaratne. Optimal Placement of Actuators and Sensors for Floor Vibration Control. *Journal of Structural Engineering*, 126(12):1380–1387, December 2000.

Linda. M. Hanagan, Thomas. M. Murray, and Kamal Premaratne. Controlling Floor Vibration with Active and Passive Devices. *The Shock and Vibration Digest*, 35(5):347–365, 2003.

J. P. Hespanha. *Undergraduate Lecture Notes on LQG/LQR controller design*. April 2007.

K Hiramoto, H Doki, and G Obinata. Optimal Sensor/Actuator Placement for Active Vibration Control Using Explicit Solution of Algebraic Riccati Equation. *Journal of Sound and Vibration*, 229(5):1057–1075, 2000. doi: 10.1006/jsvi.1999.2530.

Chih-Chergn Ho and Chih-Kao Ma. Active vibration control of structural systems by a combination of the linear quadratic Gaussian and input estimation approaches. *Journal of Sound and Vibration*, 301:429–449, 2007.

Arpad Horvath. Construction Materials and the Environment. *Annual Review of Environmental Resources*, 29:181–204, 2004.

G. W. Housner, Boutros A. Klink, and Eduardo Kausel. Proceedings of the first world conference on structural control. *Soil Dynamics and Earthquake Engineering*, 15(2):147–149, February 1996. ISSN 0267-7261. doi: 10.1016/S0267-7261(96)90003-2.

G. W. Housner, L. A. Bergman, T. K. Caughey, A. G. Chassiakos, R. O. Claus, S. F. Masri, R. E. Skelton, T. T. Soong, B. F. Spencer, and J. T. P Yao. Structural Control: Past, Present, and Future. *ASCE Journal of Engineering Mechanics*, 123(9):897–971, September 1997. doi: 10.1061/(ASCE)0733-9399(1997)123:9(897).

M J Hudson and P Reynolds. Analytical and Experimental Evaluation of Active Vibration Control of an Office Floor Structure. In *Proceedings of 5th World Conference on Structural Control and Monitoring*, page 10047, Tokyo, 2010.

M J. Hudson and P. Reynolds. Implementation considerations for active vibration control in the design of floor structures. *Engineering Structures*, 44:334–358, November 2012. ISSN 01410296. doi: 10.1016/j.engstruct.2012.05.034.

M J Hudson and P Reynolds. Implications of structural design on the effectiveness of AVC of floor structures. *Structural Control and Health Monitoring*, In Review, 2013a.

M J Hudson and P Reynolds. A Life Cycle Analysis of an Office Floor With Active Vibration Control. *ASCE Journal of Structural Engineering*, In Review, 2013b.

M J Hudson, P Reynolds, and D Nyawako. Efficient Design of Floor Structures Using Active Vibration Control. In *Structures Congress 2011*. Asce, 2011. ISBN 978-0-7844-1171-1. doi: 10.1061/41171(401)35.

M J. Hudson, P Reynolds, and D S. Nyawako. Comparison of passive and active mass dampers for control of floor vibrations. In *Proceedings of SPIE 2012*, April 2012. doi: 10.1117/12.915956.

M J Hudson, P Reynolds, and D Nyawako. Power requirements for active control of floor vibrations. In *Proceedings of IMAC XXXI*, California, 2013. Society for Experimental Mechanics.

J. S Hwang, H. Kim, and J. Kim. Estimation of the modal mass of a structure with a tuned-mass damper using H-infinity optimal model reduction. *Engineering structures*, 28(1):34–42, 2006.

Petros A. Ioannou and Bari Fidan. *Adaptive control tutorial*. Cambridge University Press, 2006. ISBN 9780898716153.

ISO. Evaluation of human exposure to whole-body vibration - Part 2: Continuous and shock-induced vibration in buildings (1 to 80 Hz) - 2631-2:1989(E). Technical report, Switzerland, 1989.

ISO. Bases for design of structures - Serviceability of buildings and walkways against vibrations - 10137:2007(E). Technical report, Switzerland, 2007.

IVF Industrial Research and Development Corporation. Lot 3 Personal Computers (desktops and laptops) and Computer Monitors. Technical report, European Commission DG TREN, 2007.

F. Jabbari, W. E. Schmitendorf, and J. N. Yang. H-infinity Control for Seismic-Excited Buildings with Acceleration Feedback. *Journal of Engineering Mechanics*, 121(9):994–1002, 1995.

Nader Jalili. A Comparative Study and Analysis of Semi-Active Vibration-Control Systems. *Journal of Vibration and Acoustics*, 124(4):593, 2002. ISSN 07393717. doi: 10.1115/1.1500336.

A. P. Jeary. Damping in tall buildings - a mechanism and a predictor. *Earthquake Engineering & Structural Dynamics*, 14:733–750, 1986.

C. D Johnson. Design of passive damping systems. *Transactions-American Society Of Mechanical Engineers Journal Of Mechanical Design*, 117:171–171, 1995.

C. I. Jones. Embodied Carbon: A Look Forward. Technical report, Sustain, 2011.

S. Junnila and Arpad Horvath. Life-cycle environmental effects of an office building. *Journal of Infrastructure Systems*, 9:157–166, 2003.

Joshua Kneifel. Life-cycle carbon and cost analysis of energy efficiency measures in new commercial buildings. *Energy and Buildings*, 42(3):333–340, 2010. ISSN 03787788. doi: 10.1016/j.enbuild.2009.09.011.

Í. E. Köse, W. E. Schmitendorf, F. Jabbari, and J. N. Yang. H-infinity active seismic response control using static output feedback. *Journal of Engineering Mechanics*, 122(7):651–659, 1996.

W Lawson. *Building Materials, Energy and the Environment: Towards Ecologically Sustainable Development*. Royal Australian Institute of Architects, Red Hill, 1996.

H. K Lee, S. T Chen, and A. C Lee. Optimal control of vibration suppression in flexible systems via dislocated sensor/actuator positioning. *Journal of the Franklin Institute*, 333(5):789–802, 1996.

Manfred Lenzen. Errors in Conventional and Input-Output-based Life-Cycle Inventories. *Journal of Industrial Ecology*, 4(4):127–148, October 2000. ISSN 1530-9290. doi: 10.1162/10881980052541981.

Q. S. Li, J. Q. Fang, A. P. Jeary, and D. K. Liu. Decoupling control law for structural control implementation. *International Journal of Solids and Structures*, 38:6147–6162, 2001.

Q. S. Li, D. K. Liu, J. Tang, N. Zhang, and C. M. Tam. Combinatorial optimal design of number and positions of actuators in actively controlled structures using genetic algorithms. *Journal of sound and vibration*, 270(4-5):611–624, 2004.

X. Li, Y. Zhu, and Z. Zhang. An LCA-based environmental impact assessment model for construction processes. *Building and Environment*, 45:766–775, 2010.

Li-Teh Lu, Wei-Ling Chiang, and Jhy-Pyng Tang. LQG/LTR Control Methodology in Active Structural Control. *Journal of Engineering Mechanics*, 124(4): 446–454, April 1998.

Li-Teh Lu, Wei-Ling Chiang, Jhy-Pyng Tang, Ming-Yi Liu, and Cheng-Wu Chen. Active control for a benchmark building under wind excitations. *Journal of Wind Engineering and Industrial Aerodynamics*, 91:469–493, 2003.

B. J. Lurie and P. J. Enright. *Classical Feedback Control with MATLAB*. Control Engineering. Marcel Dekker, Inc., New York, 2000.

J. P. Lynch and K. H. Law. Decentralized Control Techniques for Large-Scale Civil Structural Systems. In *Proceedings of the 20th International Modal Analysis Conference (IMAC-XX): Structural Dynamics Vols I and II*, Los Angeles, 2002.

L. E. Mackriell, K. C. S. Kwok, and B. Samali. Critical mode control of a wind-loaded tall building using an active tuned mass damper. *Engineering Structures*, 19(10):834–842, 1997.

Iain MacLeay, Kevin Harris, and Anwar Annut. Digest of United Kingdom Energy Statistics 2010. Technical report, National Statistics, London, 2010.

Maurer Söhne. Tuned Mass and Viscous Dampers - Technical Information and Products, 2004.

D.C. McFarlane and K. Glover. *Robust Controller Design Using Normalized Coprime Factor Plant Description*, volume 138 of *Lecture Notes in Control and Information Sciences*. Springer, Berlin, 1990.

Zbigniew Michalewicz and David B. Fogel. *How to solve it: Modern Heuristics*. Springer, 2nd edition, December 2004. ISBN 9783540224945.

C.J. Middleton and J.M.W. Brownjohn. Response of high frequency floors: A literature review. *Engineering Structures*, 32(2):337–352, February 2010. ISSN 0141-0296. doi: 10.1016/j.engstruct.2009.11.003.

E. J. Mishan. *Cost-benefit Analysis*. Unwin Hyman, London, 4th edition, 1988. ISBN 0044450923.

Z. Miskovic, A. Pavić, and P. Reynolds. Effects of full-height nonstructural partitions on modal properties of two nominally identical building floors. *Canadian Journal of Civil Engineering*, 36:1121–1132, 2009.

Alexandre Molter, Otávio A. A. Silveira, Valdecir Bottega, and Jun S. O. Fonseca. Integrated topology optimization and optimal control for vibration suppression in structural design. *Structural and Multidisciplinary Optimization*, pages 1–9, August 2012. ISSN 1615-147X. doi: 10.1007/s00158-012-0829-x.

A. Montazeri, J. Poshtan, and A. Choobdar. Performance and robust stability trade-off in minimax LQG control of vibrations in flexible structures. *Engineering Structures*, 31(10):2407–2413, 2009.

C. Moutinho, A. Cunha, and E. Caetano. Implementation of an active mass damper to control vibrations in a lively footbridge. In *III ECCOMAS Thematic conference on smart structures and materials*, Gdansk, Poland, 2007.

T. M. Murray, D. E. Allen, and E. E. Ungar. Floor vibrations due to human activity - DG-11 (10M797). Technical report, AISC American Institute of Steel Construction, 1997.

NHS Information Centre. Health Survey for England - 2009 trend tables, 2010.

I. Nishimura, T. Yamada, M. Sakamoto, and T. Kobori. Control performance of active-passive composite tuned mass damper. *Smart Materials and Structures*, 7:637–653, 1998.

D Nyawako, P Reynolds, and M Hudson. Investigating PID controllers for mitigation of human-induced floor vibrations. In *EURODYN 2011*, 2011.

D S. Nyawako, P Reynolds, and M J Hudson. Exploring efficiencies of SISO, multi-SISO and MIMO AVC schemes for floor vibration control. In *Proceedings of SPIE 2012*, April 2012.

Donald Nyawako. *An Active Control Approach for Mitigation of Human-Induced Vibrations in Floors*. Phd thesis, The University of Sheffield, Sheffield, UK, March 2009.

Donald Nyawako and Paul Reynolds. Technologies for Mitigation of Human-induced Vibrations In Civil Engineering Structures. *The Shock and Vibration Digest*, 39(6):465–493, November 2007a. doi: 10.1177/0583102407084286.

Donald Nyawako and Paul Reynolds. Active Control of Human Induced Floor Vibrations. In *Proceedings of 12th Asia Pacific Vibration Conference (APVC2007)*, page 12, Hokkaido University, August 2007b.

Donald Nyawako and Paul Reynolds. Response-dependent velocity feedback control for mitigation of human-induced floor vibrations. *Smart Materials and Structures*, 18(075002), June 2009. doi: 10.1088/0964-1726/18/7/075002.

A. Pachi and T. Ji. Frequency and velocity of people waking. *The Structural Engineer*, 83(3):36–40, 2005.

Kwan-Soon Park and Hyun-Moo Koh. Preference-based optimum design of an integrated structural control system using genetic algorithms. *Advances in Engineering Software*, 35:85–94, 2004.

Kwan-Soon Park, Hyun-Moo Koh, and Chung-Won Seo. Independent modal space fuzzy control of earthquake-excited structures. *Engineering Structures*, 26:279–289, 2004.

A Pavic, Z Miskovic, and P Reynolds. Modal testing and finite-element model updating of a lively open-plan composite building floor. *ASCE Journal of Structural Engineering*, 133(4):550–558, 2007.

A Pavic, Z Miskovic, and S Zivanovic. Modal properties of beam-and-block precast floors. *The IES Journal Part A: Civil & Structural Engineering*, 1(3): 171–185, 2008.

Aleksandar Pavic, Paul Reynolds, Peter Waldron, and Kevin Bennett. Dynamic modelling of post-tensioned concrete floors using finite element analysis. *Finite Elements in Analysis and Design*, 37(4):305–323, April 2001. ISSN 0168-874X. doi: 10.1016/S0168-874X(00)00045-7.

Aleksander Pavić and Michael Willford. Vibration Serviceability of Post-Tensioned Concrete Floors. *Appendix G in Post-Tensioned Concrete Floors Design Handbook - Technical Report 43*, pages 99–107, 2005.

Anton C Pil and H Haruhiko. Integrated Structure/Control Design of Mechatronic Systems Using a Recursive Experimental Optimization Method. *IEEE/ASME Transactions on Mechatronics*, 1(3):191–203, 1996.

Andre Preumont. *Vibration Control of Active Structures: An Introduction*. Number 96 in Solid Mechanics and its Applications. Kluwer Academic Publishers, The Netherlands, 2nd edition, 2002.

Quarry Products Association. Sustainable Development Report 2008. Technical Report December, Quarry Products Association, London, 2008.

V Racic. *Experimental measurement and mathematical modelling of near-periodic human-induced dynamic force signals*. Phd thesis, University of Sheffield, 2009.

P Reynolds. *The Effects of Raised Access Flooring on the Vibrational Performance of Long-Span Concrete Floors*. PhD thesis, The University of Sheffield, 2000.

P. Reynolds and A. Pavić. Effects of False Floors on Vibration Serviceabitliy of Building Floors. I: Modal Properties. *Journal of Performance of Constructed Facilities*, 17(2):75–86, 2003.

P Reynolds, A Pavic, and S Prichard. Dynamic analysis and testing of a high performance floor structure. In M M Maia, M M Silva, and M R Ribeiro, editors, *International Conference on Structural Dynamics Modelling - Test, Analysis, Correlation and Validation*, pages 339–346, Madeira, Portugal, 2002.

P. Reynolds, I. M. Díaz, and Donald Nyawako. Vibration Testing and Active Control of an Office Floor. In *Proceedings of the IMAC-XXVII*, Orlando, Florida USA, 2009. Society for Experimental Mechanics Inc.

Paul Reynolds and Aleksandar Pavić. Reliability of Assessment Criteria for Office Floor Vibrations. In *Proceedings of EVACES 2011*, 2011.

Martin Gerard Rogers. *Engineering project appraisal: The Evaluation of Alternative Development Schemes*. Wiley-Blackwell, July 2001. ISBN 9780632056064.

J. Rohlfing, S. J. Elliott, and P. Gardonio. Compensation filter for feedback control units with proof-mass electrodynamic actuators, simulations and experimental studies. *University of Southampton, Institute of Sound and Vibration Research*, (ISVR Technical Memorandum No. 991), 2011a.

J. Rohlfing, P. Gardonio, and S.J. Elliott. Base impedance of velocity feedback control units with proof-mass electrodynamic actuators. *Journal of Sound and Vibration*, 330(20):4661–4675, September 2011b. ISSN 0022-460X. doi: 16/j.jsv.2011.04.028.

I. Saidi, E.F. Gad, J.L. Wilson, and N. Haritos. Development of passive viscoelastic damper to attenuate excessive floor vibrations. *Engineering Structures*, 33 (12):3317–3328, July 2011. ISSN 01410296. doi: 10.1016/j.engstruct.2011.05.017.

S. Sandun De Silva and David P. Thambiratnam. Dynamic characteristics of steel-deck composite floors under human-induced loads. *Computers & Structures*, 87(17-18):1067–1076, September 2009. ISSN 0045-7949. doi: 10.1016/j.compstruc.2009.04.005.

C. Scheuer, G. A Keoleian, and P. Reppe. Life cycle energy and environmental performance of a new university building: modeling challenges and design implications. *Energy and Buildings*, 35(10):1049–1064, 2003.

G. Schulz and G. Heimbold. Dislocated Actuator/Sensor Positioning and Feedback Design for Flexible Structures. *AIAA Journal of Guidance and Control*, 6 (5):361–367, 1983.

M. Setareh, J. K Ritchey, T. M Murray, J. H Koo, and M. Ahmadian. Semiactive tuned mass damper for floor vibration control. *Journal of Structural Engineering*, 133(2):242–250, 2007.

Mehdi Setareh. Vibration Serviceability of a Building Floor Structure. I: Dynamic Testing and Computer Modeling. *Journal of Performance of Constructed Facilities*, 24(6):497–507, December 2010. doi: 10.1061/(ASCE)CF.1943-5509.0000134.

Mehdi Setareh and R. D. Hanson. Tuned Mass Dampers to Control Floor Vibration from Humans. *Journal of Structural Engineering*, 118(3):741–762, March 1992a.

Mehdi Setareh and R. D. Hanson. Tuned Mass Dampers for Balcony Vibration Control. *Journal of Structural Engineering*, 118(3):723–740, March 1992b.

Mehdi Setareh, J. K Ritchey, Anthony J. Baxter, and Thomas. M. Murray. Pendulum Tuned Mass Dampers for Floor Vibration Control. *Journal of Performance of Constructed Facilities*, 20(1):64–73, 2006. doi: 10.1061/(ASCE)0887-3828(2006)20:1(64).

Erfan Shahabpoor, Paul Reynolds, and Donald Nyawako. A comparison of direct velocity, direct and compensated accleration feed-back control systems in mitigation of low-frequency floor vibrations. In *Proceedings of IMAC XXVIII*, Jacksonville, Florida USA, 2010.

Yan Sheng, Chao Wang, Ying Pan, and Xinhua Zhang. Modified LQG/LTR Control Methodology in Active Structural Control. *Journal of Low Frequency Noise, Vibration and Active Control*, 22(2):97–108, 2003.

Sigurd Skogestad and Ian Postlethwaite. *Multivariable Feedback Control*. John Wiley & Sons Ltd, Sussex, 2nd edition, 2005.

A. L. Smith, S. J. Hicks, and P. J. Devine. *Design of floors for vibration: A new approach (SCI P354)*. SCI, Ascot, Berkshire, 2007. ISBN 10: 1-85942-176-8; 1.

H. A. Smith and J. G. Chase. Comparison of LQR and H-infinity Algorithms for Vibration Control of Structures in Seismic Zones. In *Proceedings of ASCE Structures Congress*, 1996.

L. Son, S. Hara, H. Matsuhisa, H. Utsuno, and K. Yamada. Proposal of Active Momentum Exchange Impact Damper and Its Application to Floor Shock Vibration Control. In *SICE Annual Conference*, pages 806–811, The University Electro-Communications, Japan, 2008.

Lovely Son, Susumu Hara, Keisuke Yamada, and Hiroshi Matsuhisa. Experiment of Shock Vibration Control Using Active Momentum Exchange Impact Damper. *Journal of Vibration and Control*, 16(1):49–64, 2010.

T. T. Soong. State-of-the-art Review: Active Structural Control in Civil Engineering. *Engineering Structures*, 10(2):74–84, April 1988.

T. T. Soong and B. F. Spencer. Supplemental energy dissipation: state-of-the-art and state-of-the-practice. *Engineering Structures*, 24(3):243–259, March 2002. ISSN 0141-0296. doi: 10.1016/S0141-0296(01)00092-X.

B. F. Spencer and T. T. Soong. New applications and development of active, semi-active and hybrid control techniques for seismic and non-seismic vibration in the USA. In *Proceedings of International Post-SMiRT Conference Seminar on Seismic Isolation, Passive Energy Dissipation and Active Control of Vibration of Structures*, Cheju, Korea, 1999.

B. F. Spencer, J. Suhardjo, and M. K. Sain. Frequency domain optimal control strategies for aseismic protection. *Journal of Engineering Mechanics*, 120(1): 135–158, 1994.

M Spielmann, C Bauer, R Dones, and M Tuchschmid. Transport Services. ecoinvent report no. 14. Technical Report 14, Swiss Centre for Life Cycle Inventories, Dubendorf, Siwtizerland, 2007.

G.E. Stavroulakis, D.G. Marinova, E. Hadjigeorgiou, G. Foutsitzi, and C.C. Baniotopoulos. Robust active control against wind-induced structural vibrations. *Journal of Wind Engineering and Industrial Aerodynamics*, 94(11):895–907, November 2006. ISSN 0167-6105. doi: 10.1016/j.jweia.2006.06.012.

J. Suhardjo, B. F. Spencer, and A. Kareem. Active Control of Wind Excited Builldings: A Frequency Domain Based Design Approach. *Journal of Wind Engineering and Industrial Aerodynamics*, 41-44:1985–1996, 1992.

Michael D. Symans and Michael C. Constantinou. Semi-active control systems for seismic protection of structures: a state-of-the-art review. *Engineering Structures*, 21(6):469–487, June 1999. ISSN 0141-0296. doi: 10.1016/S0141-0296(97)00225-3.

Tata Steel. Advance sections price list 5. Technical Report February, Tata Steel, Scunthorpe, 2012.

Catarina Thormark. A low energy building in a life cycle–its embodied energy, energy need for operation and recycling potential. *Building and Environment*, 37(4):429–435, April 2002. ISSN 0360-1323. doi: 10.1016/S0360-1323(01)00033-6.

A. J. Todd, D. Crawley, S. Geissler, and G. Lindsey. Comparative assessment of environmental performance tools and the role of the Green Building Challenge. *Building Research & Information*, 29(5):324–335, 2001. ISSN 0961-3218. doi: 10.1080/09613210110064268.

P. J. Torvik. The Analysis and Design of Constrained Layer Damping Treatments - AFIT TR 80-4. Technical report, Air Force Institute of Technology, Ohio, 1980.

G J Treloar, R Fay, B Ilozor, and P E D Love. An analysis of the embodied energy of office buildings by height. *Facilities*, 19(5/6):204–214, 2001a.

Graham Treloar, Roger Fay, Benedict Ilozor, and Peter Love. Building materials selection: greenhouse strategies for built facilities. *Facilities*, 19(3/4):139–149, 2001b.

H. C. Tsai and G. C. Lin. Explicit Formulae For Optimum Absorber Parameters For Force-Excited And Viscously Damped Systems. *Journal of Sound and Vibration*, 176(5):585–596, October 1994. ISSN 0022-460X. doi: 10.1006/jsvi.1994.1400.

E. E. Ungar and R.W. White. Footfall-induced vibrations of floors supporting sensitive equipment. *Sound and Vibration*, pages 10–13, 1979.

Wendell D. Varela and Ronaldo C. Battista. Control of vibrations induced by people walking on large span composite floor decks. *Engineering Structures*, 33(9):2485–2494, September 2011. ISSN 01410296. doi: 10.1016/j.engstruct.2011.04.021.

VHK. MEEUP Methodology Report. Technical report, 2005.

S. Živanović, A. Pavić, and P. Reynolds. Probability-based prediction of multi-mode vibration response to walking excitation. *Engineering Structures*, 29(6):942–954, 2007. ISSN 0141-0296.

Stana Živanović and Aleksander Pavić. Probabilistic Modeling of Walking Excitation for Building Floors. *Journal of Performance of Constructed Facilities*, 23(3):132–143, 2009.

Stana Živanović, A. Pavić, and Paul Reynolds. Vibration serviceability of footbridges under human-induced excitation: a literature review. *Journal of Sound and Vibration*, 279(1-2):1–74, 2005. ISSN 0022-460X. doi: 10.1016/j.jsv.2004.01.019.

Q Wang and C M Wang. A Controllability Index for optimal Design of Piezoelectric Actuators in Vibration Control of Beam Structures. *Journal of Sound and Vibration*, 242(3):507–518, 2001. doi: 10.1006/jsvi.2000.3357.

G. B. Warburton. Optimum absorber parameters for various combinations of response and excitation parameters. *Earthquake Engineering & Structural Dynamics*, 10:381–401, 1982.

A. C Webster and R Vaicaitis. Application of Tuned Mass Dampers to control vibrations of composite floor systems. *AISC Engineering Journal*, Quarter 3: 116–124, 1992.

M. Wells. Active Structural Control: An Appraisal For A Practical Application. The Royal Victoria Footbridge. London Docklands. In *Proceedings of Second World Conference on Steel in Construction*, volume Paper 59, 1998.

Y. K. Wen and M. Shinozuka. Cost-effectiveness in active structural control. *Engineering Structures*, 20(3):216–221, March 1998. ISSN 0141-0296. doi: 10.1016/S0141-0296(97)00080-1.

Michael Willford and Peter Young. A Design Guide for Footfall Induced Vibrations of Structures. *The Concrete Society*, 016, December 2006.

Michael Willford, Peter Young, and William H. Algaard. A constrained layer damping system for composite floors. *The Structural Engineer*, 84(4):31–38, 2006.

Martin S. Williams and Shahram Falati. Modal testing of a post-tensioned concrete model floor slab. In *Proceedings of 17th International Modal Analysis Conference*, pages 14–20. Society for Experimental Mechanics, 1999.

M. G. Wright. *Discounted Cash Flow*. McGraw-Hill Book Company, Maidenhead, 2nd edition, 1973.

J. C. Wu, J. N. Yang, and W. E. Schmitendorf. Reduced-order H-infinity and LQR control for wind-excited tall buildings. *Engineering Structures*, 20(3):222–236, 1998.

Jong-Cheng Wu, Hsin-Hsien Chih, and Chern-Hwa Chen. A robust control method for seismic protection of civil frame building. *Journal of Sound and Vibration*, 294:314–328, 2006.

T.A. Wyatt. Mechanisms of damping. In *Symposium on Dynamic Behaviour of Bridges*, pages 10–21, Crowthorne, 1977.

T.A. Wyatt. *Design guide on the vibration of floors*. The Steel Construction Institute, Construction Industry Research and Information Association, London, 1989.

S. M. Yang and Y. J. Lee. Optimization of non-collocated sensor/actuator location and feedback gain in control systems. *Smart Materials and Structures*, 2:96–102, 1993.

Y. G. Yohanis and B. Norton. Life-cycle operational and embodied energy for a generic single-storey office building in the UK. *Energy*, 27(1):77–92, 2002.

P. Young. Improved floor vibration prediction methodologies. In *Proceedings of Arup Vibration Seminar on Engineering for Structural Vibration - Current Developments in Research and Practice*, London, 2001. Institution of Mechanical Engineers.

G. Zames. Feedback and Optimal Sensitivity: Model Reference Transformations, Multiplicative Seminorms, and Approximate Inverses. *IEEE Transactions on Automatic Control*, 26(2):301–320, 1981.

J. Zhang and P. N. Roschke. Active control of a tall structure excited by wind. *Journal of Wind Engineering and Industrial Aerodynamics*, 83:209–223, 1999.

W. S. Zhang and Y. L. Xu. Closed form solution for alongwind response of actively controlled tall buildings with LQG controllers. *Journal of Wind Engineering and Industrial Aerodynamics*, 89:785–807, 2001.

Tianxin Zheng, Tianjian Ji, and Brian R. Ellis. The significance of continuity in a multi-panel composite floor. *Engineering Structures*, 32(1):184–194, January 2010. ISSN 01410296. doi: 10.1016/j.engstruct.2009.09.005.

Conference papers produced during work on thesis

Hudson, M.J., Reynolds, P. & Nyawako, D., 2013. Power requirements for active control of floor vibrations. In 31st International Modal Analysis Conference (IMAC XXXI). California: Society for Experimental Mechanics.

Hudson, M.J., Reynolds, P., & Nyawako, D.S., 2012. Comparison of passive and active mass dampers for control of floor vibrations. Proceedings of SPIE 2012.

Hudson, M.J., Reynolds, P. & Nyawako, D., 2011. Efficient Design of Floor Structures Using Active Vibration Control. Structures Congress 2011, Las Vegas, pp.35-35.

Hudson, M.J. & Reynolds, P., 2010. Analytical and Experimental Evaluation of Active Vibration Control of an Office Floor Structure. In Proceedings of 5th World Conference on Structural Control and Monitoring. Tokyo, p. 10047.

Nyawako, D., Reynolds, P. & **Hudson, M.J.** 2012. Exploring efficiencies of SISO, multi-SISO and MIMO AVC schemes for floor vibration control. Proceedings of SPIE 2012.

Nyawako, D., Reynolds, P. & **Hudson, M.J.**, 2011. Investigating PID controllers for mitigation of human-induced floor vibrations. In EURODYN 2011.

Nyawako, D., Diaz, I.M., Reynolds P., & **Hudson, M.J.**, 2011. Enhancing velocity feedback with inner loop compensators for the actuators, SMART Conference 2011, Germany, 629-639.

Nyawako DS, Reynolds P, & **Hudson M.J.**, 2011. Independent modal space control technique for mitigation of human-induced vibrations in floors. In 29th International Modal Analysis Conference (IMAC XXVIII). Jacksonville: Society for Experimental Mechanics.

Journal papers produced during work on thesis

Hudson, M.J. & Reynolds, P., 2012. Implementation considerations for active vibration control in the design of floor structures. Engineering Structures, 44, pp.334-358.

Hudson, M.J. & Reynolds, P., 2013a. A Life Cycle Analysis of an Office Floor with Active Vibration Control. Smart Materials & Structures, Submitted for review.

Hudson, M.J. & Reynolds, P., 2013b. Implications of structural design on the effectiveness of AVC on floor structures. Structural Control & Health Monitoring, Revised manuscript submitted for review.

Diaz, I.M., Pereira, E., **Hudson, M.J.** Reynolds, P., 2012. Enhancing active vibration control of pedestrian structures using inertial actuators with local feedback control. Engineering Structures, 41, pp.157-166.

Appendix A

Assumptions for EE and EC coefficients used

A number of databases with EE and EC coefficients were utilised to determine the total EE and EC of the AVC installation from the bill of quantities. These provide data for the vast majority of the materials considered in this study. For example, the EE and EC coefficients for aluminium, mild steel, stainless steel and glass were taken from the ICE database (Hammond and Jones, 2008). Whilst this database was developed with the construction industry in mind, it is believed that the processes required to produce these materials for the mechanical domain here will be of a similar nature. Of these materials, there was no available data on the CO_2e for stainless steel; only CO_2. Therefore, the CO_2 value was increased by 6% to allow for the effects of other GHG's based on the average mixture of fuels used in the UK industry (Hammond and Jones, 2008). No additional contributions for transportation from gate to site were considered because the net effect when applied to these high EE materials was negligible for the current study. In addition to this database, the database found in the MEEUP Methodology Report (VHK,

2005) was utilised to determine EE and EC coefficients for the fibre-glass found in the cheek end plates and the copper winding wire. This database was chosen preferentially over the ICE database for these materials as this was considered a more appropriate source for these particular materials.

Further to this, a number of assumptions had to be made when determining the total EE and EC for the bill of quantities shown in Table 6.3 from the coefficient data. These are detailed below.

Firstly, no coefficients for laminated steel could be found so these were approximated as virgin sheet steel to account for the more involved manufacturing process of laminated steel. The linear bearings were off-the-shelf and used a sliding film within the aluminium surround. Data for this film was not readily available but its effect on the overall EE and EC for the bearings is likely to be small because of its small size and because of the very high EE of aluminium. Therefore, this film was not considered in the analysis. The encoder was also an off-the-shelf product. This was approximated as an aluminium bar with mass as specified in the product datasheet, along with a small glass scale of size 18mm $\times$ 58.2mm $\times$ 335mm. No additional EE or EC was considered for the drilling of holes etc. in the steel and aluminium components, nor for the assembly of the parts together. Details for the components within the accelerometer were unknown. However, this will likely have a relatively high EE for its mass. Therefore, this was approximated as an average of the small and large integrated circuits from the MEEUP Methodology Report (VHK, 2005). This is expected to be a conservative estimate. In addition, a 100g HDPE mount was included to allow for steady accelerometer placement, with EE and EC coefficients also from the MEEUP Methodology Report. The combined controller and amplifier for the actuator along with the embedded controller used to implement the AVC control algorithm were approximated as having

the same constituent components as a desktop PC. The EE and EC coefficients for a desktop pc were taken from the IVF Industrial Research and Development Corporation's Lot 3 Report (IVF Industrial Research and Development Corporation, 2007). The calculated total EE and EC values here were scaled by mass to apply to each component in the bill of quantities. An allowance for additional miscellaneous cables has been included. A total of 3m of additional cabling has been allowed for, with the EE and EC being calculated by calculating approximate masses of copper and pvc in 3 core cables (40 strands of 0.2mm diameter).

No data for the EE or EC of the NdFeB magnets could be sourced. Therefore, these coefficients had to be approximated as the combination of Neodymimum Oxide and Iron Sinter (Dahlsten, 2009). These coefficients were calculated manually, using data provided by Classen et al. (2009); Spielmann et al. (2007); Althaus et al. (2007) for the majority of the processes, with fuel EE and EC coefficients calculated from data in the Digest of United Kingdom Energy Statistics (DUKES) (MacLeay et al., 2010), and weighting factors for GHG emissions taken from the MEEUP Methodology Report (VHK, 2005). The proportion of neodymium oxide and iron sinter that were combined to form the NdFeB magnets was calculated by atomic weights. Neodymium constitutes 86% of Nd_2O_3 by weight, and it was assumed that iron constitutes 56% of iron sinter by weight, calculated from typical ratios of the key mineral phases (Fisher, 2010). Therefore, 0.314kg neodymium oxide and 1.30kg iron sinter were used per kg NdFeB to achieve neodymium and iron in a ratio of 1:2.71 as per their respective atomic weights in $Nd_2Fe_{14}B$. This resulted in EE and EC coefficients of 37.90MJ/kg and 7.51kgCO_2e/kg respectively for the NdFeb magnets.

The carbon dioxide emissions for any electricity used in these processes were taken as 0.617kgCO_2/kWh (Jones, 2011). The EE of electricity at the grid was

calculated using data from MacLeay et al. (2010) on power generation in the UK, with the process detailed here. In 2009, the total fuel used by generating companies was 913,396GJ and the total net supplied energy was 354,346GJ, i.e. after allowing for the power required to run the power stations themselves. In addition to this, there were approximately 7.1% losses. 22% of these were attributable to transmission losses from the high voltage power cables, 74% to distribution losses from the public supply to the customer and 4% losses due to theft or fraud (MacLeay et al., 2010). It was decided to ignore the effect of theft/fraud on the losses for the calculation of the EE of electricity, though the effect of this decision is actually very small. Therefore, the EE of 1kWh of grid electricity was calculated as 2.766kWh or 9.96MJ/kWh$_{grid}$. Given that over 99% of electricity used in the UK is generated in the UK (MacLeay et al., 2010), this coefficient was assumed to apply for all UK electricity used.

In this study, when a particular process generated several co-products (differing to by-products which are considered as of minor importance relative to the main product) the EE and EC was attributed to each, weighted by its financial price. This differs to the methodology in the MEEUP Methodology Report (VHK, 2005) which considers only the main product as having the majority of the EE/EC, with the co-products only having the EE/EC required to convert them to their final state from the state at which they would otherwise have left the process. A similar difference occurs when a product is produced through several processes - here a weighted average of the EE/EC for each major process is used, though only the major process is used in the MEEUP Methodology Report. The ICE database (Hammond and Jones, 2008) is a compilation of many sources so it is likely that each source used different assumptions here too. These differences are not expected to affect the end result significantly, but are nonetheless important to note.

The average of two quotes for manufacturing parts for the actuator were used in determining the total economic cost of the actuator. Meanwhile, it was possible to use the commercial prices for the off-the-shelf components, such as the controller, accelerometer and encoder. The resultant cost is that for the prototype actuators considered in this study so is therefore higher than would be expected once the technology has been developed further.

Appendix B

Data tables used for derivation of EE and EC of NdFeB magnets

Table B.1: EE/EC breakdown for NdFeB

Name	Amount	Unit	EE	EC	Notes
NdFeB Magnets	1.00E+0	kg	3.79E+1	7.51E+0	$Nd_2Fe_{14}B$. Amounts added by ratio of atomic weight
Neodymium Oxide	3.14E-1	kg	3.49E+1	7.07E+0	Taking atomic weight of Nd in Nd_{203}
Iron Sinter	1.30E+0	kg	3.00E+0	4.40E-1	Assuming 56% total iron in sinter

Table B.2: EE/EC breakdown for Rare Earth Concentrate (REC)

Name	Amount	Unit	EE	EC	Notes
Rare Earth Concentrate	1.00E+0	kg	1.11E+1	2.59E+0	70% REO, from bastnasite, at beneficiation
Diesel	1.00E-1	MJ	1.00E-1	9.00E-2	Burned in building machine
Electricity	1.45E-1	kWh	1.44E+0	8.95E-2	Medium voltage, at grid
Heavy fuel oil	1.12E+0	MJ	1.12E+0	1.07E+0	Burned in industrial furnace
Steam	1.80E+0	kg	1.80E-2	1.80E-3	For chemical processes
Soda	1.80E-3	kg	6.03E-3	5.14E-3	Powder
Sodium sulphate	5.80E-2	kg	4.13E-1	1.20E-1	Powder
Fatty acids	1.90E-2	kg	1.04E-1	2.04E-2	From vegetarian oil
Hydrochloric acid	6.20E-1	kg	7.73E+0	1.17E+0	30% in H_2O
Transport (road)	2.20E-1	tkm	1.47E-1	1.10E-2	
Transport (rail)	4.94E-1	tkm	5.70E-2	4.07E-3	

Table B.3: EE/EC breakdown for Rare Earth Oxide (REO)

Name	Amount	Unit	EE	EC	Notes
Neodymium oxide	3.77E-1	kg	4.19E+1	8.49E+0	
Rare earth concentrate	1.59E+0	kg	1.77E+1	4.12E+0	70% REO, from bastnasite, at beneficiation
Electricity	3.50E-1	kWh	3.49E+0	2.16E-1	Medium voltage, at grid
Heavy fuel oil	1.47E+0	MJ	1.47E+0	1.41E+0	Burned in industrial furnace
Sulphuric acid	1.30E+0	kg	4.15E-1	2.66E-2	Liquid
Sodium hydroxide	7.00E-1	kg	1.22E+1	9.39E-1	50% in H_2O, at production
Hydrochloric acid	4.50E-1	kg	5.61E+0	8.52E-1	30% in H_2O, at plant
Transport (road)	7.75E-1	tkm	5.17E-1	3.88E-2	
Transport (rail)	4.26E+0	tkm	4.91E-1	3.51E-2	
Transport (ocean)	3.70E-1	tkm	3.77E-2	2.92E-3	Calculated as 18500km to China via Mediterranean, Suez and Malacca straits. 50,000dwt bulk carrier
CO_2	8.55E-1	kg	0.00E+0	8.55E-1	

Table B.4: EE/EC breakdown for Unrefined Fe

Name	Amount	Unit	EE	EC	Notes
Unrefined iron ore	1.00E+0	kg	3.96E-2	2.38E-2	46% Fe, at mine
Mined material	2.85E+0	kg	0.00E+0	0.00E+0	
Diesel	2.55E-2	MJ	2.55E-2	2.30E-2	Burned in building machine
Electricity	1.42E-3	kWh	1.41E-2	8.76E-4	

Table B.5: EE/EC breakdown for Refined Fe

Name	Amount	Unit	EE	EC	Notes
Refined iron ore	1.00E+0	kg	2.52E-1	5.11E-2	65% Fe, at benefication
Unrefined iron ore	1.66E+0	kg	6.58E-2	3.96E-2	46% Fe, at mine
Electricity	1.87E-2	kWh	1.86E-1	1.15E-2	Medium voltage, at grid

Table B.6: EE/EC breakdown for Sinter Fe

Name	Amount	Unit	EE	EC	Notes
Sinter	1.00E+0	kg	2.30E+0	3.37E-1	
Refined iron ore	1.00E+0	kg	2.52E-1	5.11E-2	65% Fe, at beneficiation
Transport (ocean)	2.84E+0	tkm	2.90E-1	2.24E-2	transoceanic freight ship
Transport (coastal)	3.15E-2	tkm	1.18E-2	9.47E-4	barge
Transport (rail)	2.89E-1	tkm	1.42E-1	9.16E-3	
Lime	5.00E-3	kg	2.65E-2	3.90E-3	quicklime, loose pieces
Transport (rail)	2.00E-2	tkm	9.83E-3	6.34E-4	
Transport (road)	2.00E-3	tkm	1.34E-3	1.00E-4	
Fuel gas for heating	3.63E-2	MJ	3.63E-2	0.00E+0	Exhausts cleaned, so only CO_2 values as given
Coke chippings	1.43E+0	MJ	1.43E+0	0.00E+0	Exhausts cleaned, so only CO_2 values as given
Electricity	1.00E-2	kWh	9.96E-2	6.17E-3	Medium voltage, at grid
CO_2	2.04E-1	kg	0.00E+0	2.04E-1	
CO	2.47E-2	kg	0.00E+0	3.88E-2	

Table B.7: EE/EC breakdown for Transport (road)

Name	Amount	Unit	EE	EC	Notes
Transport (road)	1.60E+1	tkm	1.07E+1	8.01E-1	<16t lorry, fleet average for Europe (converted from 1vkm)
Diesel	2.49E-1	kg	1.07E+1	0.00E+0	
CO_2	7.88E-1	kg	0.00E+0	7.88E-1	
CO	1.64E-3	kg	0.00E+0	2.57E-3	
CH_4	7.67E-5	kg	0.00E+0	1.61E-3	
N_2O	3.00E-5	kg	0.00E+0	8.88E-3	

Table B.8: EE/EC breakdown for Transport (rail)

Name	Amount	Unit	EE	EC	Notes
Operation, freight train	1.00E+0	tkm	4.91E-1	3.17E-2	Europe average for diesel / electricity
Electricity	3.96E-2	kWh	3.94E-1	2.44E-2	
Diesel	2.26E-3	kg	9.70E-2	0.00E+0	
CH_4	2.94E-7	kg	0.00E+0	6.17E-6	
CO	3.57E-5	kg	0.00E+0	5.60E-5	
CO_2	7.12E-3	kg	0.00E+0	7.12E-3	
N_2O	2.26E-7	kg	0.00E+0	6.69E-5	

Table B.9: EE/EC breakdown for Transport (China rail)

Name	Amount	Unit	EE	EC	Notes
Operation, freight train	1.00E+0	tkm	1.15E-1	8.25E-3	China. Coal freight train on diesel (70% of trains are diesel.)
Freight train	7.50E-1	tkm	8.04E-2	5.99E-3	Diesel powered
Freight train	2.50E-1	tkm	3.49E-2	2.25E-3	Electricity powered

Table B.10: EE/EC breakdown for Transport (China rail electric)

Name	Amount	Unit	EE	EC	Notes
Freight train	1.00E+0	tkm	1.40E-1	9.02E-3	Electricity powered
Electricity	1.11E-2	kWh	1.11E-1	6.85E-3	
Diesel	6.77E-4	kg	2.90E-2	0.00E+0	
CO_2	2.13E-3	kg	0.00E+0	2.13E-3	
CO	1.07E-5	kg	0.00E+0	1.68E-5	
N_2O	6.77E-8	kg	0.00E+0	2.00E-5	
CH_4	8.79E-8	kg	0.00E+0	1.85E-6	

Table B.11: EE/EC breakdown for Transport (China rail diesel)

Name	Amount	Unit	EE	EC	Notes
Freight train	1.00E+0	tkm	1.07E-1	7.99E-3	Diesel powered
Diesel	2.50E-3	kg	1.07E-1	0.00E+0	
CH_4	3.25E-7	kg	0.00E+0	6.83E-6	
CO	3.95E-5	kg	0.00E+0	6.20E-5	
CO_2	7.85E-3	kg	0.00E+0	7.85E-3	
N_2O	2.50E-7	kg	0.00E+0	7.40E-5	

Table B.12: EE/EC breakdown for Transport (ocean)

Name	Amount	Unit	EE	EC	Notes
Operation, transoceanic freight	1.00E+0	tkm	1.02E-1	7.88E-3	
Heavy fuel oil	2.50E-3	kg	1.02E-1	0.00E+0	
CH_4	1.55E-7	kg	0.00E+0	3.26E-6	
CO	1.76E-5	kg	0.00E+0	2.76E-5	
CO_2	7.79E-3	kg	0.00E+0	7.79E-3	
N_2O	2.00E-7	kg	0.00E+0	5.92E-5	

Table B.13: EE/EC breakdown for Transport (coastal)

Name	Amount	Unit	EE	EC	Notes
Operation, barge	1.00E+0	tkm	3.75E-1	3.01E-2	
Diesel	8.74E-3	kg	3.75E-1	0.00E+0	
CH_4	2.25E-7	kg	0.00E+0	4.73E-6	
CO	2.54E-5	kg	0.00E+0	3.99E-5	
CO_2	2.98E-2	kg	0.00E+0	2.98E-2	
N_2O	7.52E-7	kg	0.00E+0	2.23E-4	

Table B.14: EE/EC breakdown for Soda

Name	Amount	Unit	EE	EC	Notes
Soda	3.00E+0	kg	1.00E+1	8.56E+0	Made through Solvay process
$CaCl_2$	1.50E+0	kg	1.00E+1	8.56E+0	Made through Solvay process
Sodium chloride	1.50E+0	kg	1.51E+0	4.73E-1	
Limestone	1.20E+0	kg	7.44E-1	3.84E-2	
Ammonia	2.00E-3	kg	6.64E-2	4.43E-3	
Electricity	4.00E-2	kWh	3.98E-1	2.47E-2	
Heat (coal furnace)	7.23E+0	MJ	7.23E+0	8.02E+0	
Transport (road)	1.53E-1	tkm	1.02E-1	7.66E-3	

Table B.15: EE/EC breakdown for Sodium Sulphate (production mix)

Name	Amount	Unit	EE	EC	Notes
Sodium sulphate	1.00E+0	kg	7.12E+0	2.08E+0	Production Mix
Sodium sulphate	6.00E-1	kg	1.13E+0	1.75E-1	From natural sources
Sodium sulphate	1.50E-1	kg	6.70E-1	3.71E-1	From Mannheim process
Electricity	3.33E-1	kWh	3.32E+0	2.05E-1	
Natural gas	2.00E+0	MJ	2.00E+0	1.32E+0	Burned

Table B.16: EE/EC breakdown for Sodium Sulphate (natural sources)

Name	Amount	Unit	EE	EC	Notes
Sodium sulphate	1.00E+0	kg	1.89E+0	2.92E-1	From Natural Sources
Electricity	1.70E-1	kWh	1.69E+0	1.05E-1	
Light fuel oil	1.91E-1	MJ	1.91E-1	1.83E-1	Burned
Diesel	4.28E-3	MJ	4.28E-3	3.85E-3	Burned

Table B.17: EE/EC breakdown for Sodium Sulphate (from Mannheim Process)

Name	Amount	Unit	EE	EC	Notes
Sodium sulphate	1.00E+0	kg	4.47E+0	2.47E+0	From Mannheim process
Hydrochloric acid	5.13E-1	kg	1.46E+0	8.07E-1	From Mannheim process
Sodium chloride	8.66E-1	kg	8.70E-1	2.73E-1	
Sulphuric acid	7.27E-1	kg	2.32E-1	1.49E-2	
Electricity	6.50E-2	kWh	6.47E-1	4.01E-2	
Natural gas	1.80E+0	MJ	1.80E+0	1.19E+0	Burned
Heavy fuel oil	1.80E+0	MJ	1.80E+0	1.72E+0	Burned
Transport (rail)	9.56E-1	tkm	4.70E-1	3.03E-2	
Transport (road)	1.59E-1	tkm	1.06E-1	7.96E-3	

Table B.18: EE/EC breakdown for Hydrochloric Acid (Production Mix)

Name	Amount	Unit	EE	EC	Notes
Hydrochloric Acid	1.00E+0	kg	1.25E+1	1.89E+0	Production mix
Hydrochloric Acid	5.00E-1	kg	1.11E+1	1.11E+0	Reaction of hydrogen with chlorine
Hydrochloric Acid	5.00E-1	kg	1.42E+0	7.87E-1	From Mannheim process

Table B.19: EE/EC breakdown for Hydrochloric Acid (Direct HCl Production)

Name	Amount	Unit	EE	EC	Notes
Hydrochloric Acid	1.00E+0	kg	2.21E+1	2.21E+0	Direct HCl production
Chlorine	9.73E-1	kg	1.69E+1	1.31E+0	
Electricity	3.30E-1	kWh	3.29E+0	2.04E-1	
Hydrogen	2.70E-2	kg	1.81E+0	6.97E-1	
Transport (rail)	1.00E-1	tkm	4.91E-2	3.17E-3	
Transport (road)	5.00E-2	tkm	3.34E-2	2.50E-3	

Table B.20: EE/EC breakdown for Sulphuric Acid

Name	Amount	Unit	EE	EC	Notes
Sulphuric Acid	1.00E+0	kg	3.19E-1	2.04E-2	Liquid
Secondary Sulphur	2.15E-1	kg	0.00E+0	0.00E+0	Assume EE/EC is 0. Byproduct of oil refining, so resources allocated there.
Diesel	7.44E-5	kg	3.19E-3	2.35E-4	
Electricity	1.75E-2	kWh	1.74E-1	1.08E-2	
Transport (rail)	2.35E-1	tkm	1.15E-1	7.45E-3	
Transport (road)	3.93E-2	tkm	2.62E-2	1.97E-3	

Table B.21: EE/EC breakdown for Sodium Hydroxide

Name	Amount	Unit	EE	EC	Notes
Sodium Hydroxide	2.16E+0	kg	3.75E+1	2.89E+0	Production by mercury cell
Chlorine (gaseous)	2.16E+0	kg	3.75E+1	2.89E+0	Production by mercury cell
Sodium Chloride	1.75E+0	kg	1.76E+0	5.51E-1	
Mercury	6.75E-6	kg	0.00E+0	0.00E+0	Data not available
Soda	1.15E-2	kg	3.85E-2	3.28E-2	
Barite	3.50E-3	kg	0.00E+0	0.00E+0	Data not available
Calcium chloride	1.78E-2	kg	1.19E-1	1.02E-1	
Sulphite	1.00E-4	kg	0.00E+0	0.00E+0	Data not available
Sulphuric acid	8.62E-3	kg	2.75E-3	1.76E-4	
Electricity	3.56E+0	kWh	3.54E+1	2.20E+0	
Carbon tetrachloride	1.00E-5	kg	0.00E+0	0.00E+0	Data not available
Transport (road)	1.89E-1	tkm	1.26E-1	9.46E-3	
Transport (rail)	1.40E-2	tkm	6.88E-3	4.44E-4	

Table B.22: EE/EC breakdown for Hydrogen

Name	Amount	Unit	EE	EC	Notes
Hydrogen	1.00E+0	kg	6.69E+1	2.58E+1	Cracking, APME
Crude Oil	7.56E-1	kg	3.28E+1	2.43E+0	
Natural Gas	9.21E-1	m^3	3.28E+1	2.17E+1	
Coal, hard	4.88E-2	kg	1.24E+0	5.41E-2	
Energy in hydropower reservoir	5.73E-2	MJ	5.73E-2	0.00E+0	
CO	2.51E-3	kg	0.00E+0	3.94E-3	
CO_2	1.23E+0	kg	0.00E+0	1.23E+0	
CH_4	1.82E-2	kg	0.00E+0	3.82E-1	

Table B.23: EE/EC breakdown for Ammonia (liquid)

Name	Amount	Unit	EE	EC	Notes
Ammonia	1.00E+0	kg	3.32E+1	2.22E+0	Liquid
Ammonia	8.50E-1	kg	2.73E+1	1.82E+0	From steam reforming
Ammonia	1.50E-1	kg	5.54E+0	3.72E-1	From partial oxidation
Transport (road)	1.00E-1	tkm	6.68E-2	5.01E-3	
Transport (rail)	6.00E-1	tkm	2.95E-1	1.90E-2	

Table B.24: EE/EC breakdown for Ammonia (from steam reforming)

Name	Amount	Unit	EE	EC	Notes
Ammonia	1.00E+0	kg	3.21E+1	2.14E+0	From steam reforming
Natural gas	2.34E+1	MJ	2.34E+1	0.00E+0	Feedstock
Heavy fuel oil	1.97E-1	kg	8.04E+0	6.34E-1	
Electricity	6.94E-2	kWh	6.91E-1	4.28E-2	
Transport (road)	4.00E-5	tkm	2.67E-5	2.00E-6	
Transport (rail)	2.28E-4	tkm	1.12E-4	7.22E-6	
CO_2	1.46E+0	kg	0.00E+0	1.46E+0	
CO	8.40E-5	kg	0.00E+0	1.32E-4	
N_2O	1.53E-5	kg	0.00E+0	4.53E-3	

Table B.25: EE/EC breakdown for Ammonia (from partial oxidation)

Name	Amount	Unit	EE	EC	Notes
Ammonia	1.00E+0	kg	3.70E+1	2.48E+0	From partial oxidation
Heavy fuel oil	8.57E-1	kg	3.50E+1	0.00E+0	Feedstock
Electricity	2.00E-1	kWh	1.99E+0	1.23E-1	
Transport (road)	5.00E-6	tkm	8.55E-4	6.41E-5	
Transport (rail)	1.80E-5	tkm	8.84E-6	5.70E-7	
CO_2	2.34E+0	kg	0.00E+0	2.34E+0	
CO	2.20E-4	kg	0.00E+0	3.45E-4	
N20	5.65E-5	kg	0.00E+0	1.67E-2	

Table B.26: EE/EC breakdown for Sodium Chloride

Name	Amount	Unit	EE	EC	Notes
Sodium chloride	1.00E+0	kg	1.01E+0	3.15E-1	
Water	3.82E-3	m^3	0.00E+0	0.00E+0	Natural origins
Heat	1.69E-1	MJ	1.69E-1	1.62E-1	Heavy fuel oil
Heat	1.69E-1	MJ	1.69E-1	1.12E-1	Natural gas
Electricity	6.70E-2	kWh	6.67E-1	4.13E-2	

Table B.27: EE/EC breakdown for Soya Oil

Name	Amount	Unit	EE	EC	Notes
Soya oil	3.57E+0	kg	1.95E+1	3.84E+0	
Pentane	2.24E-3	kg	9.81E-2	0.00E+0	Assume as 'petroleum product'
Soybeams IP	5.60E+0	kg	0.00E+0	0.00E+0	In ground
Natural gas	2.29E+0	MJ	2.29E+0	1.52E+0	Burned
Light fuel oil	1.24E+0	MJ	1.24E+0	1.19E+0	Burned
Electricity	2.58E-1	kWh	2.57E+0	1.59E-1	
Transport (road)	8.15E+0	tkm	5.44E+0	4.08E-1	
Transport (rail)	1.96E+0	tkm	4.00E+0	2.58E-1	
Transport (ocean)	6.74E+1	tkm	8.31E-1	6.42E-2	
Transport (coastal)	4.50E+0	tkm	3.06E+0	2.45E-1	

Appendix C

Design Calculations for Column, Piles and Pile Caps

C.1 Column Design

C.1.1 Column Load Calculation

First, calculate the total design load due to the floors and roof above for a single column in the centre of the building:

For 130mm, 170mm and 210mm slab depths, the volume of concrete is given as $0.097m^3/m^2$, $0.137m^3/m^2$ and $0.177m^3/m^2$ respectively. This gives a concrete

dead load as:

$$\text{Concrete DL } (130mm) = \frac{9.81}{1000} kN/kg \times 2400 kg/m^3 \times 0.097 m^3/m^2$$
$$= 2.28 kN/m^2 \quad \text{(C.1)}$$
$$\text{Concrete DL } (170mm) = \frac{9.81}{1000} kN/kg \times 2400 kg/m^3 \times 0.137 m^3/m^2$$
$$= 3.23 kN/m^2 \quad \text{(C.2)}$$
$$\text{Concrete DL } (210mm) = \frac{9.81}{1000} kN/kg \times 2400 kg/m^3 \times 0.177 m^3/m^2$$
$$= 4.17 kN/m^2 \quad \text{(C.3)}$$

The primary and secondary steel beams have masses of 74.0kg/m and 72.2kg/m respectively. Given the beam arrangement shown in Figure 6.4 the total lengths of steel beam per column were calculated as 6m and 15 $\times$ 2=30m respectively. This gives a total steel weight of:

$$\text{Steel weight } = \frac{9.81}{1000} kN/kg \times (74.0 kg/m \times 6m + 72.2 kg/m \times 30m)$$
$$= 25.6 kN \quad \text{(C.4)}$$

Other dead loads are assumed to be services (0.5kN/m^2), raised floor (0.3kN/m^2), ducting (0.1kN/m^2) and decking (0.1kN/m^2), totalling 1kN/m^2.

An imposed load of 2.5kN/m^2 plus 1kN/m^2 for internal partitions was assumed for office loading, resulting in a total imposed load of 3.5kN/m^2 (BSI, 1996).

The area around each central column over which these uniform loads act is 15m $\times$ 6m = 90m. Therefore, the design loads for each floor around each central column are given as (using 1.35 and 1.5 as factors of safety for dead and imposed loads

respectively):

$$\begin{aligned} \text{130mm floor load} &= (3.5kN/m^2 \times 1.5 + (2.28 + 1.0)kN/m^2 \times 1.35) \times 90m^2 \\ &\quad + (25.6kN \times 1.35) \\ &= 906kN \end{aligned} \tag{C.5}$$

$$\begin{aligned} \text{170mm floor load} &= (3.5kN/m^2 \times 1.5 + (3.23 + 1.0)kN/m^2 \times 1.35) \times 90m^2 \\ &\quad + (25.6kN \times 1.35) \\ &= 1021kN \end{aligned} \tag{C.6}$$

$$\begin{aligned} \text{210mm floor load} &= (3.5kN/m^2 \times 1.5 + (4.17 + 1.0)kN/m^2 \times 1.35) \times 90m^2 \\ &\quad + (25.6kN \times 1.35) \\ &= 1135kN \end{aligned} \tag{C.7}$$

For simplicity, the roof was assumed to have the same structural layout as the most slender floor design (130mm slab depth). This roof is assumed to have services, ducting and decking as additional loads, but no raised floor. A minimum imposed load of 1.5kN/m^2 was assumed for access (BSI, 1988). Therefore, the total roof load per column is:

$$\begin{aligned} \text{Roof load} &= (1.5kN/m^2 \times 1.5 + (2.28 + 0.7)kN/m^2 \times 1.35) \times 90m^2 \\ &\quad + (25.6kN \times 1.35) \\ &= 600kN \end{aligned} \tag{C.8}$$

It is assumed that the cross section of the column does not vary with storey. Therefore, the highest loaded case of the bottom storey of the five storey building was considered.

The self weight of the steel column is assumed for design purposes to be 198kg/m, resulting in a total self weight load resulting from the upper four storeys of:

$$\begin{aligned}\text{Column self weight } &= \frac{9.81}{1000}kN/kg198kg/m \times (3.8m \times 4) \times 1.35 \\ &= 40kN \end{aligned} \tag{C.9}$$

Therefore, the total design vertical loads for each column are given by:

$$\begin{aligned}\text{130mm vertical load} &= (906kN/\text{floor} \times 4\text{floors}) + 600kN + 40kN \\ &= 4264kN \end{aligned} \tag{C.10}$$

$$\begin{aligned}\text{170mm vertical load} &= (1021kN/\text{floor} \times 4\text{floors}) + 600kN + 40kN \\ &= 4721kN \end{aligned} \tag{C.11}$$

$$\begin{aligned}\text{210mm vertical load} &= (1135kN/\text{floor} \times 4\text{floors}) + 600kN + 40kN \\ &= 5179kN \end{aligned} \tag{C.12}$$

C.1.2 Column Specification

An initial size of 305 $\times$ 305 $\times$ 198UC was assumed for the columns. The design capacity of this section was calculated by checking the maximum compressive resistance and the maximum flexural buckling resistance about both the major and minor axes, assuming the columns were simply supported and loaded axially only.

The compressive resistance check is given by (Baddoo et al., 1993):

$$N_{Sd} \leq N_{c,Rd} = \frac{Af_y}{\gamma_{M0}} \tag{C.13}$$

where N_{Sd} is the design applied compressive force, $N_{c,Rd}$ is the compressive re-

sistance of the section, A is the cross sectional area of the section, f_y is the characteristic strength, γ_{M0} is the partial safety factor.

Therefore,

$$N_{c,Rd} = \frac{252 \times 10^2 \times 275}{1.05 \times 10^3} = 6600kN \tag{C.14}$$

The flexural buckling check is given by (Baddoo et al., 1993):

$$N_{Sd} \leq N_{b,Rd,y} \qquad \text{and} \qquad N_{Sd} \leq N_{b,Rd,z} \tag{C.15}$$

where

$$N_{b,Rd} = \frac{\beta_A \times f_c \times A}{\gamma_{M1}} \tag{C.16}$$

$\beta_A = 1$ for class 1 elements, $\gamma_{M1} = 1.05$ and f_c is the reduced characteristic strength based on the slenderness ratio of the element.

The slenderness ratio, λ is given by (Baddoo et al., 1993):

$$\lambda_y = \frac{l}{i_y} = \frac{1.0L}{i_y} = \frac{3800}{142} = 26.8 \tag{C.17}$$

$$\lambda_z = \frac{l}{i_z} = \frac{1.0L}{i_z} = \frac{3800}{80.2} = 47.4 \tag{C.18}$$

For buckling about the $y - y$ axis, curve 'b' is used from Table 5.14 (Baddoo et al., 1993), whilst for buckling about the $z - z$ axis, curve 'c' is used. This gives $f_c = 263$N/mm^2 and $f_c = 225$N/mm^2 for $y - y$ and $z - z$ buckling respectively. Therefore, checking the buckling design resistance gives:

$$N_{b,Rd,y} = \frac{1.0 \times 263 \times 252 \times 10^2}{1.05 \times 10^3}$$
$$= 6312kN \tag{C.19}$$
$$N_{b,Rd,z} = \frac{1.0 \times 225 \times 252 \times 10^2}{1.05 \times 10^3}$$
$$= 5400kN \tag{C.20}$$

With reference to Equations C.14, C.19 and C.20 for the design resistances and Equations C.10-C.12 for the design loads, it is observed that this column size is suitable for all three design scenarios, namely 130mm, 170mm and 210mm. However, it may be possible to reduce this column size for some of the lighter load cases.

Therefore, a 305 $\times$ 305 $\times$ 158UC was considered. Here, the compressive resistance is given by:

$$N_{c,Rd} = \frac{201 \times 10^2 \times 275}{1.05 \times 10^3}$$
$$= 5264kN \tag{C.21}$$

The slenderness ratios are given by:

$$\lambda_y = \frac{l}{i_y} = \frac{1.0L}{i_y} = \frac{3800}{139} = 27.3 \tag{C.22}$$
$$\lambda_z = \frac{l}{i_z} = \frac{1.0L}{i_z} = \frac{3800}{78.9} = 48.2 \tag{C.23}$$

which gives reduced characteristic strengths of $f_c = 263$N/mm^2 and $f_c = 224$N/mm^2 for $y-y$ and $z-z$ buckling respectively. Using these strengths,

the buckling design resistances are:

$$N_{b,Rd,y} = \frac{1.0 \times 263 \times 201 \times 10^2}{1.05 \times 10^3}$$
$$= 5035kN \tag{C.24}$$
$$N_{b,Rd,z} = \frac{1.0 \times 224 \times 201 \times 10^2}{1.05 \times 10^3}$$
$$= 4288kN \tag{C.25}$$

Now, comparing Equations C.10-C.12 with Equations C.21, C.24 and C.25 it is observed that this smaller column size is suitable for the 130mm slab depth scenario but is insufficient for the 170mm and 210mm scenarios. Given how close the design resistance is to the design load for the 130mm case it is unlikely that any further improvement can be made.

C.2 Pile Design

C.2.1 Pile Load Calculation

The load at the top of the piles was calculated using Equations C.10-C.12 for the column loads, and adding the appropriate additional loads. These are: the self weight of the column for the first storey only, the floor load for the ground floor, and an assumed weight for the pile cap. For simplicity, the ground floor is assumed to be of a similar construction type to the upper storeys. However, vibrations are not likely to be a problem on this floor so it has a fixed slab depth of 130mm. This is considered a reasonable approximation because this assumption is only used to calculate the floor's self weight for the purposes of designing the pile caps and piles - it is not directly considered later in any material savings calculations.

The design of the piles is performed before the design of the pile caps. This is

because the two designs are linked, but it is easier to approximate the size of the pile cap than the size of the piles. Therefore, each column is assumed to be supported by a 2.0m $\times$ 2.0m $\times$ 1.0m concrete pad, which is itself supported by 4 piles.

The additional load to each pile is therefore given by:

$$\begin{aligned}\text{Pile Cap SW} &= \frac{9.81}{1000}kN/kg \times 2400kg/m^3 \\ &\quad \times (2.0m \times 2.0m \times 1.0m) \times 1.35 \\ &= 127kN \end{aligned} \tag{C.26}$$

$$\begin{aligned}\text{Column SW} &= \frac{9.81}{1000}kN/kg \times 198kg/m \times 3.8m \times 1.35 \\ &= 10kN \end{aligned} \tag{C.27}$$

$$\text{Ground Floor SW} = 906kN \quad \text{(from Equation C.5)} \tag{C.28}$$

Therefore, the total design loads to be carried by the piles for each design scenario are:

$$\begin{aligned}\text{130mm pile load} &= 4264kN + 127kN + 10kN + 906kN \\ &= 5307kN \end{aligned} \tag{C.29}$$

$$\begin{aligned}\text{170mm pile load} &= 4721kN + 127kN + 10kN + 906kN \\ &= 5879kN \end{aligned} \tag{C.30}$$

$$\begin{aligned}\text{210mm pile load} &= 5179kN + 127kN + 10kN + 906kN \\ &= 6451kN \end{aligned} \tag{C.31}$$

C.2.2 Pile Specification

As discussed in Section 6.4.3, the building in this study is not based on an existing structure so no soil conditions were available; therefore "typical" values were assumed. These are shown in Table C.1 (repeated from Table 6.2). Four piles were designed per column, and each was assumed to be bored and checked for axial capacity only (Curtin et al., 2006).

Table C.1: Assumed soil conditions

Depth (m)	Soil type
0 to 5	Fill material. Negligible contribution to axial capacity of pile
5 to 10	Sand and gravel. Assume angle of friction 30°
10 to 15	Stiff clay. Assume strength of 150kN/m^2
15 to 30	Very stiff clay. Assume strength of 300kN/m^2

The total resistance of the piles, Q, were found by dividing the load equally between the piles and then considering each pile in isolation and summing the shaft resistance, Q_s, within each strata and the end bearing resistance, Q_b, in the final strata.

For a single soil strata, the total resistance of one pile with a circular cross section is given by:

$$\begin{aligned} Q &= Q_b + Q_s \\ &= q_b \times \left(\pi \frac{D^2}{4}\right) + \int_0^L \tau_s \pi D \, \mathrm{d}L \end{aligned} \tag{C.32}$$

where, in sand/gravel:

$$\tau_s = K tan(\delta) s' \tag{C.33}$$

Table C.2: Summary of pile design calculations

	Resistance Force (kN)					
Pile length	23m	24m	25m	26m	27m	28m
Strata 2 Q_s	390	390	390	390	390	390
Strata 3 Q_s	530	530	530	530	530	530
Strata 3 Q_b	0	0	0	0	0	0
Strata 4 Q_s	1696	1909	2121	2333	2545	2757
Strata 4 Q_b	530	530	530	530	530	530
Total Force Q	3147	3359	3571	3783	3995	4207
Force with FOS	1259	1344	1428	1513	1598	1683
All 4 Piles	5035	5375	5714	6053	6393	6732

whilst, in clay:

$$\tau_s = \alpha c_s \tag{C.34}$$

$$q_b = N_c c_b \tag{C.35}$$

D is the diameter of the pile, L is the length of the pile within that strata, K is an earth pressure coefficient (assumed $K = 0.8$ assumed for these bored piles), δ is the pile-soil adhesion (assumed to be equal to 0.75ϕ), ϕ is the angle of friction of the soil, s' is the effective overburden pressure $s' = \gamma z$, γ is the self weight of the undrained soil, z is the depth within the strata, α is an adhesion factor (assumed $\alpha = 0.45$ for London clay with bored piles), N_c is a bearing capacity (assumed $N_c = 9$ for circular piles), c_s is the undrained shear strength, c_b is the undisturbed shear strength at the base (assumed to be equal to c_s).

These calculations were performed for the soil properties shown in Table C.1 and with a pile diameter of 0.5m. The details of this calculation are not shown here but a summary table for several design scenarios is shown in Table C.2. Here, a factor of safety of 2.5 was used.

Referring to Equations C.29-C.31 and Table C.2 it is observed that for the three

structural types, piles of length 24m, 26m and 28m respectively are needed.

C.3 Pile Cap Design

C.3.1 Pile Cap Load Calculation

The load at the top of the pile cap was calculated in a similar manner to that for the pile caps but obviously without the self weight of the pile caps. Using the same procedure as discussed in Section C.2 the total design loads for each design scenario are:

$$\begin{aligned} \text{130mm pile load} &= 4264kN + 10kN + 906kN \\ &= 5180kN \end{aligned} \tag{C.36}$$

$$\begin{aligned} \text{170mm pile load} &= 4721kN + 10kN + 906kN \\ &= 5752kN \end{aligned} \tag{C.37}$$

$$\begin{aligned} \text{210mm pile load} &= 5179kN + 10kN + 906kN \\ &= 6324kN \end{aligned} \tag{C.38}$$

C.3.2 Pile Cap Specification

The pile caps were designed based on the pile layout specified in Section C.2, namely four piles on a square arrangement as shown in Figure C.1. The piles were spaced at $1.5D$ (where D is the diameter of the pile) with 100mm cover to the edges. This gives an overall width of 1.95m which was rounded up to 2.0m for the square pile caps. The depth of the piles were determined for each design scenario by considering both local shear and bending shear in the cap using the bending theory approach in accordance with (BSI, 1997).

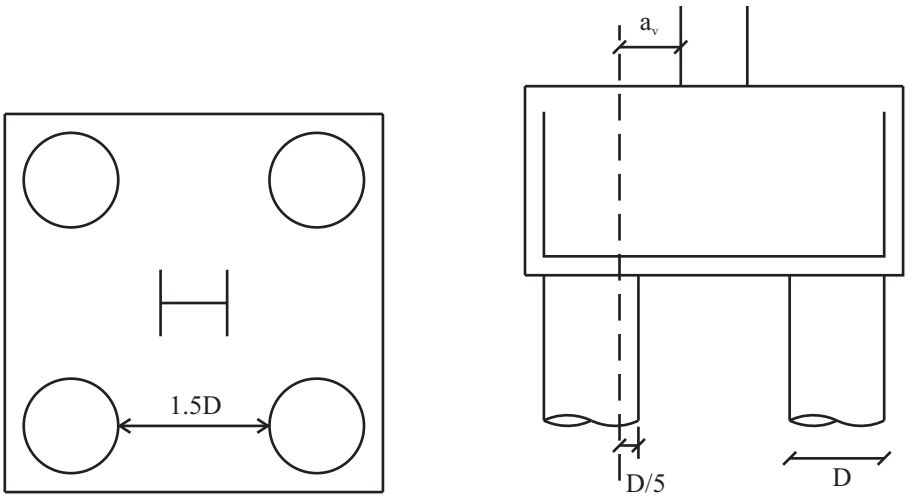

(a) Plan View (b) Elevation View

Figure C.1: Pile Cap Design

First, the local shear check (Curtin et al., 2006):

$$\nu_u = \frac{P_u}{ud} \leq 0.8\sqrt{f_{cu}} \text{ or } 5N/mm^2 \tag{C.39}$$

where ν_u is the shear stress at the face of the column, P_u is the applied vertical load, u is the column perimeter, d is the depth to reinforcement as shown in Figure C.1 and for grade C35 concrete, $0.8\sqrt{f_{cu}} = 4.73$N/mm^2. Therefore, Equation C.39 can be rearranged to give a lower limit on d:

$$d \geq \frac{P_u}{4.73u} \tag{C.40}$$

It was assumed that the column perimeter extended just to the outer edges of the column, i.e. no extra width for a base plate was accounted for. This is a slightly conservative approximation as the smaller column perimeter necessitates a larger pile cap depth.

This check was performed for the three design scenarios, as shown in Equa-

tions C.41-C.43:

$$130mm \quad d \geq \frac{5180 \times 10^3 N}{4.73 N/mm^2 \cdot (4 \times 350) mm} = 782mm \tag{C.41}$$

$$170mm \quad d \geq \frac{5752 \times 10^3 N}{4.73 N/mm^2 \cdot (4 \times 350) mm} = 869mm \tag{C.42}$$

$$210mm \quad d \geq \frac{6324 \times 10^3 N}{4.73 N/mm^2 \cdot (4 \times 350) mm} = 955mm \tag{C.43}$$

Secondly, the bending shear check which is performed across a section 20% of the diameter of the pile inside the face of the pile (Curtin et al., 2006):

$$\frac{V_u}{b_v d} \leq \left(\frac{2d}{a_v}\right) v_c \tag{C.44}$$

where V_u is the shear force across the section (given by half the applied axial force, P_u, ignoring the self weight of the pile cap), b_v is the breadth of the pile cap, a_v is the distance shown in Figure C.1, and v_c is the design concrete shear stress which for grade C35 concrete with six T25 bars (assumed) has a minimum value of 0.4N/mm^2. This can be rearranged to:

$$d \geq \sqrt{\frac{a_v V_u}{2 b_v v_c}} \tag{C.45}$$

This check was performed for the three design scenarios, as shown in Equations C.46-C.48:

$$130mm \quad d \geq \sqrt{\frac{325mm \times 5180/2 \times 10^3 N}{2 \times 2000mm \times 0.4 N/mm^2}} = 725mm \tag{C.46}$$

$$170mm \quad d \geq \sqrt{\frac{325mm \times 5752/2 \times 10^3 N}{2 \times 2000mm \times 0.4 N/mm^2}} = 764mm \tag{C.47}$$

$$210mm \quad d \geq \sqrt{\frac{325mm \times 6324/2 \times 10^3 N}{2 \times 2000mm \times 0.4 N/mm^2}} = 801mm \tag{C.48}$$

Therefore, the overall depth of the pile caps can be calculated by taking the maximum of the two calculated d values, as per Equations C.41-C.43 and C.46-C.48 and adding 25mm for the diameter of the reinforcing bars and 75mm for cover. The overall depth of the pile caps for each of the design scenarios is thus given by:

$$\begin{aligned} 130mm \quad h &\geq \max(782mm, 725mm) + 25mm + 75mm \\ &= 882mm \quad \therefore \text{ use } 900mm \end{aligned} \tag{C.49}$$

$$\begin{aligned} 170mm \quad h &\geq \max(869mm, 764mm) + 25mm + 75mm \\ &= 969mm \quad \therefore \text{ use } 1000mm \end{aligned} \tag{C.50}$$

$$\begin{aligned} 210mm \quad h &\geq \max(955mm, 801mm) + 25mm + 75mm \\ &= 1055mm \quad \therefore \text{ use } 1100mm \end{aligned} \tag{C.51}$$

It is observed that the final calculated size for the pile caps is 2.0m $\times$ 2.0m $\times$ 1.0m $\pm$ 0.1m so the original assumption used in Section C.2 for the size of the pile caps is suitable.